

1-1-1993

# Morphology and enhanced compatibility of immiscible polymers via specific interactions/

Elliot P. Douglas

*University of Massachusetts Amherst*

Follow this and additional works at: [https://scholarworks.umass.edu/dissertations\\_1](https://scholarworks.umass.edu/dissertations_1)

---

## Recommended Citation

Douglas, Elliot P, "Morphology and enhanced compatibility of immiscible polymers via specific interactions/" (1993). *Doctoral Dissertations 1896 - February 2014*. 806.

[https://scholarworks.umass.edu/dissertations\\_1/806](https://scholarworks.umass.edu/dissertations_1/806)

This Open Access Dissertation is brought to you for free and open access by ScholarWorks@UMass Amherst. It has been accepted for inclusion in Doctoral Dissertations 1896 - February 2014 by an authorized administrator of ScholarWorks@UMass Amherst. For more information, please contact [scholarworks@library.umass.edu](mailto:scholarworks@library.umass.edu).

312066008193064

MORPHOLOGY AND ENHANCED COMPATIBILITY  
OF IMMISCIBLE POLYMERS VIA SPECIFIC  
INTERACTIONS

A Dissertation Presented  
by  
ELLIOT P. DOUGLAS

Submitted to the Graduate School of the  
University of Massachusetts in partial fulfillment  
of the requirements for the degree of

DOCTOR OF PHILOSOPHY

February 1993

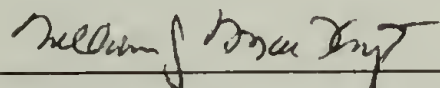
Department of Polymer Science and Engineering

© Copyright by Elliot Paul Douglas 1993  
All Rights Reserved

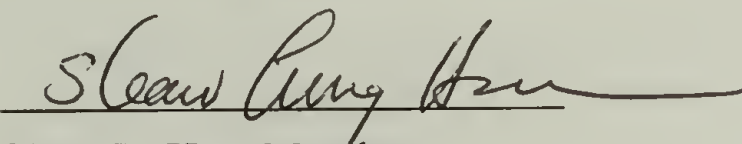
# MORPHOLOGY AND ENHANCED COMPATIBILITY OF IMMISCIBLE POLYMERS VIA SPECIFIC INTERACTIONS

A Dissertation Presented  
by  
ELLIOT P. DOUGLAS

Approved as to style and content by:



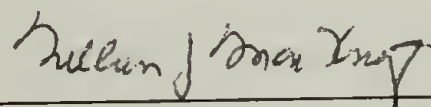
William J. MacKnight, Chair



Shaw L. Hsu, Member



Michael F. Malone, Member



William J. MacKnight, Department Head  
Polymer Science and Engineering

This work is dedicated to my family: my mother and my brothers for their love and support, and especially to Heidi, who has given this work meaning and life.

## ACKNOWLEDGMENTS

I am deeply indebted to a number of people, without whom this work would not have been possible. I would especially like to thank my advisor, Dr. William J. MacKnight, and the other members of my committee, Dr. Shaw L. Hsu and Dr. Michael F. Malone for their help and guidance. Helpful discussions and critique were also provided by Dr. Dennis G. Peiffer, Dr. Robert D. Lundberg, Mr. Kazuo Sakurai, Ms. Deborah Vezie, Ms. Karla Gagnon, Mr. Robert Jennings, Dr. Michelle Bellinger, and Dr. Alan Waddon.

Technical help was also provided by a great number of people. I would like to thank the following people: Dr. Fotios Papadimitrakopoulos (polymer synthesis), Dr. J. Michael Connolly (DMTA), Dr. Alan Waddon (optical microscopy and SAXS), Mr. Satoshi Osawa (density measurements), Mr. Eric Kendall (GPC), Mr. Robert Jennings (mechanical properties), and Mr. Louis Raboin (SEM). I am extremely grateful to Dr. Dennis G. Peiffer, Dr. Robert D. Lundberg, and Exxon Research and Engineering Company for providing the sulfonated polystyrenes used in this work.

## ABSTRACT

### MORPHOLOGY AND ENHANCED COMPATIBILITY OF IMMISCIBLE POLYMERS VIA SPECIFIC INTERACTIONS

FEBRUARY 1993

ELLIOT P. DOUGLAS

S.B., MASSACHUSETTS INSTITUTE OF TECHNOLOGY

PH.D., UNIVERSITY OF MASSACHUSETTS

Directed by: Professor William J. MacKnight

This work describes the phase behavior and morphology of otherwise immiscible polymer blends that contain small numbers of specific interactions. The experimental results are explained in terms of a new model for phase separation, termed the "ionic crosslink model".

Sulfonated polystyrene in both the acid and zinc-neutralized forms was blended with either ethyl acrylate/4-vinylpyridine copolymers or styrene/4-vinylpyridine copolymers. The blends were investigated using differential scanning calorimetry (DSC), dynamic mechanical thermal analysis (DMTA), and optical microscopy. At substitution levels of 2%, 5%, and 8% the blends are macrophase separated, microphase separated, and phase mixed, respectively. Microscopy shows that the macrophase separated blends exhibit smaller, more uniform sized domains compared to the unfunctionalized blend. The experimental results are qualitatively consistent with the proposed "ionic crosslink model" for phase separation, in which the chains between ionic groups phase-separate due to an unfavorable free energy of mixing, but the presence of ionic interactions restricts the size of the domains.



Aggregation of the ionic groups within the blends was examined using DMTA and small angle x-ray scattering (SAXS). Viscoelastic measurements show the existence of a high temperature loss peak, similar to the peak observed in ionomers. However, the temperature of the transition is depressed relative to the parent ionomers due to internal plasticization. The presence of ionic aggregates was confirmed by calculating the average network functionalities. Activation energies for the high temperature transition are related to the relative strengths of the interactions, which is consistent with the transition being due to motion of the ionic groups. SAXS measurements show that the "ionic peak" present in ionomers is destroyed upon blending. The combined DMTA and SAXS results are consistent with intraparticle scattering models for ionomer morphology and are inconsistent with interparticle scattering models.

Tensile properties show enhanced toughness and strength due to the presence of specific interactions. The improved properties are attributed to two factors: the presence of interactions which enhance the interfacial adhesion between phase separated domains and the presence of ionic aggregates which act as filler particles. Examination of freeze-fractured surfaces shows evidence for improved interfacial adhesion and enhanced formation of crazes.

# TABLE OF CONTENTS

	Page
ACKNOWLEDGMENTS.....	v
ABSTRACT.....	vi
LIST OF TABLES.....	x
LIST OF FIGURES.....	xi
 Chapter	
1. REVIEW OF THE PHASE BEHAVIOR AND MORPHOLOGY OF POLYMER BLENDS AND IONOMERS.....	1
1.1 Polymer Blends.....	1
1.1.1 Thermodynamics of Polymer Mixing.....	1
1.1.2 Phase Behavior and Mixing of Polymer Blends.....	3
1.2 Ionomers.....	9
1.2.1 Viscoelastic Behavior.....	10
1.2.2 Morphology.....	12
1.3 References.....	15
2. PHASE BEHAVIOR OF IONOMER BLENDS.....	19
2.1 Introduction.....	19
2.2 Results and Discussion.....	21
2.2.1 Experimental.....	21
2.2.2 Thermal Analysis.....	26
2.2.3 Morphology.....	54
2.3 Conclusions.....	61
2.4 References.....	63
3. AGGREGATION PHENOMENA IN IONOMERS AND IONOMER BLENDS.....	66
3.1 Introduction.....	66
3.2 Results and Discussion.....	69
3.2.1 Experimental.....	69
3.2.2 Viscoelastic Behavior.....	77
3.2.3 Morphology.....	110
3.3 Conclusions.....	125
3.4 References.....	128

4. MECHANICAL PROPERTIES AND DEFORMATION BEHAVIOR.....	130
4.1 Introduction.....	130
4.2 Results and Discussion.....	132
4.2.1 Experimental.....	132
4.2.2 Mechanical Properties and Deformation Behavior.....	133
4.3 Conclusions.....	150
4.4 References.....	151
5. GENERAL CONCLUSIONS AND FUTURE WORK.....	153
5.1 Conclusions and Future Work.....	153
5.2 References.....	159
BIBLIOGRAPHY.....	160

## LIST OF TABLES

Table		Page
2.1	Characteristics of blend precursors.....	22
2.2	Characteristics of blends.....	24
2.3	DSC and DMTA data for blend precursors.....	27
2.4	DSC data for blends.....	29
2.5	DMTA data for blends.....	41
2.6	Glass transitions of styrene/styrene blends.....	43
3.1	Densities and absorption parameters for x-ray analysis.....	71
3.2	Ionic cluster transition temperatures and activation energies.....	84
3.3	Comparison of experimental shear moduli and moduli calculated from ideal rubber elasticity.....	92
3.4	Calculated network functionalities.....	95
3.5	WLF constants.....	109
3.6	Scattering parameters determined from Guinier and Porod analyses.....	121
4.1	Tensile test data for blend precursors.....	136
4.2	Tensile test data for ionomer blends.....	140

## LIST OF FIGURES

Figure		Page
2.1	Schematic diagram of ionic crosslink model.....	20
2.2	DSC curves for (a) acid blends and (b) zinc blends.....	28
2.3	DSC annealing curves for blend 2H2 at 185° C.....	32
2.4	DSC annealing curves for blend 2Z2 at 185° C.....	32
2.5	DSC annealing curves for blend 5H5 at 185° C.....	33
2.6	DSC annealing curves for blend 5Z5 at 185° C.....	33
2.7	DSC annealing curves for blend 8H10 at 185° C.....	34
2.8	DSC annealing curves for blend 7Z10 at 185° C.....	34
2.9	Multifrequency DMTA plot for blend 00 of (a) storage modulus and (b) $\tan \delta$ in bending.....	36
2.10	Multifrequency DMTA plot for blend 8H10 of (a) storage modulus and (b) $\tan \delta$ in bending.....	37
2.11	Multifrequency DMTA plot for blend 7Z10 of (a) storage modulus and (b) $\tan \delta$ in bending.....	38
2.12	DMTA plots of (a) storage modulus and (b) $\tan \delta$ for acid blends at 1 Hz in bending.....	39
2.13	DMTA plots of (a) storage modulus and (b) $\tan \delta$ for zinc blends at 1 Hz in bending.....	40
2.14	Calculated Kwei parameters for styrene/styrene blends.....	44
2.15	Calculated phase compositions and overall bulk compositions for (a) acid blends and (b) zinc blends.....	46
2.16	Effect of conversion on EAVP copolymer composition.....	50
2.17	Effect of conversion on ethyl acrylate sequence distribution for (a) 2EAVP, (b) 5EAVP, and (c) 10EAVP.....	51
2.18	Optical micrograph for blend 00.....	55
2.19	Optical micrographs for acid blends.....	56
2.20	Optical micrographs for zinc blends.....	58

3.1	Schematic diagram of the depleted zone core-shell model.....	67
3.2	Schematic diagram of x-ray collimation system.....	72
3.3	Effect of (a) convergence factor, (b) smoothing parameter, and (c) number of iterations on the desmeared SAXS curves of 7ZSPS.....	74
3.4	Comparison of smeared and desmeared SAXS curves of 7ZSPS.....	76
3.5	Multifrequency DMTA plots of (a) storage modulus and (b) $\tan \delta$ for 5ZSPS in shear.....	78
3.6	Multifrequency DMTA plots of (a) storage modulus and (b) $\tan \delta$ for 8HSPS in shear.....	79
3.7	$\tan \delta$ at 1 Hz in shear for (a) 2%, (b) 5%, and (c) 8% substitution levels....	81
3.8	Ionic cluster transition temperatures.....	83
3.9	Arrhenius plots of the ionic cluster transition for blends and ionomers at 5% substitution level.....	87
3.10	Ionic cluster transition activation energies.....	87
3.11	Shear storage moduli at 1 Hz for (a) acid styrene/styrene and (b) acid styrene/ethyl acrylate blends.....	89
3.12	Shear storage moduli at 1 Hz for (a) zinc styrene/styrene and (b) zinc styrene/ethyl acrylate blends.....	90
3.13	Isothermal shear data for polystyrene.....	99
3.14	Master curves of (a) storage modulus and (b) $\tan \delta$ for polystyrene.....	100
3.15	WLF plot for polystyrene.....	101
3.16	Master curves of (a) storage modulus and (b) $\tan \delta$ for 2H2S.....	102
3.17	Master curves of (a) storage modulus and (b) $\tan \delta$ for 5H5S.....	103
3.18	Master curves of (a) storage modulus and (b) $\tan \delta$ for 8H8S.....	104
3.19	Master curves of (a) storage modulus and (b) $\tan \delta$ for 2Z2S.....	105
3.20	Master curves of (a) storage modulus and (b) $\tan \delta$ for 5Z5S.....	106
3.21	Master curves of (a) storage modulus and (b) $\tan \delta$ for 7Z8S.....	107
3.22	WLF plots for (a) acid blends and (b) zinc blends.....	108
3.23	SAXS plots for sulfonated polystyrene zinc ionomers.....	114
3.24	SAXS plots for acid form of sulfonated polystyrene.....	114

3.25	SAXS plots for acid styrene/ethyl acrylate blends.....	116
3.26	SAXS plots for acid styrene/styrene blends.....	116
3.27	SAXS plots for zinc styrene/ethyl acrylate blends.....	117
3.28	SAXS plots for zinc styrene/styrene blends.....	117
3.29	Guinier plots for (a) zinc ionomers, (b) zinc styrene/ethyl acrylate blends, and (c) zinc styrene/styrene blends.....	119
3.30	Porod plots for (a) zinc ionomers, (b) zinc styrene/ethyl acrylate blends, and (c) zinc styrene/styrene blends.....	123
4.1	Stress-strain curves for zinc neutralized polystyrene ionomers.....	134
4.2	Stress-strain curves for acid forms of sulfonated polystyrene.....	134
4.3	Stress-strain curves for EAVP's.....	135
4.4	Stress-strain curve or blend 00.....	138
4.5	Stress-strain curves for zinc blends.....	139
4.6	Stress-strain curves for acid blends.....	139
4.7	SEM of freeze-fractured surface of blend 00.....	144
4.8	SEM of freeze-fractured surface of (a) blend 2Z2, (b) blend 5Z5 and (c) blend 7Z10.....	145
4.9	SEM of freeze-fractured surface of (a) blend 2H2, (b) blend 5H5 and (c) blend 8H10.....	147

CHAPTER 1  
REVIEW OF THE PHASE BEHAVIOR AND  
MORPHOLOGY OF POLYMER BLENDS  
AND IONOMERS

1.1 Polymer Blends

Polymer blends provide the opportunity for creating new materials with properties that can not be achieved with individual polymers. In the case of miscible polymer blends, the properties are usually an average of the properties of the two components. In the case of immiscible blends synergistic enhancement of the properties can occur, as in the case of high impact polystyrene, but often the properties are undesirable.

Because of the technological importance of polymer blends, there have been many studies which have examined the nature of mixing in polymer blends. A brief review of some of the results is given here.

1.1.1 Thermodynamics of Polymer Mixing

The first theory to describe the thermodynamics of mixing for polymers is the well-known Flory-Huggins theory. First described for polymer solutions,<sup>1-3</sup> it was extended to polymer mixtures by Scott and Tompa.<sup>4,5</sup> The basic characteristics of this approach are that the entropy of mixing is determined solely by a combinatorial term and the enthalpy of mixing is described by the interaction parameter,  $\chi$ , which is a mean-field parameter. For most high molecular weight polymers the combinatorial entropy term is very small and  $\chi$  is slightly positive, so the lattice theory predicts immiscibility of the UCST type. In order to account for the loss of entropy associated with the orientational requirements for forming specific interactions,  $\chi$  is often described as having a temperature dependence of the form



$A+B/T$ , where the constant  $A$  describes the enthalpic contribution and  $B$  describes the entropic contribution.<sup>6</sup> Using this temperature dependence for  $\chi$  it is possible to predict both UCST and LCST behavior.

A mean-field theory that does not require a lattice is the equation of state theory developed by Flory and his coworkers.<sup>7,8</sup> In this theory the system is described in terms of a characteristic pressure, temperature, and volume. By removing the restrictions of a lattice the equation of state theory can allow for volume changes upon mixing.

An interesting effect occurs in the case of random copolymers. In this case the effective value of  $\chi$  is related to the  $\chi$  parameters for the different pairs of monomers in the blend.<sup>9</sup> Through the appropriate choice of copolymers, the effective value of  $\chi$  can be negative, even if the individual values of  $\chi$  are all positive. For example, in a blend of homopolymer A with a random copolymer of B and C repulsion between monomers A and B can be overcome by a stronger repulsion between B and C, resulting in a miscible blend. These theoretical predictions have been confirmed experimentally.<sup>9</sup>

One of the difficulties in the mean-field theories is accounting for highly directional specific interactions, since by definition the mean-field is the average enthalpic contribution resulting from all entities in the system. There have been several attempts to deal with specific interactions. One of the least satisfying is that of Lu and Weiss.<sup>10</sup> They combine the Couchman equation with thermodynamic arguments to derive an equation relating the glass transition temperature to  $\chi$ . Although it is somewhat successful in predicting  $T_g$  for blends containing specific interactions,  $\chi$  has been reduced to an empirical parameter with no physical meaning. This is because, as stated above,  $\chi$  is a mean-field parameter and can not be applied to the case of specific interactions.

Coleman and Painter have described the behavior of blends containing hydrogen bonds.<sup>11-13</sup> Their approach uses the equilibrium constants for the formation of the various hydrogen bonded species in the blend to determine the free energy change upon mixing. The result is an equation identical to the Flory-Huggins equation, with an

additional term related to the enthalpy of formation of hydrogen bonds. Their theory is successful in predicting the qualitative features of a large number of polymer blends, although in some cases the quantitative agreement is poor.

Brereton and Vilgis have recently proposed a theoretical model of mixing in blends of polymers containing highly specific interactions, such as positively and negatively charged groups.<sup>14</sup> Using a mean field approach and including the effect of charge-charge interactions, they conclude that the size of the domains is determined by the distance between the interacting groups. Such a blend will appear mixed on a scale greater than the distance between interacting groups, and phase separated on a scale less than the distance between interacting groups.

Kohklov and Nyrkova have examined the behavior of charged polymers in solution.<sup>15</sup> When one of a pair of initially immiscible polymers becomes charged, a window of miscibility is obtained due to the translational entropy of the counterions. This window can further be divided into two regions. In one region true molecular compatibility occurs, while in the other a microdomain structure forms. These results are similar to those of Brereton and Vilgis, although the underlying reasons for the microphase separation are different.

Thus it is clear from theoretical considerations that the introduction of specific interactions can have a profound effect on the phase behavior of polymer blends. The following section presents some experimental results.

### 1.1.2 Phase Behavior and Mixing of Polymer Blends

It is well-known that polymer blends are generally not miscible. As explained in the previous section, this is due to the very low entropy of mixing of long polymer chains, and the unfavorable enthalpy of mixing of most polymer pairs due to van der Waals repulsion. Recently, however, a large number of polymer pairs that exhibit miscibility have been

discovered. Krause has surveyed the literature and found close to 300 blends which are miscible over at least part of the composition range.<sup>16</sup> One classic example is the blend of polystyrene and poly(vinyl methyl ether), which exhibits miscibility over the entire composition range.<sup>17</sup> Miscible homopolymer blends generally require some type of interaction between the two components to provide a negative enthalpy of mixing. In the case of polystyrene and PVME it is believed that there is an interaction that occurs between the ether oxygen and the phenyl ring.<sup>18</sup> In many other cases the source of the interaction can be positively identified as being, for example, hydrogen bonding or interactions between charged species. General aspects of polymer blends have been reviewed thoroughly<sup>6,18,19</sup> and will not be discussed further here.

Specific interactions have been used extensively to enhance compatibility in polymers. Of interest to this work are systems containing only a small number of interacting groups on otherwise incompatible polymer chains. These interactions can be covalent cross-links, physical entanglements, hydrogen-bonding, donor/acceptor complexes, acid/base interactions, ion/ion and ion/dipole interactions, and coordination complexes. Examples of each of these types of interactions will be discussed below.

Covalent bonds as compatibilizers have been investigated in the curing of rubbers. In one study<sup>20</sup> various uncured rubber blends showed two glass transitions in their dynamic mechanical loss spectra. Subsequent vulcanization of the blends resulted in the appearance of a third intermediate loss peak. Optical microscopy of the cured blends showed a two-phase structure, and it was assumed that the intermediate loss peak results from material compatibilized at the interface. In another study<sup>21</sup> unvulcanized blends showed two well-separated loss peaks, while the vulcanized blends showed a single, although highly broadened, peak.

Similar results have been obtained on interpenetrating polymer networks (IPN's). In an early study Sperling et al. examined IPN's of poly(methyl methacrylate) and poly(ethyl acrylate).<sup>22</sup> Using shear modulus measurements and dilatometry they showed that a blend

of the two polymers exhibits two transitions while the IPN exhibits a single, highly broadened transition. In a later study Xiao et al. studied IPN's of polyurethanes containing a tertiary amine and poly(methyl methacrylate-methacrylic acid copolymers) containing 10 to 20% of the acid units.<sup>23</sup> IPN's containing no acid groups showed two T<sub>g</sub>'s by DSC, while the IPN's containing the acid groups showed a single T<sub>g</sub>. Scanning electron microscopy showed particle sizes decreasing with increasing amounts of acid groups.

Non-covalent bonds have been investigated extensively for miscibility enhancement. In a series of experiments, Pearce et al. investigated the miscibility of a modified polystyrene with a wide variety of polymers.<sup>24-26</sup> The polystyrene was modified to contain hexafluorodimethyl carbinol groups as hydrogen-bonding groups. Blends of this modified polystyrene containing as few as 4% hydroxyl groups showed enhanced miscibility with poly(ethylene oxide) and various methacrylate polymers by DSC and NMR T<sub>1</sub> measurements.

Complexes of donor and acceptor containing polymers have also been investigated. Ohno and Kumanotani have reported that even polymers in which all of the monomer units contain donor or acceptor species exhibit a two phase structure by DSC, dynamic mechanical measurements, and SEM.<sup>27</sup> In a complementary study, Schneider et al. have shown that blends of poly(methyl methacrylate) and poly(butyl methacrylate) with less than 10% complexing groups show dynamic plateau moduli that extend to lower frequencies and higher temperatures than blends without the complexing groups.<sup>28,29</sup> Simmons and Natahnson have recently examined blends and copolymers in which all of the monomer units contain either an electron donor or an electron acceptor group.<sup>30,31</sup> They find that these systems are miscible by both DSC and NMR T<sub>1ρ</sub> measurements when the amount of the electron donor-containing monomer is greater than about 30%. Heating the system to temperatures greater than 170° C decomplexes the charge transfer interaction, resulting in phase separation.

The most extensive set of experiments performed in this area have been carried out by a group led by Eisenberg. His group has examined miscibility in otherwise immiscible polymers that are modified to contain acid/base, ion/ion, and ion/dipole interactions.<sup>32-52</sup> In general, his experiments show that polymers containing a sulfonic acid group mixed with polymers containing vinyl pyridine show a single dynamic loss peak above a substitution level of 5%, even when the parent polymers are completely immiscible. This result holds for a wide variety of polymer pairs, including polystyrene and poly(ethyl acrylate),<sup>32,33</sup> polystyrene and polyisoprene,<sup>33</sup> and polyphenylene and poly(ethyl acrylate).<sup>37</sup> Investigations using both one dimensional and two dimensional NMR have shown that the mechanism of interaction is a proton transfer from the acid group to the basic pyridine nitrogen.<sup>38,42</sup> The type of interaction can be modified by neutralizing the acid group with a tetraalkyl ammonium cation and quarternizing the pyridine group. This type of ion/ion interaction gives the same miscibility enhancement as the acid/base interactions.<sup>50,51</sup> Eisenberg's group has also investigated ion pair/ion pair interactions with a sodium neutralized sulfonate group and a pyridinium ion and ion/dipole interactions with a sodium neutralized sulfonate group and unquarternized pyridine, as well as the effect of substituting carboxylate groups for the sulfonate groups.<sup>51</sup> As a result of these experiments he presents the following ranking of interacting groups based on the level of miscibility enhancement seen in the polystyrene/poly(ethyl acrylate system):<sup>51</sup>

acid/base = ion/ion (sulfonate) > ion/ion (carboxylate) = ion pair/ion pair > ion/dipole

Similar systems which involve a metal-neutralized sulfonate group have been investigated by Lundberg et al.<sup>53-55</sup> Melt viscosity data of sulfonated EPDM/poly(styrene-co-4-vinyl pyridine) blends show that zinc-neutralized materials have a higher viscosity than sodium- or magnesium-neutralized materials, and the highest viscosity is at a 1:1 ratio of sulfonate to pyridine groups.<sup>53</sup> Further investigation of the zinc-neutralized

materials showed that the presence of an interaction between the zinc sulfonate and pyridine increased the tensile strength and elongation to break, increased the dynamic plateau modulus, and resulted in smaller domain sizes.<sup>54</sup> The results are interpreted as being due to a coordination interaction between zinc and pyridine, resulting in a compatibilized blend. Belfiore et al. have found similar mechanical properties for blends of zinc-neutralized ethylene/methacrylic acid copolymers blended with poly(4-vinylpyridine). Infrared and NMR spectroscopy showed that there is metal-ligand  $\pi$  bonding between zinc and pyridine.<sup>56</sup>

One study on a copper-neutralized carboxy-terminated polybutadiene blended with a copolymer of styrene and 4-vinyl pyridine by Register et al.<sup>57</sup> using DSC showed that there is some enhanced miscibility, although the blends were not fully miscible. Extended x-ray absorption fine structure (EXAFS) spectroscopy showed that there is a local change in the arrangement of the copper atoms upon blending. Their results support the concept of coordination between the metal ion and pyridine.

Infrared spectroscopy was used to examine the nature of the interactions in blends of sulfonated polystyrene and ethyl acrylate/4-vinylpyridine copolymers.<sup>58,59</sup> When the sulfonated polystyrene was in the acid form the interaction occurred by proton transfer from the sulfonic acid to pyridine. In the case of the zinc ionomer, pyridine was shown to displace water and coordinate to the zinc ion. Quantitative analysis of the extent of interaction showed for the blends containing sulfonic acid that all of the acid groups were converted to sulfonate anion. The blends containing the zinc ionomer contained some pyridine that was not coordinated, but it was not possible to quantitatively determine the amount due to the complicated infrared spectra.

Djadoun et al. have studied the ternary phase behavior of styrene/4-vinyl pyridine copolymers, methyl methacrylate/methacrylic acid copolymers, and a solvent.<sup>60-63</sup> They found that the introduction of the interacting groups resulted in a one phase solution at low concentrations and a two phase solution at high concentrations. The two phases were both

solutions of the polymers in the solvent, one having a low concentration of polymer and the other having a high concentration of polymer.

Blends in which the parent polymers are both butadiene have been investigated by Ostocka and Eirich.<sup>64-67</sup> Upon blending, polybutadiene containing methacrylic acid units and polybutadiene containing pyridine units showed an increased glass transition and an increased modulus which persisted to higher temperatures compared with the individual components. Similar studies using the lithium salts of the acid copolymer did not show significant changes over the individual components.

In summary, it appears clear from the literature that even a small amount of interacting groups incorporated into otherwise immiscible polymers is enough to significantly alter the properties of the blends. The presence of as few as 5% interacting groups is enough to give a single glass transition by dynamic mechanical measurements in certain systems. It is interesting to note that the same results are obtained with IPN's and co-crosslinking. In these systems phase separation is prevented by covalent bonds and entanglements, which do not contribute to the free energy of mixing. These observations lead to a model of these blend systems, which has been postulated by a few authors. Pearce et al. in their study of modified polystyrene blended with hydrogen-bond acceptor polymers note that only the few modified segments are truly compatible with the acceptor polymer, and thus even those blends exhibiting a single Tg should be phase separated on very small scales.<sup>24</sup> Subsequent NMR measurements, however, did not detect such phase separation.<sup>25</sup> Similarly, Yoshimura and Fujimoto in their study of vulcanized rubber blends<sup>21</sup> and Sperling et al. in their study of IPN's<sup>22</sup> postulate that a single glass transition is seen because physical restrictions prevent individual motion of the polymer chains. In other words, the scale of phase separation being measured is larger than the distance between physical restrictions, and thus an average Tg is seen. On a more sophisticated level, Brereton and Vilgis have recently proposed a theoretical model of mixing in such systems,<sup>14</sup> which was discussed in Section 1.1.1. The basic results of their calculations

are that such a blend will appear mixed on a scale greater than the distance between interacting groups, and phase separated on a scale less than the distance between interacting groups. Many of the interactions described above, such as the acid/base and coordination interactions, may be considered to be essentially chemical cross-links, and thus fit the above model.

## 1.2 Ionomers

Ionomers are defined as hydrocarbon polymers containing 10% or less ionic groups. One of the biggest classes of ionomers is that based on copolymers of ethylene and methacrylic acid.<sup>68</sup> These materials currently account for the largest commercial use of ionomers, as golf ball covers. The perfluorinated versions have found extensive use as membranes. One complication in interpreting the behavior of these ionomers is the presence of crystallinity. As a simpler system, sulfonated polystyrene ionomers have been studied extensively in recent years.<sup>69</sup> Other ionomers include those based on EPDM, poly(phenylene oxide), poly(ether ether ketone), polypentenamer, and segmented polyurethanes, to name a few.<sup>69</sup>

Because of the difference in polarity between the ionic groups and the hydrocarbon chains, there is an electrostatic driving force for aggregation of the ionic groups. The first theory describing this aggregation is that due to Eisenberg.<sup>70</sup> In his work, a "multiplet" is defined as an aggregate in which the ions are in contact with each other with no intervening hydrocarbon chain. A "cluster" is an aggregate of multiplets which contains some hydrocarbon chains. The size of the clusters is determined by a balance of the forces resulting from electrostatic attraction between multiplets and elasticity of the polymer chains. However, the morphology of the clusters is not described by this theory. More detailed theories will be described in Section 1.2.2.



The properties of ionomers have been extensively reviewed by a number of authors.<sup>68,69,71</sup> What follows is only a brief review of the behavior of polystyrene ionomers of interest to this work.

### 1.2.1 Viscoelastic Behavior

The first studies on polystyrene ionomers were performed by Eisenberg and Navratil.<sup>72-75</sup> They examined the dynamic mechanical behavior of neutralized copolymers of styrene and methacrylic acid, and found that below 6% ionic group content time-temperature superposition held, while above 6% time-temperature superposition failed. These results were interpreted as being due to the formation of clusters above 6% ionic group content, resulting in a new relaxation mechanism. Thus, 6% was identified as the critical ion content for cluster formation. Examination of the loss spectra for the same materials showed that below this critical level two peaks appeared in the plots of  $\tan \delta$  versus temperature, while above the critical level there was only one peak followed by a large increase in  $\tan \delta$ . At the lower ion contents, the peaks were assigned to the Tg of polystyrene and the motion of ions within multiplets, respectively. At the higher ion contents, the peak was also assigned to with the Tg of polystyrene, followed by increasing loss due to relaxations within clusters.

Sulfonated polystyrene ionomers have been examined by Connolly and Weiss et al.<sup>76,77</sup> Connolly found two loss peaks for the ionomers at all ionic contents studied, which is in contrast to the results for styrene/methacrylic acid ionomers. It was also found that frequency-temperature superposition failed for all ionomers, due to the presence of the two relaxations. The storage modulus curves showed extended rubbery plateaus. Analysis of the plateaus on the basis of rubber elasticity resulted in calculated functionalities that were infinite. This result indicates that rubber elasticity is not sufficient to describe the plateau, and the aggregates may be acting as filler particles instead of as simple crosslinks.

Calculation of filler volume fractions on the basis of composite theory gave cluster volume fractions between 0.06 and 0.15. Weiss et al., however, found excellent frequency-temperature superposition over an extended frequency range. Calculation of the relaxation time spectra from the master curves showed that the formation of ionic domains causes an increase in the long relaxation times, which is responsible for the higher viscosities and rubbery plateau's seen in the ionomers.

The effect of different counterions has been examined in several different studies. Eisenberg and Navratil found that the rubbery plateau is lower and extends over a shorter range for cesium ionomers than for sodium ionomers.<sup>75</sup> This was correlated with the charge densities of the counterions. Sodium, which has a higher charge density, resulted in more stable ionic crosslinks. Barium, however, showed unusual behavior in that, although the height of the plateau was lower than for sodium, it extended over a longer range. The greater stability of the ionic crosslinks for barium ionomers can not be rationalized on the basis of charge density.

Connolly found that the high temperature transition was lower for zinc ionomers than for sodium ionomers.<sup>76</sup> This is similar to the result of Weiss et al., who found that sodium increased the relaxation times more than zinc.<sup>77</sup>

The effect of neutralization was studied by Eisenberg and Navratil<sup>75</sup> and Connolly.<sup>76</sup> Both studies showed that the rubbery plateau diminishes as the percentage of unneutralized acid groups increases. Interestingly, Connolly found that the matrix T<sub>g</sub> is higher for the partially neutralized ionomers than for the fully neutralized ionomers, and explained it as being due to the counterions reducing the amount of hydrogen bonding between acid groups.

Connolly also examined the effect of thermal history on ionomers, and found that both the cluster transition temperature and the height of the rubbery plateau increase with either increasing annealing time or temperature. Apparently, higher temperatures and longer

times allow greater phase separation of ionic groups into clusters. This illustrates the difficulty of attaining equilibrium structures in ionomers due to their long relaxation times.

The effect of low molecular weight compounds on the viscoelastic properties of ionomers has also been studied. Lundberg et al. found that glycerol was much more effective in reducing the viscosity of sulfonated polystyrene ionomers than dioctyl phthalate, despite the fact that glycerol had no effect on the matrix glass transition temperature.<sup>78</sup> Weiss et al. found that dioctyl phthalate lowered the matrix Tg with no effect on the ionic cluster transition.<sup>79,80</sup> Glycerol, on the other hand, lowered the ionic cluster transition with no effect on Tg. The results were explained as being due to selective plasticization of either the hydrocarbon matrix or the ionic aggregates, depending on the polarity of the solvent

An interesting effect was seen by Yano et al. in transition metal-neutralized ethylene ionomers.<sup>81</sup> The neat ionomer did not show an ionic cluster transition in dielectric measurements. Addition of the complexing agent 1,3-bis(aminomethyl)cyclohexane (BAC) resulted in the presence of an ionic transition. Apparently BAC coordinates to the metal ion and enhances the formation of clusters.

### 1.2.2 Morphology

The morphology of ionomers has been studied extensively using small angle x-ray scattering (SAXS).<sup>68,69</sup> The general features of the SAXS curves for ionomers are a peak at scattering vectors between 1 and 3 nm<sup>-1</sup>, corresponding to Bragg spacings of between 20 and 60 Å, and an upturn at low angles. The ionic peak is affected by such variables as the sulfonation level, counterion, thermal treatment, and the presence of low molecular weight compounds. However, the exact interpretation of the features is still a matter of question.

Taggart<sup>82</sup> and MacKnight et al.<sup>83</sup> studied the SAXS behavior of ethylene ionomers, and described the general features as explained above. Based on a Guinier analysis of the upturn, a Porod analysis at high angles, and a radial distribution function fit to the data, they proposed a core-shell model for the morphology. In this model the multiplets aggregate into an ionic core containing some hydrocarbon chains, surrounded by a shell depleted in ions. Beyond the shell the matrix contains a few isolated multiplets. Guinier and Porod analyses gave core radii of approximately 10 Å. The ionic peak is considered to arise from the preferred distance between multiplets defined by the shell, resulting in a shell thickness of approximately 30 Å. The key feature of the core-shell model is that it attributes the scattering to intraparticle effects.

On the other hand, an interparticle scattering model has been proposed by Yarusso and Cooper.<sup>84</sup> Fits of theoretical models to the experimental scattering data showed that a better fit is obtained with a hard sphere liquid-like interference model than with the core-shell model. In the hard sphere liquid-like interference model the clusters are arranged with a liquid-like degree of order, and the peak occurs due to discrete scattering effects between clusters, while the upturn is attributed to some undefined inhomogeneity in the distribution of the clusters. This model also fit scattering data obtained during the deformation of ionomers.<sup>85</sup>

It should be noted that a third model of ionomer morphology has been proposed by Eisenberg et al., although it is not based on scattering data.<sup>86</sup> In their restricted mobility model the cluster is considered to consist of regions of hydrocarbon chains that are restricted in mobility due to the crosslinking effect of the multiplets. Although not stated explicitly, this is presumably an interparticle scattering model, with the ionic peak resulting from interference effects between multiplets.

The effect of sulfonation level on the SAXS curves of sulfonated polystyrene ionomers has been studied by Fitzgerald and Weiss.<sup>87</sup> The ionic peak was found to increase in height and move to slightly higher scattering angles with increasing sulfonation

level. There was no difference between the sodium and zinc ionomers in the unannealed samples. Transition metal salts, on the other hand, showed an ionic peak at slightly higher scattering angles.

Thermal treatment can greatly affect the SAXS curves. An extensive study on sodium and zinc sulfonated polystyrene ionomers has been performed by Weiss and Lefelar.<sup>88</sup> With increasing annealing temperature or time the ionic peak for the zinc ionomers was found to decrease in intensity, while for the sodium ionomer the peak was found to increase in intensity. Examination of the scattering curves as a function of temperature found that the peak for the zinc ionomer decreased in intensity and became broader at higher temperatures, while the peak for the sodium ionomer increased in intensity and became narrower at higher temperatures. The results were explained as being due to differences in the packing of the ions in the aggregates, and would appear to be consistent with the viscoelastic measurements.

The effect of added small molecules on the SAXS curves has been investigated in several studies. MacKnight et al. found that in ethylene ionomers saturated with water the ionic peak was destroyed.<sup>83</sup> A similar result was found by Fitzgerald, et al. for the addition of methanol to sulfonated polystyrene ionomers.<sup>89</sup> On the other hand, Yarusso and Cooper found that the addition of small amounts of water sharpened the ionic peak.<sup>90</sup> The difference is probably due to the amounts of solvents added. When only small amounts are added, the polar solvent acts to solvate the ions, resulting in a greater charge separation and a greater electrostatic driving force for aggregation. At saturation, however, the solvent increases the local dielectric constant, screening the charges and reducing the electrostatic attraction between ionic groups.

Although it seems clear that the nature of aggregation in ionomers is affected by the type of counterion or presence of small molecules, there have been no studies describing aggregation in ionomer blends. One goal of this work will be to examine the distribution of interacting groups within blends containing ionic interactions.

### 1.3 References

1. Flory, P. J. *J. Chem. Phys.*, **9**, 660 (1941)
2. Flory, P. J. *J. Chem. Phys.*, **10**, 51 (1942)
3. Huggins, M. L. *J. Chem. Phys.*, **9**, 440 (1941)
4. Scott, R. L. *J. Chem. Phys.*, **17**, 279 (1949)
5. Tompa, H. *Trans. Faraday Soc.*, **45**, 1142 (1949)
6. MacKnight, W. J.; Karasz, F. E. in *Comprehensive Polymer Science*, Vol. 7, S. L. Aggarwal, eds., Pergamon Press, New York, 1989, pp. 135
7. Flory, P. J.; Orwell, R. A.; Vrij, A. *J. Am. Chem. Soc.*, **86**, 3507 (1964)
8. Flory, P. J. *J. Am. Chem. Soc.*, **87**, 1833 (1965)
9. ten-Brinke, G.; Karasz, F. E.; MacKnight, W. J. *Macromolecules*, **16**, 1827 (1983)
10. Lu, X.; Weiss, R. A. *Poly. Mat. Sci. Eng.*, **64**, 75 (1991)
11. Painter, P. C.; Park, Y.; Coleman, M. M. *Macromolecules*, **21**, 66 (1988)
12. Painter, P. C.; Park, Y.; Coleman, M. M. *Macromolecules*, **22**, 580 (1989)
13. Coleman, M. M.; Lichkus, A. M.; Painter, P. C. *Macromolecules*, **22**, 586 (1989)
14. Brereton, M. G.; Vilgis, T. A. *Macromolecules*, **23**, 2044 (1990)
15. Kokhlov, A. R.; Nyrkova, I. A. *Macromolecules*, **25**, 1493 (1992)
16. Krause, S. *Pure and Appl. Chem.*, **58**, 1553 (1986)
17. Kwei, T. K.; Nishi, T.; Roberts, R. F. *Macromolecules*, **7**, 667 (1974)
18. Walsh, D. J.; Rostani, S. *Adv. Poly. Sci.*, **70**, 119 (1985)
19. Paul, D. R.; Newman, S., eds. *Polymer Blends*, Academic Press, New York, 1978
20. Bauer, R. F.; Dudley, E. A. *Rub. Chem. Tech.*, **50**, 35 (1977)
21. Yoshimura, N.; Fujimoto, K. *Rub. Chem. Tech.*, **42**, 1009 (1969)
22. Sperling, L. H.; Taylor, D. W.; Kirkpatrick, M. L.; George, H. F.; Bardman, D. R. *J. Appl. Poly. Sci.*, **14**, 73 (1970)
23. Xiao, H. X.; Frisch, K. C.; Frisch, H. L. *J. Poly. Sci. : Chem.*, **22**, 1035 (1984)

24. Pearce, E. M.; Kwei, T. K.; Min, B. Y. *J. Macromol. Sci.-Chem.*, **A21**, 1181 (1984)
25. Jong, L.; Pearce, E. M.; Kwei, T. K.; Dickinson, L. C. *Macromolecules*, **23**, 5071 (1990)
26. Ting, S. P.; Bulkin, B. J.; Pearce, E. M.; Kwei, T. K. *J. Poly. Sci. : Poly. Chem. Ed.*, **19**, 1451 (1981)
27. Ohno, N.; Kumanotani, J. *Polymer Journal*, **11**, 947 (1979)
28. Schneider, H. A.; Cantow, H.-J.; Percec, V. *Poly. Bull.*, **6**, 617 (1982)
29. Schneider, H. A.; Cantow, H.-J.; Maben, U.; Northfleet-Neto, H. *Poly. Bull.*, **7**, 263 (1982)
30. Simmons, A.; Natansohn, A. *Macromolecules*, **24**, 3651 (1991)
31. Simmons, A.; Natansohn, A. *Macromolecules*, **25**, 1272 (1992)
32. Smith, P.; Eisenberg, A. *J. Poly. Sci. : Letters*, **21**, 223 (1983)
33. Eisenberg, A.; Smith, P.; Zhou, Z.-L. *Poly. Eng. Sci.*, **22**, 1117 (1982)
34. Murali, R.; Eisenberg, A. *J. Poly. Sci. : Part B : Phys.*, **26**, 1385 (1988)
35. Zhou, Z.-L.; Eisenberg, A. *J. Poly. Sci. : Phys.*, **21**, 595 (1983)
36. Simmons, A.; Eisenberg, A. *Poly. Prep.*, **27**, 341 (1986)
37. Murali, R.; Eisenberg, A. *Poly. Prep.*, **27**, 343 (1986)
38. Natansohn, A.; Eisenberg, A. *Poly. Prep.*, **27**, 349 (1986)
39. Hara, M.; Eisenberg, A. *Macromolecules*, **20**, 2160 (1987)
40. Hara, M.; Eisenberg, A. *Macromolecules*, **17**, 1335 (1984)
41. Eisenberg, A.; Hara, M. *Poly. Eng. Sci.*, **24**, 1306 (1984)
42. Natansohn, A.; Eisenberg, A. *Macromolecules*, **20**, 323 (1987)
43. Rutkowska, M.; Eisenberg, A. *Macromolecules*, **17**, 821 (1984)
44. Rutkowska, M.; Eisenberg, A. *J. Appl. Poly. Sci.*, **30**, 3317 (1985)
45. Rutkowska, M.; Eisenberg, A. *J. Appl. Poly. Sci.*, **33**, 2833 (1987)
46. Rutkowska, M.; Eisenberg, A. *J. Appl. Poly. Sci.*, **29**, 755 (1984)
47. Natansohn, A.; Rutkowska, M.; Eisenberg, A. *Polymer*, **28**, 885 (1987)
48. Natansohn, A.; Rutkowska, M.; Eisenberg, A. *Poly. Eng. Sci.*, **27**, 1504 (1987)

49. Natansohn, A.; Murali, R.; Eisenberg, A. *Makromol. Chem., Macromol. Symp.*, **16**, 175 (1988)
50. Zhang, X.; Eisenberg, A. *Poly. Adv. Tech.*, **1**, 9 (1990)
51. Zhang, X.; Eisenberg, A. *J. Poly. Sci. : Part B : Phys.*, **28**, 1841 (1990)
52. Smith, P.; Hara, M.; Eisenberg, A. in *Current Topics in Polymer Science, Vol. II*, R. M. Ottenbrite, L. A. Utracki and S. Inoue, eds., Carl Hanser Verlag, New York, 1987, pp. 256
53. Peiffer, D. G.; Duvdevani, I.; Agarwal, P. K.; Lundberg, R. D. *J. Poly. Sci.: Letters*, **24**, 581 (1986)
54. Agarwal, P. K.; Duvdevani, I.; Peiffer, D. G.; Lundberg, R. D. *J. Poly. Sci. : Part B: Phys.*, **25**, 839 (1987)
55. Lundberg, R. D.; Phillips, R. R.; Peiffer, D. G. *J. Poly. Sci. : Part B : Phys.*, **27**, 245 (1989)
56. Belfiore, L. A.; Pires, A. T. N.; Wang, Y.; Graham, H.; Ueda, E. *Macromolecules*, **25**, 1411 (1992)
57. Register, R. A.; Sen, A.; Weiss, R. A.; Li, C.; Cooper, S. *J. Poly. Sci. : Part B : Phys.*, **27**, 1911 (1989)
58. Sakurai, K.; Douglas, E. P.; MacKnight, W. J. *Macromolecules*, in press
59. Sakurai, K.; Douglas, E. P.; MacKnight, W. J. *Macromolecules*, submitted
60. Aouadj, O.; Lassoued, A.; Djadoun, S. *Phys. Opt. Dyn. Phen. in Macr. Sys.*, p. 525 (1985)
61. Djadoun, S. *Poly. Bull.*, **9**, 313 (1983)
62. Djadoun, S. *Poly. Bull.*, **7**, 607 (1982)
63. Djadoun, S.; Goldberg, R. N.; Morawetz, H. *Macromolecules*, **10**, 1015 (1977)
64. Otocka, E. P.; Eirich, F. R. *J. Poly. Sci. : Part A-2*, **6**, 895 (1968)
65. Otocka, E. P.; Eirich, F. R. *J. Poly. Sci. : Part A-2*, **6**, 913 (1968)
66. Otocka, E. P.; Eirich, F. R. *J. Poly. Sci. : Part A-2*, **6**, 921 (1968)
67. Otocka, E. P.; Eirich, F. R. *J. Poly. Sci. : Part A-2*, **6**, 933 (1968)
68. MacKnight, W. J.; Earnest, T. R. *J. Poly. Sci. : Macromol. Rev.*, **16**, 41 (1981)
69. Fitzgerald, J. J.; Weiss, R. A. *J. Macromol. Sci.-Rev. Macromol. Chem. Phys.*, **C28**, 99 (1988)
70. Eisenberg, A. *Macromolecules*, **3**, 147 (1970)



71. Eisenberg, A.; King, M. *Ion-Containing Polymers*, Academic Press, New York, 1977
72. Eisenberg, A.; Navratil, M. *J. Poly. Sci. : Part B*, **10**, 537 (1972)
73. Eisenberg, A.; Navratil, M. *Macromolecules*, **6**, 604 (1973)
74. Eisenberg, A.; Navratil, M. *Macromolecules*, **7**, 90 (1974)
75. Navratil, M.; Eisenberg, A. *Macromolecules*, **7**, 84 (1974)
76. Connolly, J. M., Ph.D. Thesis, University of Massachusetts, 1989
77. Weiss, R. A.; Fitzgerald, J. J.; Kim, D. *Macromolecules*, **24**, 1071 (1991)
78. Lundberg, R. D.; Makowski, H. S.; Westerman, L. *Poly. Prep.*, **19**, 310 (1978)
79. Fitzgerald, J. J.; Kim, D.; Weiss, R. A. *J. Poly. Sci. : Part C : Letters*, **24**, 263 (1986)
80. Weiss, R. A.; Fitzgerald, J. J.; Kim, D. *Macromolecules*, **24**, 1064 (1991)
81. Yano, S.; Nagao, N.; Hattori, M.; Hirasawa, E.; Tadano, K. *Macromolecules*, **25**, 368 (1992)
82. Taggart, W. P., Ph.D. Thesis, University of Massachusetts, 1973
83. MacKnight, W. J.; Taggart, W. P.; Stein, R. S. *J. Poly. Sci. : Symp.*, **45**, 113 (1974)
84. Yarusso, D. J.; Cooper, S. L. *Macromolecules*, **16**, 1871 (1983)
85. Visser, S. A.; Cooper, S. L. *Macromolecules*, **25**, 2230 (1992)
86. Eisenberg, A.; Hird, B.; Moore, R. B. *Macromolecules*, **23**, 4098 (1990)
87. Fitzgerald, J. J.; Weiss, R. A. *Proc. Annu. Tech. Conf. Soc. Plast. Eng.*, 341 (1985)
88. Weiss, R. A.; Lefelar, J. A. *Polymer*, **27**, 3 (1986)
89. Fitzgerald, J. J.; Kim, D.; Weiss, R. A. *J. Poly. Sci. : Letters*, **24**, 263 (1986)
90. Yarusso, D. J.; Cooper, S. L. *Polymer*, **26**, 371 (1985)

## PHASE BEHAVIOR OF IONOMER BLENDS

2.1 Introduction

There have been many studies recently on the effect of specific interactions on polymer blends. A review of the relevant literature was given in Chapter 1. It has been found that as few as 5% interacting groups is enough to give a single glass transition as measured by dynamic mechanical measurements,<sup>1-21</sup> which suggests the presence of a single mixed phase. However, a single transition is also seen for co-crosslinked blends and interpenetrating networks. The similarity among the ionic blends, co-crosslinked blends, and IPN's suggests that the ionic interactions are best considered to be crosslinks. In this case the two components are still immiscible, but the scale of phase separation is constrained by the presence of the (ionic) crosslinks. This "ionic crosslink model" for phase separation is shown schematically in Figure 2.1. It is clear from this figure that the scale of phase separation is determined by the distance between interacting groups. As more interacting groups are placed on the chain the domain size becomes smaller, until the domain size is smaller than the resolution limit of the experiment being conducted. At this point the blend is considered to be mixed as measured by that technique, even though it is still phase separated on smaller scales. The presence of a single transition in dynamic mechanical measurements does not necessarily indicate thermodynamic miscibility. It should be noted that this model is similar to the result of a calculation by Brereton and Vilgis,<sup>22</sup> in which they use a mean field approach but include the effect of charge-charge correlations.

In order to investigate the ionic crosslink model, this chapter discusses the phase behavior of blends of sulfonated polystyrene and poly(ethyl acrylate-co-(4-vinylpyridine)).

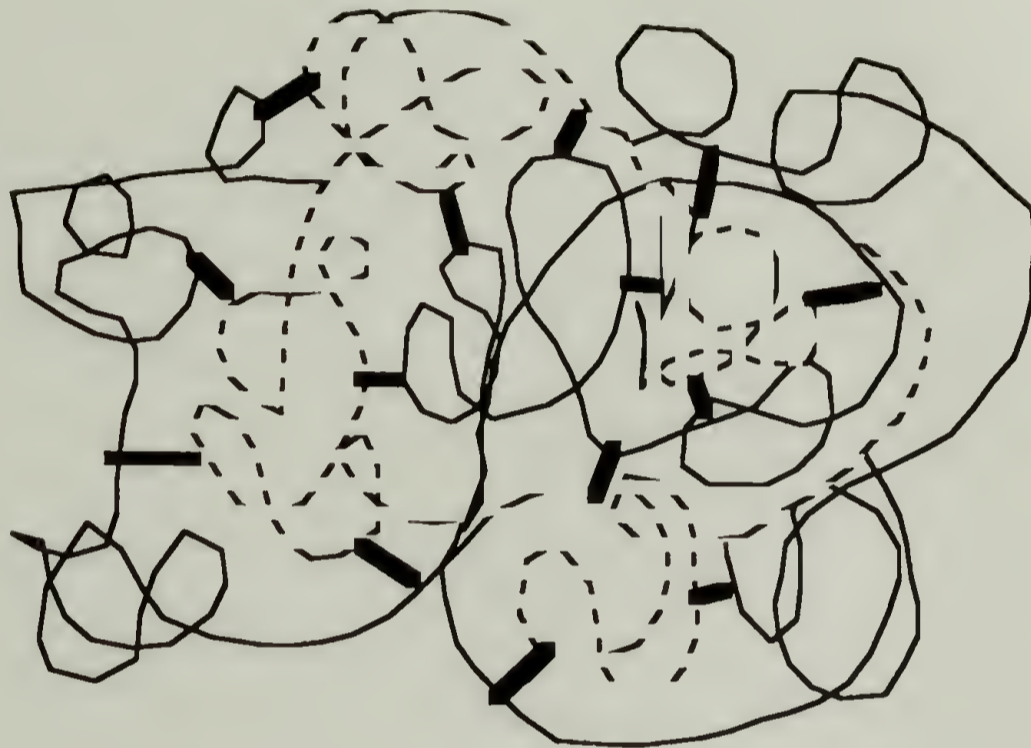


Figure 2.1: Schematic diagram of ionic crosslink model. Thin solid lines represent one type of polymer chain, thin dotted lines represent a different type of polymer chain, and thick solid lines represent ionic interactions between the two chains.

Previous work has focused exclusively on dynamic mechanical analysis. This work extends the measurements to other techniques. The sulfonated polystyrene is used in both the acid and zinc-neutralized forms. Infrared spectroscopy studies on these blends have shown that the interactions occurring are a proton transfer from the sulfonic acid to pyridine (acid/base) and coordination of pyridine to the zinc metal.<sup>23,24</sup> It is interesting to compare the different types of interactions because the ionic crosslink model predicts no difference, as long as the number of interactions are equal. A direct comparison between the two has not been made before now.

## 2.2 Results and Discussion

### 2.2.1 Experimental

**Polymer Synthesis.** The sulfonated polystyrenes in both the acid (HSPS) and zinc neutralized (ZSPS) forms were kindly provided by Exxon Research and Engineering Company. Sulfonation levels and molecular weights are given in Table 2.1. The sulfonation levels were provided by Exxon Research and Engineering Company as determined from elemental analysis. The molecular weights are those of the unfunctionalized polystyrene, since the polymer is sulfonated in a post-polymerization reaction.

The copolymers of ethyl acrylate and 4-vinyl pyridine (EAVP) were prepared by free radical polymerization in solution. The reactivity ratios for this polymerization are  $r_{EA} = 0.29$  and  $r_{VP} = 2.58$ .<sup>25</sup> A typical polymerization consisted of reacting 300 g of monomer and 7 g of AIBN in 700 ml of methanol at 60° C for times varying from 20 to 90 minutes, depending on the pyridine content. Total monomer conversions for the polymerizations were approximately 20 to 30%.

Table 2.1: Characteristics of Blend Precursors

polymer	ionic content (mole%)	Mn (g/mole)	Mw (g/mole)
0SPS	0	100,000	250,000
2HSPS	1.71	100,000	250,000
5HSPS	5.7	100,000	250,000
8HSPS	7.6	100,000	250,000
2ZSPS	2.1	100,000	250,000
5ZSPS	5.5	100,000	250,000
7ZSPS	7.25	100,000	250,000
0EAVP	0	230,000	890,000
2EAVP	2.4	230,000	730,000
5EAVP	5.2	201,000	406,000
10EAVP	10.6	161,000	315,000
2SVP	2.2	27,800	280,000
5SVP	4.2	4,500	16,500
8SVP	7.4	13,500	57,800

Styrene/4-vinylpyridine copolymers (SVP) were prepared by free radical polymerization in the bulk. Reactivity ratios for this polymerization have been reported as  $r_S = 0.54$  and  $r_{VP} = 0.70$ .<sup>26</sup> A typical polymerization consisted of reacting 150 g of monomer and 0.375 g of AIBN at 60° C for four hours. Total monomer conversions for the reaction were approximately 10 to 20%.

All of the copolymers containing vinylpyridine were purified by precipitating into water and drying for 3 days at 60° C under vacuum. Pyridine contents determined by elemental analysis and molecular weights determined by GPC based on polystyrene standards are given in Table 2.1.

**Blending.** All blends were prepared to have equal numbers of sulfonate and pyridine groups. The acid blends were prepared according to the procedure of Smith and Eisenberg.<sup>1</sup> The HSPS and EAVP (or SVP) were dissolved separately in THF at a concentration of 1% (w/v). The EAVP solution was added to the HSPS solution dropwise over a period of about 45 minutes while stirring, and stirring was continued an additional 30 minutes after addition ended. In all cases a gel was formed, and this gel was removed from the solvent. The zinc blends were prepared in the same fashion, except that DMF was used as the solvent due to the limited solubility of zinc ionomers in THF, and the blends were isolated by precipitating into distilled water. The low concentration of the initial solutions and the slow addition of one solution into the other is expected to maximize the number of interactions that occur upon blending. All blends were dried at 60° C for 3 days under vacuum. The nomenclature of the blends is as follows: the first number indicates the sulfonation level of the SPS in mol%, the letter indicates the counterion, and the second number indicates the pyridine content of the ethyl acrylate/4-vinyl pyridine copolymer in mole%. An "S" at the end of the name indicates that the blend contains SVP. Characteristics of the blends are given in Table 2.2.

Table 2.2: Characteristics of blends.

blend designation	counterion in sulfonated polystyrene	sulfonation level in sulfonated polystyrene (mole%)	vinylpyridine content in copolymer (mole%)	weight fraction of vinylpyridine copolymer in blend
00	----	0	0	0.50
2H2	H <sup>+</sup>	1.71	2.4	0.40
5H5	H <sup>+</sup>	5.7	5.2	0.50
8H10	H <sup>+</sup>	7.6	10.6	0.40
2Z2	Zn <sup>2+</sup>	2.1	2.4	0.45
5Z5	Zn <sup>2+</sup>	5.5	5.2	0.51
7Z10	Zn <sup>2+</sup>	7.25	10.6	0.37
2H2S	H <sup>+</sup>	1.71	2.2	0.43
5H5S	H <sup>+</sup>	5.7	4.2	0.56
8H8S	H <sup>+</sup>	7.6	7.4	0.49
2Z2S	Zn <sup>2+</sup>	2.1	2.2	0.48
5Z5S	Zn <sup>2+</sup>	5.5	4.2	0.55
7Z8S	Zn <sup>2+</sup>	7.25	7.4	0.47

**Differential Scanning Calorimetry (DSC).** DSC analysis was done on a DuPont Instruments DSC 10. Calibration was done with indium and mercury standards. The sample size for all DSC runs was approximately 10 mg. The precursor polymers were first heated to 150° C for 1 minute to obtain good contact between the sample and the pan, then quenched with liquid nitrogen and scanned from 30° to 150° C at 20° C/minute for the SPS's and from -120° to 25° C at 20° C/minute for the EAVP's. The blends were placed in the DSC pan as-blended, heated to 150° C for 2 minutes to obtain good contact between the sample and the pan, quenched with liquid nitrogen, and scanned from -120° C to 150° C at 20° C/minute. Annealing studies were performed by maintaining the sample in the DSC at 185° C for a certain time, performing a heating scan, and then returning the sample to 185° C for further annealing. Determination of glass transition temperatures, changes in heat capacity, and transition widths were determined manually. The glass transition is given as the temperature at which half the change in heat capacity occurs; the transition width is the total temperature range over which the heat capacity change occurs. For all materials at least two different samples were run to check reproducibility.

**Dynamic Mechanical Thermal Analysis (DMTA).** Dynamic mechanical thermal analysis (DMTA) was done on a Polymer Laboratories DMTA in the single cantilever bending mode. Samples were prepared by compression molding at 175° C under vacuum for 6 minutes. All samples were run at 2° C/minute at five frequencies (0.33, 1, 3, 10, and 30 Hz) using a constant 64  $\mu\text{m}$  peak-to-peak displacement and an active sample size of 2 mm x 10 mm x 0.5 mm. The EAVP's were run from -100° to 20° C, the SPS's and SVP's from 30° to 140° C, the SPS/SVP blends from 50° to 150° C, and the SPS/EAVP blends from -100° to 130° C. All of the blends and some of the precursors were run twice each to check reproducibility. Transition temperatures are given as the peak in  $\tan \delta$  at 1 Hz.

**Optical Microscopy.** Samples for optical microscopy were prepared by compression molding the blends at 175° C for 6 minutes into films a few microns thick.



Since the blends are completely amorphous, Hoffman modulation contrast was used to form the images. Hoffman modulation contrast depends on the refractive index difference between the two components.<sup>27</sup> The interface between the two regions of different refractive index can be considered a prism. A slit is placed in the front focal plane of the condenser lens, and a special modulator with bright, dark, and grey regions is placed at the back focal plane of the objective lens. As the slit image passes through the prism, it is shifted by an amount that depends on the angle the incident light rays make with the interface (Snell's Law). The modulator is situated such that an undeflected image passes through the grey region, while deflected images pass through either the dark or bright region, depending on the direction of the deflection. In the case of a spherical particle, the angle at which incident light rays meet the interface varies continuously across the interface. Thus the image formed is a circle which changes gradually from bright on one side to dark on the other, with a grey background. Such images appear to be three dimensional to the human eye, but it must be remembered that the depth of the image occurs due to the shape of the particle forming the image, and not surface features.

### 2.2.2 Thermal Analysis

Thermal analysis data from both DSC and DMTA for all the precursor polymers are summarized in Table 2.3. The glass transition temperatures increase with increasing substitution level for each type of polymer, which has been noted for ionomers previously. It is generally believed that this increase is caused by both a cross-linking effect due to interactions between ionic groups and the well-known copolymer effect.<sup>28</sup> It should also be noted that the widths of the transitions are very narrow.

Figure 2.2 shows the initial DSC scans for all of the blends, and the data are summarized in Table 2.4. The unfunctionalized and 2% functionalized blends clearly show two glass transitions, indicating that these blends are phase-separated. However, it is

Table 2.3: DSC and DMTA data for blend precursors.

polymer	DSC T <sub>g</sub> (°C)	ΔC <sub>p</sub> (J/g°C)	DMTA T <sub>g</sub> (°C) <sup>a</sup>
0SPS	97.5 ± 3.0	0.30 ± 0.05	105.0 ± 1.0
2HSPS	103.3	0.31	110.3
5HSPS	110.2	0.34	117.0
8HSPS	111.1	0.33	119.5
2ZSPS	108.2	0.28	118.5
5ZSPS	115.5	0.30	121.0
7ZSPS	120.5	0.32	128.5
0EAVP	-15.9	0.44	-8.5
2EAVP	-13.9	0.49	-4.0
5EAVP	-10.0	0.42	-2.0
10EAVP	-7.3	0.48	2.0
2SVP	-----	-----	122.0
5SVP	-----	-----	124.0
8SVP	-----	-----	126.0

<sup>a</sup> Taken as the peak in tan δ at 1 Hz.

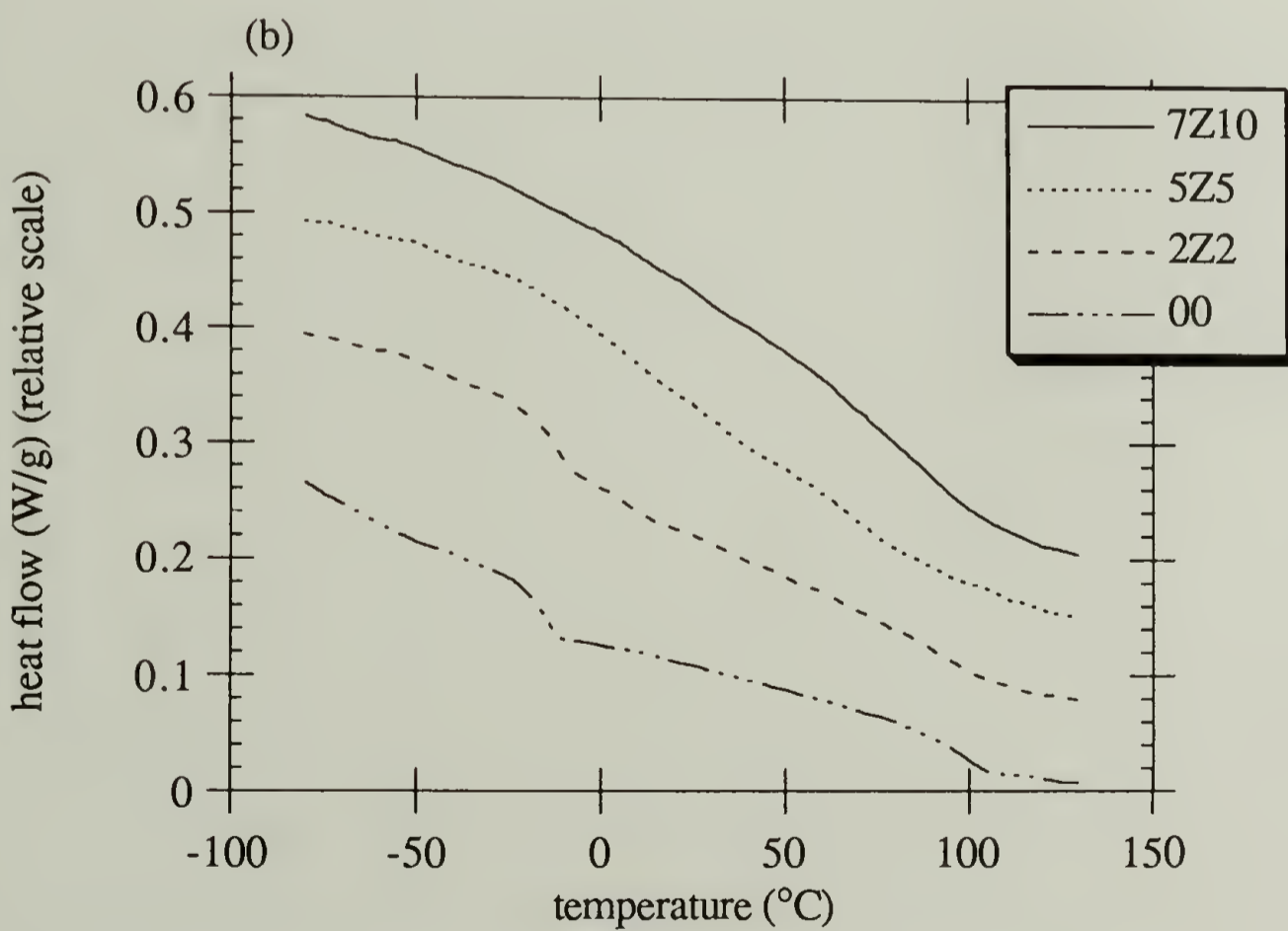
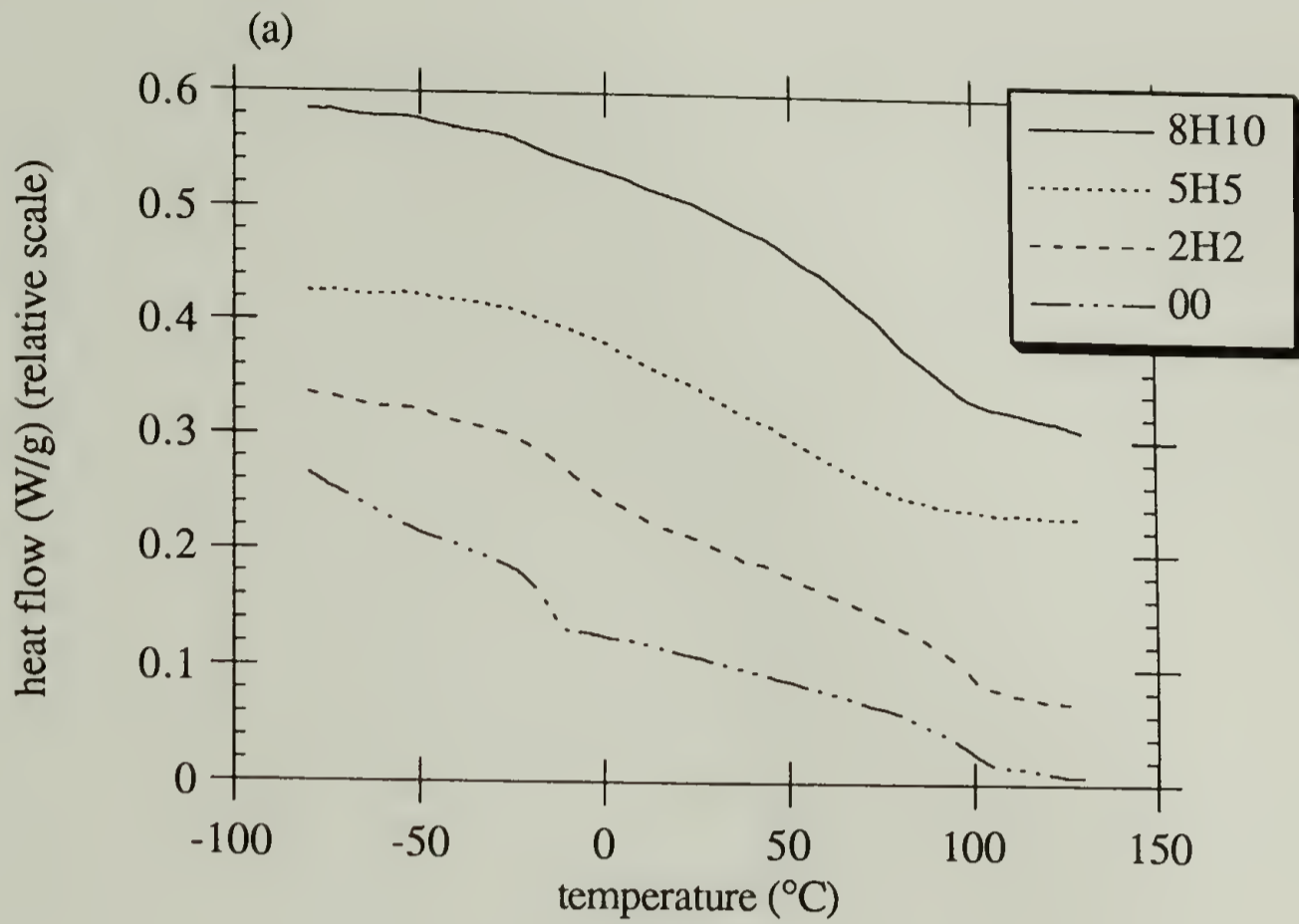


Figure 2.2: DSC curves for (a) acid blends and (b) zinc blends.

Table 2.4: DSC data for blends.

blend	T <sub>g</sub> (°C)	ΔC <sub>p</sub> (J/g°C)	ΔT <sub>g</sub> (°C)
00	-16.4±5.0	0.17±0.1	8.0±5.0
	94.5	0.17	17.6
2H2	-11.5	0.15	15.9
	96.5	0.17	21.5
5H5	37.9	0.52	97.0
8H10	72.9	0.51	47.7
2Z2	-13.2	0.17	10.7
	91.3	0.10	10.6
5Z5	0.4	0.23	29.6
	66.9	0.13	20.7
7Z10	82.0	0.37	41.1

possible that the interactions, which must occur at the interface between the two phases, result in an increase in interfacial mixing. In order to determine the presence of any enhanced compatibility for these blends, the weight fraction of interface material was calculated using the equation of Beckman et al.<sup>29</sup> This equation is derived from the Couchman equation:<sup>30</sup>

$$\ln T_g = \frac{w_1 \Delta C_p^{\circ} 1 \ln T_g^{\circ} 1 + w_2 \Delta C_p^{\circ} 2 \ln T_g^{\circ} 2}{w_1 \Delta C_p^{\circ} 1 + w_2 \Delta C_p^{\circ} 2} \quad (2.1)$$

where  $T_g$  is the glass transition of the mixed phase, and  $T_g^{\circ} i$ ,  $\Delta C_p^{\circ} i$ , and  $w_i$  are the glass transitions, heat capacity changes at  $T_g$ , and weight fractions of the individual components respectively. By assuming that the heat capacity change for the mixed phase is a linear weight average of the heat capacity change of the components, the weight fraction of each phase is determined from:

$$W_{\phi i} = \frac{\Delta C_p [\Delta C_p^{\circ} 1 \ln (T_g^{\circ} 1/T_g) - \Delta C_p^{\circ} 2 \ln (T_g^{\circ} 2/T_g)]}{\Delta C_p^{\circ} 1 \Delta C_p^{\circ} 2 \ln (T_g^{\circ} 1/T_g^{\circ} 2)} \quad (2.2)$$

After using equation 2.2 to calculate the weight fraction of each phase present, any material left over is assumed to lie in the interface. This is because the interface is a region of gradually changing composition, and each discrete composition within the interface has a glass transition temperature that lies intermediate between the glass transitions of the two phases. However, the amount of material at each of these discrete compositions is too small to be detected as a separate phase by the DSC, even if the total amount of interfacial material (which is the sum of the amounts at each composition) is large.

The calculations for blends 00, 2H2, and 2Z2 indicate that the weight fraction of material in the interface is 0.05, 0.15, and 0.31 respectively, which indicates that even for phase-separated blends the presence of a small number of interacting groups provides some enhanced mixing. These values are not absolute and are subject to somewhat large errors, mainly due to the error in measuring  $\Delta C_p$  and the assumption that the component  $\Delta C_p$ 's add linearly. Nevertheless, they do provide a relative comparison between the different blends. The difference between 2H2 and 2Z2 may also be artificial, resulting from the difference in  $T_g$  between 2HSPS and 2ZSPS, particularly since the mechanical properties seem to indicate that 2H2 has better interfacial adhesion than 2Z2. (See Chapter 4.)

For blends of higher substitution level the choice of transitions as given in Table 2.4 is somewhat arbitrary. Nevertheless, it is clear that a rather dramatic change has occurred with these materials. If the blends were completely miscible then there should be a single sharp transition midway between the transitions for the two components. The presence of the very broad transitions in the DSC traces implies that the blends are still phase separated, but on a scale smaller than can be detected by DSC.

An important question in the study of blends is whether or not thermodynamic equilibrium has been reached. It has been found that the choice of solvent used to prepare a blend can affect its phase behavior. For example, the miscible blend of polystyrene and poly(vinyl methyl ether) can be one phase or two phase, depending on the solvent that is used to cast the blend.<sup>31</sup> In order to test whether or not such a situation could be occurring for these blends, annealing studies were done on the DSC samples. As can be seen in Figures 2.3-2.8, annealing at 185° C for up to two hours had no effect on the DSC curves. While this may not be proof that the blends are in a state of true thermodynamic equilibrium, it at least indicates that the mixing behavior of the blends does not change substantially with thermal treatment.

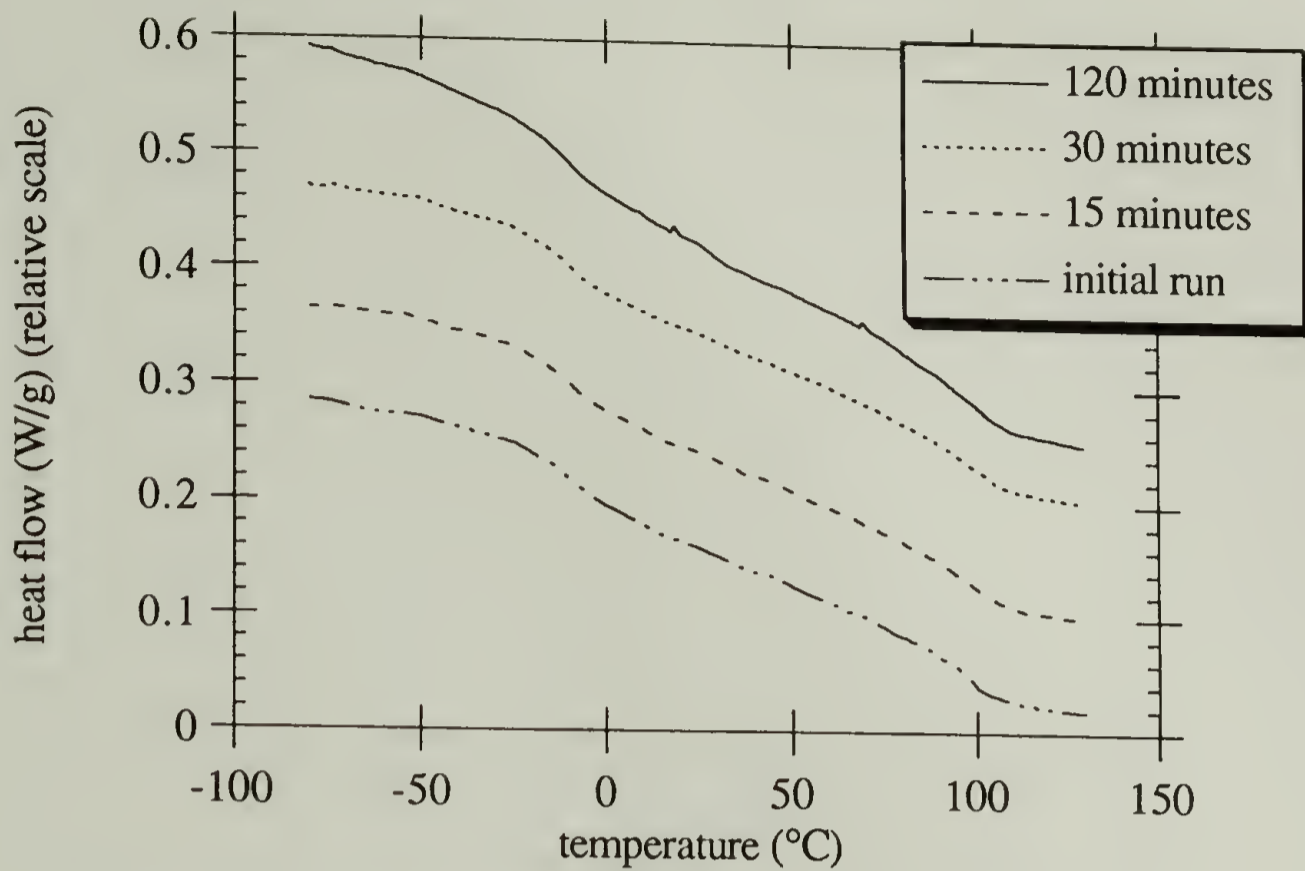


Figure 2.3: DSC annealing curves for blend 2H2 at 185° C. Times indicate the total cumulative annealing time for the sample.

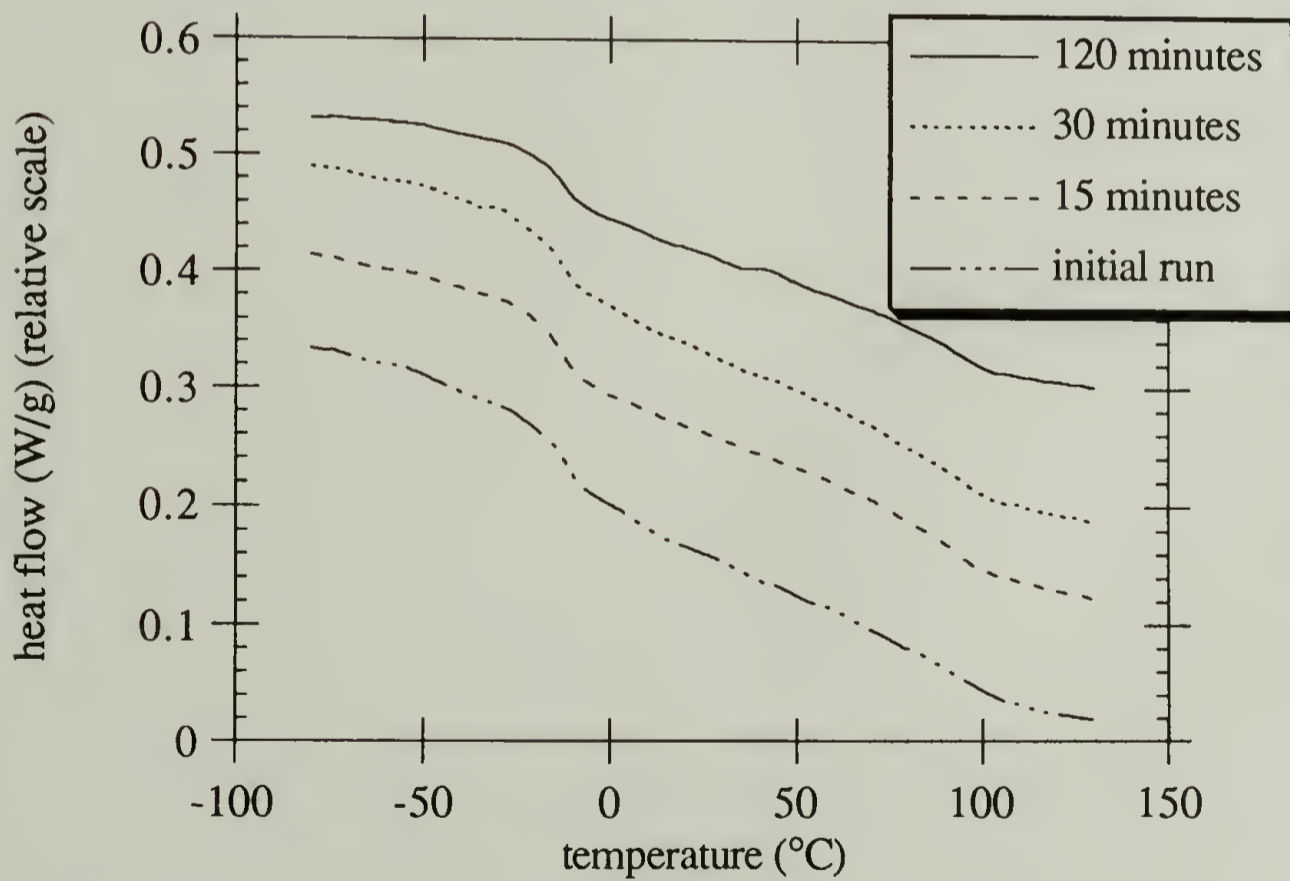


Figure 2.4: DSC annealing curves for blend 2Z2 at 185° C. Times indicate the total cumulative annealing time for the sample.

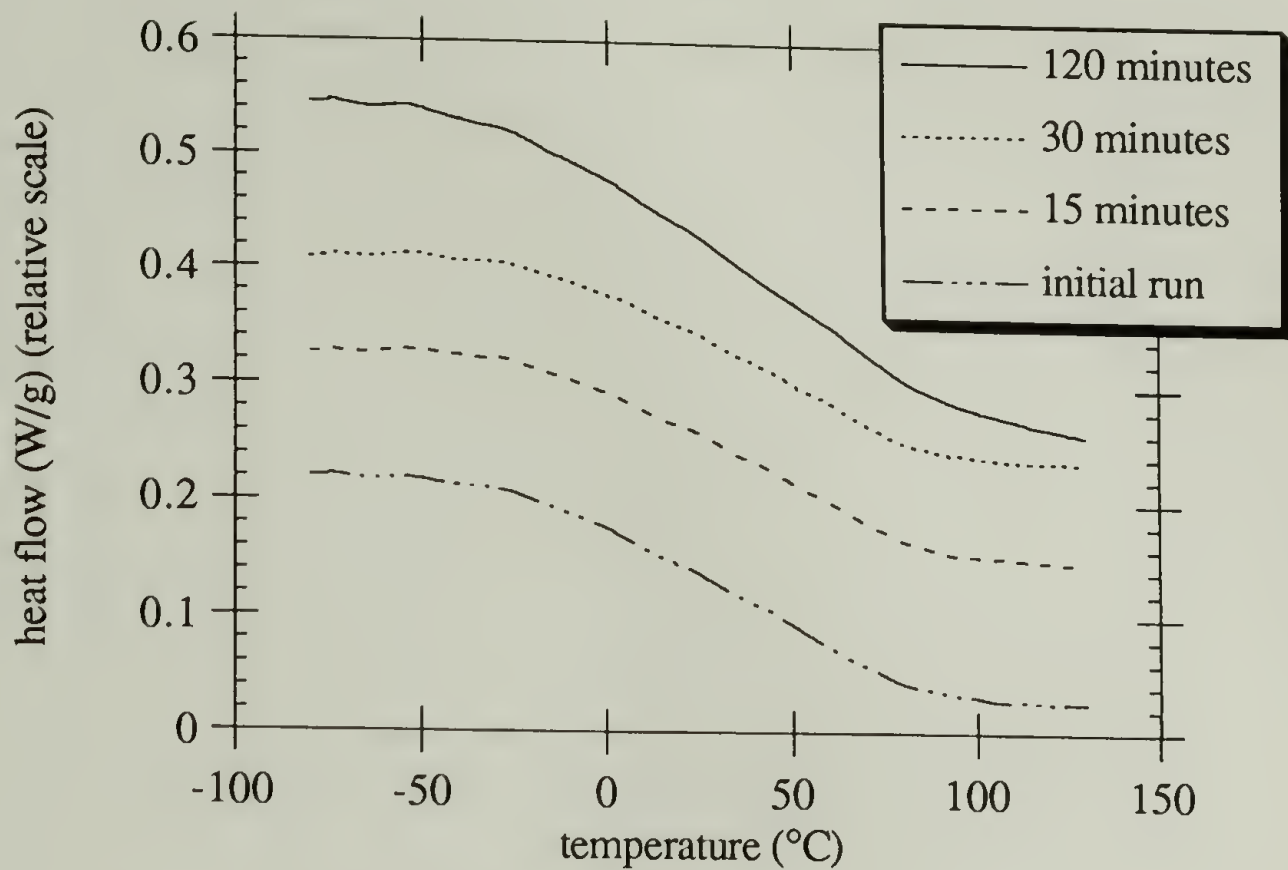


Figure 2.5: DSC annealing curves for blend 5H5 at 185° C. Times indicate the total cumulative annealing time for the sample.

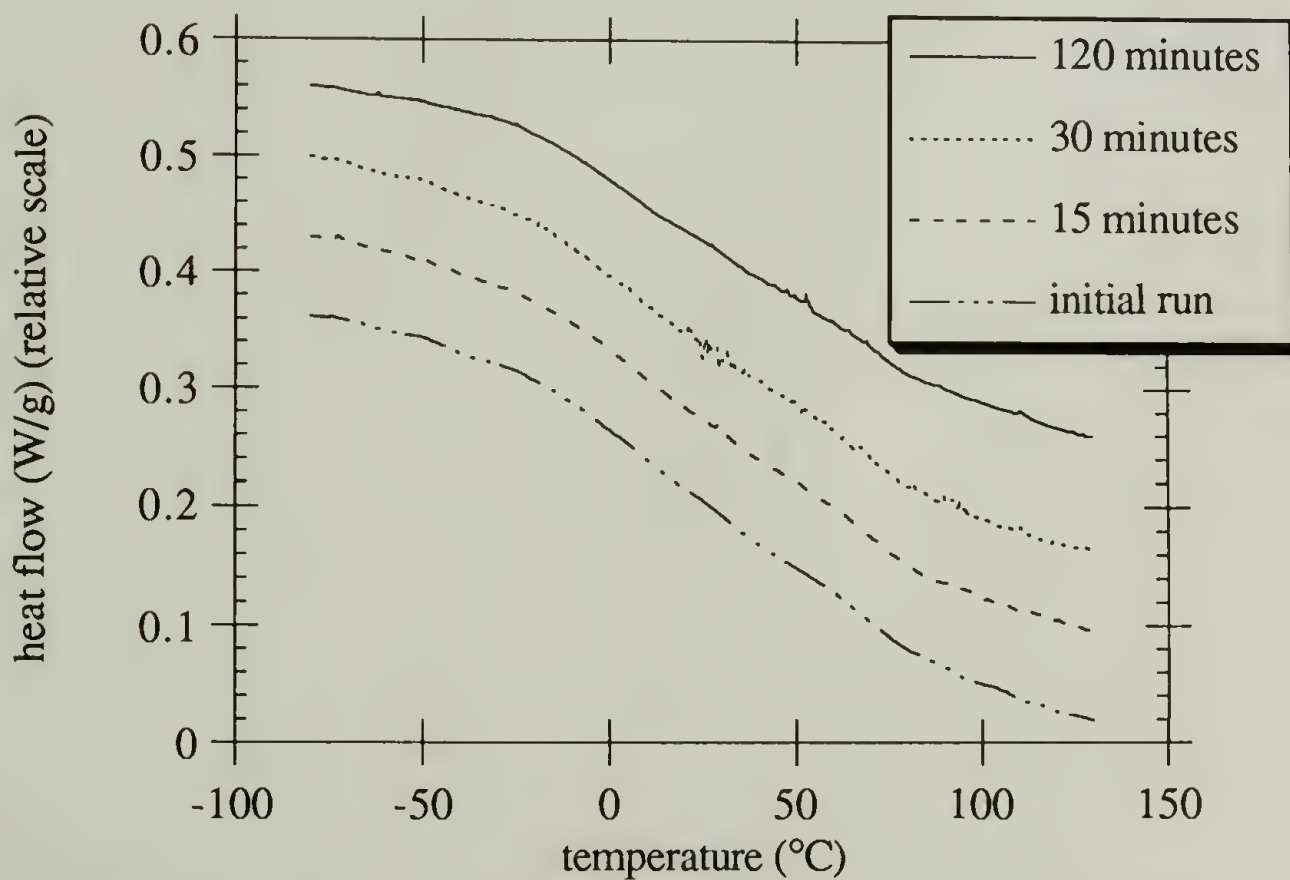


Figure 2.6: DSC annealing curves for blend 5Z5 at 185° C. Times indicate the total cumulative annealing time for the sample.



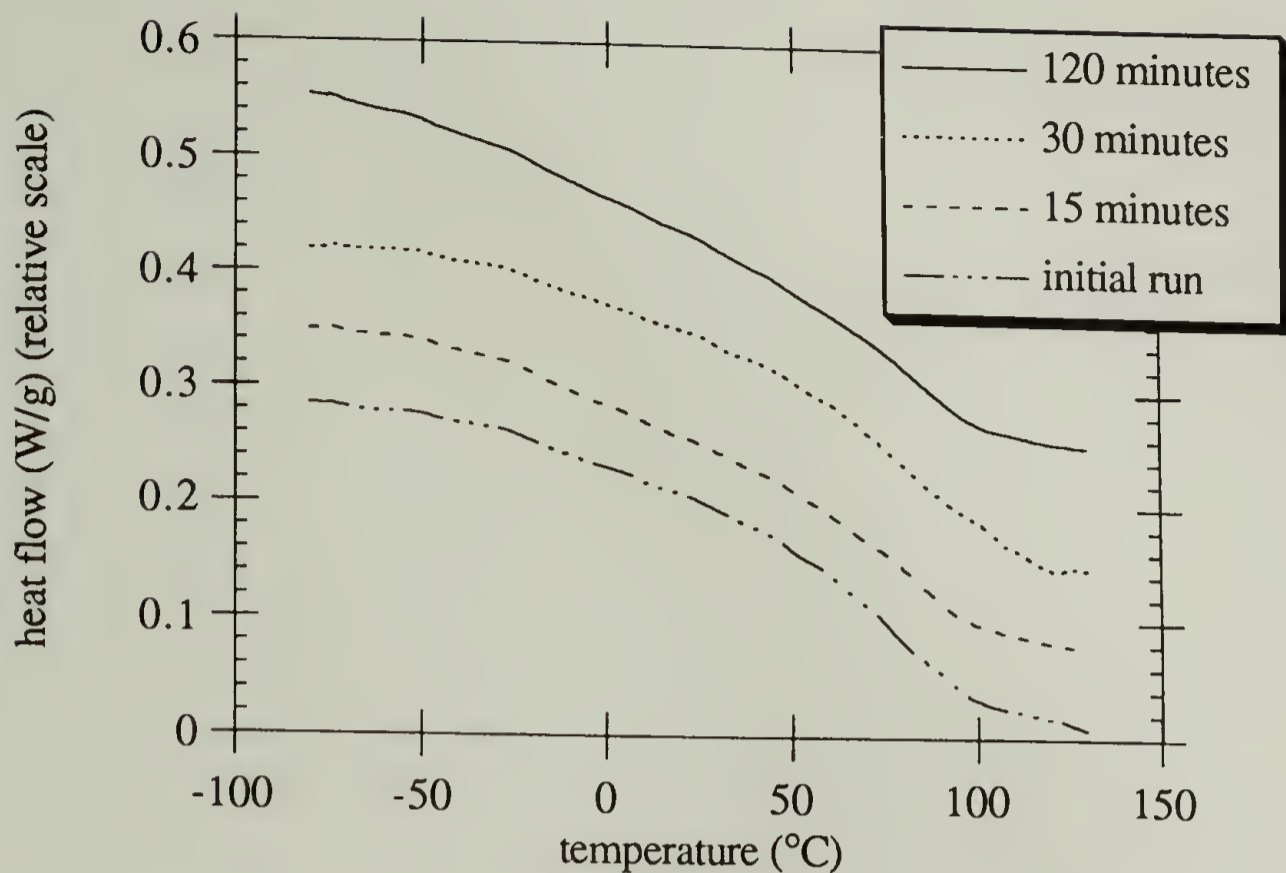


Figure 2.7: DSC annealing curves for blend 8H10 at 185° C. Times indicate the total cumulative annealing time for the sample.

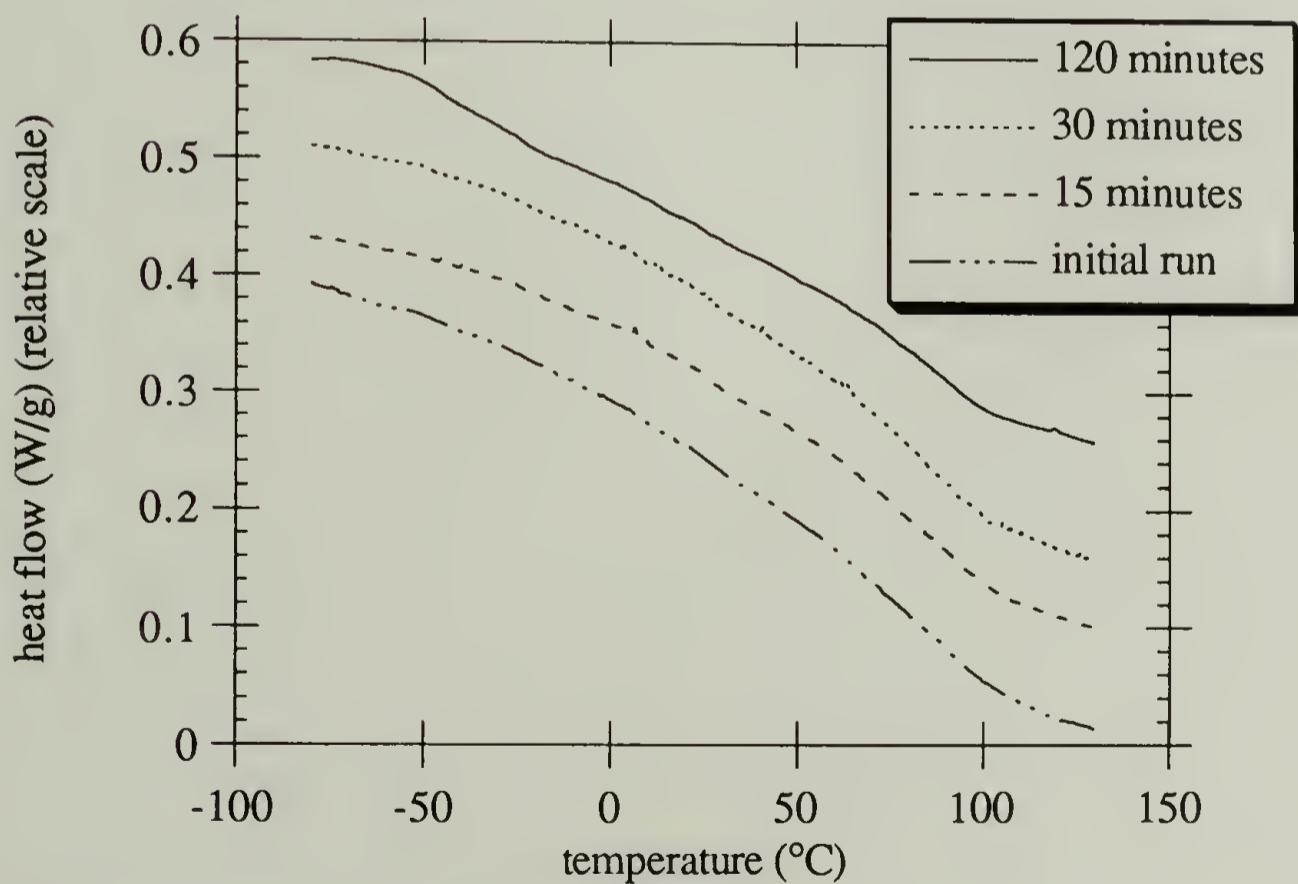


Figure 2.8: DSC annealing curves for blend 7Z10 at 185° C. Times indicate the total cumulative annealing time for the sample.

As a more sensitive probe of phase behavior, the blends were analyzed using dynamic mechanical measurements. Figures 2.9-2.11 show typical multi-frequency runs for blends 00, 8H10, and 7Z10. Figures 2.12 and 2.13 show the results for all the blends at 1 Hz. Results for all the blends are summarized in Table 2.5.

The storage modulus curves show that blends with 2% interacting groups are phase separated, as evidenced by the two step decrease in the modulus. For blends with 5% or greater interacting groups, the modulus curves show only a single, although broad, decrease. However, careful examination of the loss curves clearly indicates that even these blends exhibit some phase separation. These blends appear to consist of a single major phase and a small amount of a second phase. Further, the breadths of the transitions indicates that there is a substantial range of compositions even within a single phase. The presence of a single main peak for blends 8H10 and 7Z10 seems to show that the predominant phase in these blends is a miscible phase. However, even these blends exhibit a very shallow and broad loss peak. This peak is more apparent in the multifrequency plots in Figures 2.10 and 2.11.

In order to estimate the phase compositions based on the DMTA data it is necessary to take into account the effect of the specific interactions on  $T_g$ . Specific interactions are expected to reduce the mobility of the polymer chains, either by bringing the chains closer together and reducing the available free volume or by acting as a rigid crosslink point. Either effect results in a blend  $T_g$  higher than what would be expected from a simple mixing rule such as the Fox equation. The Kwei equation has been used extensively to fit  $T_g$  versus composition curves for a wide variety of polymer blends.<sup>32</sup> The Kwei equation in its full form is:

$$T_g = \frac{w_1 T_{g1} + k w_2 T_{g2}}{w_1 + k w_2} + q w_1 w_2 \quad (2.3)$$

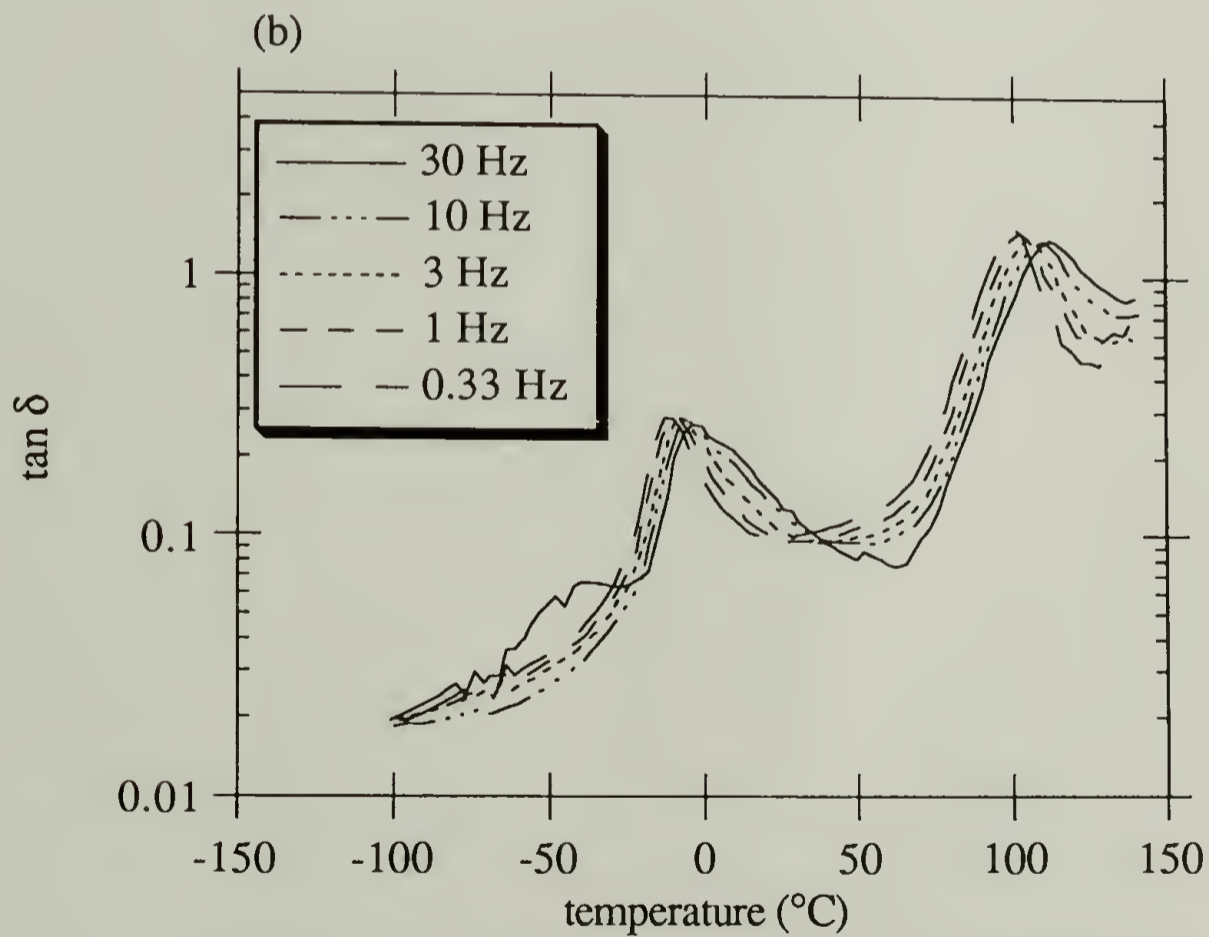
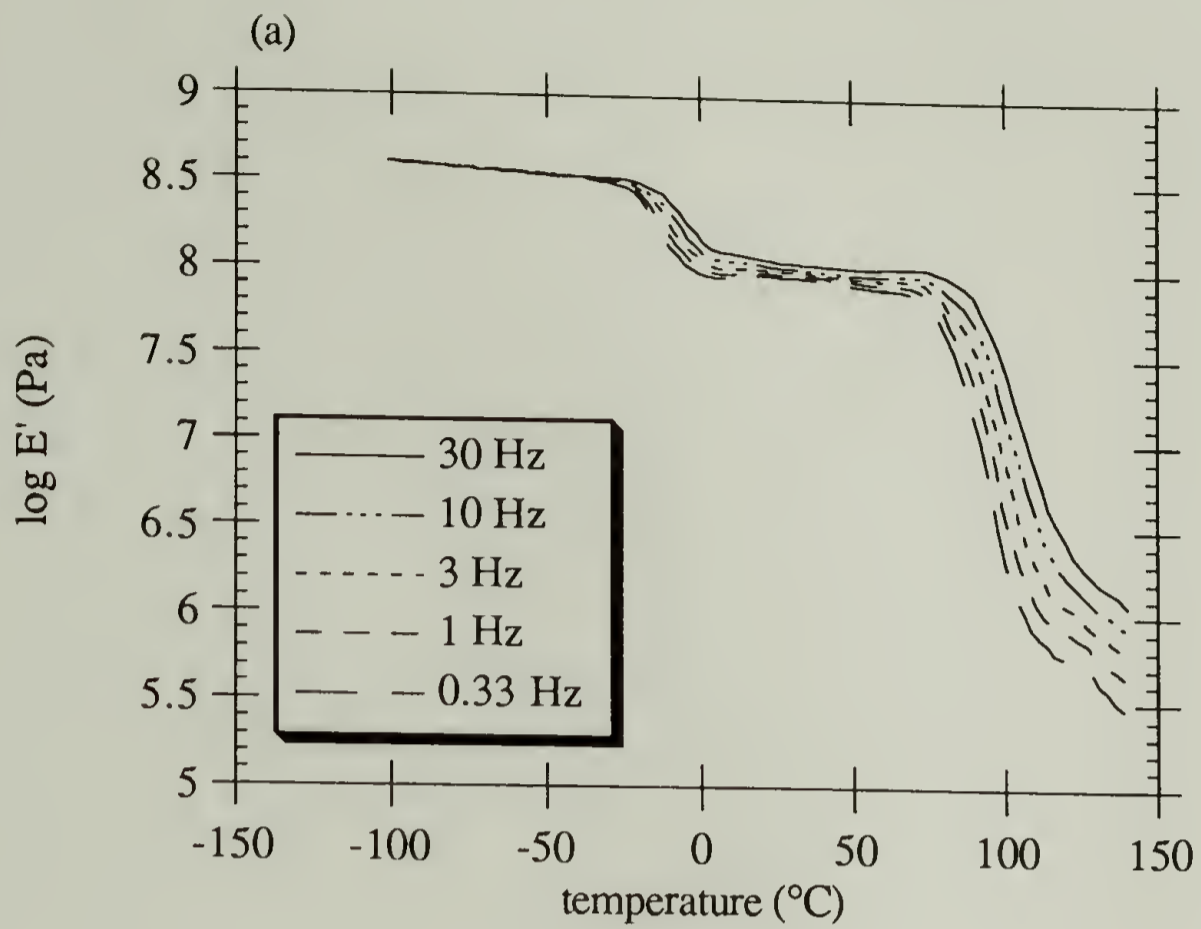


Figure 2.9: Multifrequency DMTA plot for blend 00  
of (a) storage modulus and (b) tan  $\delta$  in bending.

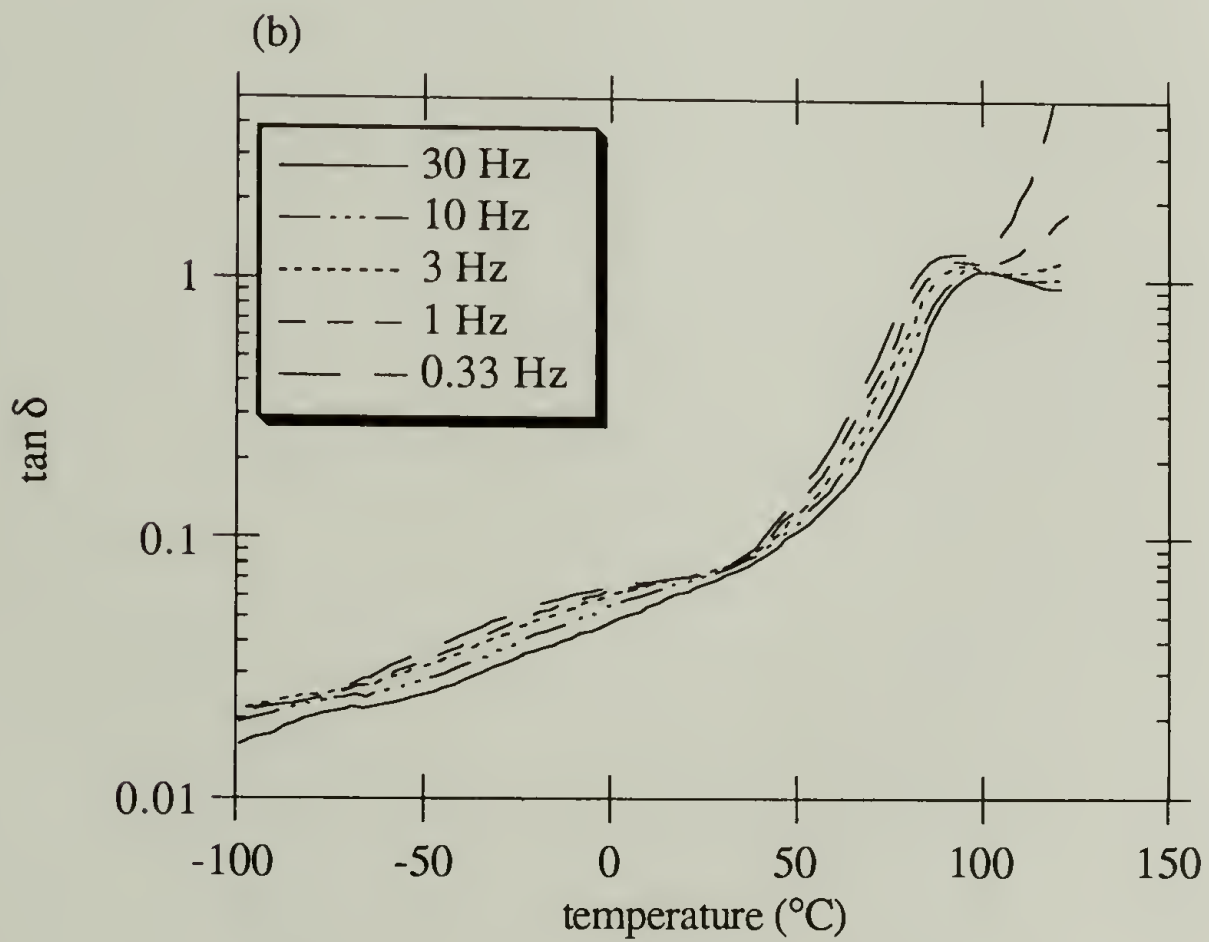
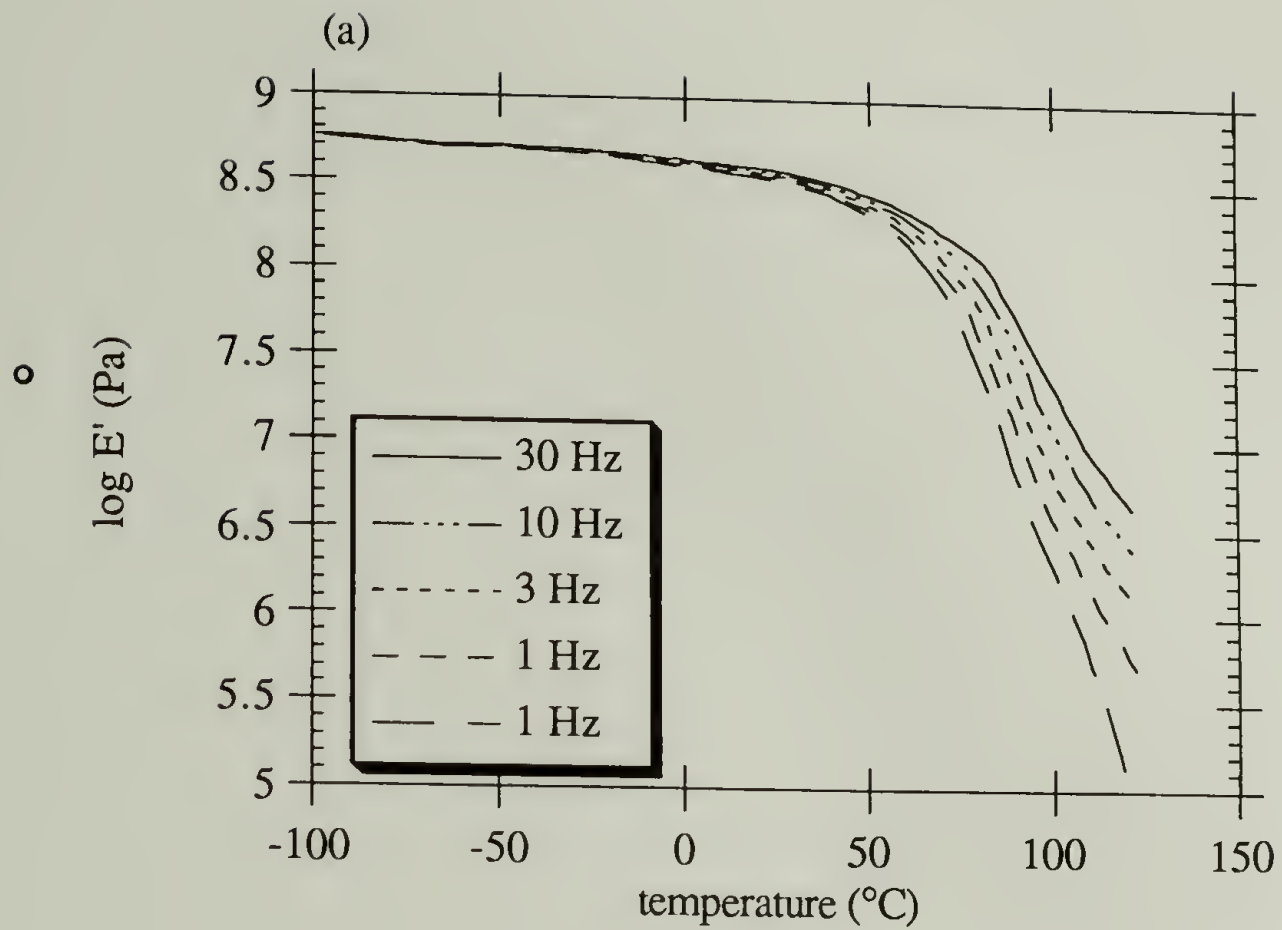


Figure 2.10: Multifrequency DMTA plot for blend 8H10 of (a) storage modulus and (b)  $\tan \delta$  in bending.

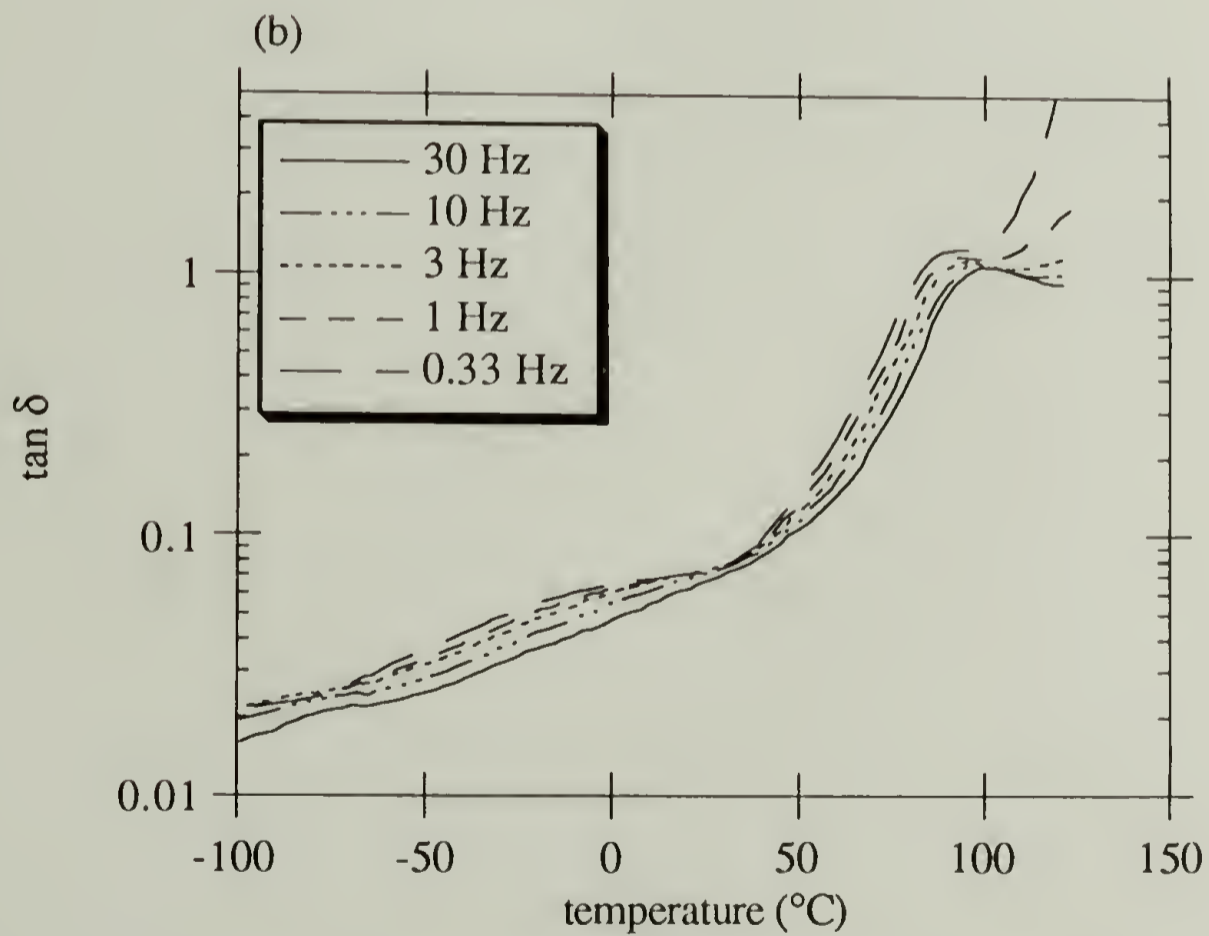
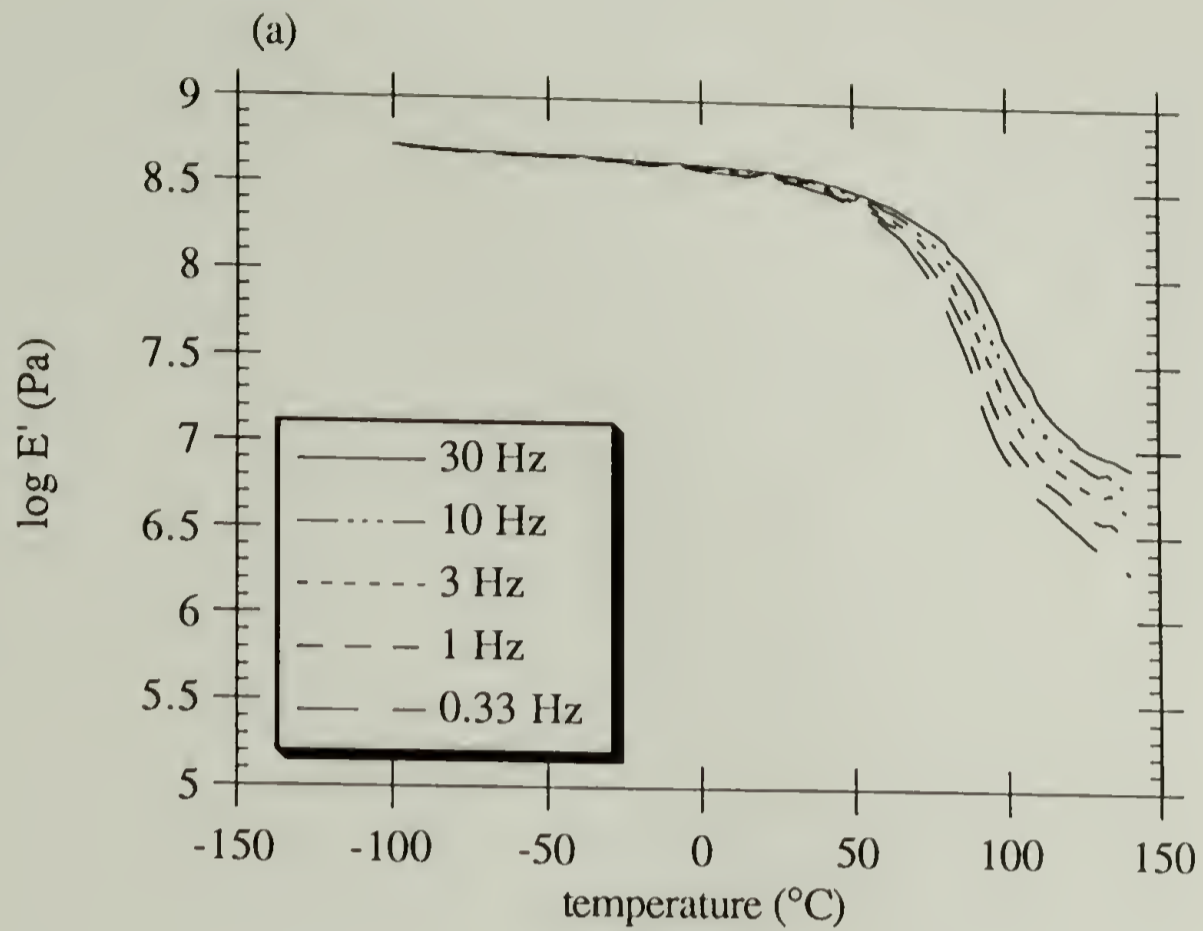


Figure 2.11: Multifrequency DMTA plot for blend 7Z10 of (a) storage modulus and (b)  $\tan \delta$  in bending.

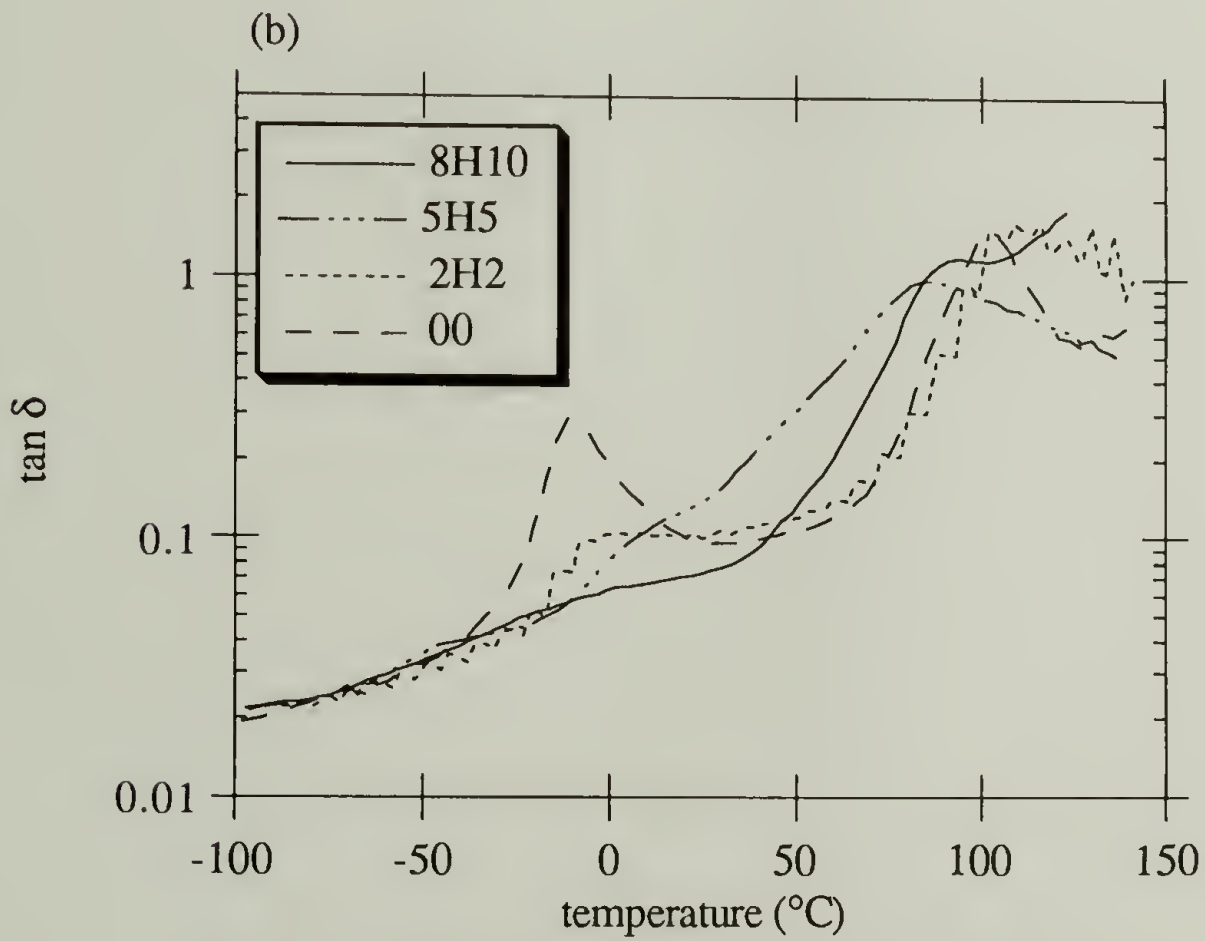
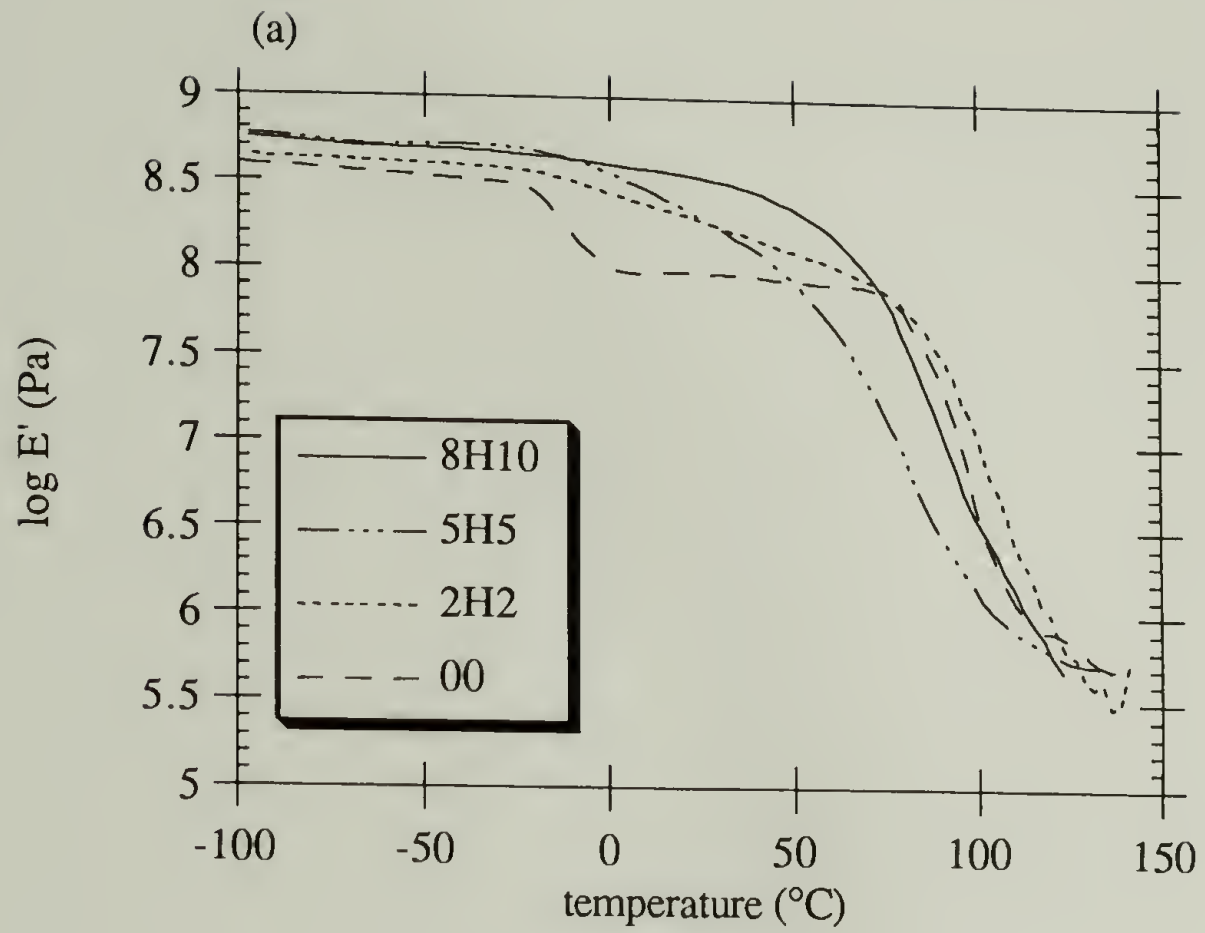


Figure 2.12: DMTA plots of (a) storage modulus and (b)  $\tan \delta$  for acid blends at 1 Hz in bending.

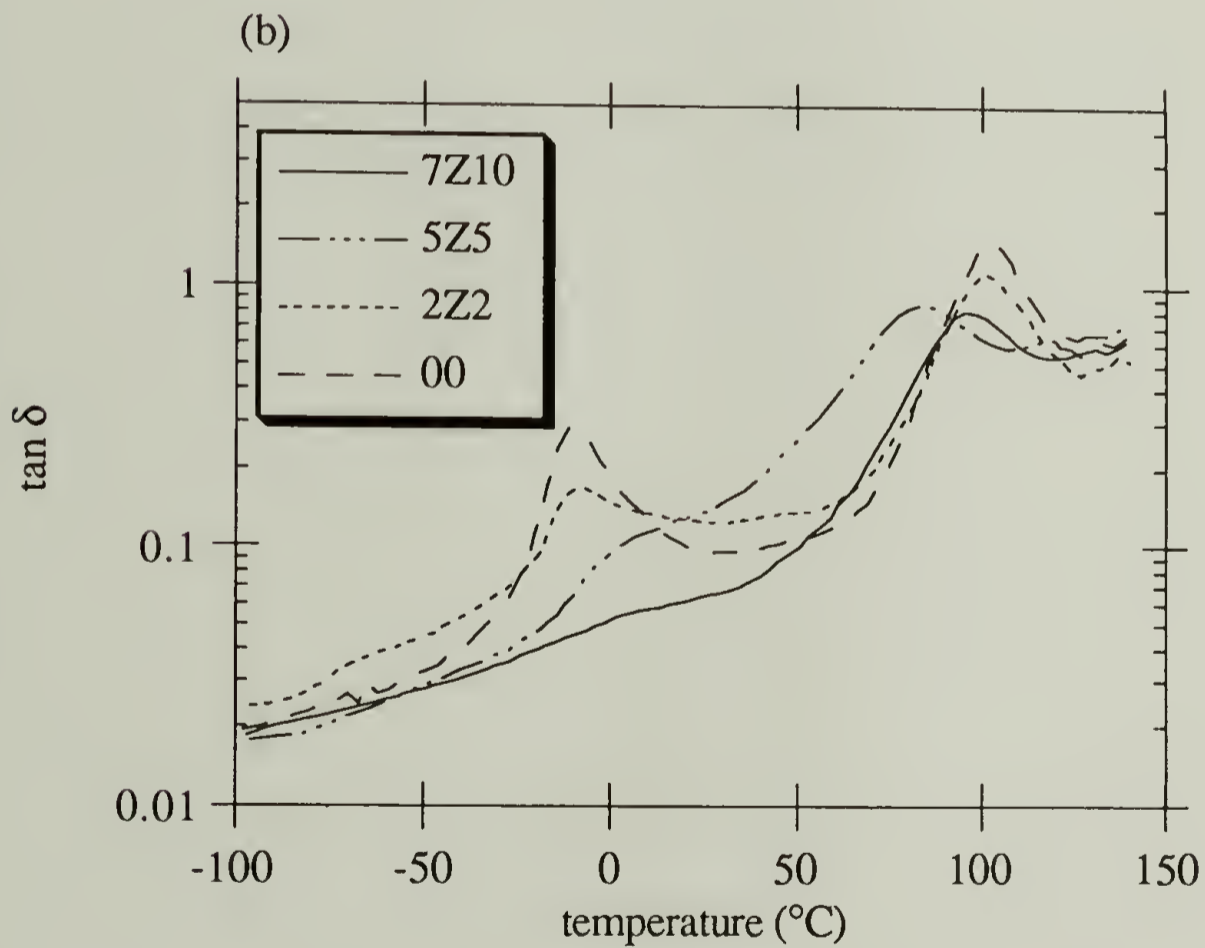
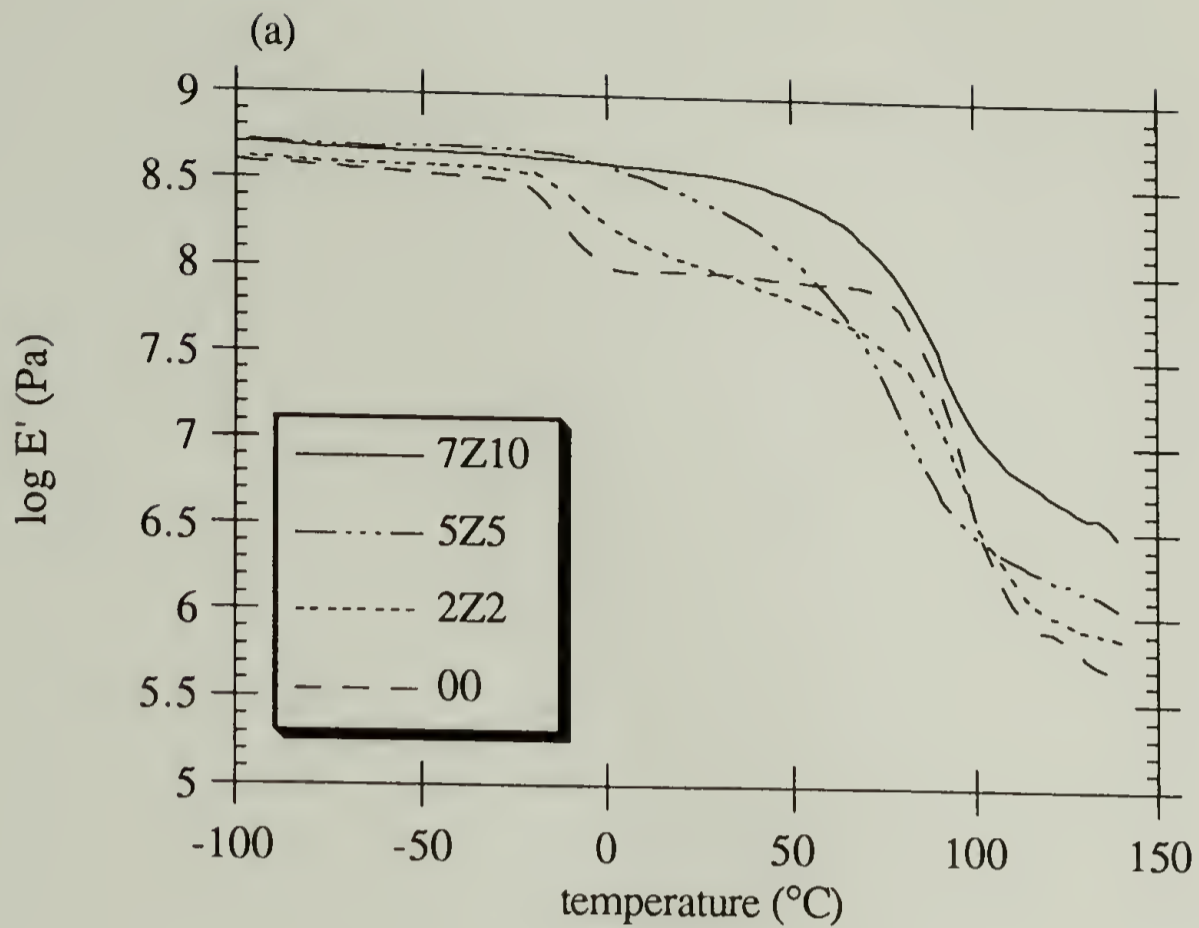


Figure 2.13: DMTA plots of (a) storage modulus and (b)  $\tan \delta$  for zinc blends at 1 Hz in bending.

Table 2.5: DMTA data for blends.

blend	T <sub>g</sub> (°C) <sup>a</sup>	ΔT <sub>g</sub> (°C) <sup>b</sup>
00	-9.0 ± 3.0	8.3 ± 3.0
	102.8	11.8
2H2	-6.0	12.0
	105.5	12.3
5H5	24.5	25.3
	90.5	25.0
8H10	10.0	54.5
	92.8	15.8
2Z2	-8.0	11.3
	100.5	13.0
5Z5	14.8	26.5
	83.8	19.5
7Z10	9.0	38.0
	96.0	16.0

<sup>a</sup> Taken as the peak in tan δ at 1 Hz.

<sup>b</sup> Taken as the half-width at half-height of the peak in tan δ at 1 Hz.



where  $k$  and  $q$  are empirically determined parameters. In comparing the values of  $k$  and  $q$  determined for a series of blends, Lin et al. found that  $k$  is related to the ratio of the molar volumes of the monomers of each of the blend components, while  $q$  is related to the interactions between the two blend components.<sup>32</sup> For example, in blends of donor and acceptor polymers where the interaction is weak  $q=0$ , whereas when there is a strong interaction  $q>0$ .

For the purposes of calculating the phase compositions of the SPS/EAVP blends, it was assumed that the parameter  $k$  is equal to unity. There is no *a priori* reason for making this assumption, but it seems reasonable since all of the monomers in these blends are vinyl monomers and thus have approximately the same size. When this assumption is made the Kwei equation reduces to:

$$T_g = w_1 T_{g1} + w_2 T_{g2} + q w_1 w_2 \quad (2.4)$$

The reason for using equation 2.4 instead of the full Kwei equation is that  $T_g$  versus composition data is not available for these blends, and so it is not possible to determine  $k$  with any reasonable degree of accuracy.

In order to determine  $q$  at the different substitution levels,  $T_g$  for each of the styrene/styrene blends was determined. Since both components of these blends are mostly styrene, they are always miscible. The glass transition temperatures of these blends from DMTA measurements are shown in Table 2.6. Since the  $T_g$ 's of the two components are close, the effect of the specific interactions on the blend  $T_g$ 's is quite pronounced; the blend  $T_g$ 's for the styrene/styrene blends are always higher than the  $T_g$ 's for the individual components.

Given the component glass transition temperatures, the blend glass transition temperature, and the blend composition, it is possible to calculate a value of  $q$  for each of the styrene/styrene blends. The results of this calculation are shown in Figure 2.14. It is

Table 2.6: Glass transitions of styrene/styrene blends

Blend	T <sub>g</sub> ,SPS (°C)	T <sub>g</sub> ,SVP (°C)	T <sub>g</sub> ,blend (°C)
2H2S	110.3 ± 1.0	122.0 ± 1.0	126.0 ± 1.0
5H5S	117.0	124.0	138.0
8H8S	119.5	126.0	145.0
2Z2S	118.5	122.0	126.0
5Z5S	121.0	124.0	133.5
7Z8S	128.5	126.0	143.0

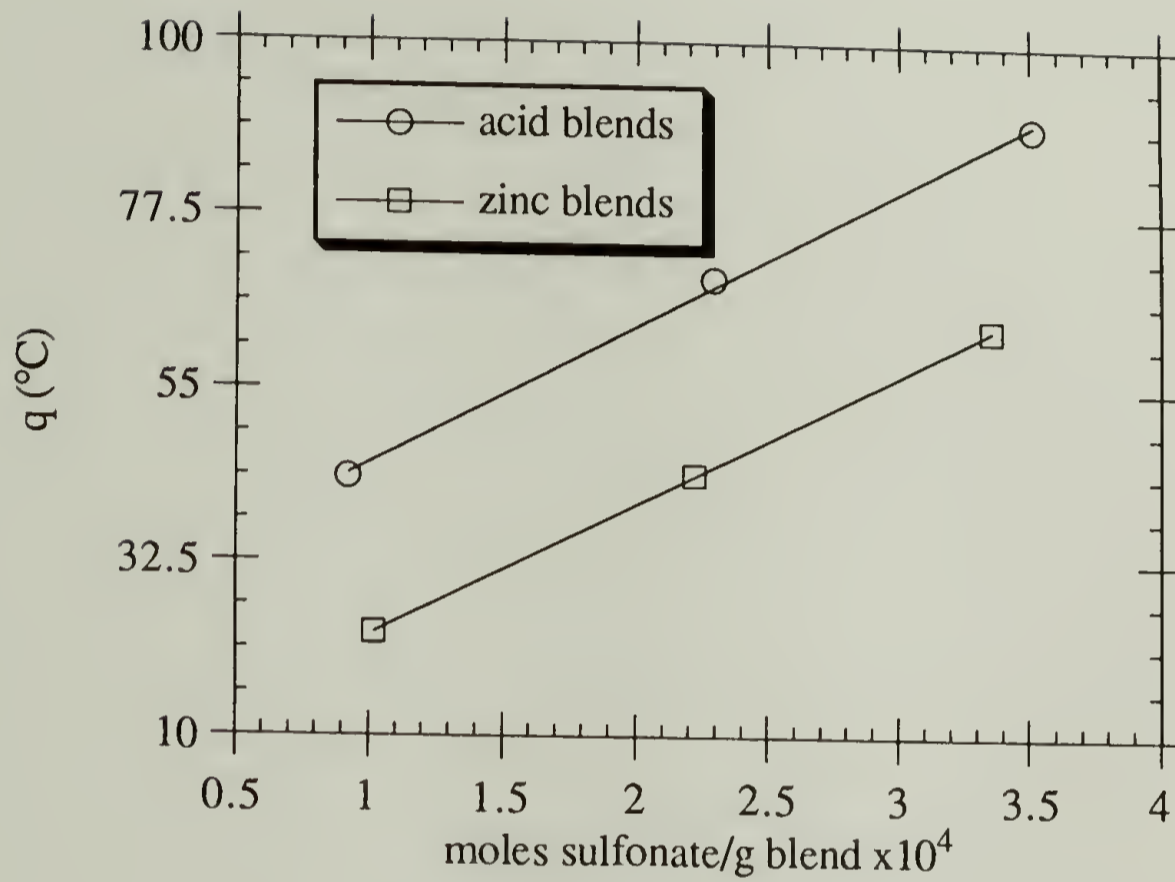


Figure 2.14: Calculated Kwei parameters for styrene/styrene blends.

interesting to note in this figure that the slopes of the lines for the zinc and acid blends are the same. As will be discussed later, this is evidence that there is essentially no difference between the acid/base and coordination interactions in determining the phase behavior.

The results from Figure 2.14 were used to determine the value of  $q$  to use for each of the styrene/ethyl acrylate blends, and that value of  $q$  was used in equation 2.4 to determine the composition of each phase as given by its transition temperature listed in Table 2.5. The results of this calculation are shown in Figure 2.15. In this figure the circles are the calculated compositions based on the DMTA data, and the crosses are the overall bulk compositions of the blends. It is clear from the figure that at 2% and 5% substitution levels the phases are predominantly polystyrene and poly(ethyl acrylate), while at the highest substitution level there is mostly a mixed phase along with a small amount of pure poly(ethyl acrylate). It should be noted that there is a fairly large error in calculating the exact compositions of the ethyl acrylate phases due to the broadness of the peaks, but within experimental error they can be considered to be essentially pure poly(ethyl acrylate).

The experimental results can now be interpreted in light of the ionic crosslink model. Phase separation is seen more clearly by DMTA than DSC at higher substitution levels because it has a higher spatial resolution. Even by DMTA, however, at the highest substitution level the main transition seen is due to a mixed phase. In terms of the model, most of the domain sizes are smaller than can be detected by DMTA and a single phase is detected.

This interpretation still does not explain the presence of the low temperature phase at the highest substitution level, however. The explanation for this phase comes from the synthesis conditions for the EAVP copolymer. As described in Section 2.2.1, the reactivity ratios for this polymerization are very different ( $r_{EA} = 0.29$  and  $r_{VP} = 2.58$ ), and the total conversions are 20-30%. Under these conditions substantial drift is expected to occur, which would lead to longer ethyl acrylate sequences later in the reaction. The amount of this drift can be estimated using models for copolymerization.

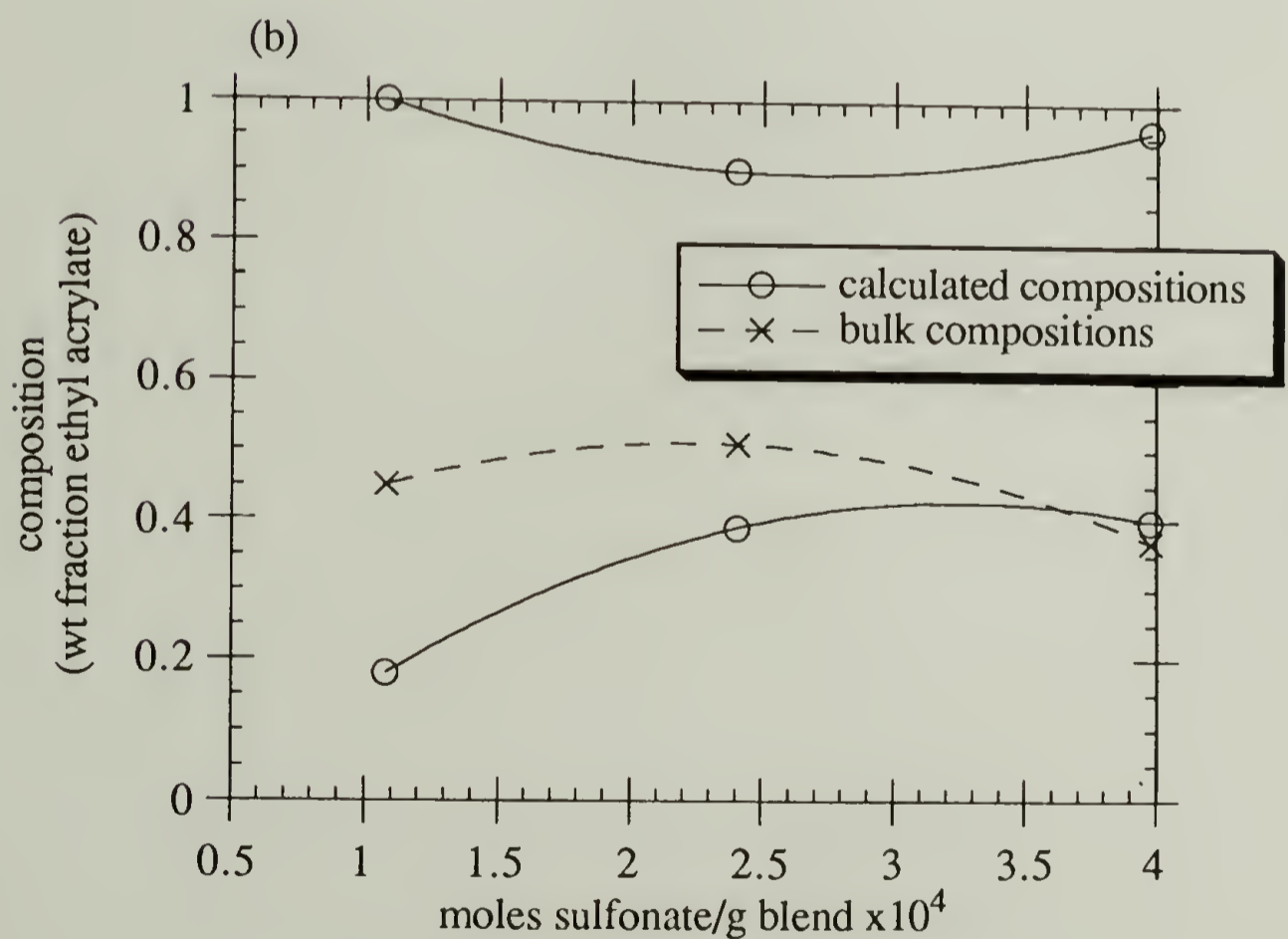
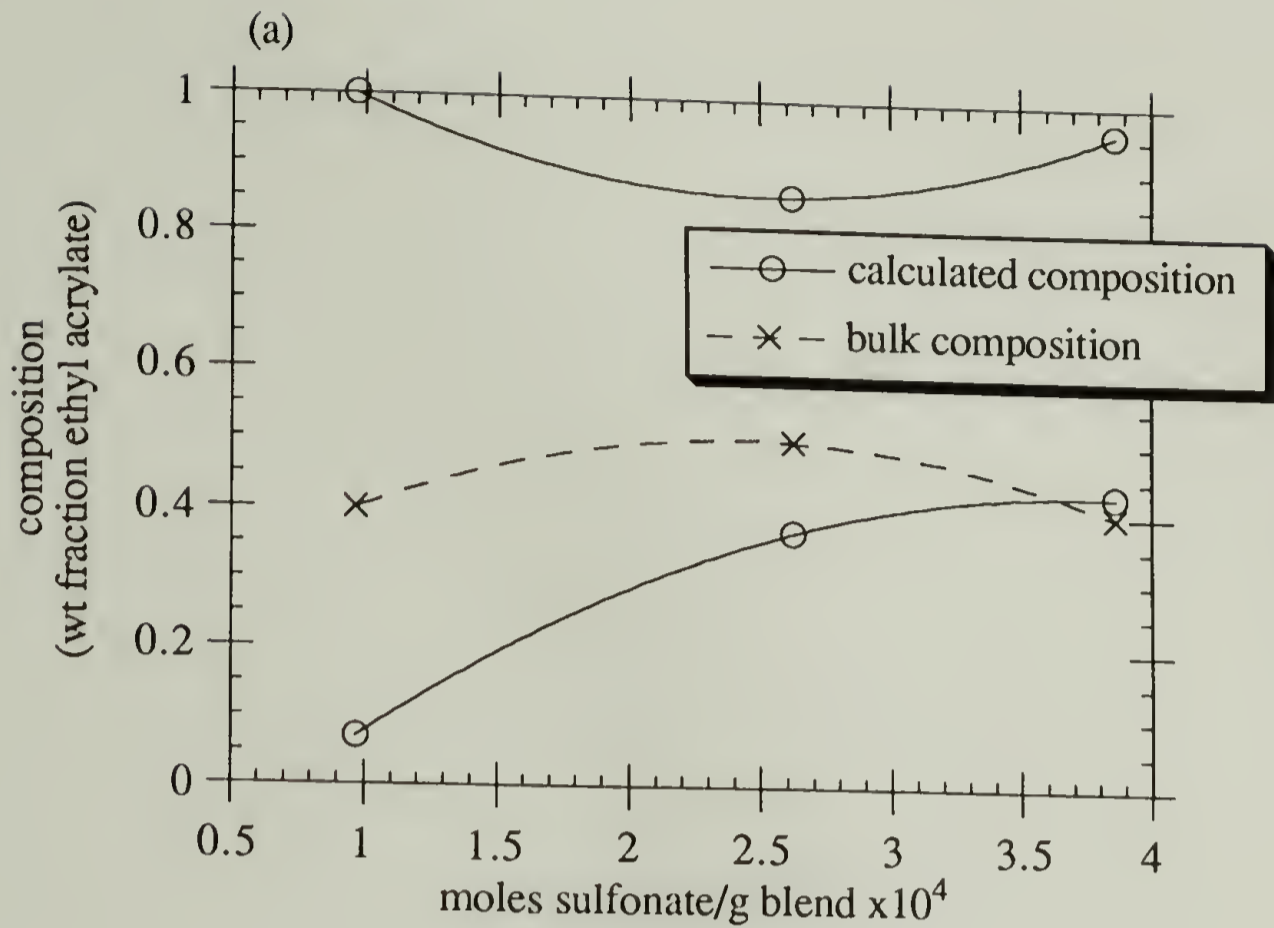


Figure 2.15: Calculated phase compositions and overall bulk compositions for (a) acid blends and (b) zinc blends.

The simplest copolymerization model is one in which the reactivity of the growing end is determined only by the nature of the end unit and of the unit attaching to that end (the terminal model).<sup>33,34</sup> Under these conditions the composition of the copolymer is given by:

$$F_1 = \frac{r_1 f_1^2 + f_1 f_2}{r_1 f_1^2 + 2f_1 f_2 + r_2 f_2^2} \quad (2.5)$$

where  $F_1$  is the mole fraction of monomer 1 in the copolymer,  $f_1$  and  $f_2$  are the mole fractions of monomers 1 and 2 in the feed, and  $r_1$  and  $r_2$  are the reactivity ratios for the two monomers, defined as the ratio of the rate constant for adding the monomer to a similar terminal unit to the rate constant for adding the monomer to a dissimilar terminal unit. This equation is strictly applicable only at the very beginning of the reaction, since a dissimilarity in reactivity ratios will result in a change in the feed composition as monomer is consumed. Meyer and Lowry have integrated this equation to give the following equations relating total monomer conversion,  $c$ , to monomer feed composition:<sup>35</sup>

$$c = 1 - (f_1/f_1^\circ)^\alpha (f_2/f_2^\circ)^\beta [(f_1^\circ - \delta)/(f_1 - \delta)]^\gamma \quad (2.6a)$$

$$\alpha = r_2 / (1 - r_2) \quad (2.6b)$$

$$\beta = r_1 / (1 - r_1) \quad (2.6c)$$

$$\gamma = (1 - r_1 r_2) / (1 - r_1)(1 - r_2) \quad (2.6d)$$

$$\delta = (1 - r_2) / (2 - r_1 - r_2) \quad (2.6e)$$

where  $f_1$  and  $f_2$  are the mole fractions of monomers 1 and 2 in the feed at conversion  $c$ , and  $f_1^\circ$  and  $f_2^\circ$  are the initial mole fractions of monomers 1 and 2 in the feed. It is also possible to calculate the sequence length distribution at different conversions. The mole fraction of sequences of monomer 1 of length  $x$  is given by:<sup>34</sup>

$$(N_1)_x = (p_{11})^{(x-1)}p_{12} \quad (2.7a)$$

where  $p_{11}$  is the probability of forming a diad of two monomers of type 1 and  $p_{12}$  is the probability of forming a diad of a type 1 monomer and a type 2 monomer. These probabilities are related to the reactivity ratios and the concentration of monomers in the feed mixture by

$$p_{11} = r_1 / (r_1 + ([M_1] + [M_2])) \quad (2.7b)$$

$$p_{12} = [M_2] / (r_1[M_1] + [M_2]) \quad (2.7c)$$

Equations 2.5-2.7 were used to determine the instantaneous and cumulative copolymer compositions as a function of conversion, as well as the instantaneous sequence length distribution at 0% conversion and the highest conversion and the average sequence length distribution at the highest conversion. The calculations were done by calculating the conversion from equation 2.6a, the mole fraction of ethyl acrylate in the copolymer formed from the instantaneous copolymerization equation (equation 2.5), and the mole fraction of sequences that are one to 100 ethyl acrylate units long from equations 2.7 ( $x$  varies from 1 to 100). The value of  $f_1$  was then incremented and the calculations repeated until the highest values of conversion used in the copolymerization was reached (typically 20 -

35%). It should be noted that the assumption that  $f_1$  increases with conversion implies that  $r_1 < 1$  and  $r_2 > 1$ .

The results of the calculations are shown in Figures 2.16 and 2.17. Figure 2.16 shows how the composition of the copolymers changes with composition. More significant for this discussion are the sequence length distribution calculations, shown in Figure 2.17. At 0% conversion only 7% of ethyl acrylate sequences in 10EAVP are longer than 50 monomer units. After 20% conversion, however, that number has increased to 16%, and the fraction of sequences greater than 85 units long has increased from none to 1.7%.

Since the proposed ionic crosslink model of phase separation states that the size of the phases depends on the distance between ionic crosslinks, an increase in the number of long sequences with conversion should result in a corresponding increase in the size of the phases formed. From Figure 2.17 it is clear that some sequences formed at later conversions in 10EAVP are as long as the average sequence length in 2EAVP. Since 2EAVP is macrophase separated, as seen by DSC, it is likely that the longer ethyl acrylate sequences in 10EAVP are also macrophase separated.

From these results it is possible to build a picture of how phase separation changes as the number of interacting groups increases. At 2% substitution level the blends remain macrophase separated. At 5% substitution level the blends are apparently no longer macrophase separated, but DMTA still detects two glass transitions, indicating that the blend is microphase separated. It is interesting to note that this change from macro- to microphase separation occurs at the same substitution level that has been reported by Eisenberg and coworkers to be the critical level for miscibility enhancement.<sup>21</sup> At the 8% substitution level most of the sequence lengths between ionic crosslinks are so short that the domain sizes are smaller than what can be detected by DMTA. The result is that only one loss peak, corresponding to a mixed phase, is detected. There are, however, a few



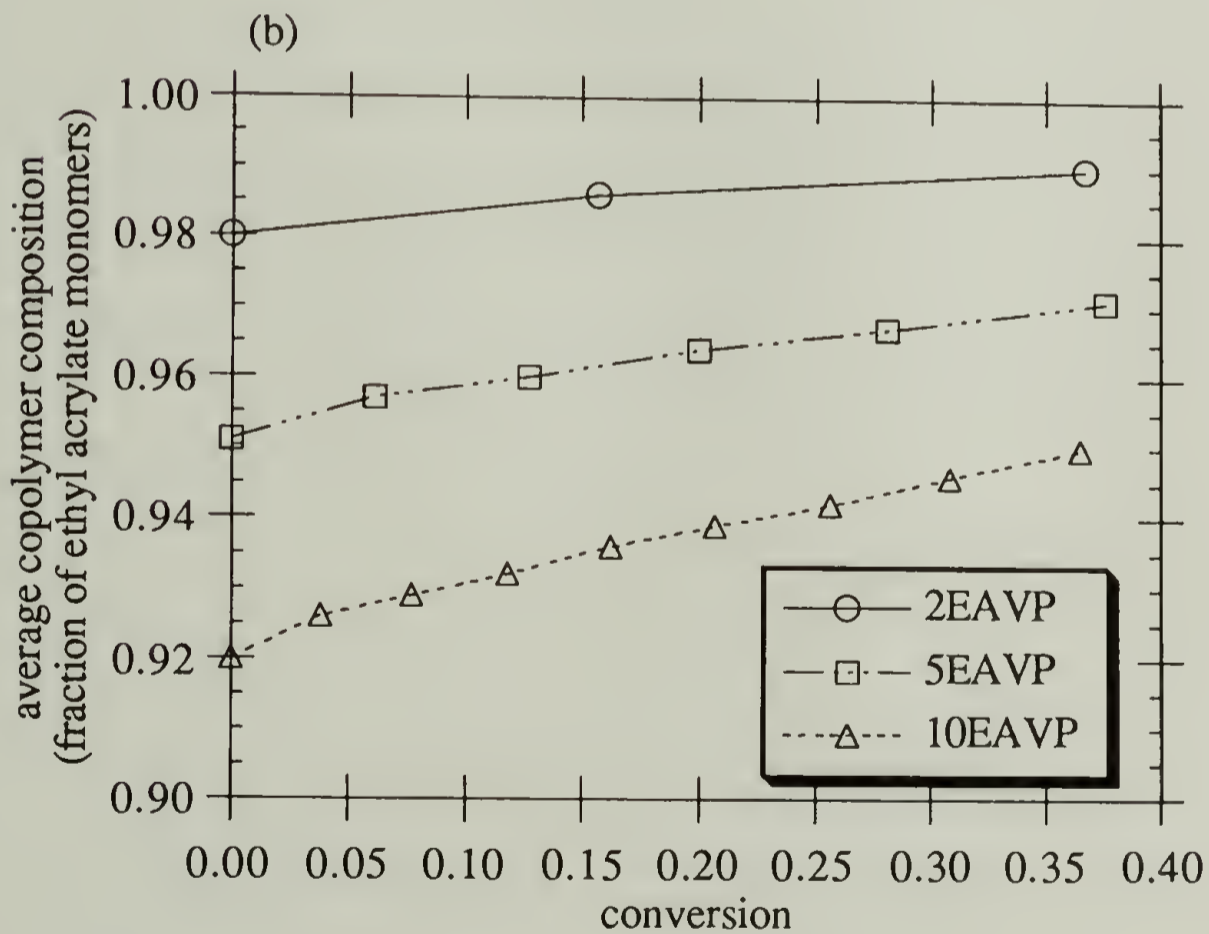
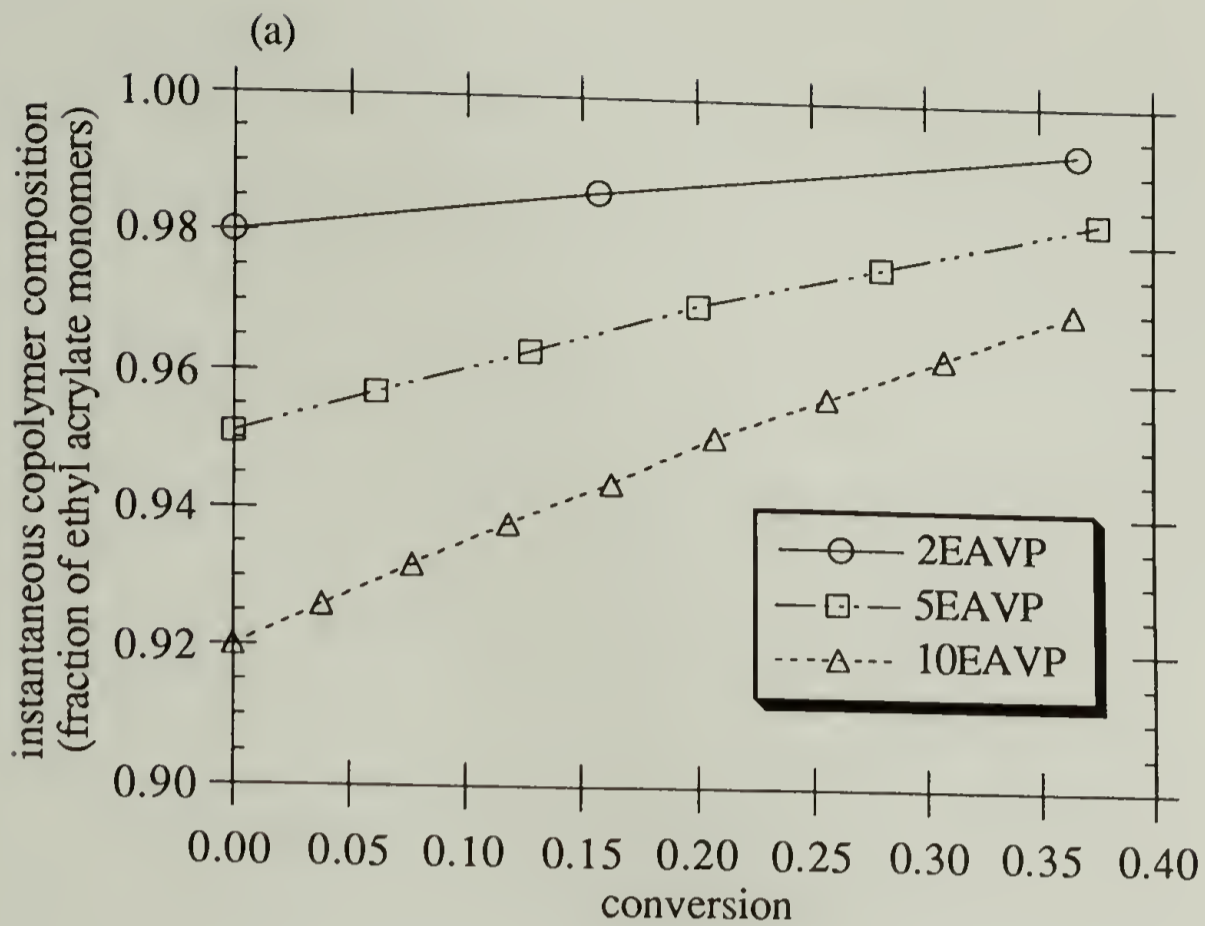


Figure 2.16: Effect of conversion on EAVP copolymer composition.  
 (a) Composition of the copolymer formed at each conversion.  
 (b) Cumulative average composition of all the copolymer formed.

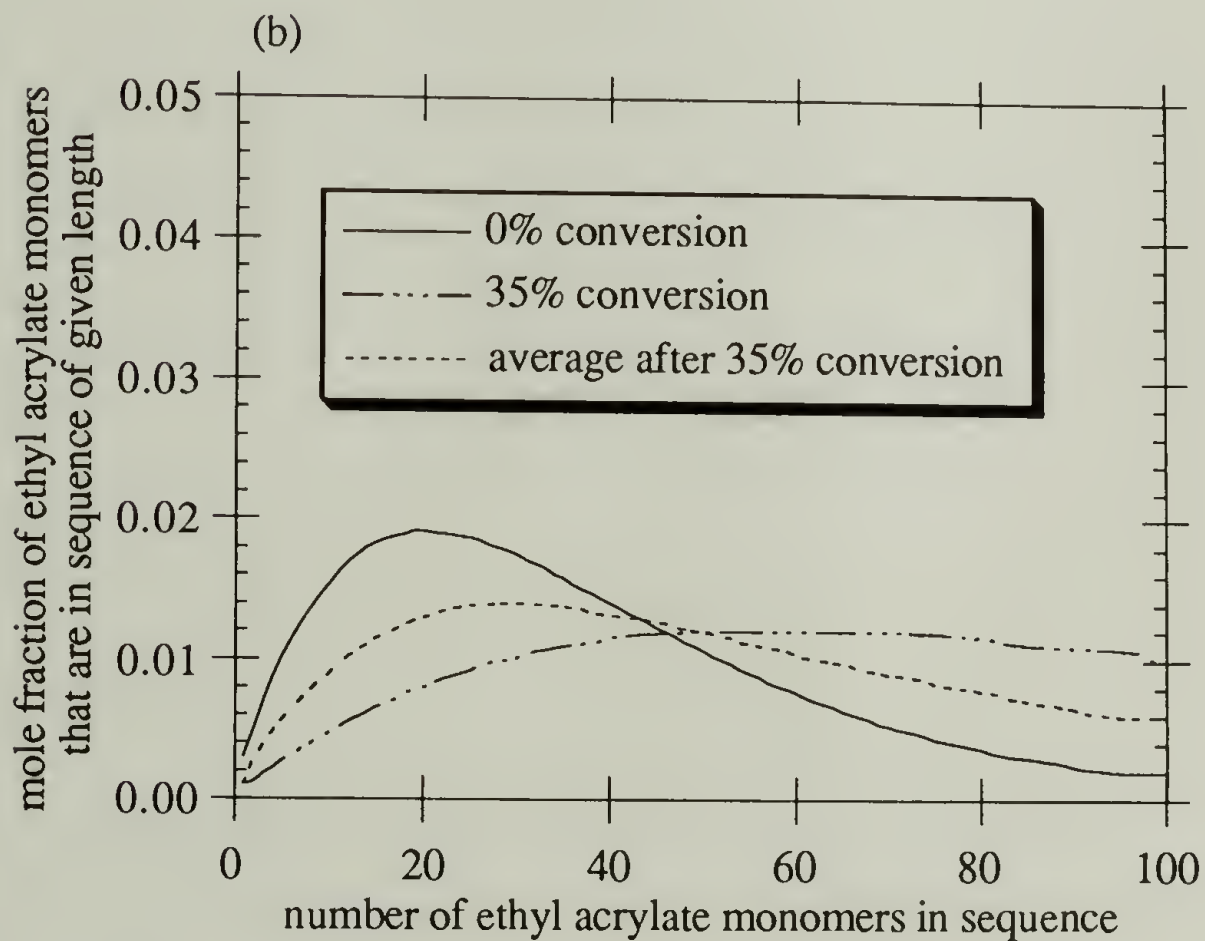
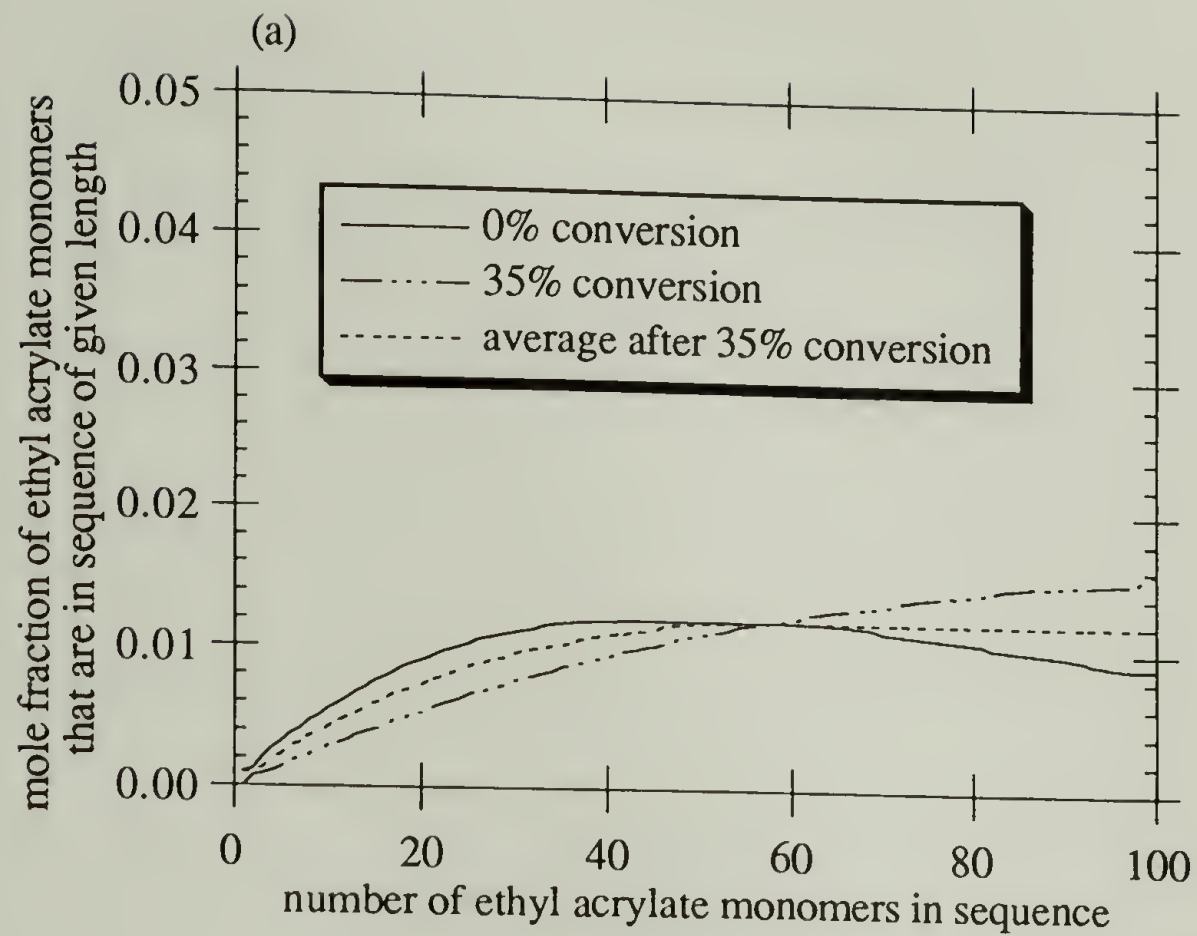


Figure 2.17: Effect of conversion on ethyl acrylate sequence distribution for (a) 2EA VP, (b) 5EA VP, and (c) 10EA VP.

continued on next page

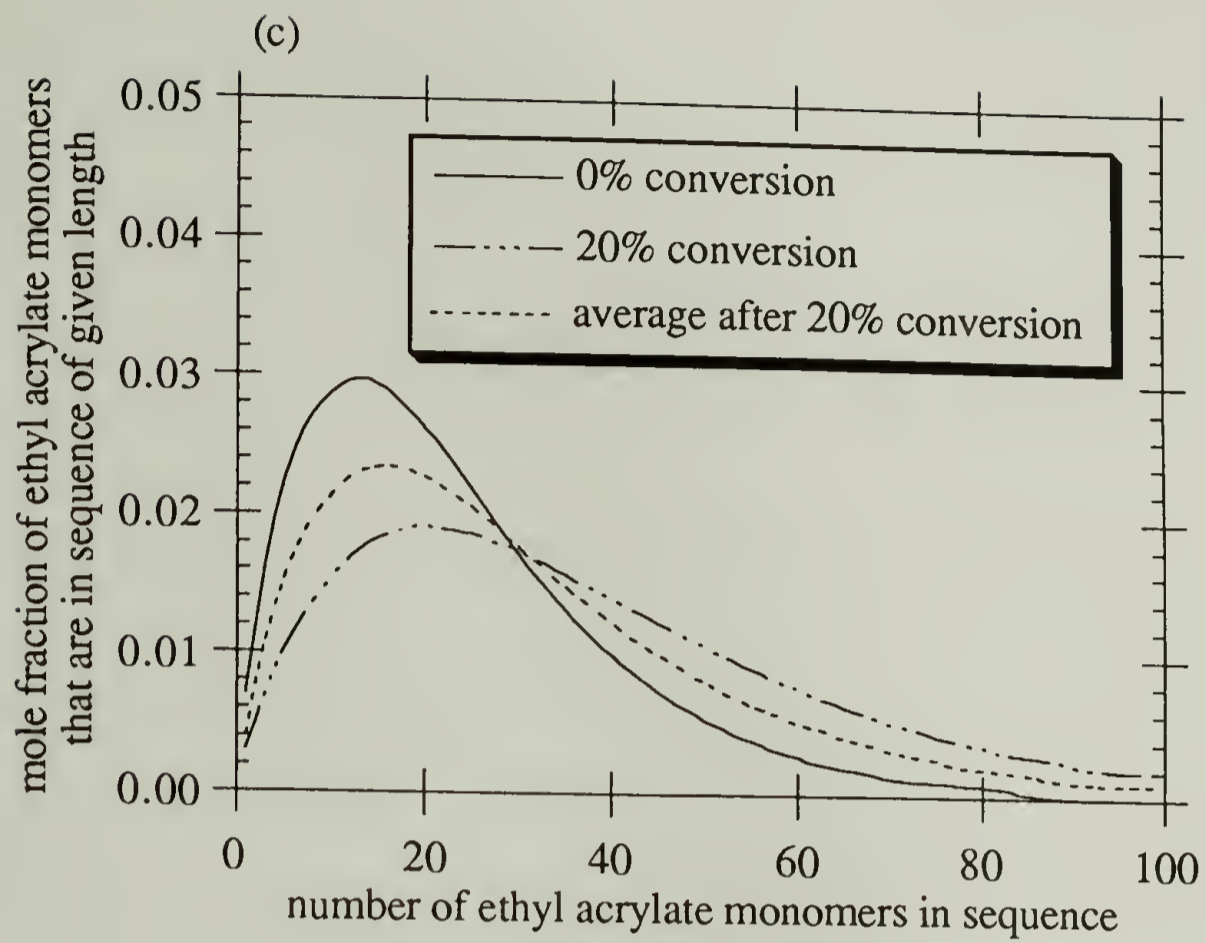


Figure 2.17 (continued)

ethyl acrylate sequences that are long enough to form domains detectable by the DMTA. These sequences result from copolymerization drift.

An estimation of the scale of phase separation can be obtained from these results. It is generally assumed that DSC detects domains that are larger than about 300 Å, while dynamic mechanical measurements are sensitive to domains greater than about 50 to 100 Å. These estimates come by comparing results using materials for which the morphology can be determined by other techniques. The best estimate can be obtained by considering the cases of ionomers and block copolymers. From small angle x-ray measurements on ionomers it has been estimated that the domains formed by the aggregation of ionic groups are a few tens of angstroms in size, depending on the exact model used to analyze the data.<sup>36</sup> Viscoelastic measurements show a high temperature loss peak associated with these aggregates, while there is no evidence of a transition in DSC scans, indicating that the aggregates are too small to be detected by DSC.<sup>37,38</sup> Block copolymers, which typically have domain sizes greater than 500 Å, do show two transitions by DSC. (block copolymers, #97) These results lead to the estimates given above.

Based on this discussion, it is clear that at 2% substitution level the domains are larger than a few hundred angstroms, since DSC shows two transitions. At 5% substitution level DSC does not show separate transitions while DMTA does, and so the domain size is in the range of 100 to 300 Å. Finally, at 8% substitution level DMTA shows a peak corresponding to a mixed phase, and so the domain sizes are smaller than 100 Å. Of course, it would be desirable to have a more accurate measure of the domain sizes, and this will be addressed in the next section.

One of the goals of this work was to determine the difference, if any, between the acid/base and coordination interactions. All of the results indicate that there is no difference, which supports the general features of the ionic crosslink model. In particular, the slopes of the lines in the plot of the Kwei parameter  $q$  versus ionic content (Figure 2.14) are the same for the two types of interactions. Since  $q$  is a measure of the

effectiveness of the interactions, a similar slope indicates that the two types of interactions are equally effective in crosslinking the chains. (The difference in the intercepts is probably an artifact resulting from the difference in  $T_g$  between HSPS and ZSPS at a given sulfonation level.)

While there does not seem to be any difference between the acid/base and coordination interactions in determining the phase behavior, there may be a subtle difference between the two related to their relative strengths. Careful comparison of the low temperature transitions of blends 2H2 and 2Z2 in Figures 2.12 and 2.13 reveals that the transition is more prominent in 2Z2. This difference reflects a greater mobility of the ethyl acrylate phase in 2Z2 compared to 2H2, and may be related to a difference in the effectiveness of the two types of interactions at the interface between the phases. This is a minor point with regard to phase behavior, but will become important in the discussion of deformation behavior in Chapter 4.

### 2.2.3 Morphology

The morphology of the blends was examined directly using Hoffman modulation contrast optical microscopy. The micrographs are shown in Figures 2.18-2.20. The domains appear slightly elongated due to the high shear the films experienced during compression molding. The features in the other micrographs are surface features that were used to aid in focusing.

The most apparent difference in the micrographs is the scale at which phase separation occurs. Blend 00 shows gross phase separation, as would be expected for this immiscible blend. Domain size varies widely, ranging from 2 microns to 20 microns across. The distribution of domains is also very inhomogeneous.

Blends 2H2 and 2Z2, while still exhibiting macrophase separation, have very different morphologies from blend 00. The domains are typically much smaller and have a more

20 microns

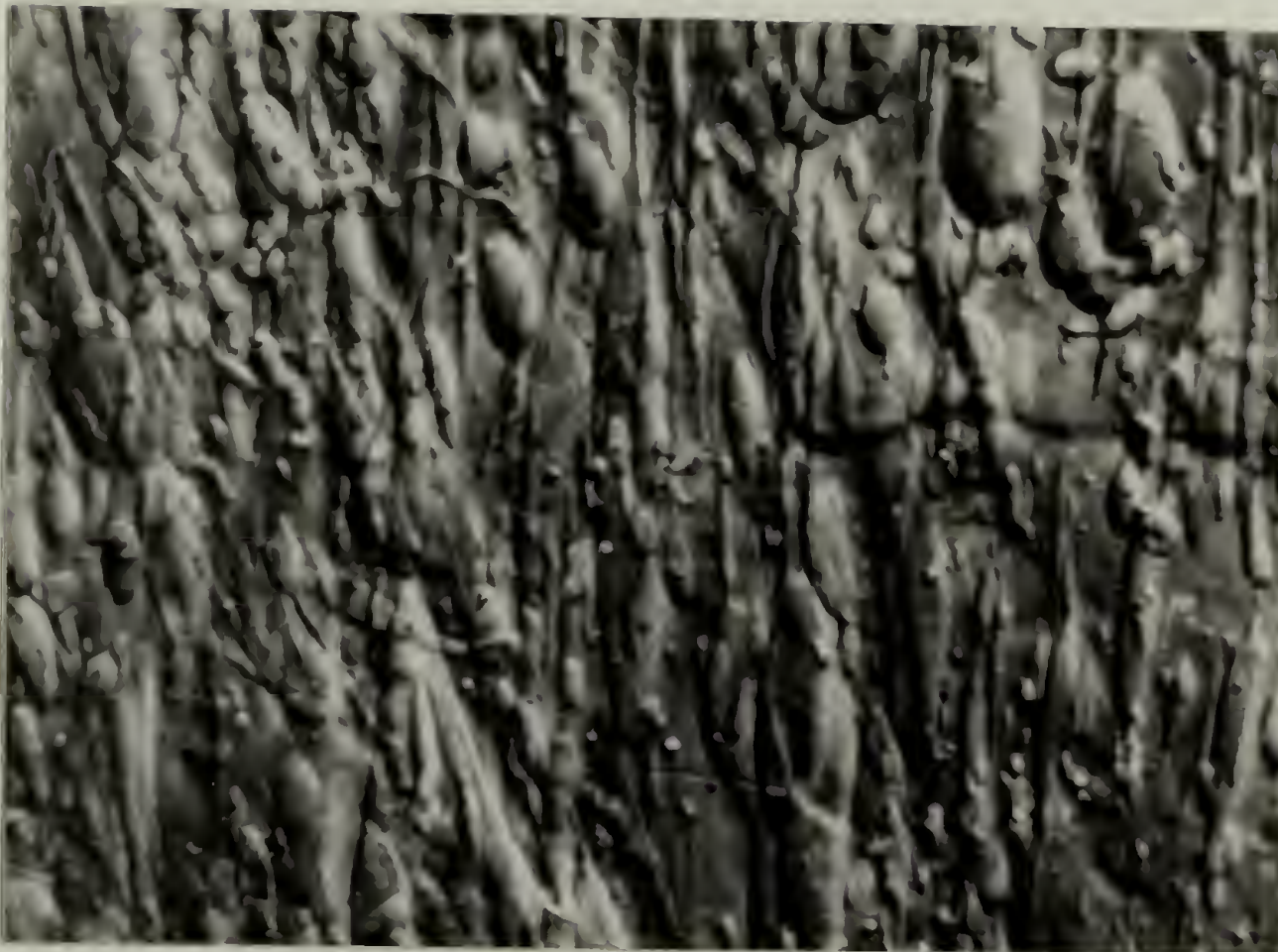
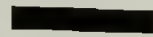


Figure 2.18: Optical micrograph for blend 00.

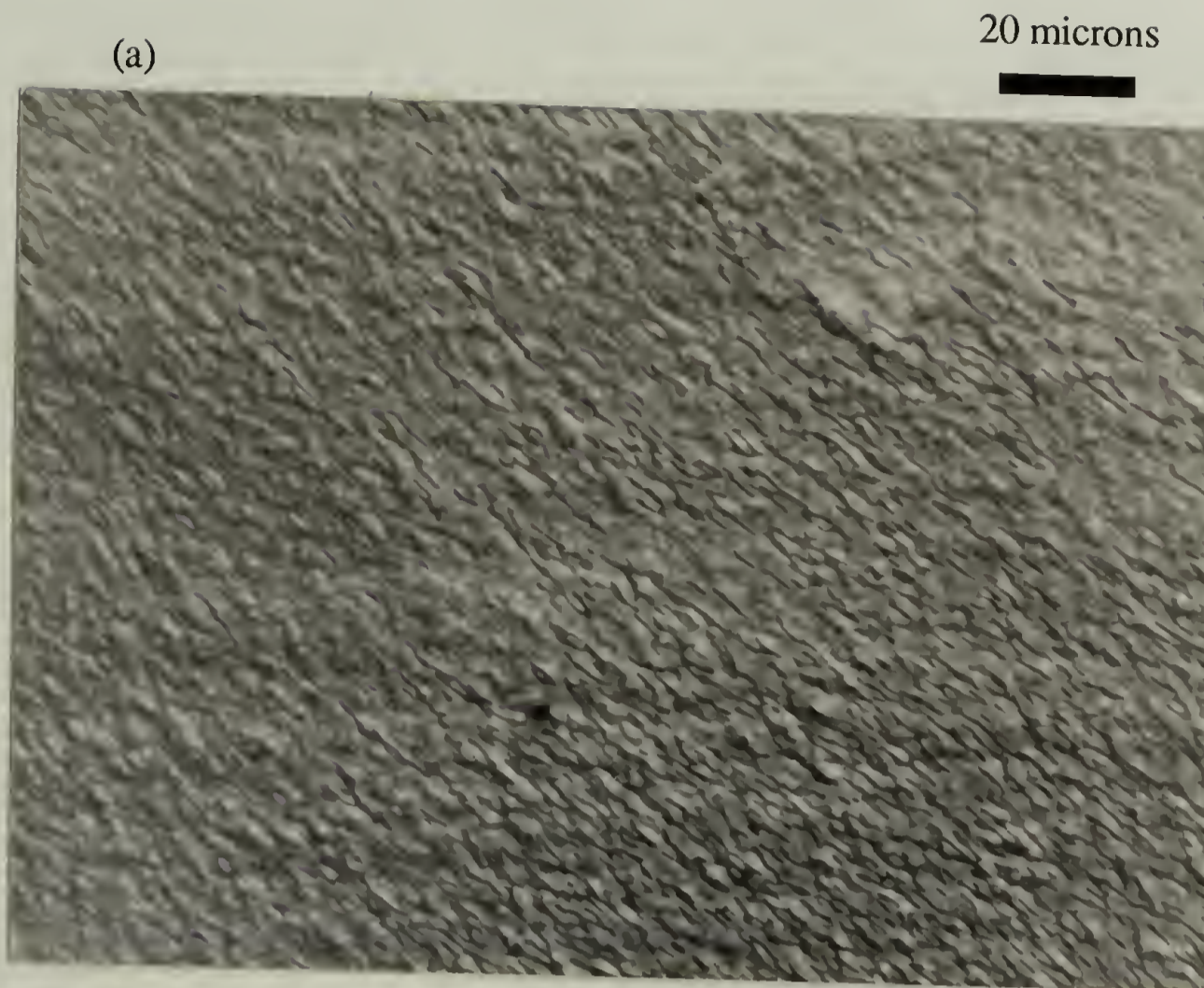


Figure 2.19: Optical micrographs for acid blends.  
(a) 2H2, (b) 5H5, (c) 8H10

continued on next page

(c)

20 microns

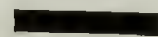


Figure 2.19 (continued)



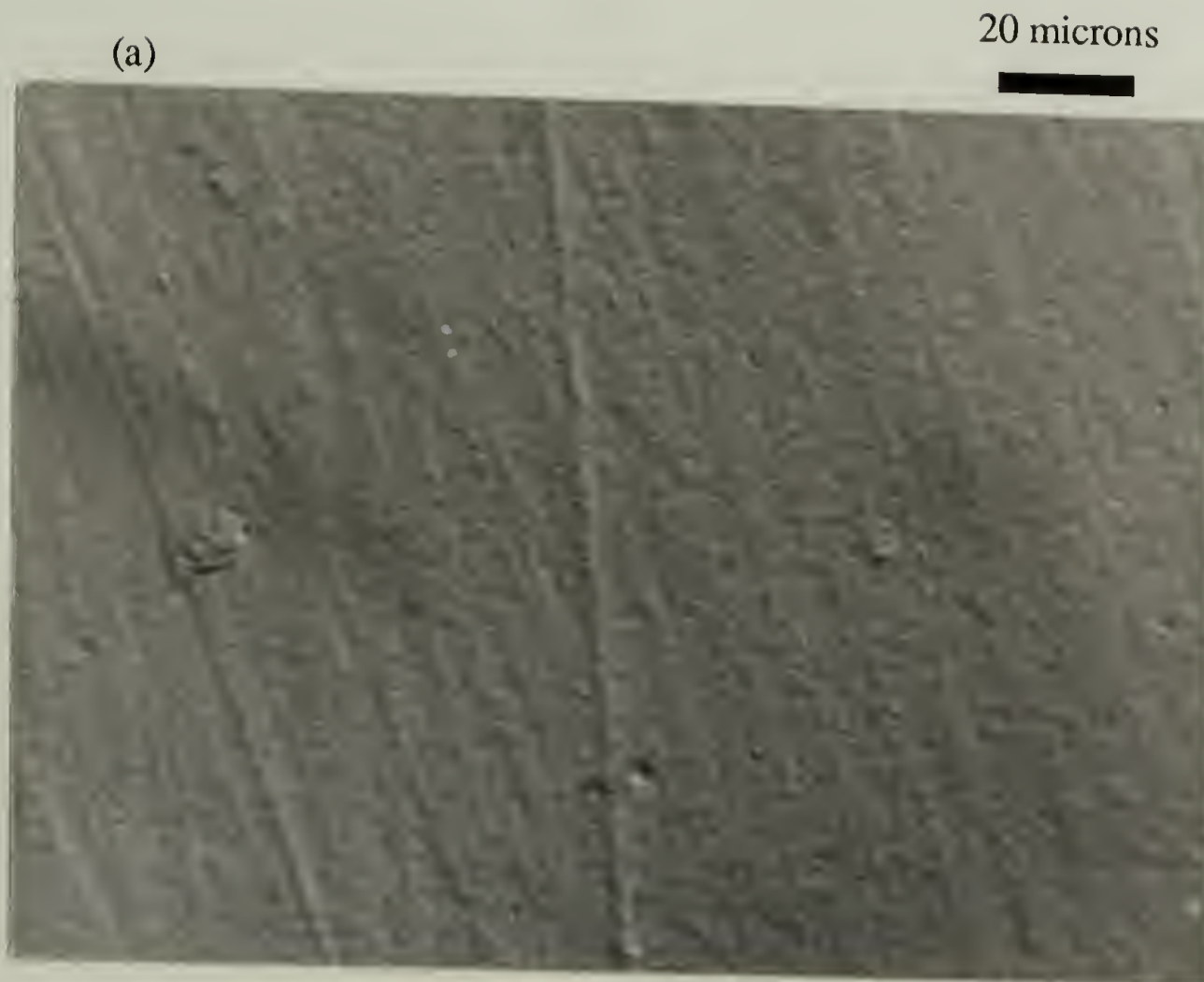


Figure 2.20: Optical micrographs for zinc blends.  
(a) 2Z2, (b) 5Z5, (c) 7Z10

continued on next page

(c)

20 microns



Figure 2.20 (continued)

uniform size distribution, ranging from 2 to 5 microns across. The domains are also distributed fairly uniformly across the sample. These are the results that would be expected from the ionic crosslink model of phase separation. Since the distance between interacting groups controls the domain size, and the interacting groups are distributed randomly along the polymer chains, the size of the domains should be smaller and the size distribution more uniform in this blend than in a blend with no interactions. Similar results have been seen previously for blends of telechelic ionomers. Russell et al. found that blending a difunctional amine-terminated polyisoprene with a monofunctional carboxylic acid-terminated polystyrene gives very coarse phase separation, while blending the same amine-terminated polyisoprene with a difunctional carboxylic acid-terminated polystyrene produces a morphology similar to that shown for blends 2H2 and 2Z2 in Figures 2.19a and 2.20a.<sup>40</sup> Interestingly, Russell et al. call their materials "block copolymers formed via ionic interactions", implying that the ionic interactions act like covalent bonds to control the morphology, similar to what the ionic crosslink model described in this work predicts.

All the blends with substitution levels of 5% or greater do not show any domains by optical microscopy. As was described in Section 2.2.2 these blends are microphase separated, and thus the domains are too small to be detected by optical microscopy. It would of course be desirable to examine the morphology of these blends with other means. For example, transmission electron microscopy (TEM) and small angle x-ray scattering (SAXS) are the primary tools used to investigate the morphology of microphase separated block copolymers. As will be described in more detail in Chapter 5, both of these techniques were attempted, but no signs of phase separation could be detected by either.

Nevertheless, it is interesting to see whether the estimates of domain size match the predictions of the ionic crosslink model. For blends at 2%, 5%, and 8% substitution level, the distance between interacting groups is 250, 100, and 60 Å respectively for fully extended chains and 25, 16, and 13 Å respectively for randomly coiled chains. (The value given for random coils is the mean end-to-end distance of the segments between interacting

groups.) Since estimates from thermal analysis and optical microscopy indicate domain sizes are approximately 20000, 200, and  $<100 \text{ \AA}$ , it is clear that the simple ionic crosslink model as described can not completely describe the behavior of these blends. One possible explanation is that not all ionic groups are participating in interactions. However, infrared spectroscopy studies show that at least for blends 5H5 and 8H10 all groups do participate in interactions.<sup>23,24</sup> The failure of the ionic crosslink model would seem to be in the assumption that the interactions act as independent crosslinks. As will be shown in Chapter 3, the interacting groups aggregate, and this may account for the discrepancies between the experimental results and the predictions of the model. Nevertheless, the model provides a good qualitative description of the phase behavior of the blends.

### 2.3 Conclusions

The experimental results show that phase separation takes place for all blends, regardless of substitution level. However, the nature of the phase separation changes. The blends with 2% interacting groups are macrophase separated, although calculation of the interface fraction from DSC data shows that even these blends exhibit some enhanced mixing. At 5% substitution level or higher the blends are microphase separated. Blends 8H10 and 7Z10 are interesting in that there appears to be a completely mixed phase and a pure poly(ethyl acrylate) phase by DMTA. In terms of the model, this result indicates a distribution of distances between interacting groups. The mixed phase results from sequence lengths smaller than the resolution of DMTA, while only a few sequences are long enough to result in domains large enough to be detected by DMTA. Even though blends 2H2 and 2Z2 are macrophase-separated, the presence of the ionic crosslinks greatly affects the morphology, causing the domains to become smaller and more uniform in size.

The experimental results also show that there is no difference between the acid/base interaction and the coordination interaction in determining the phase behavior. It is not the

type or strength of the interaction that is important in determining the phase behavior of these systems, but simply the presence of the interactions, which can be considered as crosslinks. Lu and Weiss have used a modified Flory-Huggins equation to describe mixing in similar systems.<sup>41,42</sup> In this approach the favorable interactions are considered to lead to an overall negative free energy of mixing. However, previous studies on co-crosslinked systems and interpenetrating networks have also shown enhanced compatibility.<sup>43-46</sup> These systems do not contain any favorable interactions, and thus support the concept that the interacting groups, although ionic, act as cross-links.

It should be pointed out that Eisenberg has presented a ranking of interacting group strength based on the levels of miscibility enhancement observed for different types of interactions in the polystyrene/poly(ethyl acrylate) system.<sup>19</sup> In terms of the ionic crosslink model, this ranking is due to differences in the number of interactions that take place. The differences result from an equilibrium between the formation of the interactions and the repulsion of unlike polymer pairs during blending, and this equilibrium is a function of interaction strength. Given equal numbers of interactions, the level of mixing will be the same regardless of the type of interaction.

It should also be noted that Natansohn and Eisenberg have concluded from NMR experiments that similar blends in DMSO solution are intimately mixed.<sup>7,11</sup> This result may be due to the presence of the solvent. In ionizing solvents such as DMSO it is likely that the ionic chains adopt an extended-chain conformation due to the well-known polyelectrolyte effect.<sup>28</sup> In this case, as the ionic groups form the interaction the two different chains will also be brought together along their entire length, even though they phase separate in the bulk.

Unfortunately, it has not been possible to definitively show that blends 8H10 and 7Z10 are microphase-separated on scales less than 100 Å. One intriguing piece of evidence that they are comes from an infrared spectroscopy study of these same materials. In that work it was found that the carbonyl stretching band of the poly(ethyl acrylate) component

was unchanged upon blending.<sup>23</sup> Shifts in the carbonyl band position have been used previously to infer mixing at the molecular level, since the carbonyl band is strongly influenced by its local environment.<sup>47</sup> While not definitive, the IR results for these materials would seem to suggest that the blends at the highest substitution levels are not intimately mixed.

## 2.4 References

1. Smith, P.; Eisenberg, A. *J. Poly. Sci. : Letters*, **21**, 223 (1983)
2. Eisenberg, A.; Smith, P.; Zhou, Z.-L. *Poly. Eng. Sci.*, **22**, 1117 (1982)
3. Murali, R.; Eisenberg, A. *J. Poly. Sci. : Part B : Phys.*, **26**, 1385 (1988)
4. Zhou, Z.-L.; Eisenberg, A. *J. Poly. Sci. : Phys.*, **21**, 595 (1983)
5. Simmons, A.; Eisenberg, A. *Poly. Prep.*, **27**, 341 (1986)
6. Murali, R.; Eisenberg, A. *Poly. Prep.*, **27**, 343 (1986)
7. Natansohn, A.; Eisenberg, A. *Poly. Prep.*, **27**, 349 (1986)
8. Hara, M.; Eisenberg, A. *Macromolecules*, **20**, 2160 (1987)
9. Hara, M.; Eisenberg, A. *Macromolecules*, **17**, 1335 (1984)
10. Eisenberg, A.; Hara, M. *Poly. Eng. Sci.*, **24**, 1306 (1984)
11. Natansohn, A.; Eisenberg, A. *Macromolecules*, **20**, 323 (1987)
12. Rutkowska, M.; Eisenberg, A. *Macromolecules*, **17**, 821 (1984)
13. Rutkowska, M.; Eisenberg, A. *J. Appl. Poly. Sci.*, **30**, 3317 (1985)
14. Rutkowska, M.; Eisenberg, A. *J. Appl. Poly. Sci.*, **33**, 2833 (1987)
15. Rutkowska, M.; Eisenberg, A. *J. Appl. Poly. Sci.*, **29**, 755 (1984)
16. Natansohn, A.; Rutkowska, M.; Eisenberg, A. *Polymer*, **28**, 885 (1987)
17. Natansohn, A.; Rutkowska, M.; Eisenberg, A. *Poly. Eng. Sci.*, **27**, 1504 (1987)
18. Natansohn, A.; Murali, R.; Eisenberg, A. *Makromol. Chem., Macromol. Symp.*, **16**, 175 (1988)
19. Zhang, X.; Eisenberg, A. *Poly. Adv. Tech.*, **1**, 9 (1990)

20. Zhang, X.; Eisenberg, A. *J. Poly. Sci. : Part B : Phys.*, **28**, 1841 (1990)
21. Smith, P.; Hara, M.; Eisenberg, A. in *Current Topics in Polymer Science, Vol. II*, R. M. Ottenbrite, L. A. Utracki and S. Inoue, eds., Carl Hanser Verlag, New York, 1987, pp. 256
22. Brereton, M. G.; Vilgis, T. A. *Macromolecules*, **23**, 2044 (1990)
23. Sakurai, K.; Douglas, E. P.; MacKnight, W. J. *Macromolecules*, in press
24. Sakurai, K.; Douglas, E. P.; MacKnight, W. J. *Macromolecules*, submitted
25. Niwa, M.; Matsumoto, T.; Kagami, M.; Kajiyama, K. *Sci. Eng. Rev. Doshisha Univ.*, **25**, 192 (1984)
26. Tamikado, T. *J. Poly. Sci.*, **43**, 489 (1960)
27. Hoffman, R. in *Applied Polymer Light Microscopy*, D. A. Hemsley, eds., Elsevier Applied Science, London, 1989, pp. 151
28. Fitzgerald, J. J.; Weiss, R. A. *J. Macromol. Sci.-Rev. Macromol. Chem. Phys.*, **C28**, 99 (1988)
29. Beckman, E. J.; Karasz, F. E.; Porter, R. S.; MacKnight, W. J.; Hunsel, J. V.; Koningsveld, R. *Macromolecules*, **21**, 1193 (1988)
30. Couchman, P. R. *Macromolecules*, **11**, 1156 (1978)
31. Walsh, D. J.; Rostani, S. *Adv. Poly. Sci.*, **70**, 119 (1985)
32. Lin, A. A.; Kwei, T. K.; Reiser, A. *Macromolecules*, **22**, 4112 (1989)
33. Mayo, F. R.; Lewis, F. M. *J. Am. Chem. Soc.*, **66**, 1594 (1944)
34. Odian, G. *Principles of Polymerization*, John Wiley & Sons, New York, 1981
35. Meyer, V. E.; Lowry, G. G. *J. Poly. Sci.*, **A3**, 2843 (1965)
36. Yarusso, D. J.; Cooper, S. L. *Macromolecules*, **16**, 1871 (1983)
37. Connolly, J. M., Ph.D. Thesis, University of Massachusetts, 1989
38. Weiss, R. A.; Fitzgerald, J. J.; Kim, D. *Macromolecules*, **24**, 1071 (1991)
39. Bares, J. *Macromolecules*, **8**, 244 (1975)
40. Russell, T. P.; Jérôme, R.; Charlier, P.; Foucart, M. *Macromolecules*, **21**, 1709 (1988)
41. Lu, X.; Weiss, R. A. *Poly. Mat. Sci. Eng.*, **64**, 163 (1991)
42. Lu, X.; Weiss, R. A. *Macromolecules*, **24**, 4381 (1991)
43. Bauer, R. F.; Dudley, E. A. *Rub. Chem. Tech.*, **50**, 35 (1977)

44. Yoshimura, N.; Fujimoto, K. *Rub. Chem. Tech.*, **42**, 1009 (1969)
45. Sperling, L. H.; Taylor, D. W.; Kirkpatrick, M. L.; George, H. F.; Bardman, D. R. *J. Appl. Poly. Sci.*, **14**, 73 (1970)
46. Xiao, H. X.; Frisch, K. C.; Frisch, H. L. *J. Poly. Sci. : Chem.*, **22**, 1035 (1984)
47. Coleman, M. M.; Lichkus, A. M.; Painter, P. C. *Macromolecules*, **22**, 586 (1989)



## CHAPTER 3

### AGGREGATION PHENOMENA IN IONOMERS AND IONOMER BLENDS

#### 3.1 Introduction

The viscoelastic behavior and morphology of ionomers was discussed in some detail in Chapter 1. The important points for this work are summarized here.

It is generally accepted that the polar ionic groups tend to aggregate due to electrostatic interactions, although the exact nature of the aggregation is still a matter of some speculation. The three major models of aggregation are the depleted zone core-shell model,<sup>3</sup> the hard sphere liquid-like interference model,<sup>4</sup> and the restricted mobility model.<sup>5</sup> The depleted zone core-shell model has been chosen to interpret the data in this chapter, and so will be described in some detail.

In the depleted zone core-shell model, the ionic groups are attracted to each other through electrostatic interactions to form what are termed "multiplets". The multiplets consist of ionic groups in contact with each other, and their size is limited by packing considerations. The multiplets aggregate to form "clusters", which are collections of multiplets with intervening hydrocarbon chains. Due to a balance between the electrostatic attraction and the entropic repulsion from chain stretching, a shell depleted in ionic groups is formed around the cluster core. Beyond the shell is the matrix, which contains a few isolated multiplets. A schematic diagram of this model is given in Figure 3.1.

Viscoelastic measurements on ionomers have shown the existence of a high temperature loss peak, which has been termed the ionic cluster transition.<sup>1,2</sup> This transition is interpreted as being due to motions within the clusters, although the exact

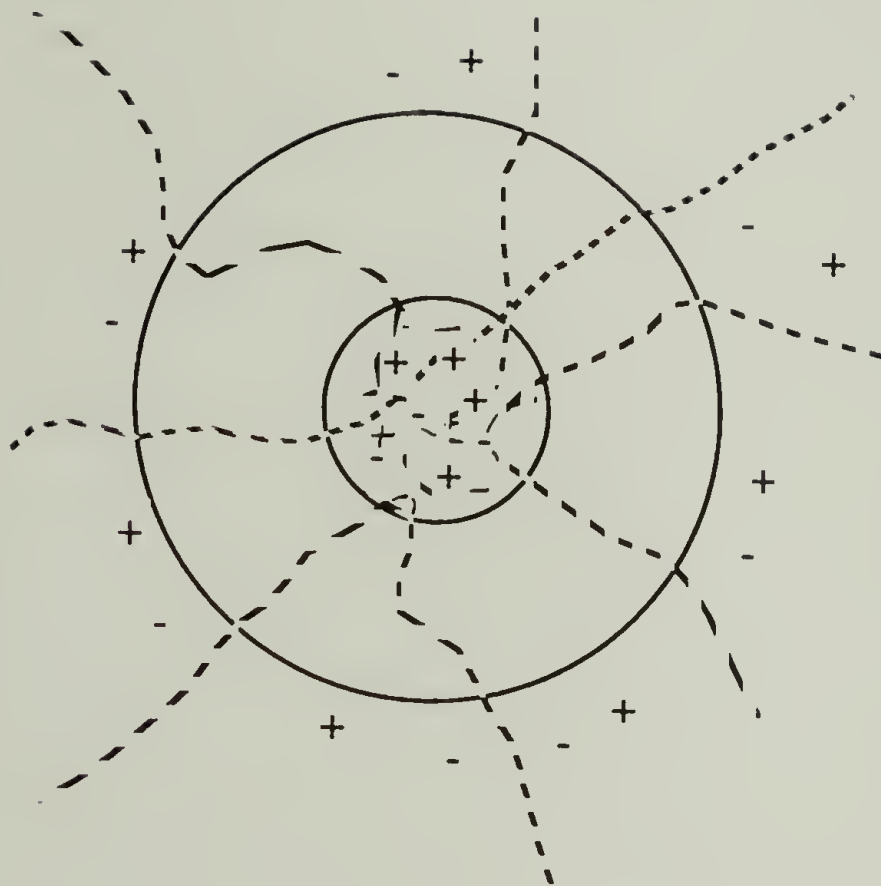


Figure 3.1: Schematic diagram of the depleted zone core-shell model.

nature of the motion is not clear. Some investigators have claimed that it is due to a glass transition within the cluster,<sup>6</sup> while others have explained it as being due to dissociation and motion of the ionic groups.<sup>2</sup> Small angle x-ray scattering measurements have shown the existence of a peak at a scattering vector  $q$  between 1 and 3 nm<sup>-1</sup>, and a low angle upturn.<sup>3,4,7</sup> The interpretation of these features is model dependent. In terms of the depleted zone core-shell model, the peak is due to the preferred distance between ionic groups determined by the thickness of the shell, and the upturn is due to Guinier scattering from isolated clusters.

It is well-known that the ionic peak in SAXS and the ionic transition in DMTA are affected by the type of cation, the amount of ionic groups, and the presence of low molecular weight compounds.<sup>1,2</sup> Investigations of plasticization in sulfonated polystyrene ionomers showed that either the polar ionic cluster or the non-polar parent matrix could be selectively plasticized, depending on the dielectric constant of the solvent used.<sup>8-10</sup> Studies on dielectric relaxations in ethylene ionomers showed that the addition of the complexing agent 1,3-bis(aminomethyl)cyclohexane (BAC) to transition metal neutralized ionomers enhanced cluster formation.<sup>11</sup>

As part of an extensive study of miscibility enhancement in ionomer blends, Simmons and Eisenberg noted that blends of ethyl acrylate/lithium acrylate copolymers with polyethyleneimine (PEI) showed a DMTA cluster transition that depended greatly on the PEI content.<sup>12</sup> However, no detailed analysis was performed. This work for the first time discusses in detail the effect of blending on ionic clusters. In addition it is hoped that the study of clustering in blends will provide some insight into the nature of clustering in ionomers.

## 3.2 Results and Discussion

### 3.2.1 Experimental

**Blending.** The blends used are the same as the ones described in Chapter 2. For a description of the blending procedure and the nomenclature for the blends, see Section 2.2.1.

**Dynamic Mechanical Thermal Analysis (DMTA).** DMTA was performed on a Polymer Laboratories DMTA operating in the shear mode. Samples were compression molded into discs approximately 1 mm thick by 12 mm in diameter. The molding temperatures were the minimum temperatures needed to cause flow, which were 175° C for the HSPS's and all SPS/EAVP blends, 200° C for the SPS/SVP blends, and 250° C for the ZSPS's. Samples were held at the molding temperature for 6 minutes, followed by quenching to room temperature. DMTA thermal scans were done from 50 to 300° C at 2° C/min at five frequencies (0.33, 1, 3, 10, 30 Hz) with a 64  $\mu\text{m}$  peak-to-peak displacement. The Polymer Labs DMTA multiplexes the frequencies, so a single scan generated the curves at all five frequencies. Two different samples were run for each material to ensure reproducibility.

DMTA isothermal scans were done on the ZSPS's and SPS/SVP blends. Isotherms were measured at every 10° C from 70 to 270° C, with 7 frequencies at each isotherm (0.033, 0.1, 0.33, 1, 3, 10, 30 Hz). The samples were allowed to equilibrate for 15 minutes at each temperature before measurement. Superposition of the isotherms was done empirically by shifting the  $\tan \delta$  isotherms to give the maximum overlap. The modulus isotherms were then superposed by applying arbitrary vertical shifts to the data.

**Density measurements.** Density measurements on all blends and SPS's were done in order to correct the small angle x-ray scattering data for absorption. Measurements were done in a density gradient column made of ethanol and aqueous sodium bromide

maintained at 23° C, which gave a density gradient of approximately 1.0 to 1.3 g/cm<sup>3</sup>. The column was calibrated with glass beads of known densities. The standards and samples were allowed to equilibrate in the column for 20 hours before measurement. The density results are given in Table 3.1

**Small angle x-ray scattering (SAXS).** Samples for SAXS measurements were prepared by compression molding into bars 20 mm x 5 mm x 1.5 mm under the same conditions as described above for the DMTA measurements. The samples were then annealed at 150° C for 24 hours followed by slow cooling over several hours to room temperature.

SAXS measurements were done on a Rigaku-Denki camera using slit collimation. A schematic diagram of the collimation system is shown in Figure 3.2. The essentials of the collimation system are as follows: the 1st and 2nd slits act to collimate the main beam; the 3rd slit eliminates scattering from the edges of the 1st and 2nd slits; the receiving and scatter slits collimate the scattered beam; and the Soller slits eliminate any x-rays scattered along the length of the slit.

The Cu k $\alpha$  x-rays were generated by a sealed tube source operating at 45 kV, 33 mA. Monochromatization was achieved by use of a pulse height analyzer. The pulse height analyzer works by discriminating the amplitudes of the pulses generated by the counter, accepting only those pulses which fall within a certain voltage range. Such a system is very effective in eliminating electronic noise and harmonics.

The x-rays were detected using a scintillation counter. The counter was placed on a stepper motor, and the scans were conducted from 0.2 to 6.5° 2 $\theta$  in 0.05° steps with a 600 second acquisition time at each angle. The data were corrected for parasitic scattering, absorption, slit smearing, and irradiated sample volume.

In order to correct for absorption, the linear absorption coefficient was calculated from the mass absorption coefficient of each element, its weight fraction in the material, and the material's density by:<sup>13</sup>

Table 3.1 : Densities and absorption parameters for x-ray analysis.

material	$\mu/\rho$ (cm <sup>2</sup> /g)	$\rho$ (g/cm <sup>3</sup> )	$\mu$ (cm <sup>-1</sup> )
polystyrene	4.278	1.042	4.457
2HSPS	4.656	1.043	4.856
5HSPS	5.885	1.044	6.144
8HSPS	6.391	1.059	6.768
2ZSPS	5.598	1.052	5.889
5ZSPS	7.580	1.109	8.406
7ZSPS	8.541	1.122	9.583
2Z2	5.971	1.112	6.639
5Z5	6.994	1.127	7.883
7Z10	7.691	1.139	8.760
2H2	5.368	1.100	5.905
5H5	6.131	1.127	6.910
8H10	6.345	1.123	7.126
2H2S	4.497	1.043	4.691
5H5S	4.990	1.050	5.240
8H8S	5.370	1.046	5.616
2Z2S	4.971	1.042	5.180
5Z5S	5.784	1.052	6.084
7Z8S	6.553	1.067	6.992

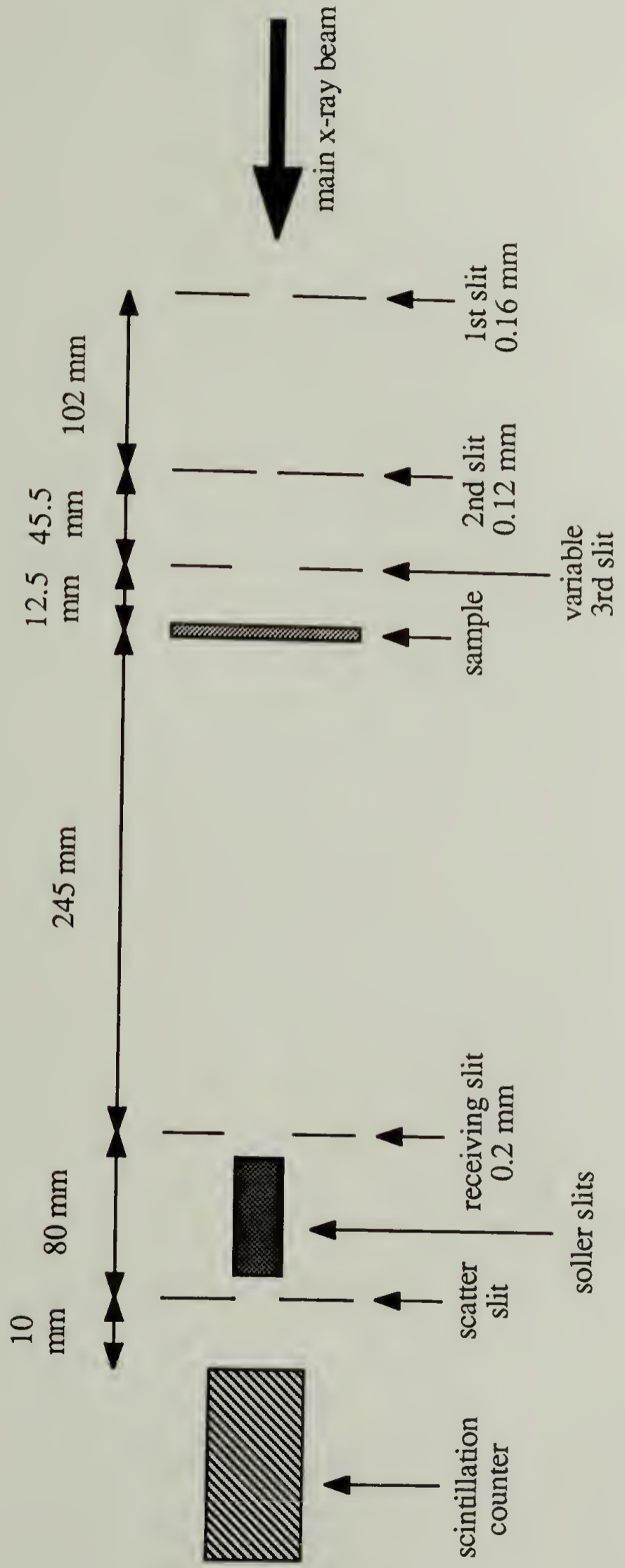


Figure 3.2: Schematic diagram of x-ray collimation system.

$$\mu = \rho \sum w_i (\mu/\rho)_i \quad (3.1)$$

The mass and linear absorption coefficients are listed in Table 3.1. The fraction of x-rays not absorbed by the sample was determined from:<sup>13</sup>

$$f = \frac{A}{\mu (1 - \sec 2\theta)} e^{-\mu t \sec 2\theta} [1 - e^{-\mu t (1 - \sec 2\theta)}] \quad (3.2)$$

where A is the irradiated sample area and t is the sample thickness. This equation accounts for the difference in path length an x-ray traverses depending on the angle at which it is scattered. In order to correct for absorption and parasitic scattering the experimentally determined background was multiplied by the calculated values of f, and the resulting curve was subtracted from the experimental curve for the sample.

Whenever slits are used for collimation it is important to correct for the slit smearing effect. Slit smearing occurs because each volume element along the slit contributes to the scattered intensity at all angles, resulting in distortion of the scattering curve. Desmearing was performed using software provided by Rigaku-Denki, which is based on the method of Glatter.<sup>14</sup> There are three parameters in the desmearing routine which must be chosen by the user: the number of iterations, the smoothing parameter, and the convergence factor. The smoothing parameter determines the range over which the data is smoothed to prevent divergence caused by noise in the data. The convergence factor determines how quickly the desmearing routine reaches a stable solution. The effect of each of these parameters is shown for 7ZSPS in Figure 3.3. The optimal parameters were chosen as the ones that give maximum intensity in the desmeared data without divergence. As can be seen from Figure 3.3, these parameters are 10 iterations, a smoothing factor of 3, and a convergence factor of 10.0. A comparison of the resulting desmeared curve and the original smeared curve for 7ZSPS is shown in Figure 3.4.



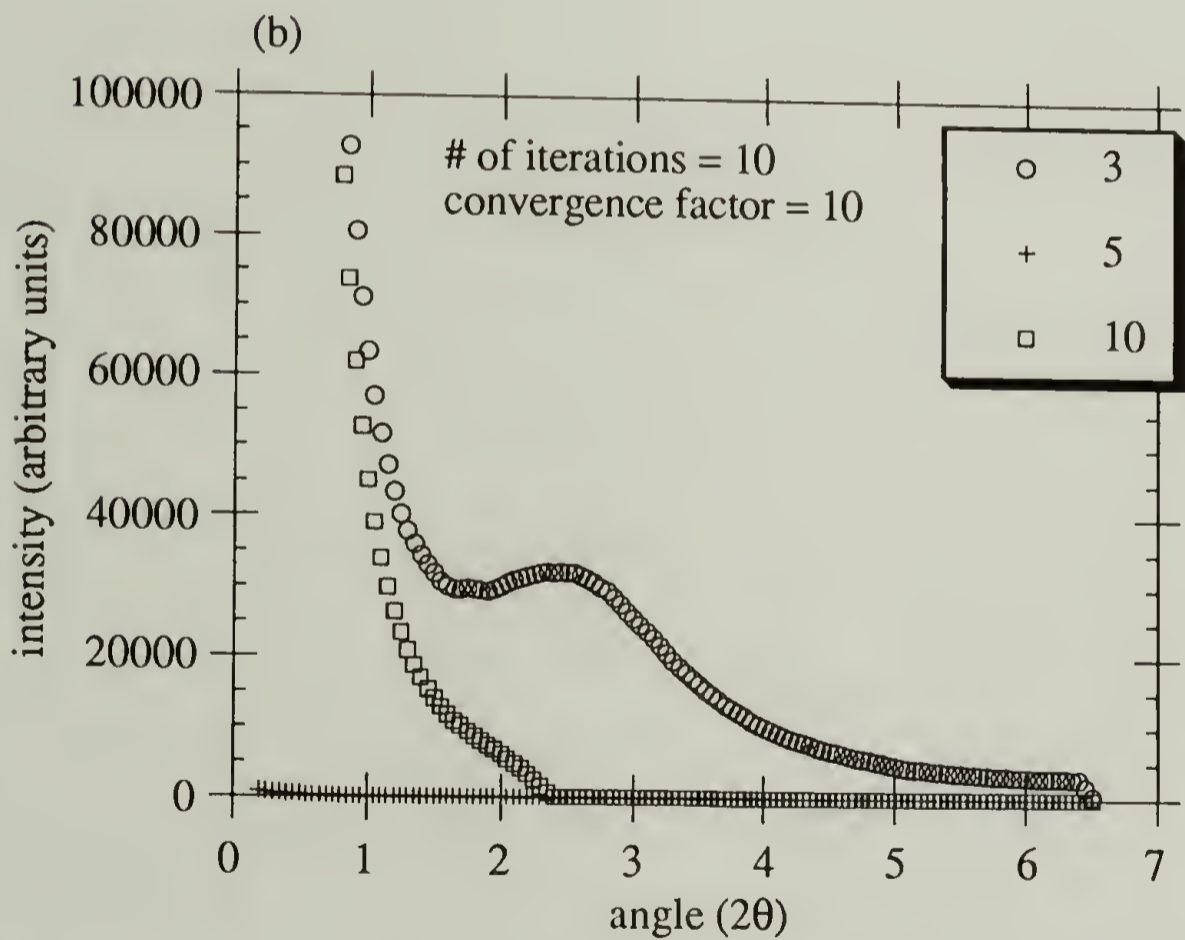
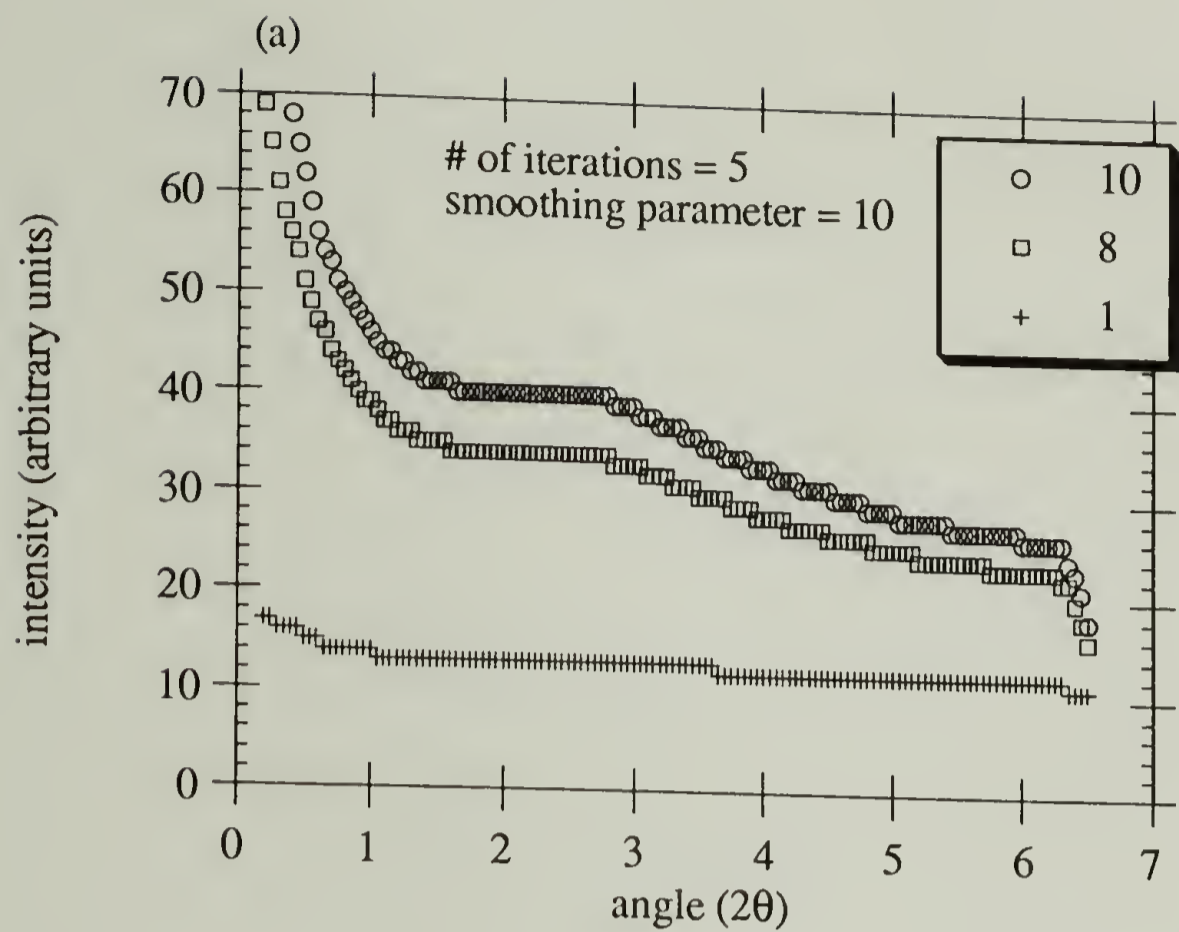


Figure 3.3: Effect of (a) convergence factor, (b) smoothing parameter, and (c) number of iterations on the desmeared SAXS curves of 7ZSPS.

continued on next page

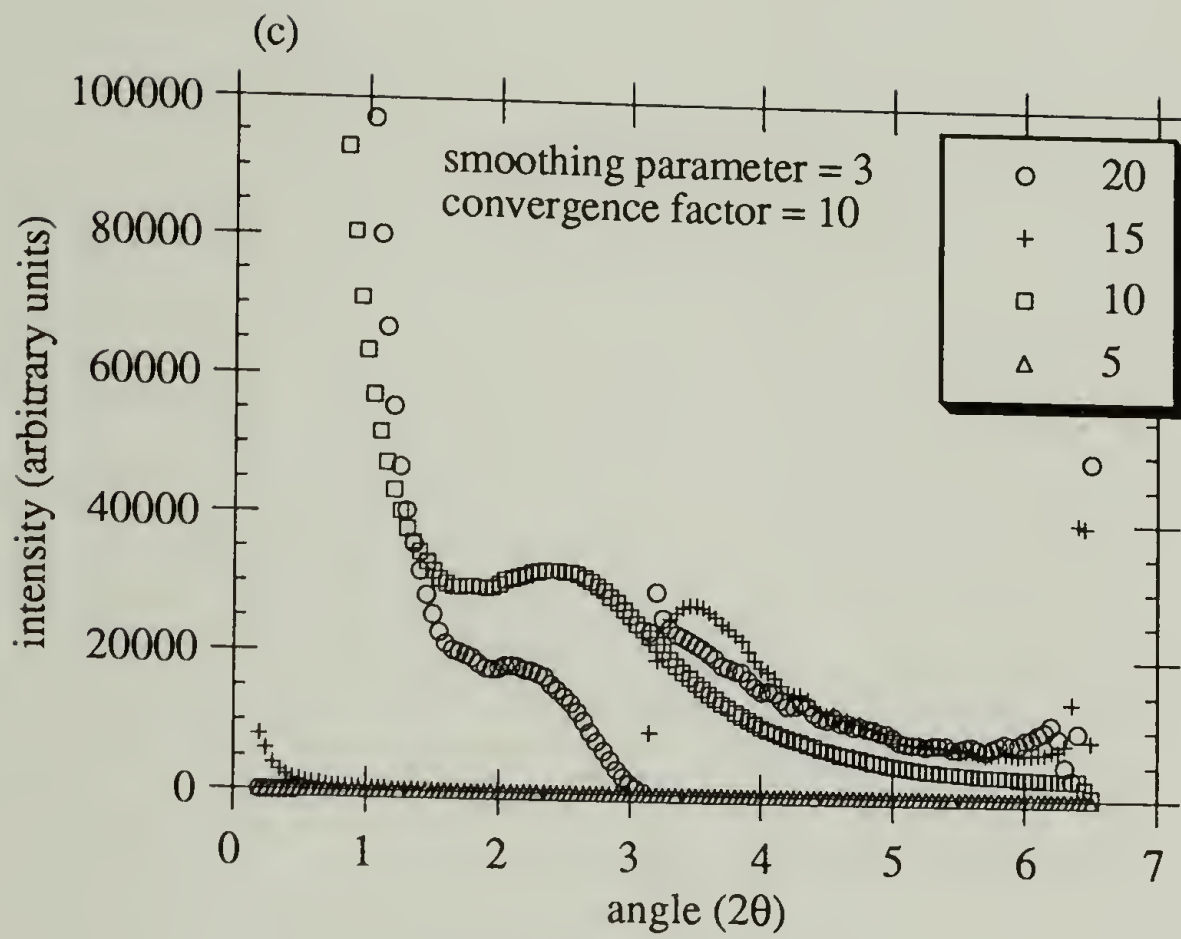


Figure 3.3 (continued)

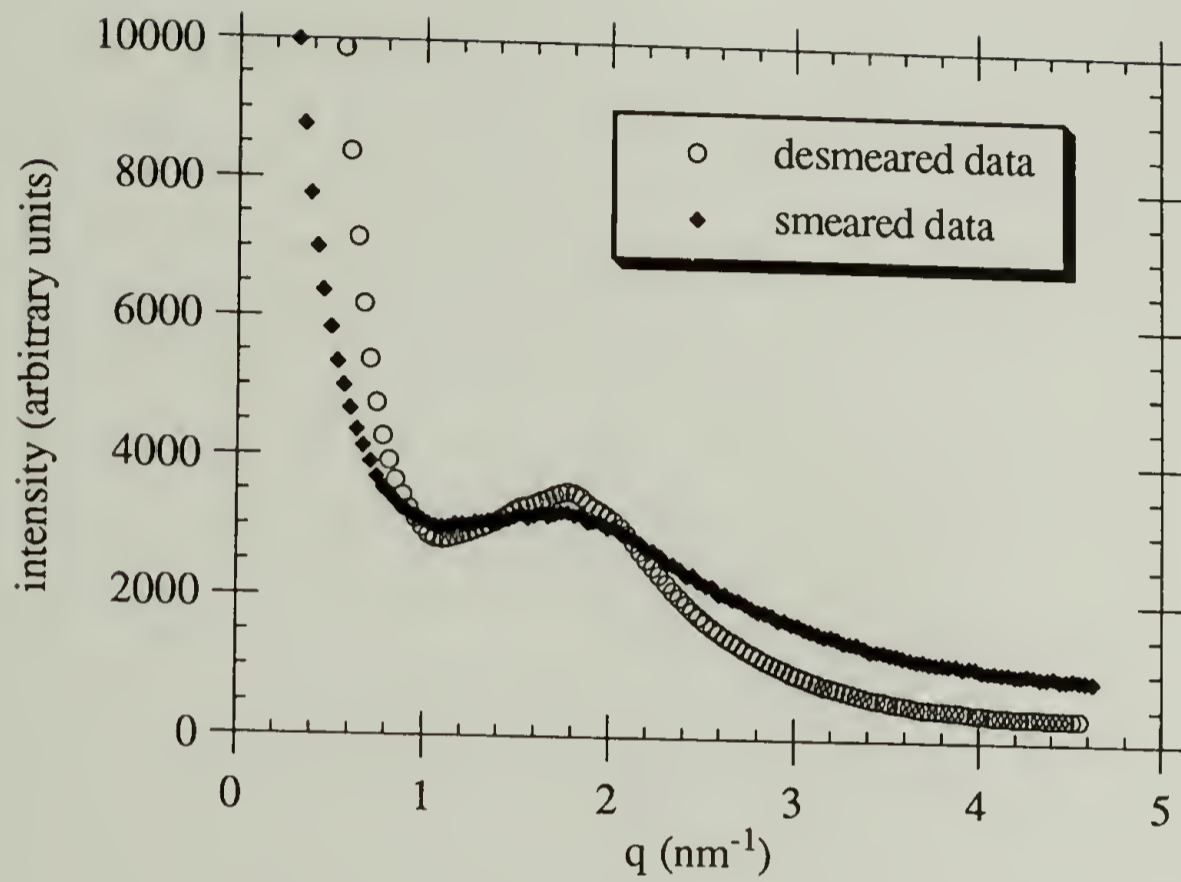


Figure 3.4: Comparison of smeared and desmeared SAXS curves of 7ZSPS.

### 3.2.2 Viscoelastic Behavior

Dynamic mechanical measurements have been used extensively to examine aggregation in ionomers.<sup>15-17</sup> Ionomers exhibit a high temperature loss peak, which has been called the ionic cluster transition. The storage modulus exhibits a plateau, reminiscent of the plateau seen in crosslinked systems. These features are evident in the multifrequency plot for 5ZSPS shown in Figure 3.5. The loss peak has been interpreted as being due to motions within the ionic aggregates, although the exact nature of these motions is not clear. They have been described as the glass transition of hydrocarbon chains associated with the cluster,<sup>6</sup> or alternatively as being due to the thermal breakup and subsequent motions of the ionic groups themselves.<sup>2</sup> The plateau in the storage modulus is generally described as being a rubbery plateau, due to ionic crosslinking by the aggregates.<sup>17</sup> In addition to the crosslinking effect, Connolly has described the plateau as being due to the two phase nature of ionomers, with the aggregates acting as reinforcing filler particles.<sup>16</sup>

Figure 3.6 shows the modulus and loss curves for 8HSPS. There is some question over whether or not the acid form of sulfonated polystyrene shows an ionic cluster transition. Most authors state that HSPS does not form clusters because the hydrogen bonding between sulfonic acid does not provide a sufficient driving force for aggregation.<sup>1,18</sup> More recently, however, there have been a few reports of a cluster transition in HSPS.<sup>16,19</sup> The data in Figure 3.6 show an apparent loss peak at approximately 220° C, but careful examination shows that the peak is independent of frequency, in contrast to the frequency dependence for the cluster transition seen in Figure 3.5. This apparent peak is more likely caused by dimensional changes of the sample due to flow. The Polymer Labs instrument measures the stiffness of the sample, which is the product of the modulus and a geometric factor. If the sample dimensions change during a scan then the stiffness will change, which is interpreted by the instrument as a change in modulus. In fact, by the end of the scan the sample has flowed out from between the

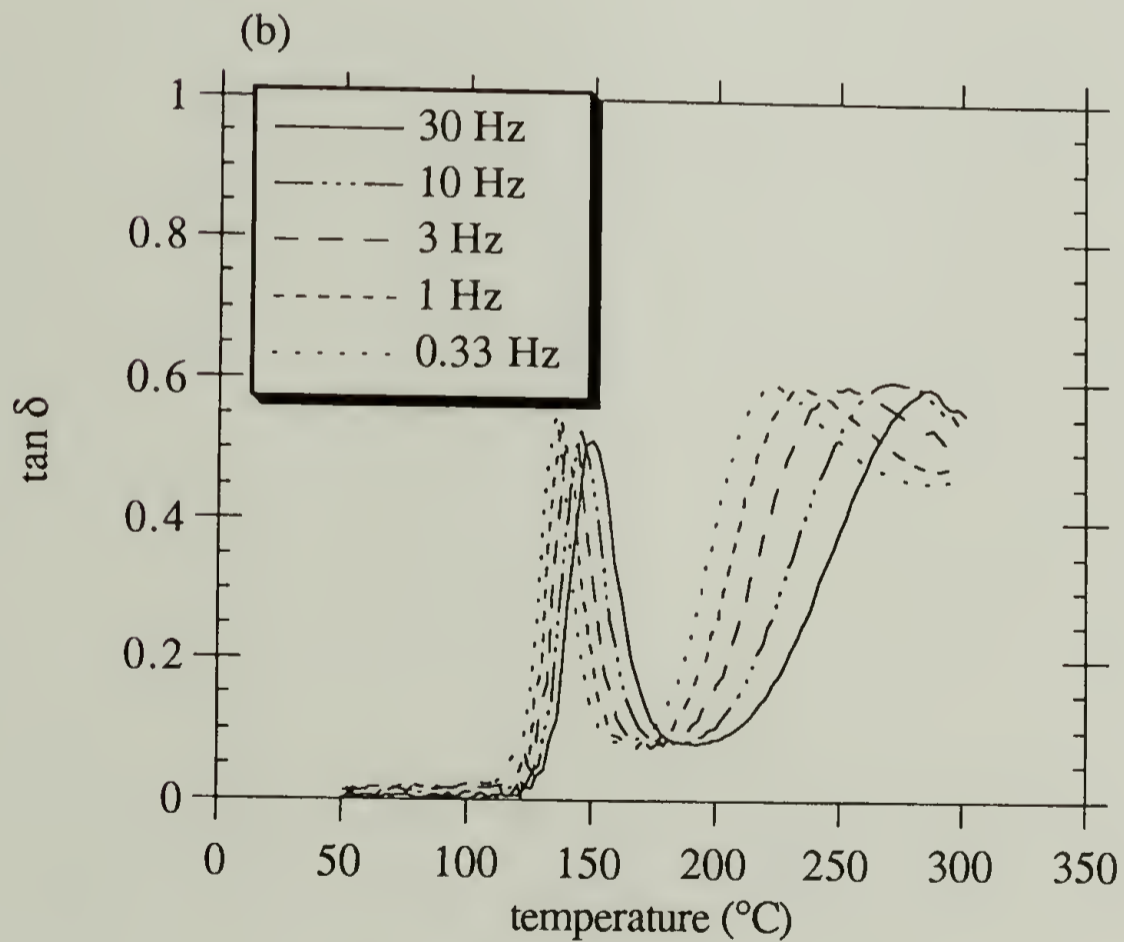
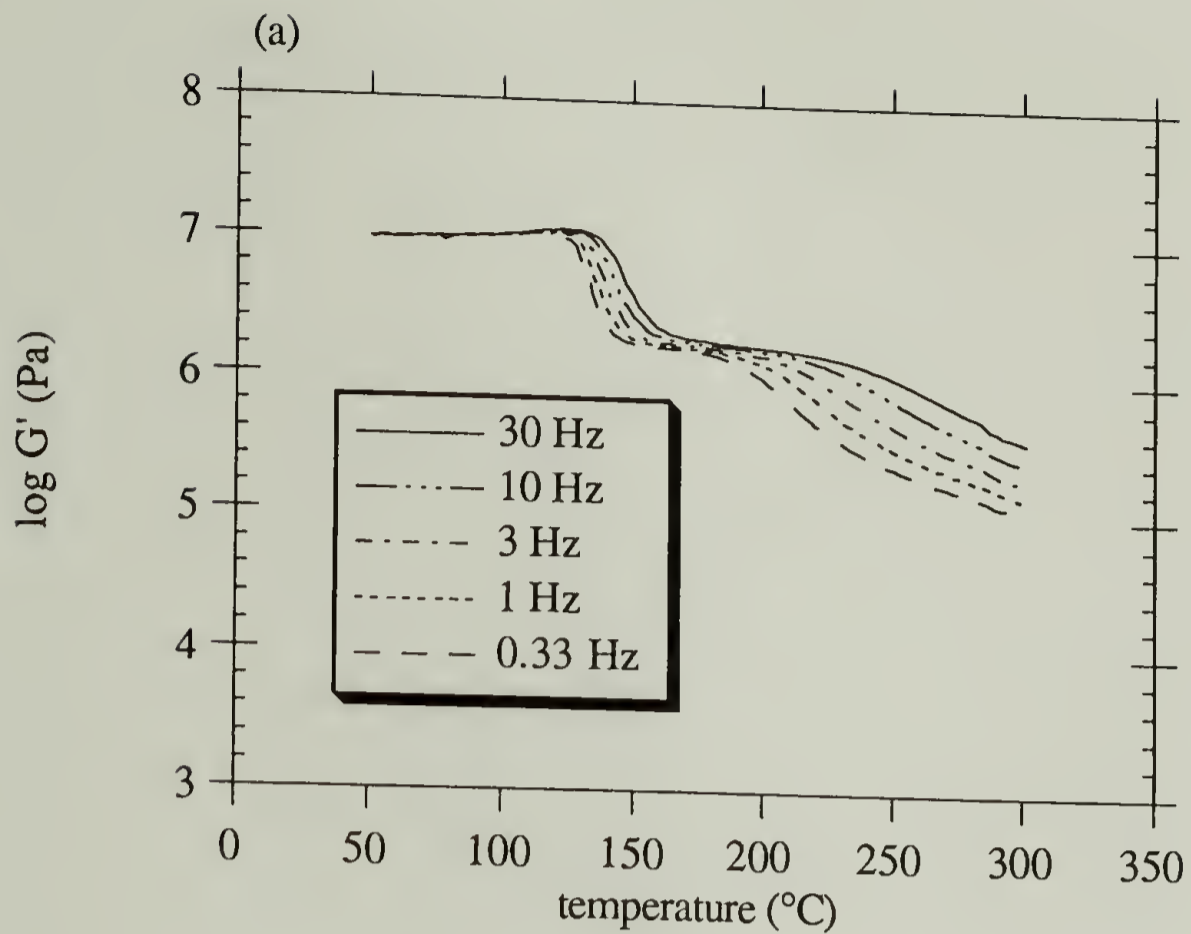


Figure 3.5: Multifrequency DMTA plots of (a) storage modulus and (b)  $\tan \delta$  for 5ZSPS in shear.

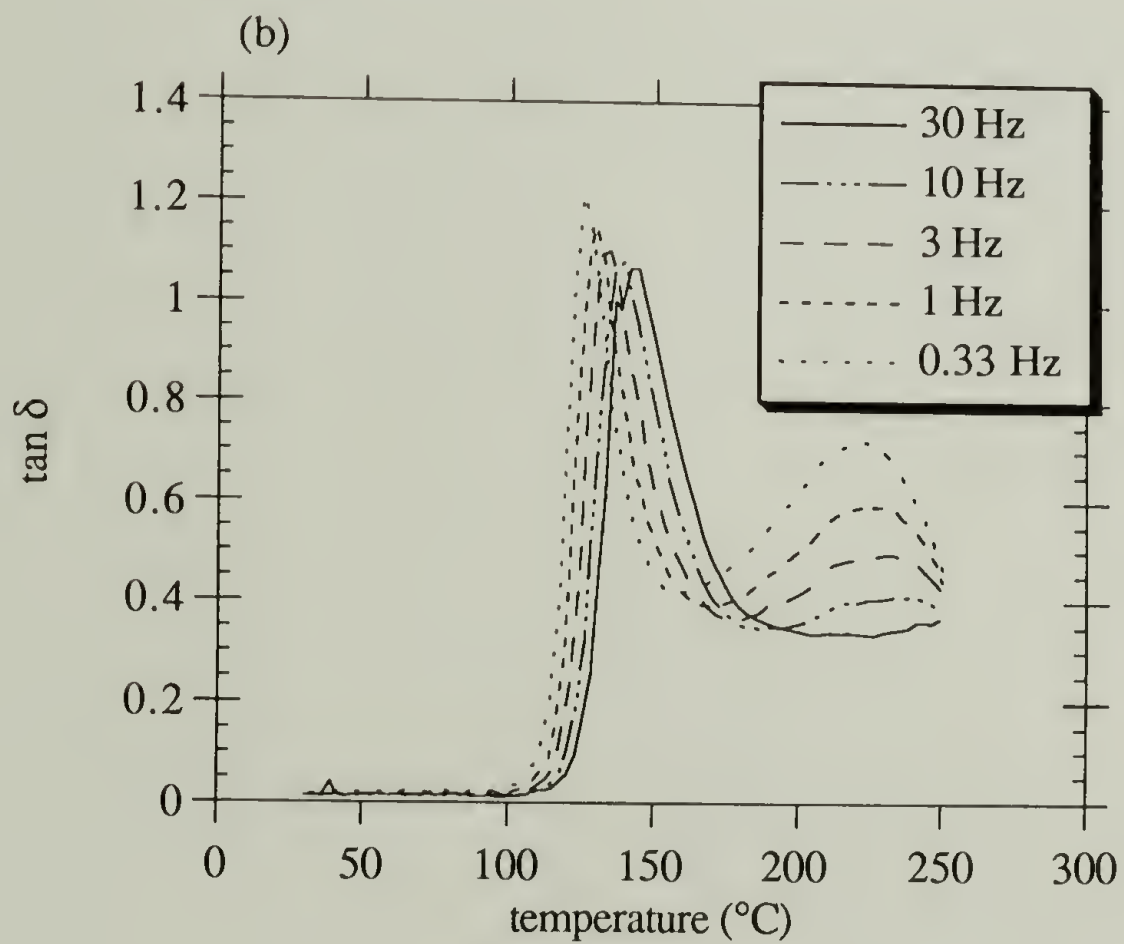
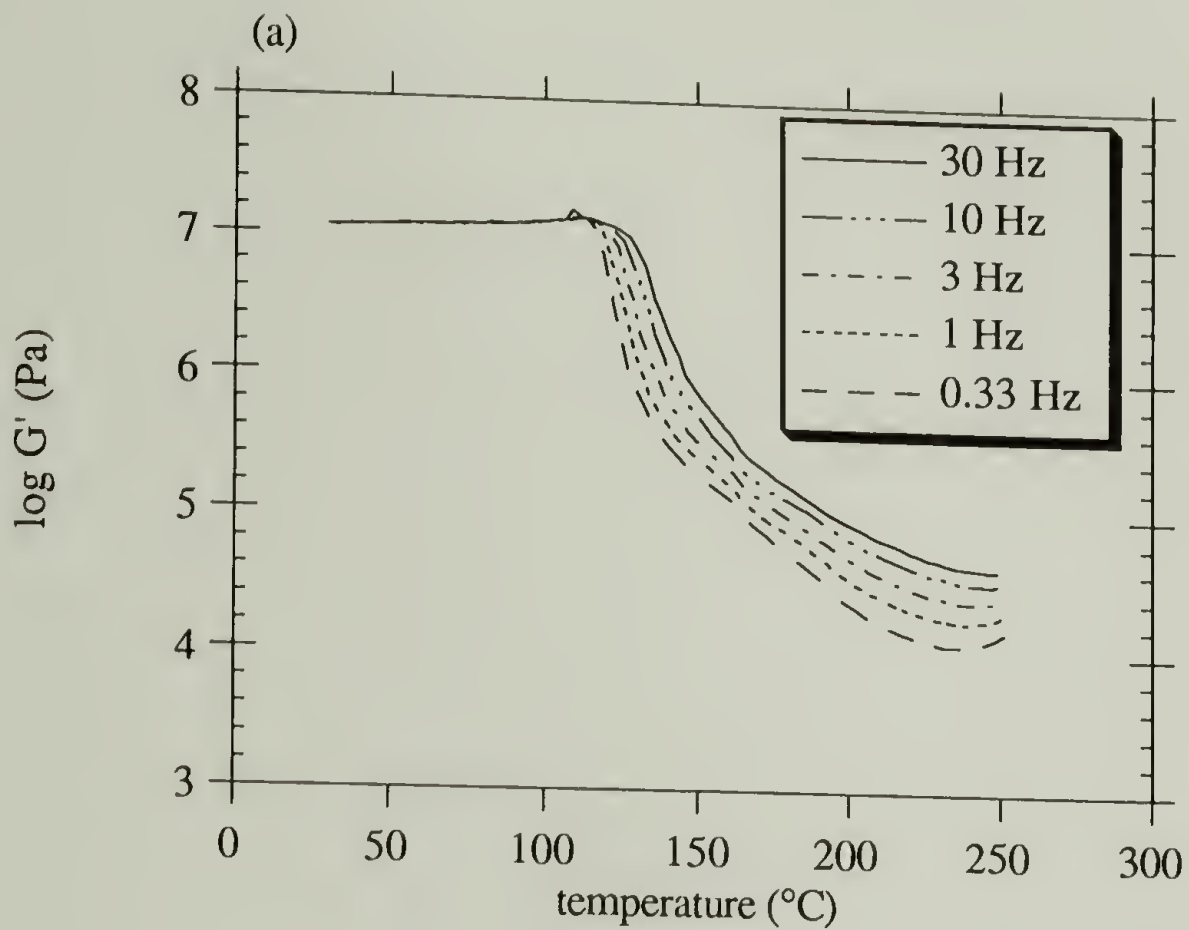


Figure 3.6: Multifrequency DMTA plots of (a) storage modulus and (b)  $\tan \delta$  for 8HSPS in shear.

clamps, which would result in a drop in the apparent modulus and the appearance of a loss peak. Thus, it must be concluded that the HSPS's used in this study do not show a cluster transition.

The loss curves for all the blends and the ZSPS ionomers at 1 Hz are shown in Figure 3.7. The arrows in the figure indicate the cluster transition. Figure 3.8 shows the cluster transition temperatures for all the materials, and the values are listed in Table 3.2. Blending obviously has a profound effect on the cluster transition temperature in the zinc-neutralized materials. The difference in the transitions between ZSPS and ZSPS/SVP blends ranges from 40 to 60° C, and is due to the bulkiness of the pyridine substituent. The bulkiness increases the free volume of the cluster, and thus acts as a classical plasticizer. The ZSPS/EAVP blends exhibit cluster transitions another 40° C lower than the ZSPS/SVP blends due to the plasticization effect of the ethyl acrylate segments incorporated into the cluster. Poly(ethyl acrylate) has a much greater mobility than polystyrene at these temperatures, since the temperature of the transition is approximately 170° C above the  $T_g$  for poly(ethyl acrylate) as opposed to only 50° C above  $T_g$  for polystyrene. Thus, the ethyl acrylate segments are expected to be an efficient plasticizer for the clusters. The amount of the decrease in the transition temperature in the ZSPS/EAVP blends is similar to what has been seen when ionomers are plasticized with a polar small molecule plasticizer such as glycerol, which is selective for the clusters.<sup>8-10</sup>

There is apparently a fairly strong dependence of the cluster transition temperatures on substitution level for the ZSPS/SVP and ZSPS/EAVP blends. The dependence in ZSPS/EAVP blends is due to the amount of ethyl acrylate incorporated into the clusters. For a given number of ionic groups in a cluster, a lower substitution level will necessarily have more ethyl acrylate present, because there are longer ethyl acrylate segments between the ionic groups. Thus the plasticization effect will be stronger at a lower substitution level. The plasticization is so strong in blend 2Z2 that the cluster transition falls below the glass transition and cannot be detected.

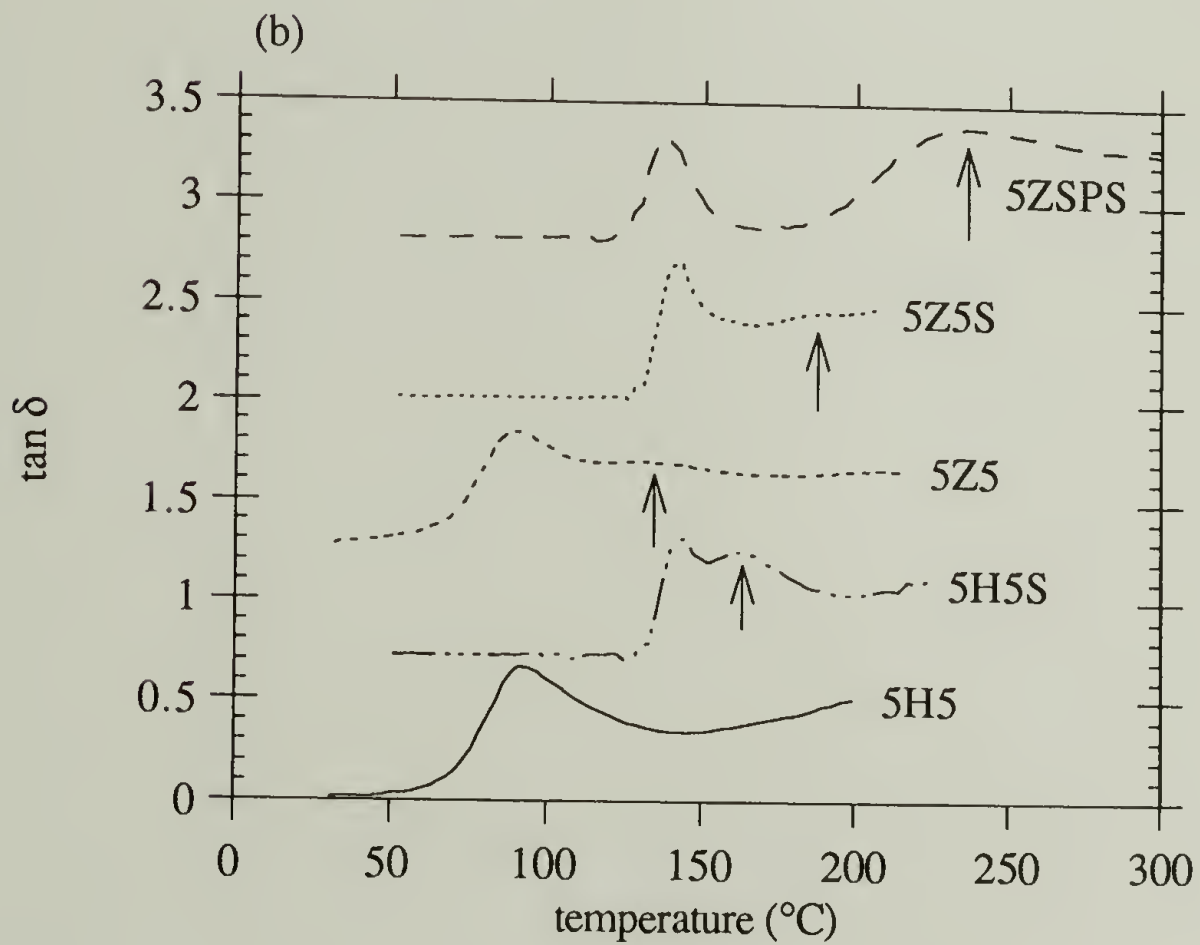
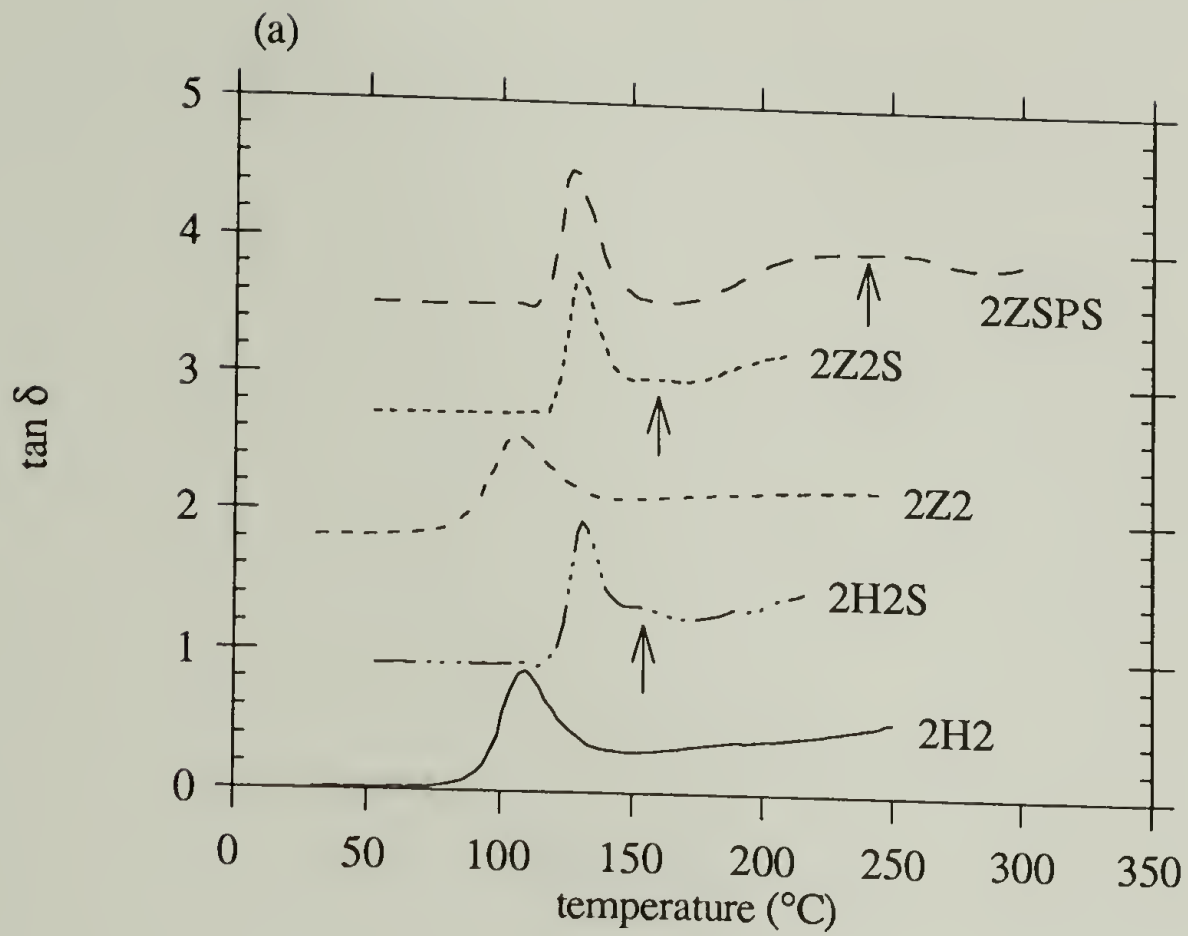


Figure 3.7: Tan  $\delta$  at 1 Hz in shear for (a) 2%, (b) 5%, and (c) 8% substitution levels. The curves have been shifted vertically for clarity. Arrows indicate the cluster transitions.

continued on next page



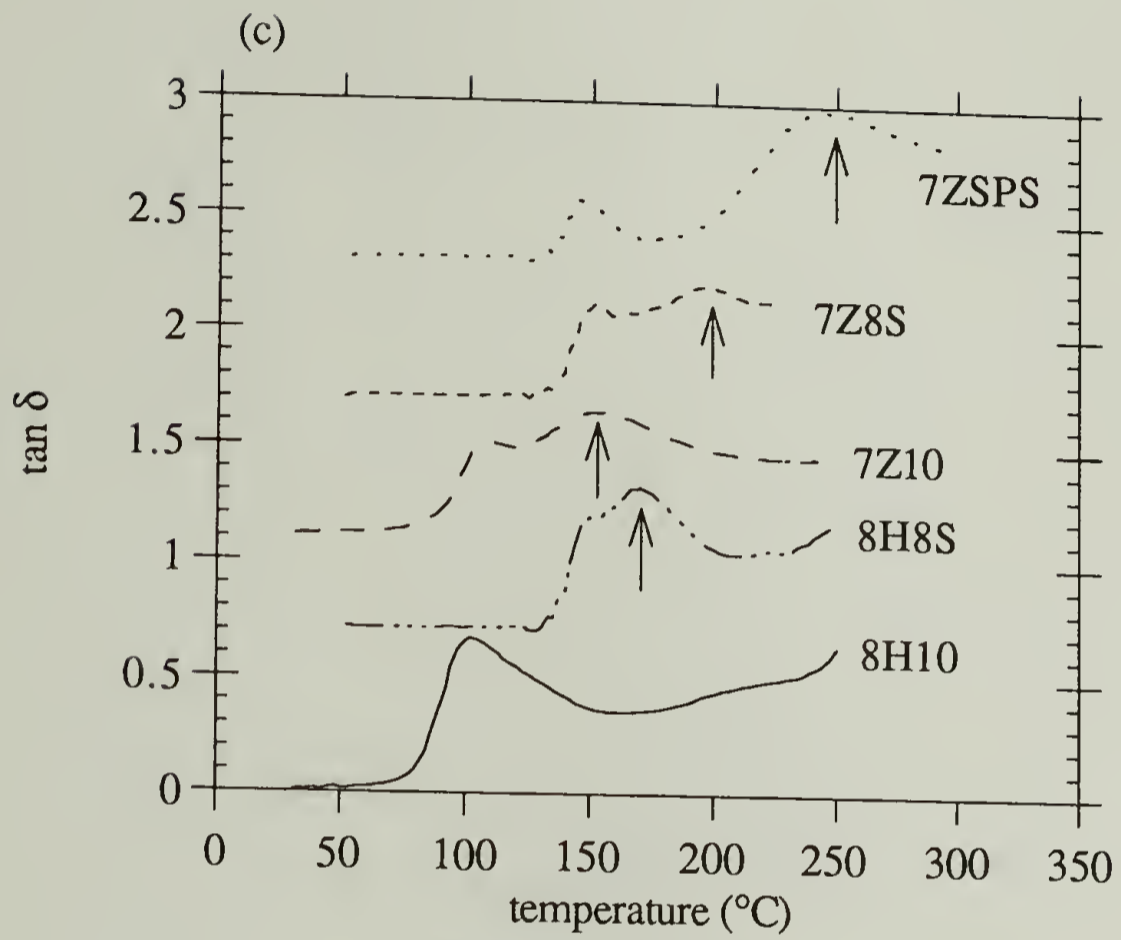


Figure 3.7 (continued)

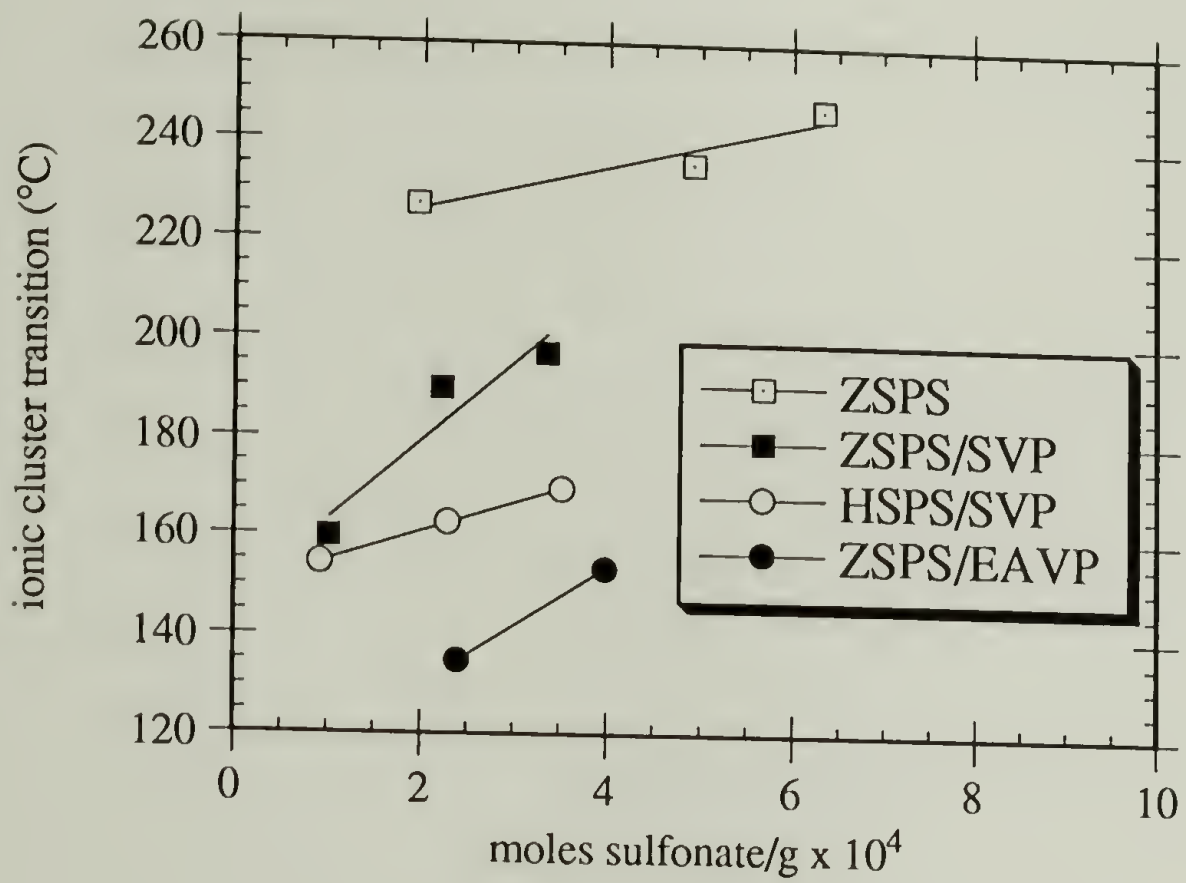


Figure 3.8: Ionic cluster transition temperatures.

Table 3.2 : Ionic cluster transition temperatures and activation energies.

material	T <sub>ionic</sub> (°C) <sup>a</sup>	E <sub>a</sub> (kJ/mole)
2ZSPS	227.0 ± 2.0	161.8 ± 5.0
5ZSPS	235.5	157.9
7ZSPS	247.0	169.8
2Z2	-----	-----
5Z5	134.9	124.8
7Z10	153.7	146.2
2Z2S	160.0	220.9
5Z5S	189.8	192.2
7Z8S	197.0	220.7
2H2S	154.5	288.1
5H5S	162.8	299.6
8H8S	169.8	305.0

<sup>a</sup>Taken as the position of the peak in tan  $\delta$  at 1 Hz

The substitution level dependence in ZSPS/SVP blends is not as easily explained, but it may be due to the greater cooperativity of motion among different chains needed to form a cluster in the blends compared to ZSPS. This greater cooperativity arises because the zinc ion is coordinated to only two sulfonates in the ionomer, while it is coordinated to two sulfonates and two pyridines in the blends.<sup>20</sup> Thus, in the ionomer only two chains need to move to allow the ionic group to become part of a cluster, while in the blend four chains need to move. It is not obvious, however, why this would cause a substitution level dependence on the cluster transition temperature.

As was stated previously, the HSPS's used in this study do not show a cluster transition. However, the HSPS/SVP blends do show a cluster transition. The driving force for aggregation in ionomers is electrostatic interactions between the charged species.<sup>21</sup> In blends containing HSPS the interaction occurs via proton transfer from the sulfonic acid to the pyridine, resulting in a sulfonate anion and a pyridinium cation.<sup>22</sup> One might think of this situation as a double ionomer, in which the neutralizing species for one ionomer is the other ionomer. The resulting electrostatic interactions result in the formation of aggregates. A similar effect has been seen by Yano et al. in transition metal neutralized ionomers using dielectric measurements.<sup>11</sup> The neat ionomer does not show a cluster transition, but the ionomer with an added complexing agent does show a cluster transition. The action of the complexing agent is apparently to increase the charge density on the transition metal, resulting in a stronger electrostatic driving force for aggregation.

The difference in transition temperatures between the zinc ionomers and the acid blends is again due to the bulkiness of pyridine. The absence of a cluster transition in HSPS/EAVP blends is because of plasticization by ethyl acrylate. The transition temperature is already so low for the HSPS/SVP blends that the incorporation of any ethyl acrylate reduces the cluster transition to below the glass transition temperature.

Activation energies for the cluster transitions can be determined according to the Arrhenius equation:

$$f = f_0 e^{-E_a/RT} \quad (3.3)$$

where  $f$  is the frequency in Hertz,  $E_a$  is the activation energy,  $R$  is the ideal gas constant, and  $T$  is the temperature of the transition. Typical Arrhenius plots for all materials at the 5% substitution level are shown in Figure 3.9. The plots are fairly linear, although the limited frequency range makes it impossible to determine whether or not the data actually follow an Arrhenius-type of dependence.

The values for the activation energies are shown in Figure 3.10 and listed in Table 3.2. It has been proposed that flow in ionomers occurs via an ion-hopping mechanism.<sup>23</sup> Dissociation of ionic groups from the clusters depends on the strength of the electrostatic interactions between the ionic groups, and thus should be related to their relative charge densities. The order in which the activation energies occurs can be rationalized on this basis. The acid blends have complete charge separation between the sulfonate anion and pyridinium cation, resulting in a high charge density and the highest activation energies. In the zinc blends the zinc ion is coordinated to pyridine, resulting in partial charges on the zinc and the pyridine and a lower charge density than in the acid blends. In the zinc ionomer the zinc is coordinated to water, which is a weaker ligand than pyridine, and so the charge separation is even lower. The ZSPS/EAVP blends are affected by the higher dielectric constant of the ethyl acrylate, which partially screens the charges and reduces the electrostatic interactions.

Since the activation energies for the cluster transitions are clearly determined by the electrostatic interactions between ionic groups, the results support the idea that the cluster transition is a result of the dissociation and motion of the ionic groups. This is in direct contrast to the statement of other authors that the cluster transition is related to a glass transition of hydrocarbon chains associated with the cluster.<sup>6</sup> This result has some implications for models of the nature of aggregation in ionomers, as will be discussed later.

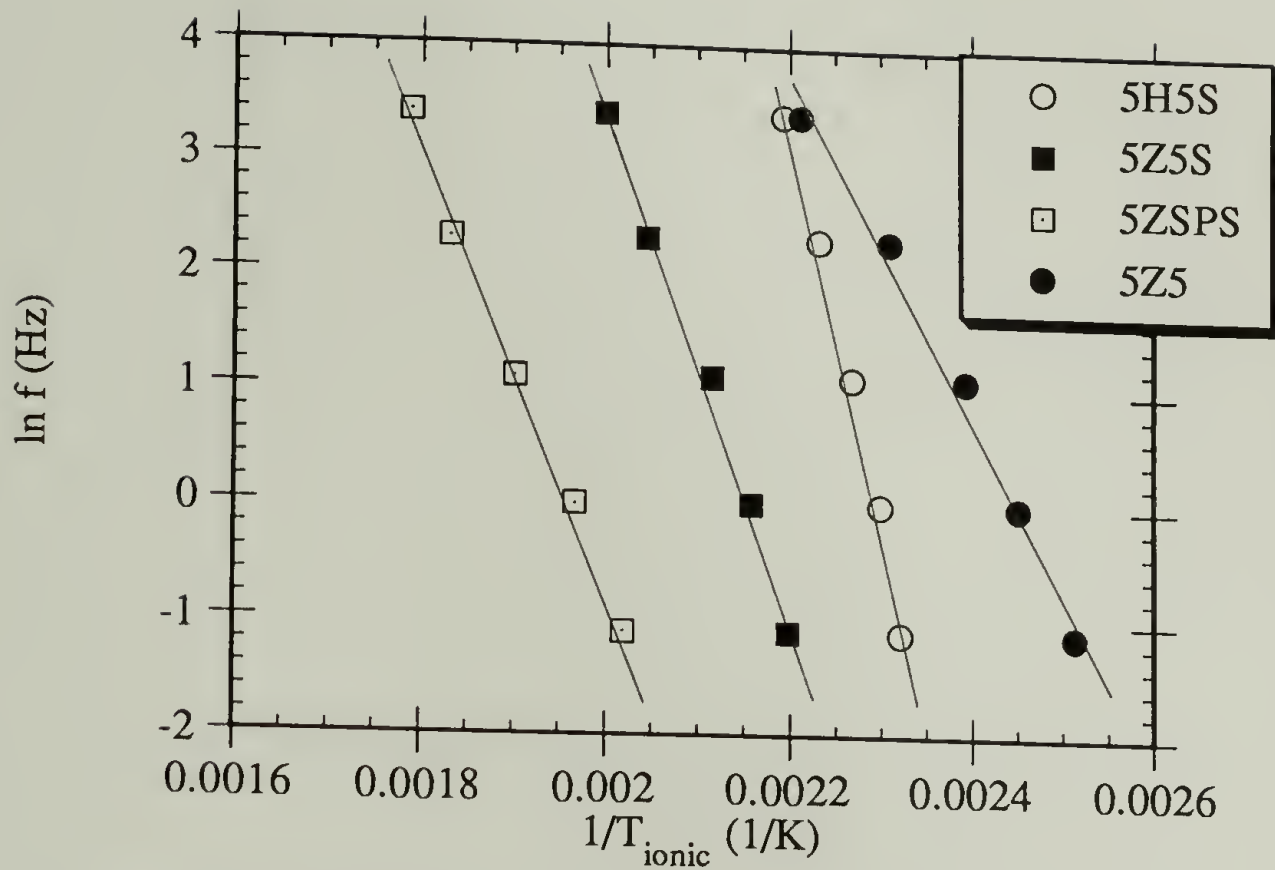


Figure 3.9: Arrhenius plots of the ionic cluster transition for blends and ionomers at 5% substitution level.

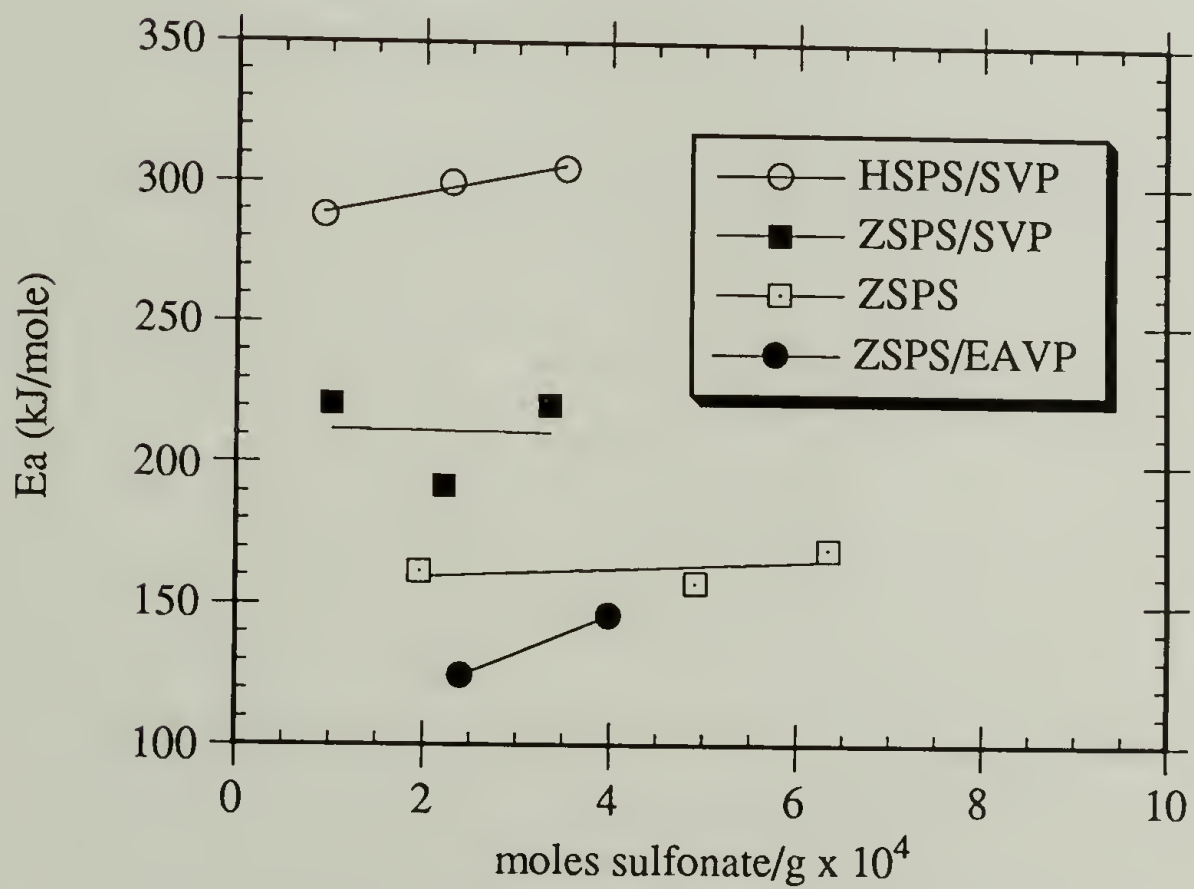


Figure 3.10: Ionic cluster transition activation energies.

The storage modulus curves for all materials at 1 Hz are shown in Figures 3.11 and 3.12. The values for the modulus in the glassy region are two orders of magnitude lower than expected due to an artifact of the instrument. The Polymer Labs DMTA only operates within a certain range of stiffness. Samples which are too stiff, as is the case for these samples in the glassy state, give modulus values which are unrealistically low. Once the samples have gone through the glass transition their stiffness drops dramatically, and the true storage modulus can be measured.

The modulus curves for the acid blends in Figure 3.11 show that the modulus is increased due to the presence of ionic crosslinks. The curve for 8HSPS is higher than for the unfunctionalized blend due to hydrogen bonding interactions between the sulfonic acid groups. The styrene/styrene acid blends all have higher moduli than 8HSPS, even at 2% substitution level, and the modulus increases with the number of interactions. This is the behavior that would be expected if the interactions act as crosslinks. It is important to note, however, that there is no rubbery plateau, as there would be for a covalently crosslinked rubber. This is because the difference between the glass transition and the cluster transition for the HSPS/SVP blends is so small that any plateau would not be detected.

The moduli for the HSPS/EAVP blends are lower than for 8HSPS. This is because the ethyl acrylate component lowers the glass transition of the blend significantly compared to 8HSPS. If the modulus curves were shifted vertically so that the glass transitions overlapped they would exhibit the same characteristics as the HSPS/SVP blends. The absence of a plateau is because the HSPS/EAVP blends do not exhibit a cluster transition, and so the crosslinks are labile at all temperatures above  $T_g$ .

The behavior of the zinc blends shown in Figure 3.12 is very different. The plateau that is present in the ionomer is no longer present in the blends, and the modulus curves lie below the curve for the ionomer. The absence of the plateau is again due to the small difference between the glass transition and the cluster transition. The drop in the modulus

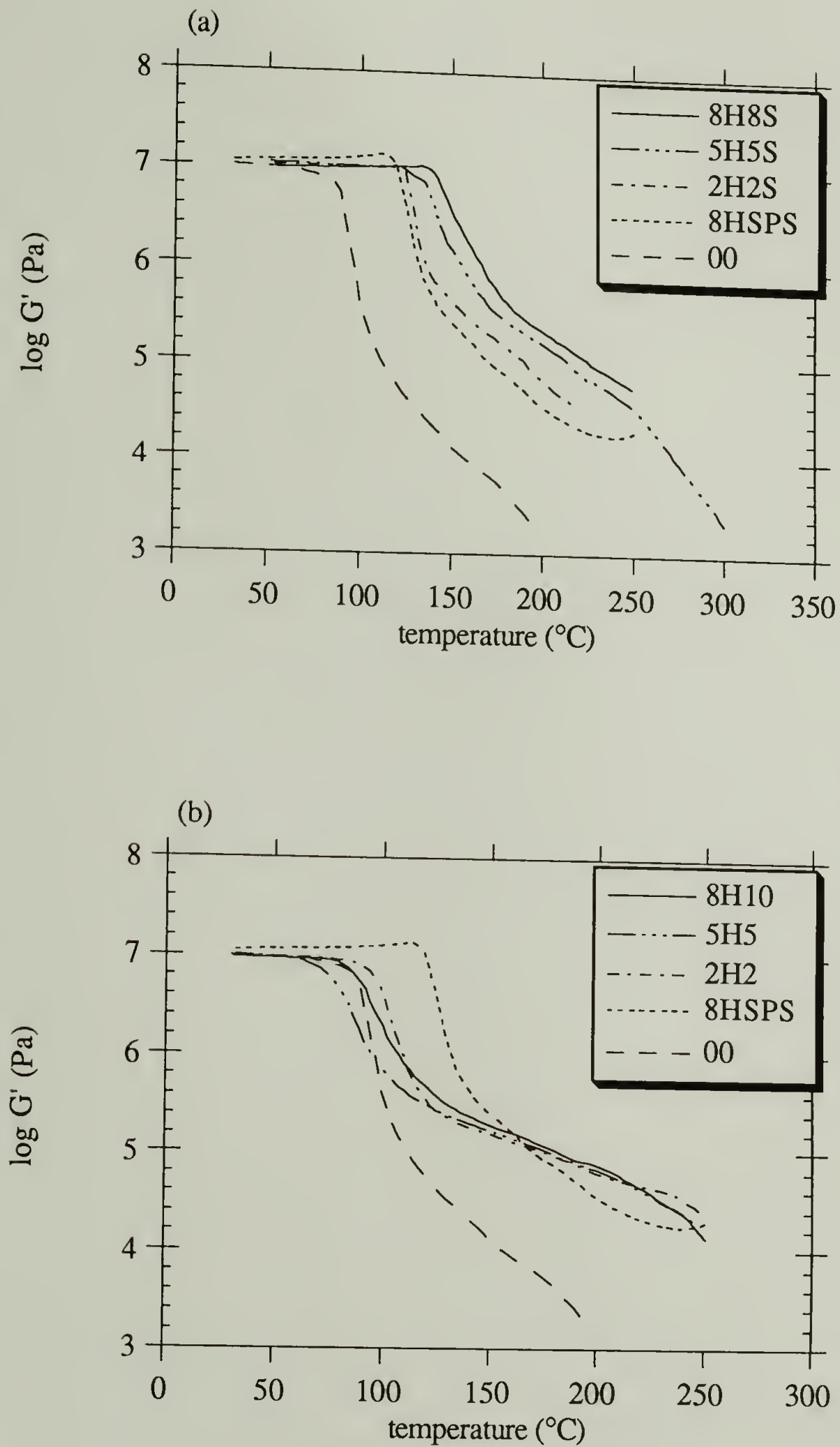


Figure 3.11: Shear storage moduli at 1 Hz for (a) acid styrene/styrene and (b) acid styrene/ethyl acrylate blends. Curves have not been corrected for machine compliance at low temperatures.



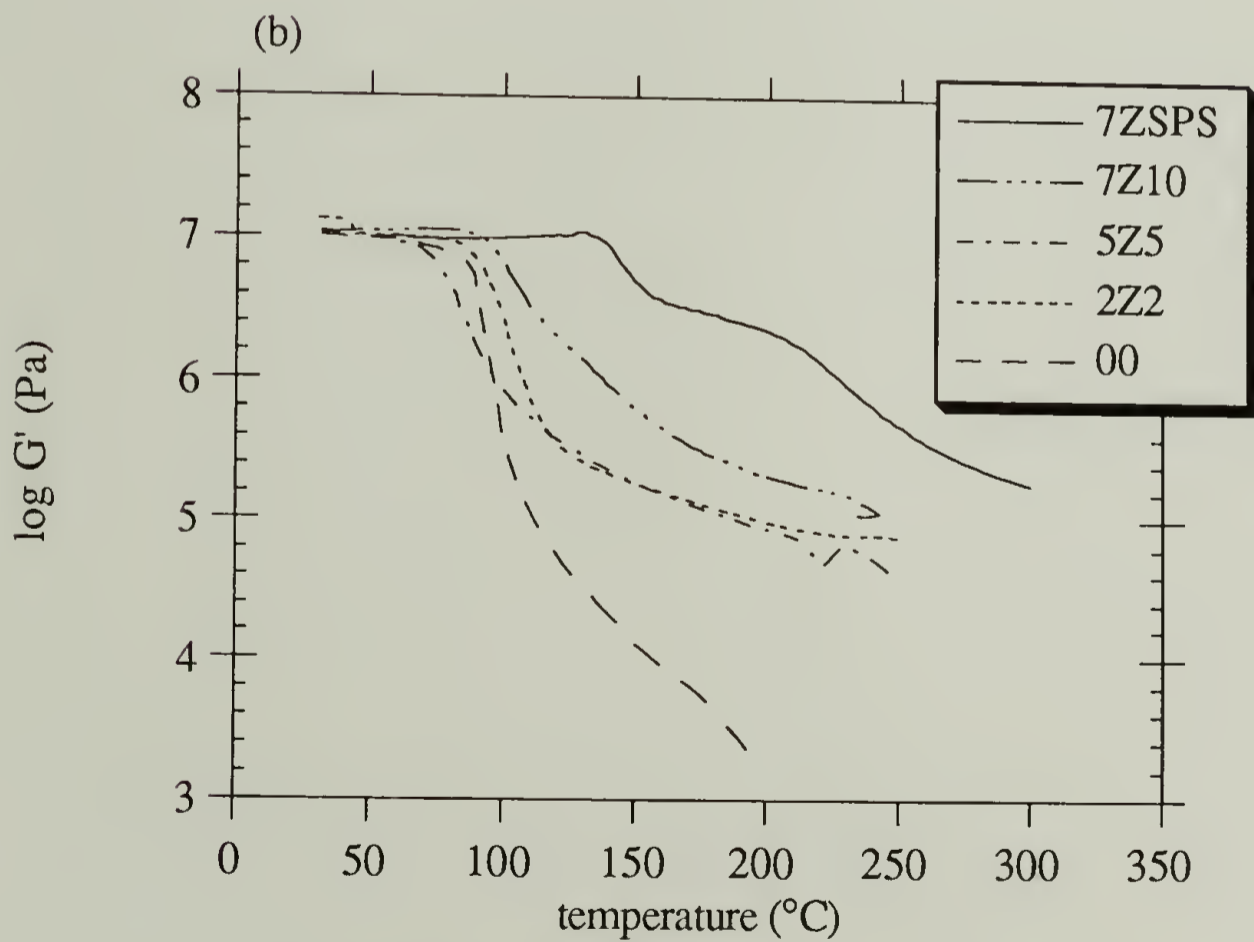
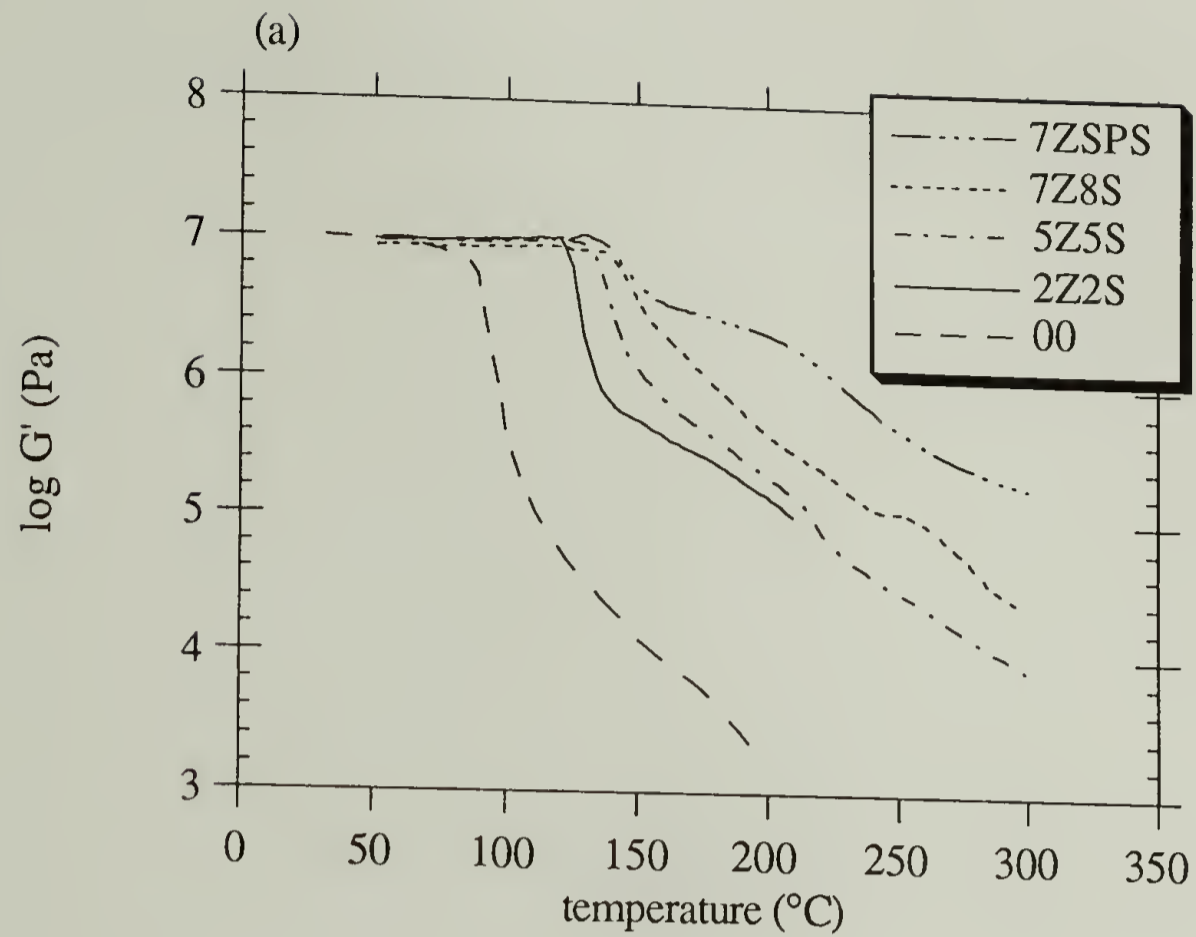


Figure 3.12: Shear storage moduli at 1 Hz for (a) zinc styrene/styrene and (b) zinc styrene/ethyl acrylate blends. Curves have not been corrected for machine compliance at low temperatures.

compared to the ionomer results from a change in the state of aggregation. The exact nature of this change will be discussed below.

Previous attempts to describe the rubbery plateau in ionomers have been based on classical rubber elasticity.<sup>17</sup> According to rubber elasticity, the shear modulus of an ideal rubber is given by:<sup>24</sup>

$$G_0 = \nu RT \quad (3.4)$$

where  $\nu$  is the crosslink density of the rubber. Results of the calculation for the ionomer blends based on this equation at 200° C are shown in Table 3.3, along with the experimental values at 200° C and 1 Hz. The temperature of 200° C was chosen somewhat arbitrarily as being a temperature where a pseudo-plateau occurs. The values of  $\nu$  used were based on the assumption that every ionic group participates in an interaction. Table 3.3 shows that ideal rubber elasticity fails to predict the moduli of the ionomer blends. Weiss et al. have also found that ideal rubber elasticity can not predict the height of the rubbery plateau for ionomers.<sup>17</sup> The failure of classical rubber elasticity can be attributed to two causes. First, it fails to account for the effect of entanglements that are trapped by the crosslinks and contribute to the network. Second, it assumes tetrafunctional crosslinks, while in ionomers and ionomer blends the crosslinks more likely have a much higher functionality because it is the aggregates that act as crosslinks. The second effect is expected to be more important for ionomers because of the large size of the aggregates.

A theory for rubbery elasticity which takes into account both effects has been described by Pearson and Graessley.<sup>25</sup> In their theory the experimentally determined modulus is the sum of two terms, the modulus due to crosslinking and the modulus due to trapped entanglements. Thus, the modulus of the rubber is given by:

Table 3.3 : Comparison of experimental shear moduli and moduli calculated from ideal rubber elasticity.

Blend	G' at 1 Hz, 200 °C (kPa)	G° <sub>ideal rubber</sub> at 200 ° C (kPa)
2H2	61.7	835.3
5H5	69.2	2088.3
8H10	77.6	3341.2
2Z2	100.0	835.3
5Z5	87.1	2088.3
7Z10	204.2	3341.2
2H2S	67.6	835.3
5H5S	160.3	2088.3
8H8S	197.2	3341.2
2Z2S	158.5	835.3
5Z5S	199.5	2088.3
7Z8S	416.9	3341.2

$$G' = G_c + G_e = \frac{\Phi (\nu - \mu) RT}{V_0} + T_e G_N^\circ \quad (3.5a)$$

where  $G_c$  is the contribution from crosslinks,  $G_e$  is the contribution from trapped entanglements,  $\Phi$  is a constant of order unity,  $\nu$  is the number of elastically active subchains,  $\mu$  is the number of elastically active crosslinks,  $V_0$  is the sample volume,  $T_e$  is an entanglement trapping factor, defined as the probability that a crosslink has permanently trapped an entanglement, and  $G_N^\circ$  is the pseudo-plateau modulus of the uncrosslinked system. At high crosslink densities (i.e. crosslink densities greater than the gel point), the modulus can be calculated from

$$T_e = (p_2)^2 \quad (3.5b)$$

$$p_2 = 1 - 2/\gamma - e^{-\gamma} \quad (3.5c)$$

$$\gamma = \alpha r \quad (3.5d)$$

$$\mu = 2\gamma N / f_n \quad (3.5e)$$

$$\nu = (\gamma - 1) / N \quad (3.5f)$$

where  $\gamma$  is the number of crosslinked units on each primary chain,  $\alpha$  is the fraction of crosslinked units,  $r$  is the number average degree of polymerization of the primary chains,  $N$  is the number of primary chains in the volume  $V_0$ , and  $f_n$  is the average functionality of a crosslink. It is important to note that there are no adjustable parameters; all variables can be determined independently from the molecular parameters of the chains.

Equations 3.5 were used to calculate the average functionalities based on the experimental modulus values. For the purposes of the calculation,  $\alpha$  was taken to be the total fraction of ionic groups on the sulfonated polystyrene. The results are shown in Table 3.4.

The functionalities are calculated for temperatures at the minimum in  $\tan \delta$ , which is between the glass transition and the cluster transition. At these temperatures the clusters are stable and expected to act as crosslinks. The ionomers show functionalities ranging from 8 to 80 as the sulfonation level is increased from 2 to 7%. Connolly has used the same approach to analyze the moduli of sulfonated polystyrene ionomers and found that the average functionality is essentially infinite.<sup>16</sup> This result has led him to conclude that the aggregates act as reinforcing filler particles, in addition to the crosslinking effect. The difference between his results and the results presented here is due to sample preparation. The samples for this work were annealed for six minutes at the molding temperature, while Connolly's samples were annealed for 30 minutes. Thus the ionomers in Connolly's work probably have larger, more developed clusters. This difference illustrates the importance of consistent sample preparation when studying ionomers.

The results in Table 3.4 shows quantitatively the effect of blending on the state of aggregation. For example, 7ZSPS has an average functionality of about 80, while the functionalities for 7Z10, 7Z8S, and 8H8S are 8, 5, and 11, respectively. (The differences among these three blends are probably insignificant.) This result explains the drop in modulus from the ionomers to the blends. A smaller functionality means that the distance between crosslinks is greater and the crosslink density is lower, resulting in a lower modulus.

There are several possible explanations for why the aggregation is less in the blends. As was explained previously, greater cooperativity among chains is required to form a cluster in the zinc blends compared to the zinc ionomer. This increased difficulty in forming a cluster would lead to a reduced cluster size. In the case of the acid blends, the

Table 3.4 : Calculated network functionalities.

Sample	Functionality at the minimum in $\tan \delta$
2H2	$2.6 \pm 1.5$
5H5	2.2
8H10	2.1
2Z2	2.8
5Z5	2.6
7Z10	7.8
2H2S	5.9
5H5S	5.6
8H8S	10.8
2Z2S	6.3
5Z5S	2.8
7Z8S	5.1
2ZSPS	7.6
5ZSPS	14.9
7ZSPS	76.7

increased electrostatic interactions between ionic groups due to the greater charge density may actually hinder the formation of clusters. Once a cluster of sufficient size has formed the electrostatic interactions holding the cluster together are large enough to reduce the mobility of the ionic groups and prevent further growth of the cluster. These explanations are only speculative, and there is at this point no experimental evidence to prove or disprove them.

In order to further examine the relaxation behavior of the blends, frequency-temperature superposition was attempted for the zinc ionomers and the SPS/SVP blends. Superposition was not attempted for the blends containing ethyl acrylate to avoid the complication caused by the ethyl acrylate phase.

Superposition is based on the observation that, for viscoelastic materials like polymers, the modulus measured at a particular time and temperature in a static experiment such as stress relaxation is the same as the modulus measured at a shorter time and a higher temperature.<sup>24,26</sup> Similarly, in dynamic experiments reducing the frequency is equivalent to increasing the temperature. In order to construct a curve of the modulus over an extended frequency range at a given temperature, one performs the experiment at various temperatures over a more limited frequency range, and then shifts the isotherms to produce a continuous master curve. The amount of shift of each isotherm relative to a reference isotherm is called the shift factor. The relationship between the modulus value on the isotherm and the corresponding shifted value on the master curve is:

$$G(T, f) = G(T_{\text{ref}}, f/a_T) \quad (3.6)$$

where  $T$  and  $T_{\text{ref}}$  are the isotherm temperature and reference temperature, respectively,  $f$  is the frequency, and  $a_T$  is the shift factor. The reference temperature is usually taken to be the glass transition temperature. The temperature dependence of the shift factor is often expressed by the WLF equation:

$$\log a_T = \frac{-C_1(T-T_g)}{C_2 + T - T_g} \quad (3.7)$$

where  $C_1$  and  $C_2$  are the WLF constants. While the WLF equation was first proposed as an empirical observation, it is possible to derive it based on the Doolittle equation for the viscosity of liquids and the assumption of a linear expansion of free volume above the glass transition.<sup>24,26</sup> Based on this derivation, the constants are given by:

$$C_1 = B/2.303f_g \quad (3.8a)$$

$$C_2 = f_g/\alpha_f \quad (3.8b)$$

where  $f_g$  is the fraction of free volume present at  $T_g$  and  $\alpha_f$  is the thermal expansion coefficient of free volume above  $T_g$ .

It is important to remember that frequency-temperature superposition is only valid when the relaxation time distribution does not change with temperature. This requirement is only strictly valid for simple polymer systems, and such a material is called "thermorheologically simple". More complicated polymer systems such as blends and semi-crystalline polymers, which do not give continuous master curves and do not follow the WLF equation, are called "thermorheologically complex". A multiphase material can be thermorheologically simple as long as the relaxation time distributions for the different components exhibit the same temperature dependence.

As an example of frequency-temperature superposition, the isothermal data and resulting master curves for polystyrene are shown in Figures 3.13 and 3.14. The superposition in the data is very good. The shift factors are plotted in Figure 3.15, along with a fit to the WLF equation. The best fit WLF parameters are  $C_1=11.8$  and  $C_2=52.5$ ,



which is in excellent agreement with the results of Connolly ( $C_1=9.2$ ,  $C_2=51$ )<sup>16</sup> who also used a Polymer Laboratories DMTA and in reasonable agreement with the detailed analysis of Plazek ( $C_1=14.5$ ,  $C_2=50.4$ ).<sup>27</sup>

The master curves for the SPS/SVP blends are shown in Figures 3.16-21. The failure of superposition, especially at the lowest frequencies, indicates that these materials are thermorheologically complex. The shift factors are plotted in Figure 3.22 along with fits to the WLF equation, and the resulting WLF constants are given in Table 3.5. The sigmoidal shapes of the plots in Figure 3.22 are typical for thermorheologically complex materials. The sigmoidal shape results from the superposition of two different relaxation time distributions, each of which follows a different WLF equation.

The values of  $C_1$  are fairly independent of the material, which is in agreement with the iso-free volume theory of the glass transition.<sup>24</sup> The iso-free volume theory states that the glass transition occurs when the free volume becomes so small that the large scale cooperative motions typical of the glass transition are no longer possible. The values of  $C_2$  are much higher than the values for polystyrene. Since Equation 3.8b shows that  $C_2$  is inversely proportional to the expansion coefficient of free volume ( $\alpha_f$ ), the increase in  $C_2$  represents a decrease in  $\alpha_f$ , due to the restricted mobility of the polymer chains caused by the interactions. There is no obvious trend in the effect of substitution level on  $C_2$ . A previous studies on ionomers by Connolly has found a similar increase in  $C_2$  and failure of superposition.<sup>16</sup> However, Weiss, et al. found good superposition over at least 20 decades of frequency.<sup>17</sup> It is not clear why superposition succeeded in their case. Nevertheless, it is evident that the failure of superposition in the ionomer blends described here confirms the presence of phase-separated ionic clusters with a distinct relaxation time distribution.

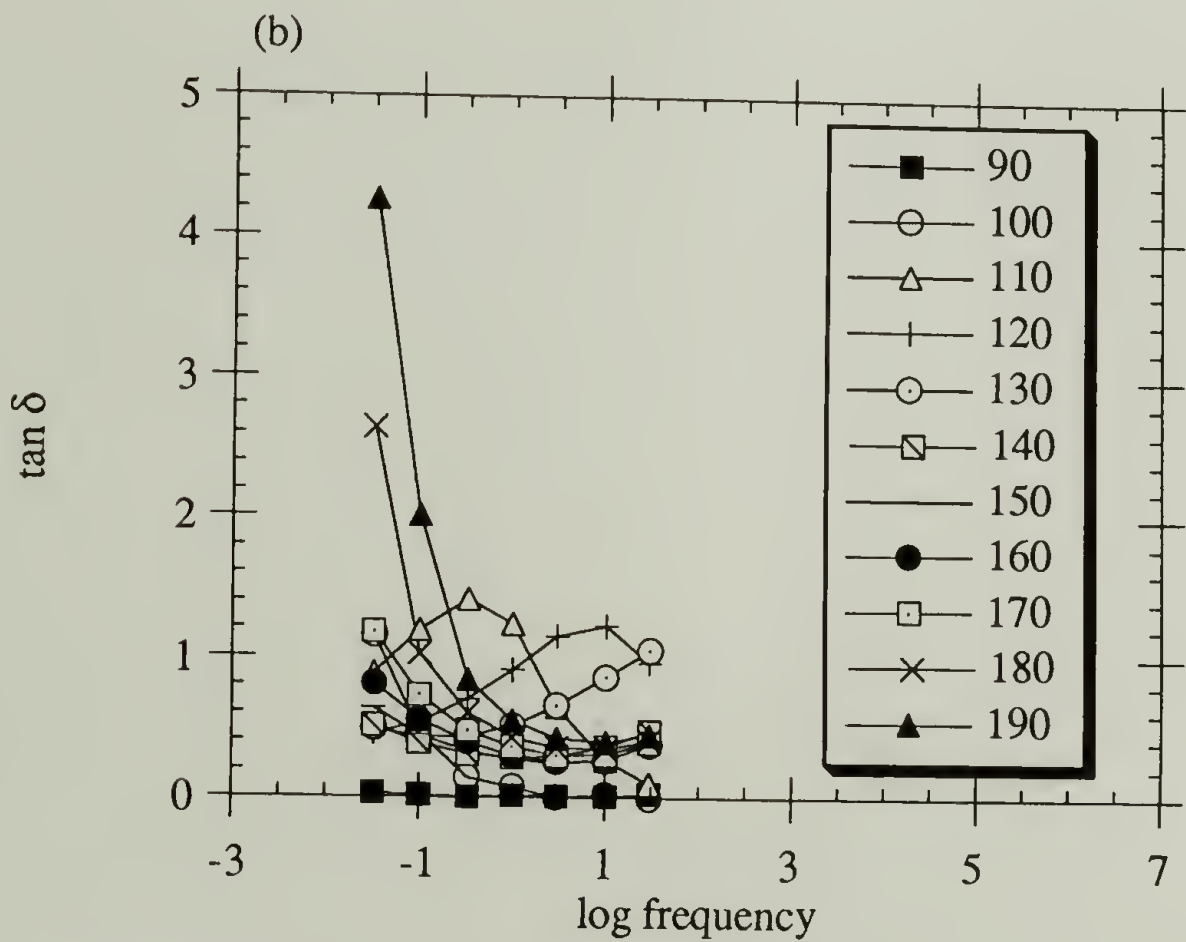
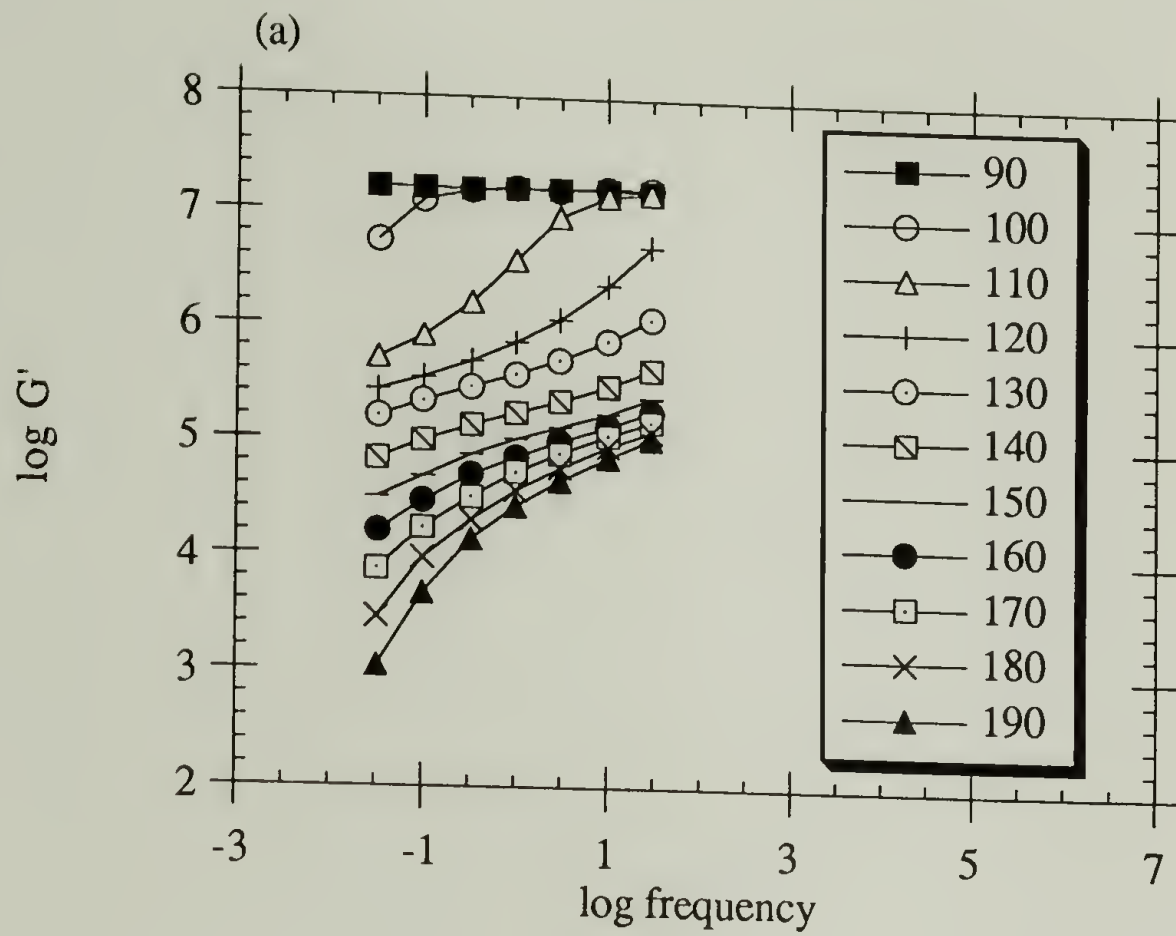


Figure 3.13: Isothermal shear data for polystyrene. Numbers indicate the temperature in  $^{\circ}\text{C}$  at which the isotherm was measured.

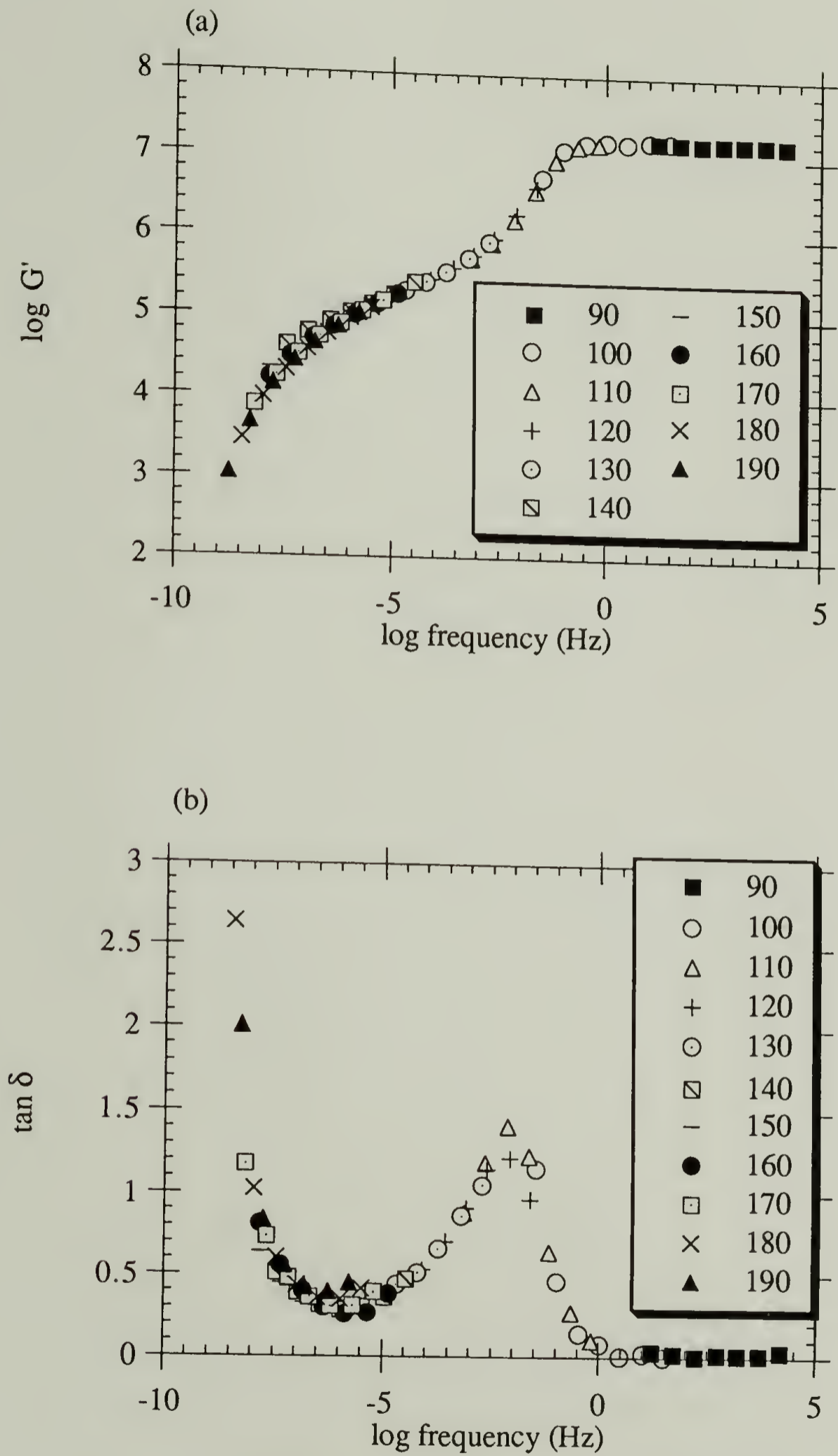


Figure 3.14: Master curves of (a) storage modulus and (b)  $\tan \delta$  for polystyrene. Numbers indicate the temperature in  $^{\circ}\text{C}$  at which each isotherm was measured.

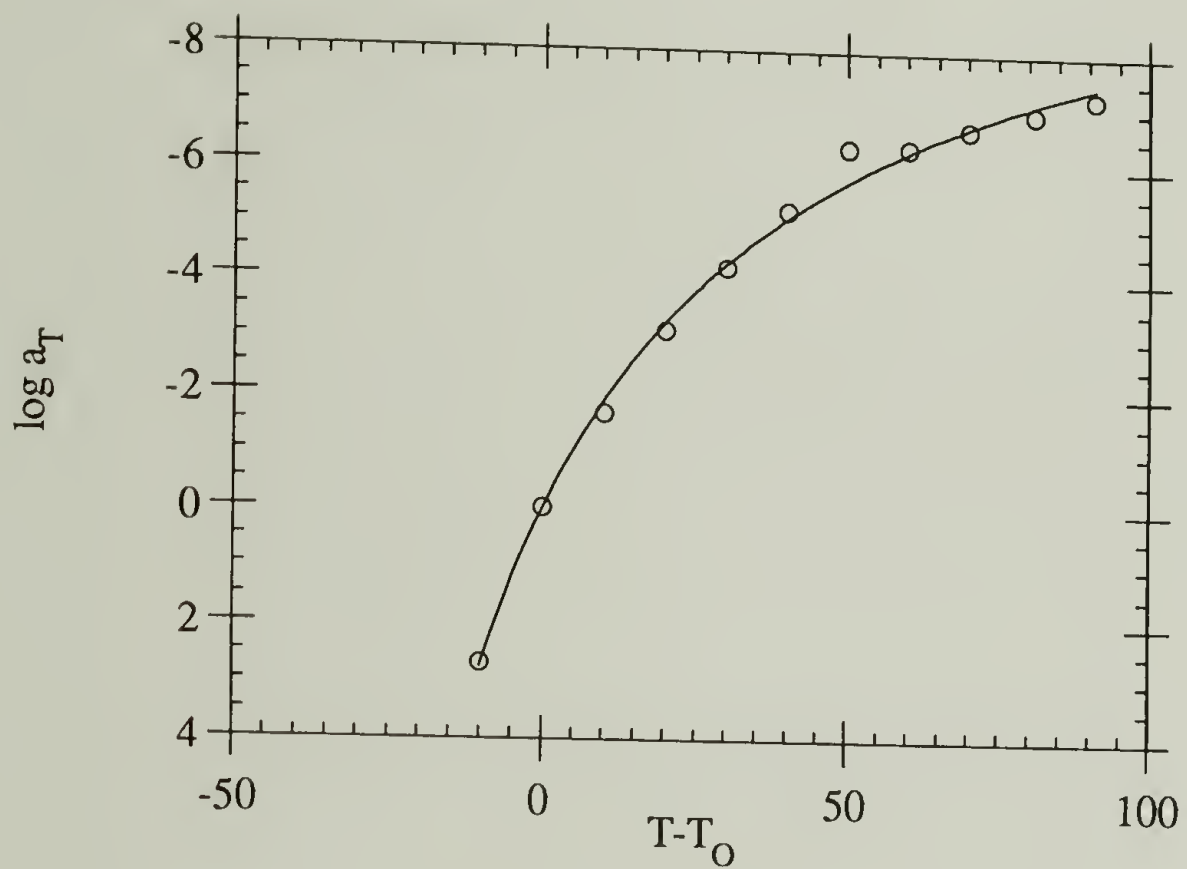


Figure 3.15: WLF plot for polystyrene. Points are the experimentally determined shift factors. The line is a fit of the data to the WLF equation.

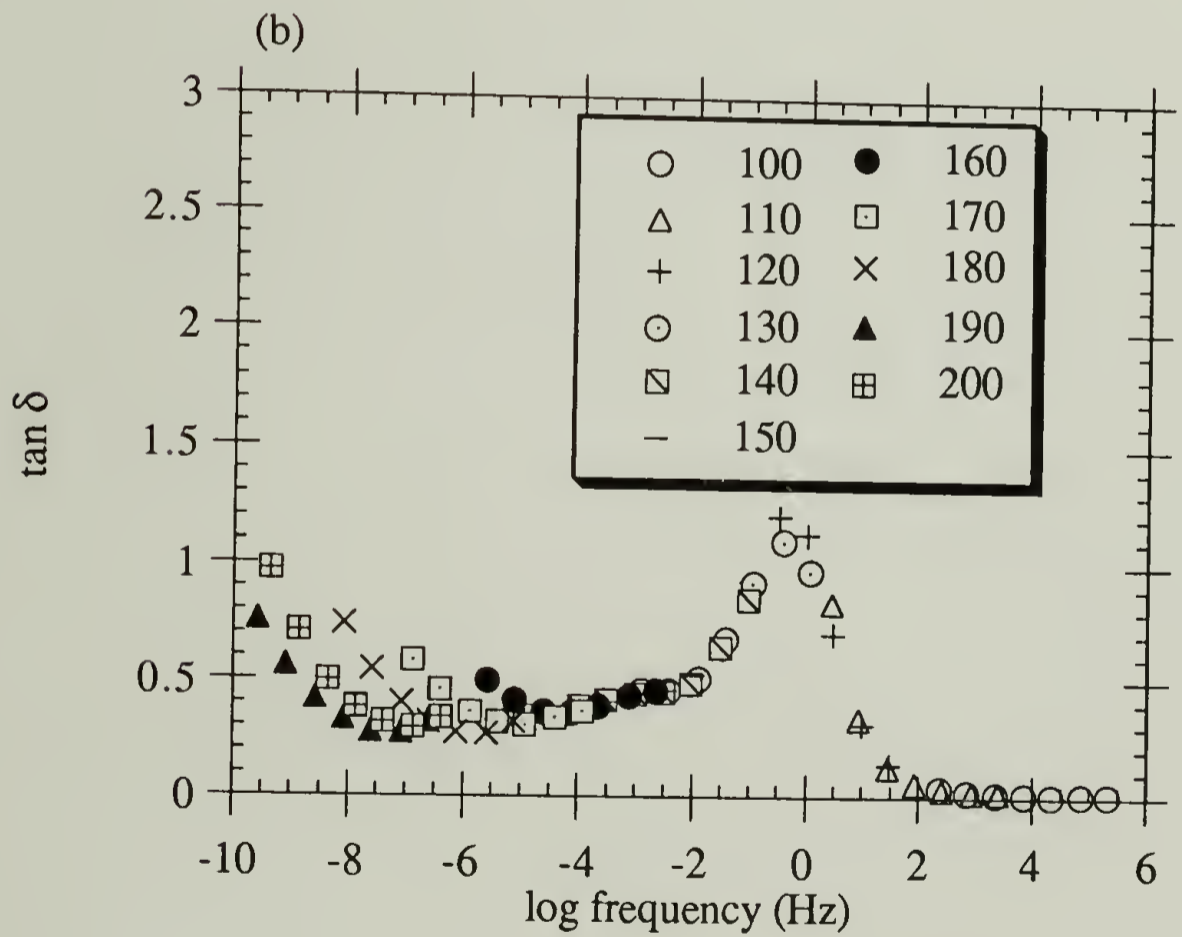
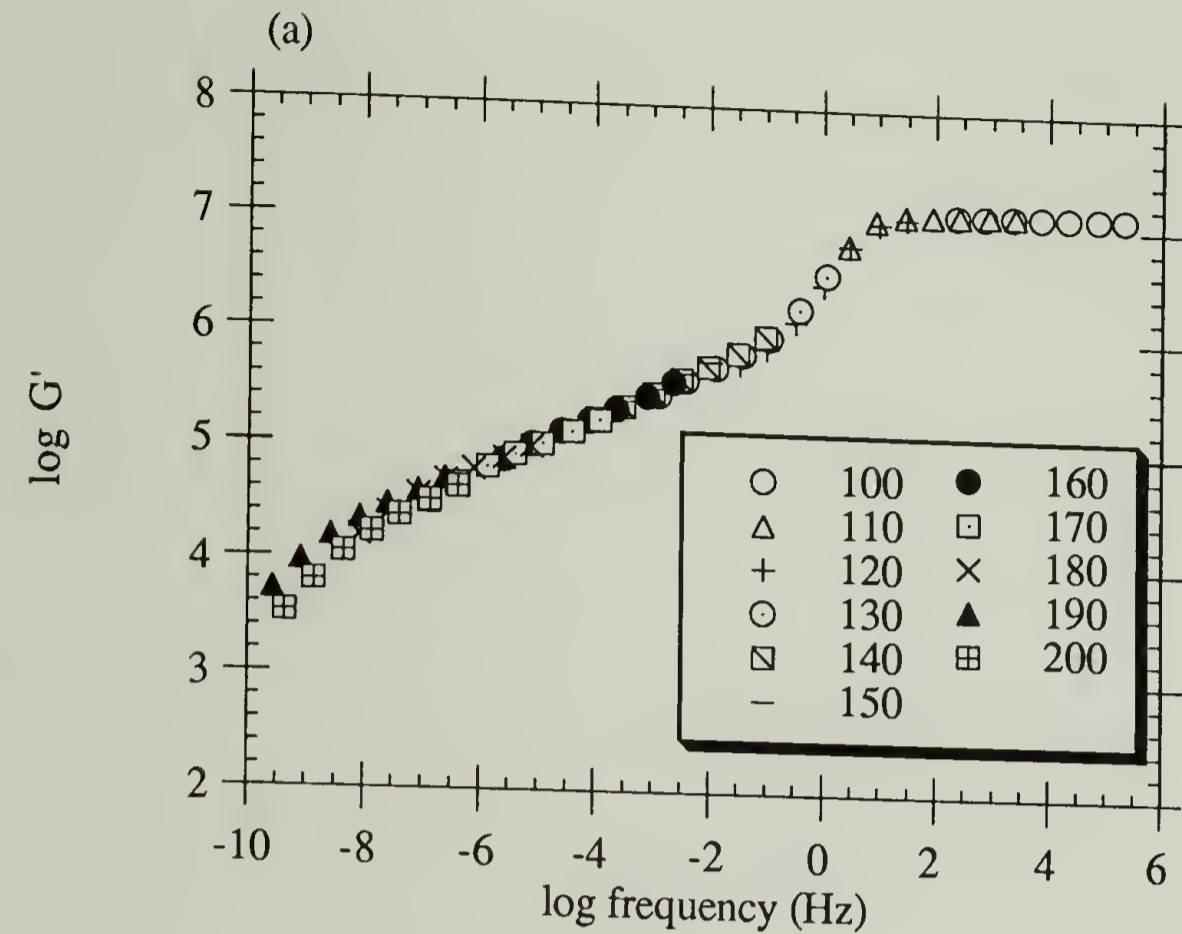


Figure 3.16: Master curves of (a) storage modulus and (b)  $\tan \delta$  for 2H2S. Numbers indicate the temperature in  $^{\circ}\text{C}$  at which each isotherm was measured.

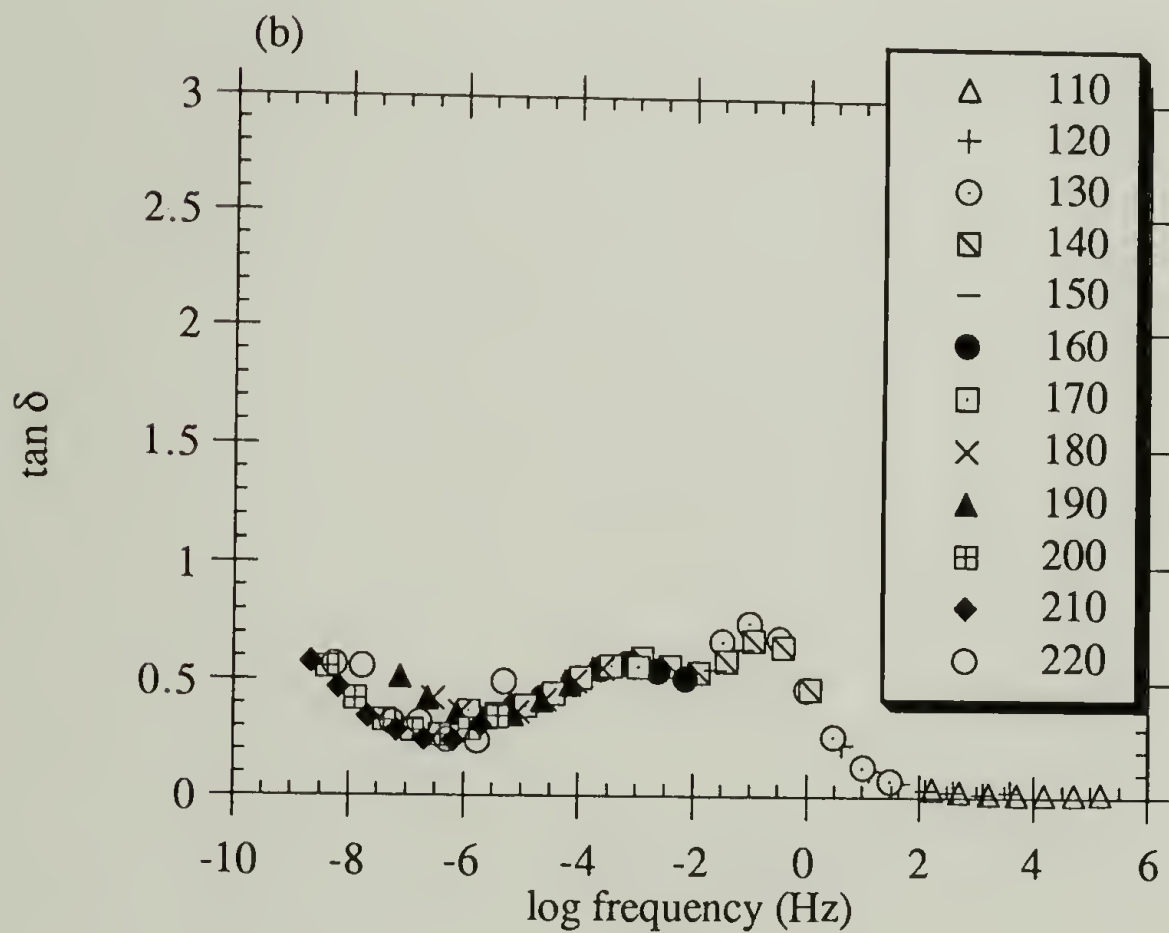
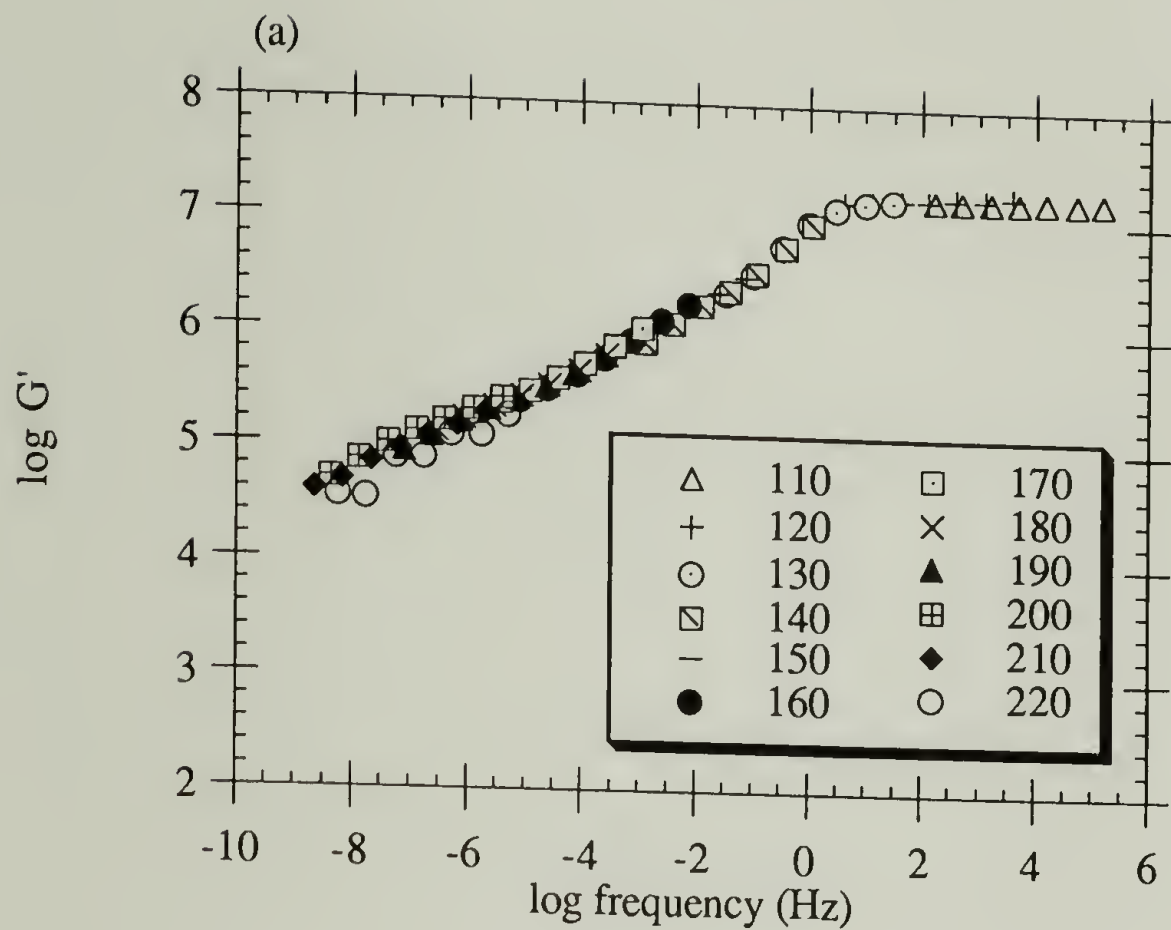


Figure 3.17: Master curves of (a) storage modulus and (b)  $\tan \delta$  for 5H5S. Numbers indicate the temperature in  $^{\circ}\text{C}$  at which each isotherm was measured.

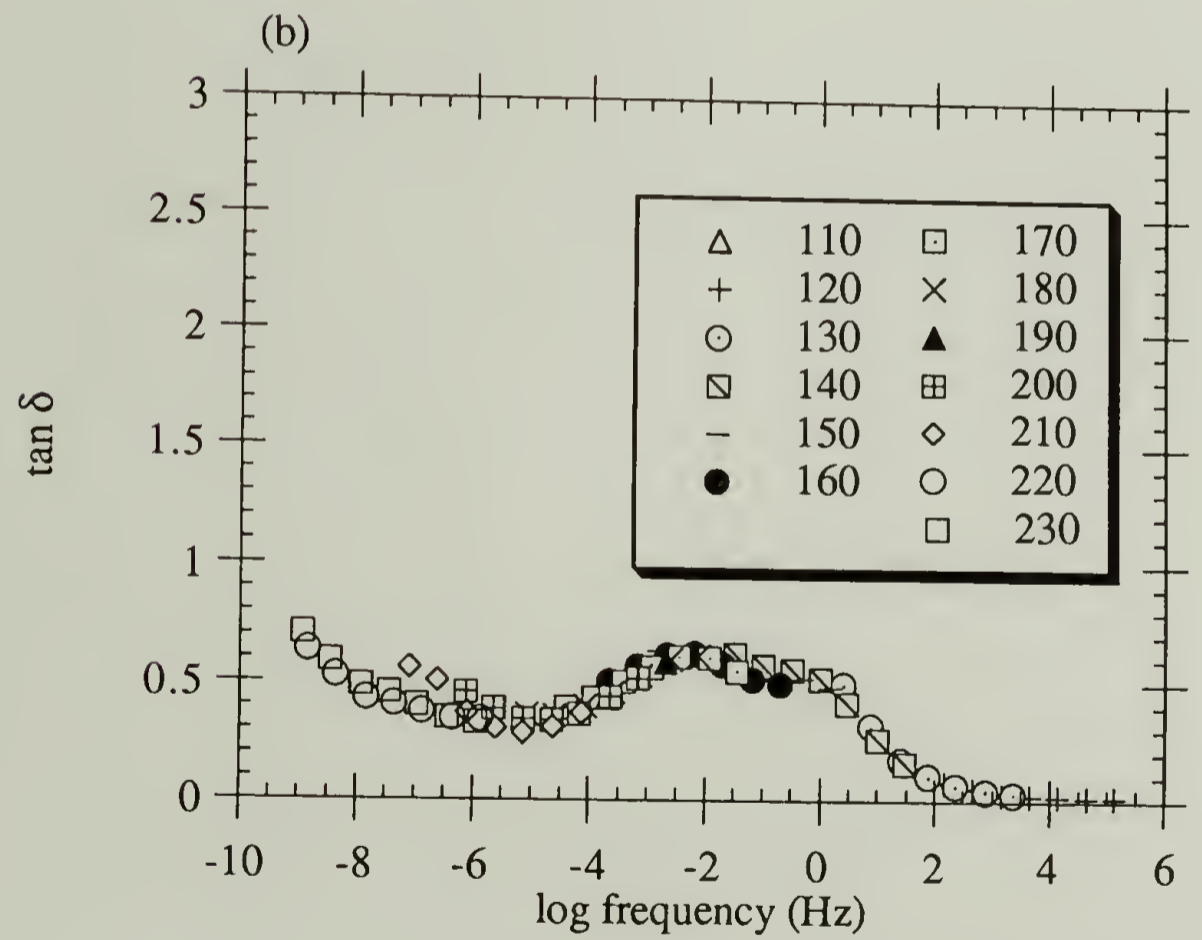
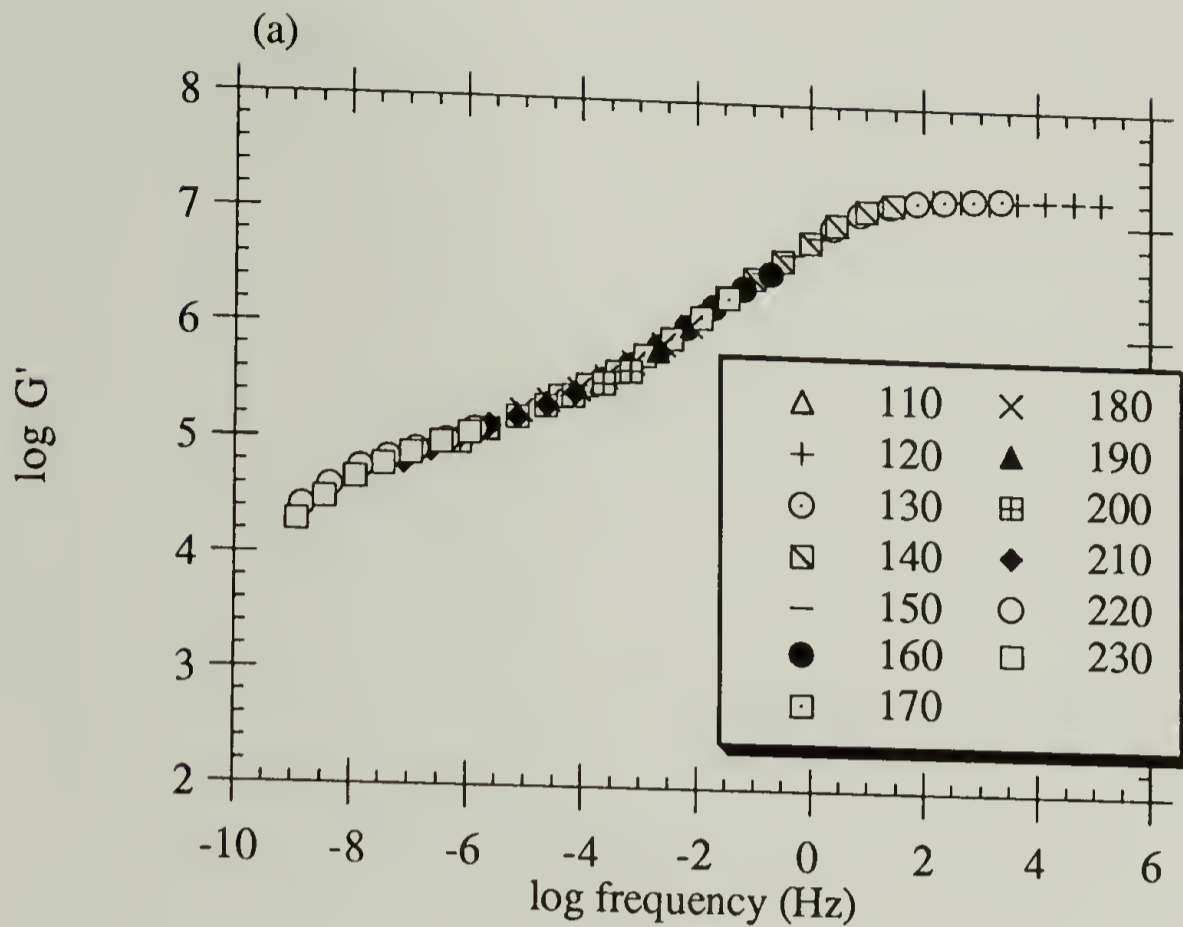


Figure 3.18: Master curves of (a) storage modulus and (b)  $\tan \delta$  for 8H8S. Numbers indicate the temperature in  $^{\circ}\text{C}$  at which each isotherm was measured.

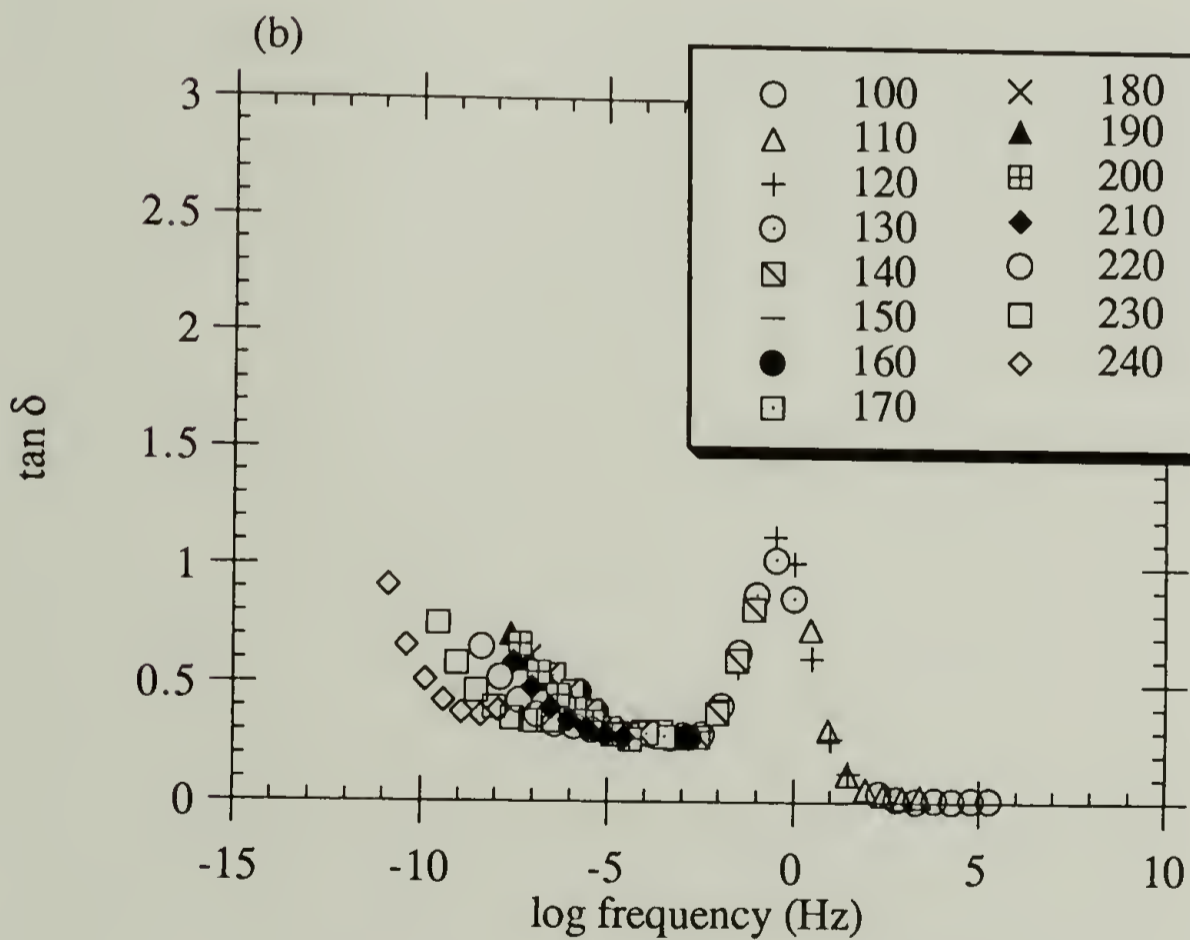
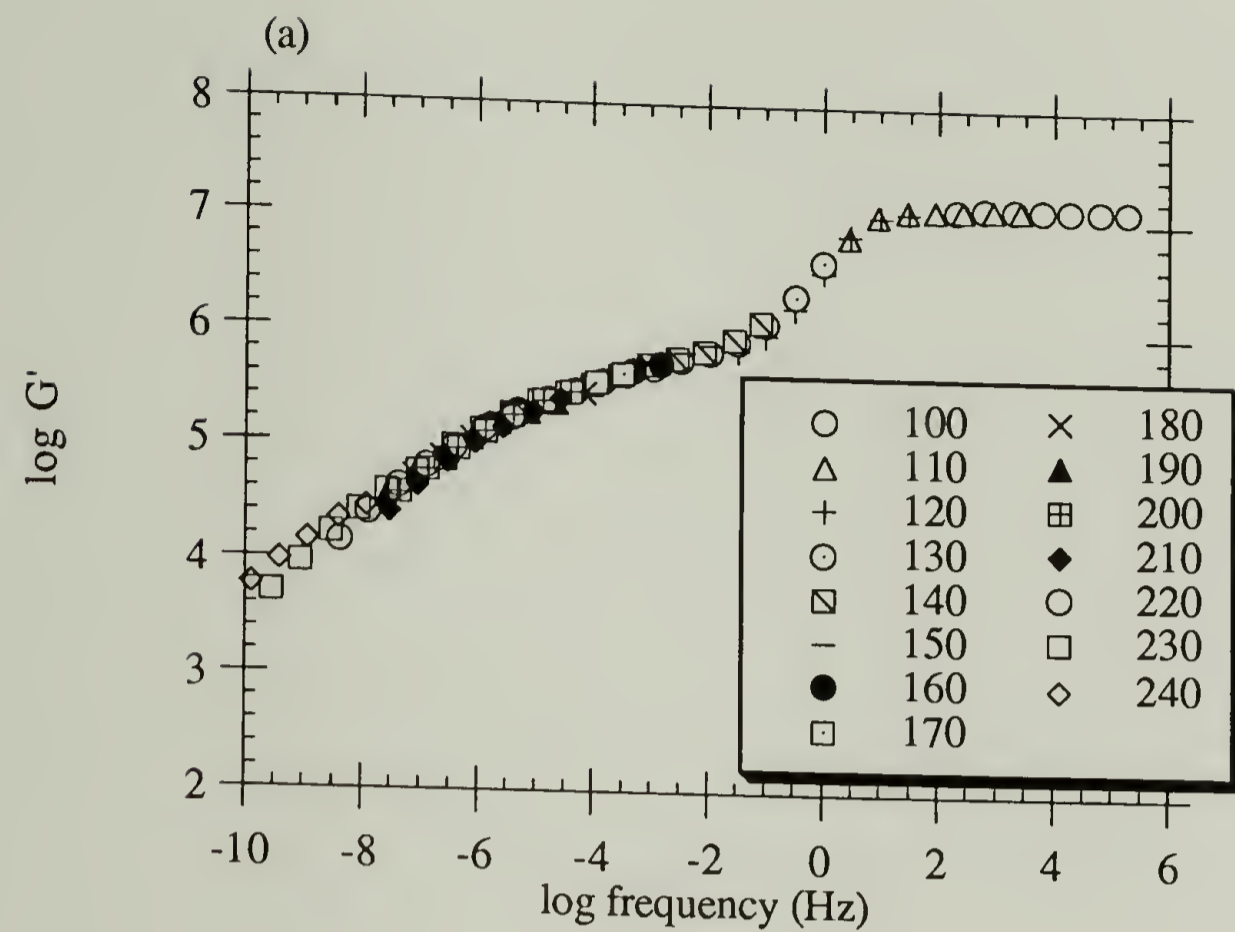


Figure 3.19: Master curves of (a) storage modulus and (b)  $\tan \delta$  for 2Z2S. Numbers indicate the temperature in  $^{\circ}\text{C}$  at which each isotherm was measured.



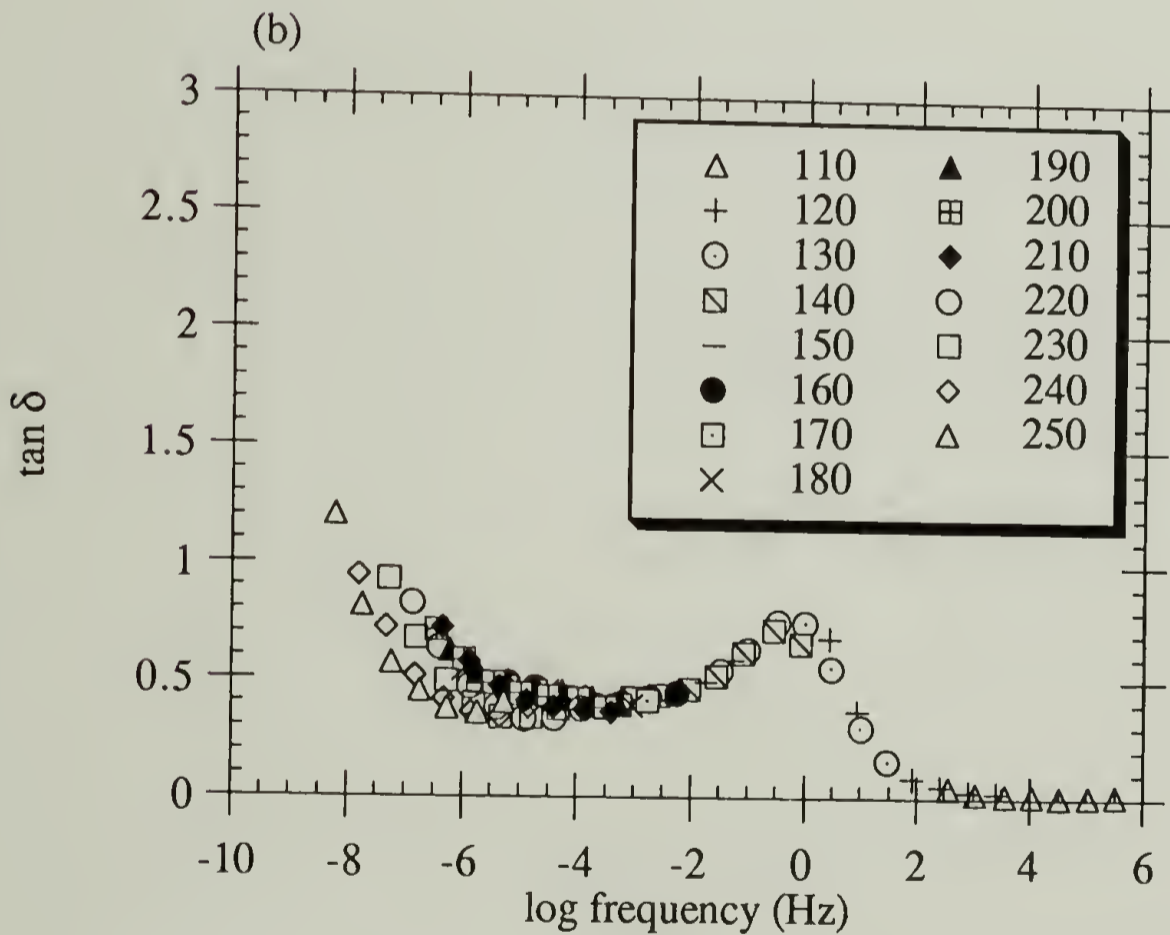
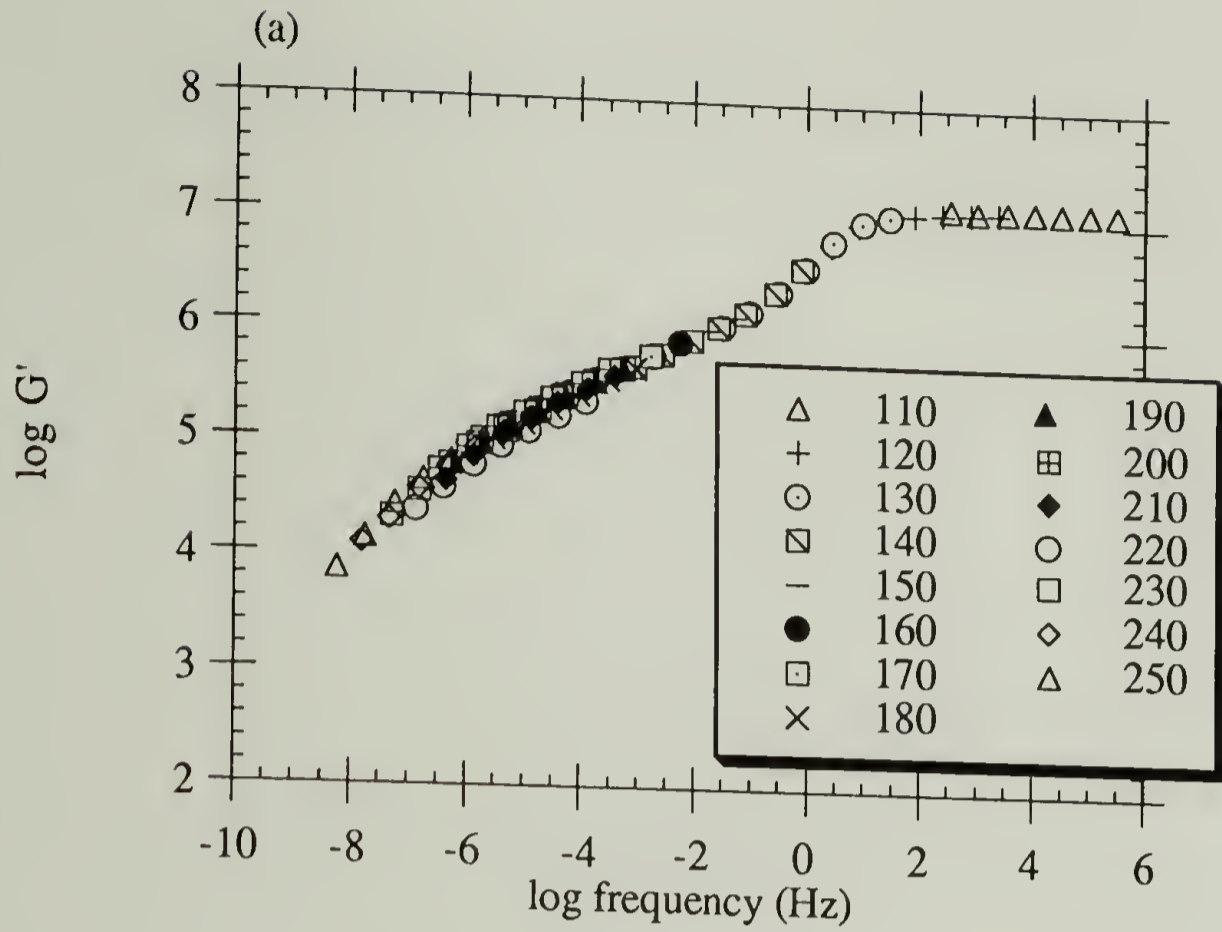


Figure 3.20: Master curves of (a) storage modulus and (b)  $\tan \delta$  for 5Z5S. Numbers indicate the temperature in  $^{\circ}\text{C}$  at which each isotherm was measured.

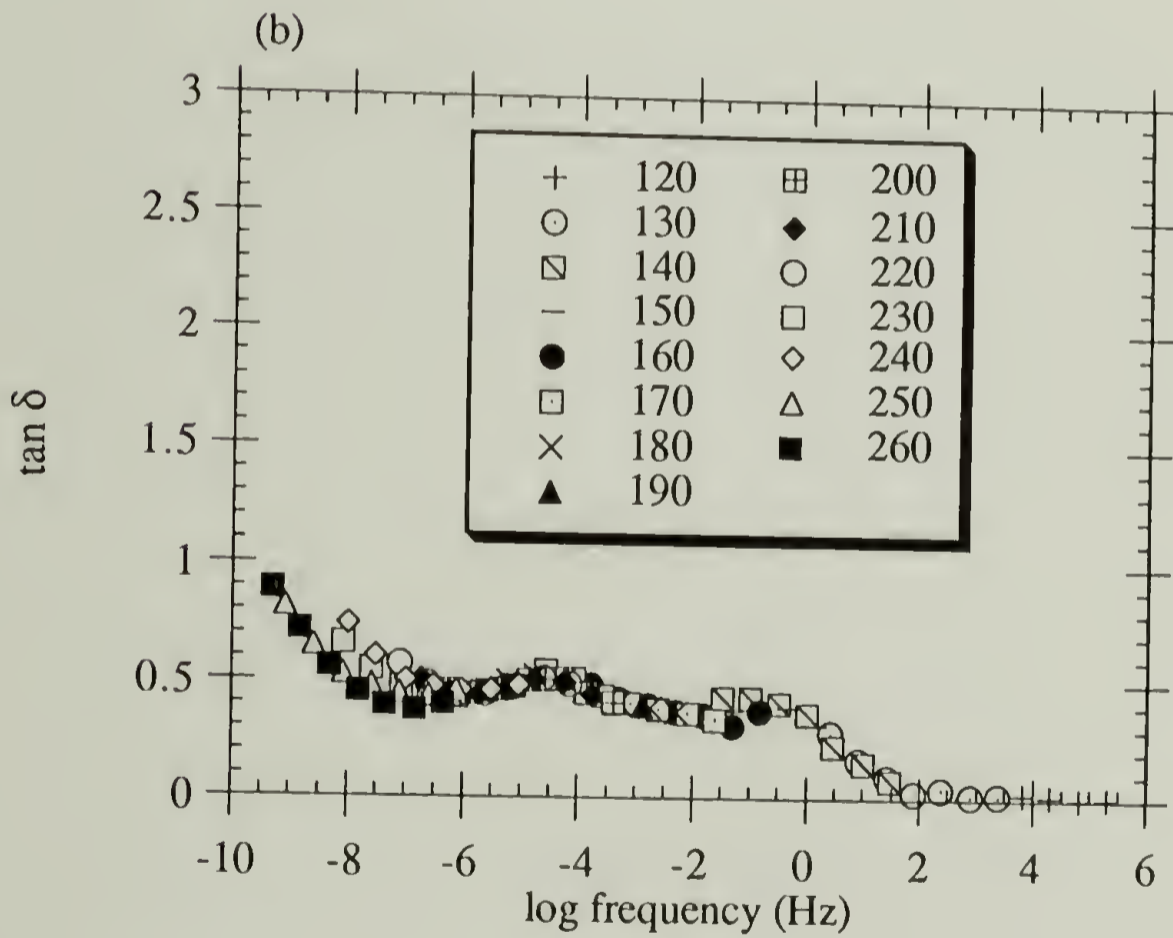
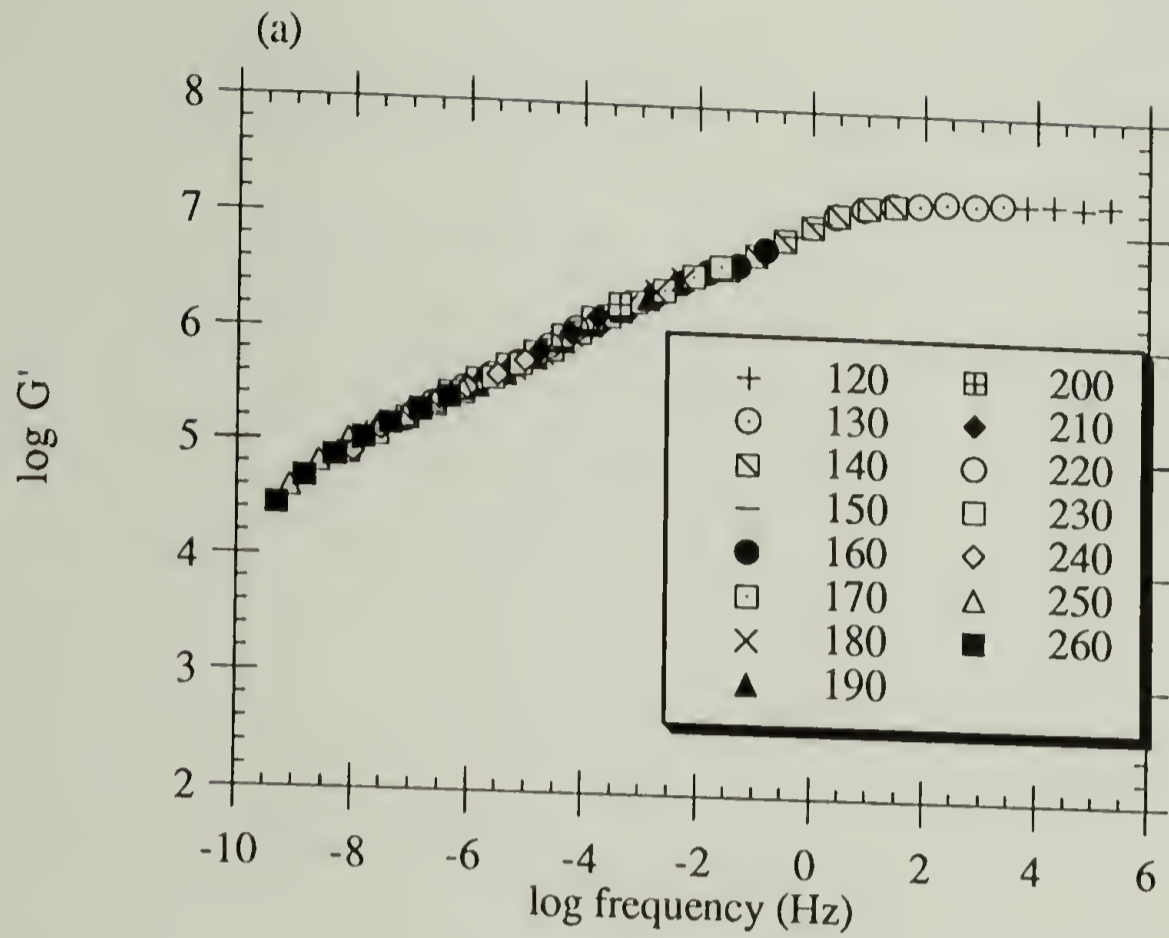


Figure 3.21: Master curves of (a) storage modulus and (b)  $\tan \delta$  for 7Z8S. Numbers indicate the temperature in  $^{\circ}\text{C}$  at which each isotherm was measured.

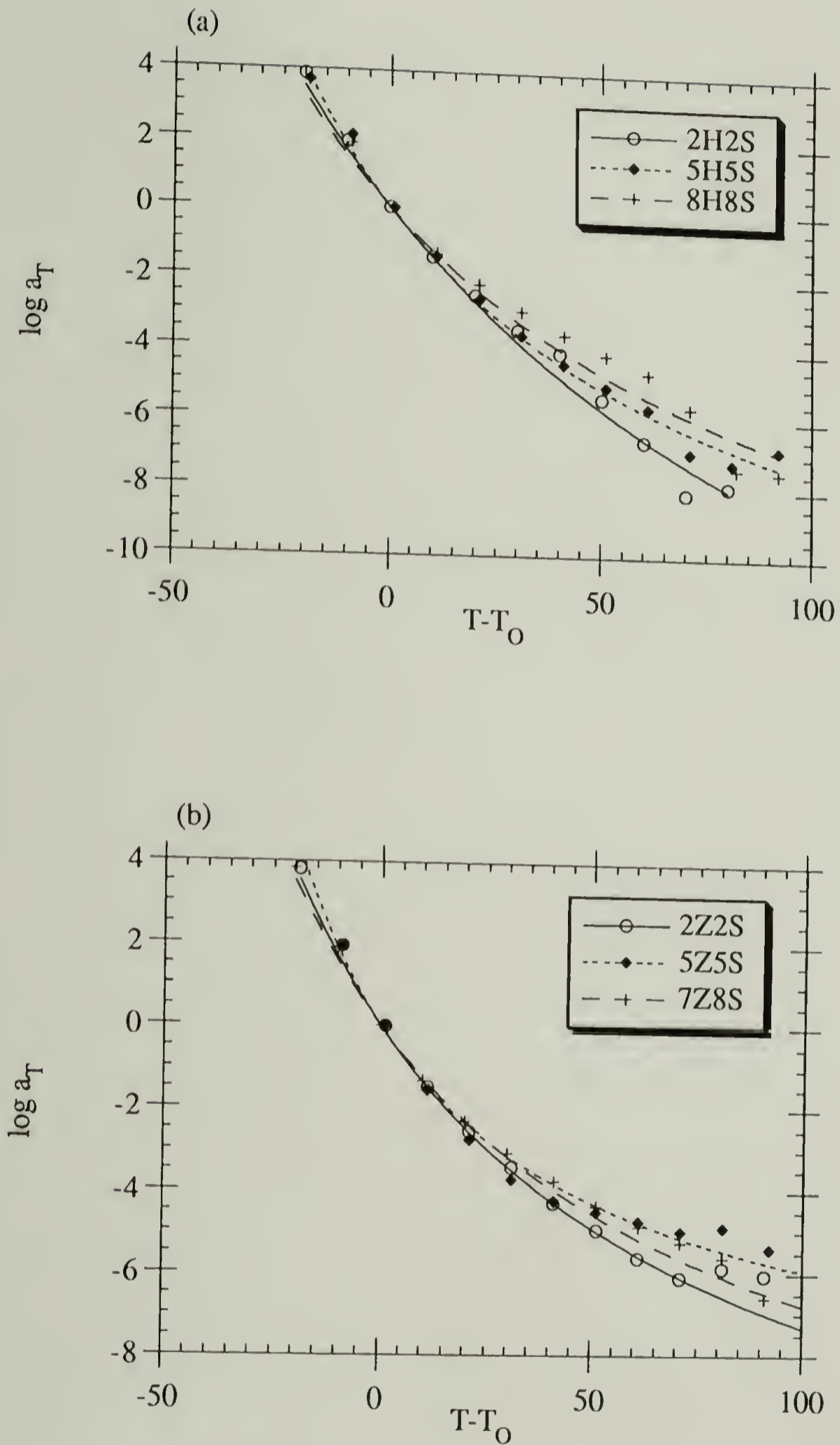


Figure 3.22: WLF plots for (a) acid blends and (b) zinc blends. Points are the experimentally determined shift factors. The line are fits of the data to the WLF equation.

Table 3.5 : WLF constants.

sample	$T_0$ (°C)	$C_1$	$C_2$
polystyrene	100	$11.8 \pm 0.5$	$52.5 \pm 4.6$
2H2S	120	$23.0 \pm 3.9$	$151.2 \pm 34.4$
5H5S	130	$14.5 \pm 1.1$	$91.5 \pm 10.3$
8H8S	140	$15.4 \pm 2.8$	$114.4 \pm 30.5$
2Z2S	120	$14.3 \pm 1.4$	$95.8 \pm 16.3$
5Z5S	130	$9.6 \pm 0.4$	$61.5 \pm 4.3$
7Z8S	140	$13.2 \pm 0.8$	$95.2 \pm 9.8$

### 3.2.3 Morphology

The principal means of studying the morphology of ionomers is by the use of small angle x-ray scattering (SAXS).<sup>1,2</sup> Unfortunately, the interpretation of scattering data is model dependent, and so the only quantity that can be determined unambiguously is the mean-square electron density fluctuation in the sample. As was explained in Section 3.1, the model that the analysis in this work will be based on is the depleted zone core-shell model, shown schematically in Figure 3.1. Although the choice appears somewhat arbitrary, a careful examination will show later that this model best explains all the data.

Guinier's Law describes the diffuse scattering from a two-phase system composed of isolated spheres in a matrix.<sup>13</sup> Assuming the spheres are monodisperse in size, a sharp interface between the spheres and the matrix, and a uniform electron density within each phase, the scattering at low angles can be expressed by:

$$I(q) = I(0) e^{-1/3q^2r^2} \quad (3.9)$$

where  $r$  is the radius of the spheres and  $q$ , the scattering vector, is given by:

$$q = \frac{4\pi \sin \theta}{\lambda} \quad (3.10)$$

where  $2\theta$  is the scattering angle and  $\lambda$  is the wavelength of the x-rays. A plot of  $\ln I$  versus  $q^2$  at low  $q$  for a system that follows Guinier's Law will be linear, and the slope will be inversely proportional to the square of the radius of the spheres.

The scattering at high angles can be described by Porod's Law.<sup>13</sup> For a two phase system in which the interface is sharp and the two phases each have a uniform electron

density, the intensity of the scattering is proportional to  $q^{-4}$  for pinhole collimation and  $q^{-3}$  for collimation by infinitely long, narrow slits. Mathematically, this can be expressed as:

$$I(q) = K_1 q^{-4} \quad (\text{pinhole collimation}) \quad (3.11a)$$

$$I(q) = K_1 q^{-3} \quad (\text{slit collimation}) \quad (3.11b)$$

where  $K_1$  is a constant, usually expressed as:

$$K_1 = \lim_{q \rightarrow \infty} (Iq^4) \quad (\text{pinhole collimation}) \quad (3.12a)$$

$$K_1 = \lim_{q \rightarrow \infty} (Iq^3) \quad (\text{slit collimation}) \quad (3.12b)$$

Systems that follow Porod's Law give a straight line with zero slope when  $Iq^4$  is plotted against  $q^4$  for pinhole collimation or when  $Iq^3$  is plotted against  $q^3$  for collimation by infinitely long, narrow slits. Systems that deviate from Porod's Law will show a positive slope in such a plot. Such deviations usually arise from either an interface that is not sharp or electron density fluctuations within the phases. In such a case there is an additional term that must be added to equations 3.11:

$$I(q) = K_1 q^{-4} + K_2 \quad (\text{pinhole collimation}) \quad (3.13a)$$

$$I(q) = K_1 q^{-3} + K_2 \quad (\text{slit collimation}) \quad (3.13b)$$

In this case  $K_1$  is determined from the slope of a plot of  $I$  versus  $q^{-4}$  (for pinhole collimation) or  $q^{-3}$  (for slit collimation).

Based on Porod's Law, an inhomogeneity length can be determined from the following equations:

$$Q = \int q^2 I dq \quad (\text{pinhole collimation}) \quad (3.14a)$$

$$Q = \int q I dq \quad (\text{slit collimation}) \quad (3.14b)$$

$$O_s = \pi \phi_1 \lim_{q \rightarrow \infty} (q^4 I) \quad (\text{pinhole collimation}) \quad (3.15a)$$

$$O_s = \pi \phi_1 \lim_{q \rightarrow \infty} (q^3 I) \quad (\text{slit collimation}) \quad (3.15b)$$

$$O_s = 4 \phi_1 \phi_2 / L \quad (3.16)$$

where  $Q$  is the invariant,  $O_s$  is the inner specific surface, defined as the ratio of the interface surface area to the volume of the disperse phase,  $\phi_1$  and  $\phi_2$  are the volume fractions of the disperse and continuous phases, respectively, and  $L$  is the inhomogeneity length.

It is important to note that the analyses described above strictly apply only to the idealized systems for which they were developed. Ionomers do not meet those requirements, because the electron density within a cluster is not uniform, and the interface may not be sharp. Keeping in mind these limitations, the use of Guinier's Law and Porod's Law may allow comparisons within a similar set of materials.

Discrete scattering effects can be analyzed using Bragg's Law:<sup>13</sup>

$$n\lambda = 2d \sin \theta \quad (3.17)$$

where  $n$  is an integer and  $d$  is the distance between scattering sites.

The general features of the scattering from ionomers are a peak at intermediate scattering angles and a low angle upturn. These features are evident in the scattering curves for the ZSPS's shown in Figure 3.23. In terms of the depleted zone core-shell model, the peak is due to the preferred distance between ionic groups determined by the thickness of the shell, and the upturn is due to Guinier scattering from isolated clusters. As has been reported previously, the ionic peak increases in intensity and moves to slightly higher scattering angles with increasing sulfonation.<sup>3,7,28</sup> The values for the core plus shell radii obtained from a Bragg analysis of the peak positions are 37.0 and 34.9 Å for 5ZSPS and 7ZSPS, respectively. These values are similar to what has been reported previously.<sup>3,7,28</sup> Calculation of the network functionalities in Section 3.2.2 showed that the number of ionic groups per cluster increases with increasing substitution level. The decrease in shell thickness with substitution level seen from the Bragg analysis of the peak position results from the greater electrostatic force when more ionic groups are present in a cluster.

The curves for the HSPS's shown in Figure 3.24 do not show any appreciable scattering. There has been some question recently over whether or not the acid form of sulfonated polystyrene shows an ionic peak. Most studies do not show any scattering,<sup>1,2,7,29</sup> but a study by Yarusso and Cooper did show an ionic peak.<sup>4</sup> Weiss and Lefelar<sup>7</sup> have speculated that the peak seen by Yarusso and Cooper may have been due to the effect of residual solvent, which enhanced the contrast. The absence of any scattering in the data of Figure 3.24 supports the view that there is insufficient contrast in the acid form of sulfonated polystyrene to result in scattering.



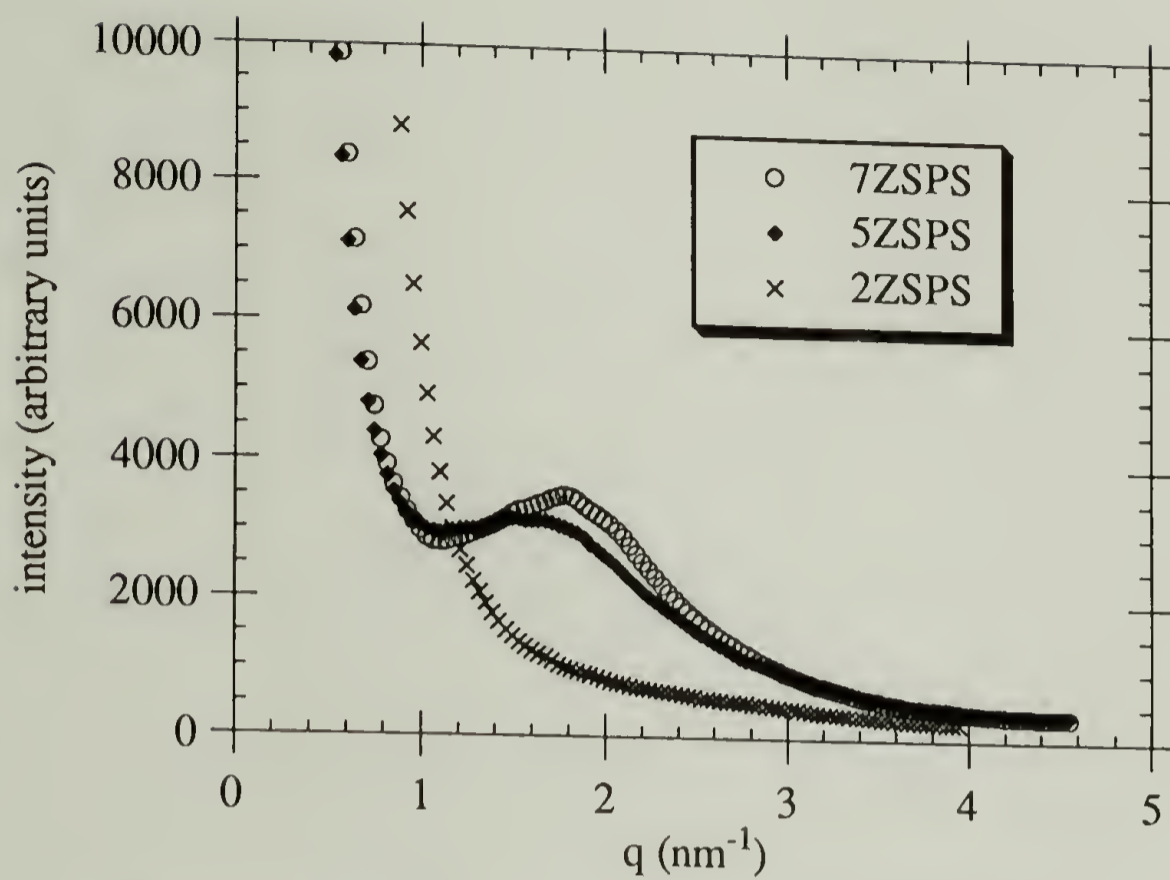


Figure 3.23: SAXS plots for sulfonated polystyrene zinc ionomers.

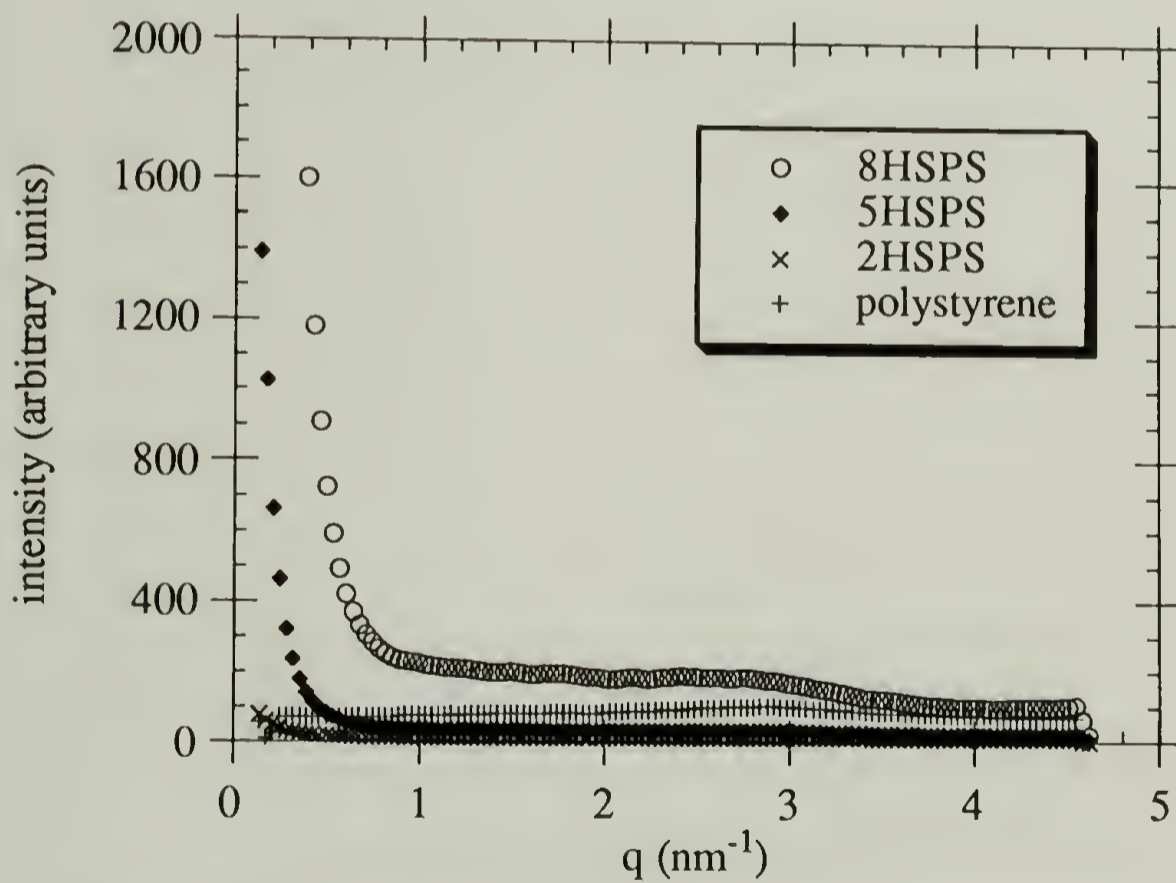


Figure 3.24: SAXS plots for acid form of sulfonated polystyrene.

The scattering curves for the blends are shown in Figures 3.25-28. The most obvious features are that there is no ionic peak in the zinc blends, although the upturn is still present, and there is no scattering at all from the acid blends. The absence of scattering in the acid blends, even though the viscoelastic behavior shows the presence of clusters, again demonstrates that there is insufficient contrast for scattering when no metal is present. It is important to be sure that the absence of a peak in the data for the zinc blends is also not a result of insufficient contrast. The electron density for polystyrene has been reported as  $340 \text{ e}^-/\text{nm}^3$  and the electron density for zinc benzenesulfonate hexahydrate as  $510 \text{ e}^-/\text{nm}^3$ .<sup>4</sup> Assuming these two species represent the matrix and cluster compositions, respectively, the electron density contrast for the ionomers is  $170 \text{ e}^-/\text{nm}^3$ . Assuming no change in the mass density, the replacement of two of the water molecules with pyridine gives an electron density for zinc benzenesulfonate bipyridine tetrahydrate of  $534 \text{ e}^-/\text{nm}^3$ . Thus, the electron density contrast in the blends has actually increased by approximately  $24 \text{ e}^-/\text{nm}^3$ . While these are only rough estimates, they do illustrate that there is sufficient contrast in the blends to detect an ionic peak if one is present.

The absence of an ionic peak in the zinc blends is due to the effect of blending. Absence of an ionic peak was also seen by MacKnight et al. in ethylene ionomers that were saturated with water.<sup>3</sup> In that case, the result was explained as being due to the water increasing the local dielectric constant and screening the electrostatic interactions between ionic groups, thus eliminating the depleted shell region. Fitzgerald, et al. have also seen a decrease in the peak intensity with the addition of methanol.<sup>30</sup> On the other hand, Yarusso and Cooper have found that the addition of water to sulfonated polystyrene ionomers sharpened the ionic peak,<sup>31</sup> and Fitzgerald and Weiss found that the addition of small amounts of glycerol substantially increased the intensity of the peak.<sup>32</sup> The difference is

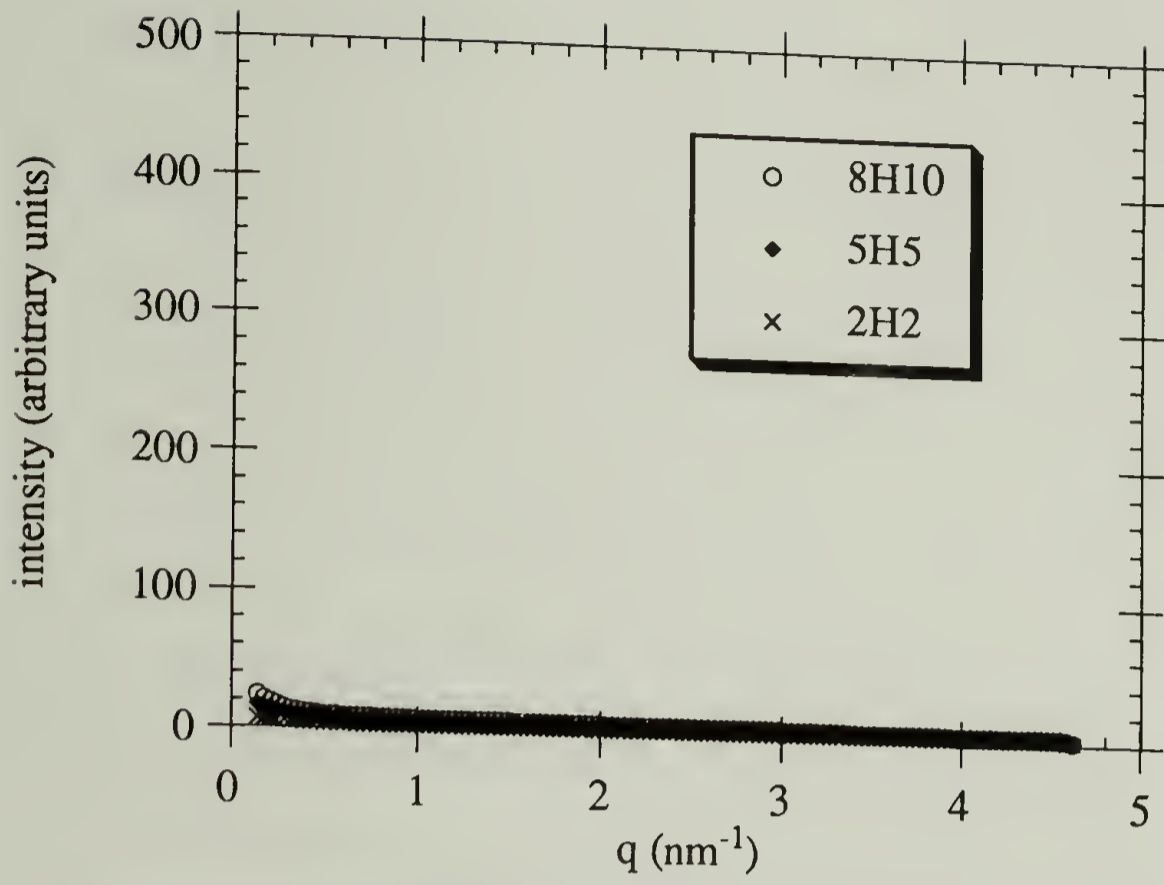


Figure 3.25: SAXS plots for acid styrene/ethyl acrylate blends.

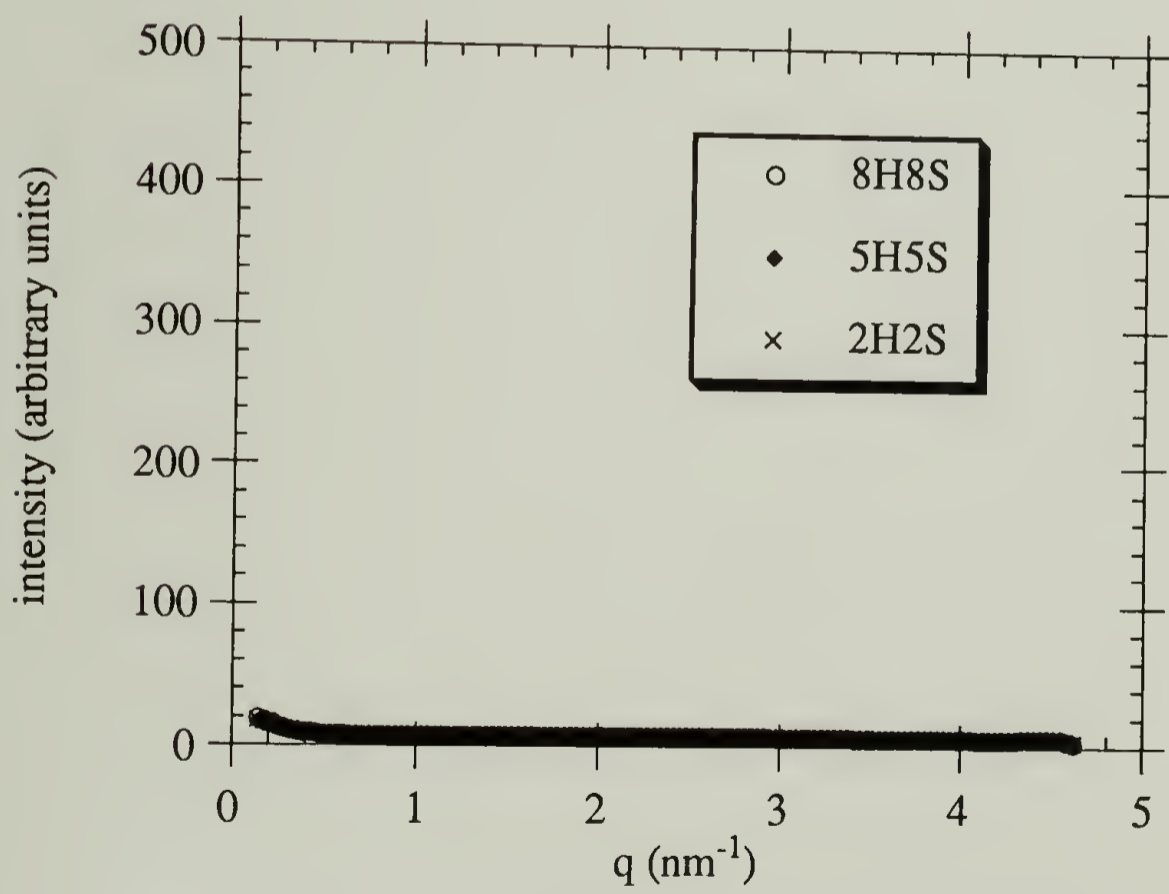


Figure 3.26: SAXS plots for acid styrene/styrene blends.

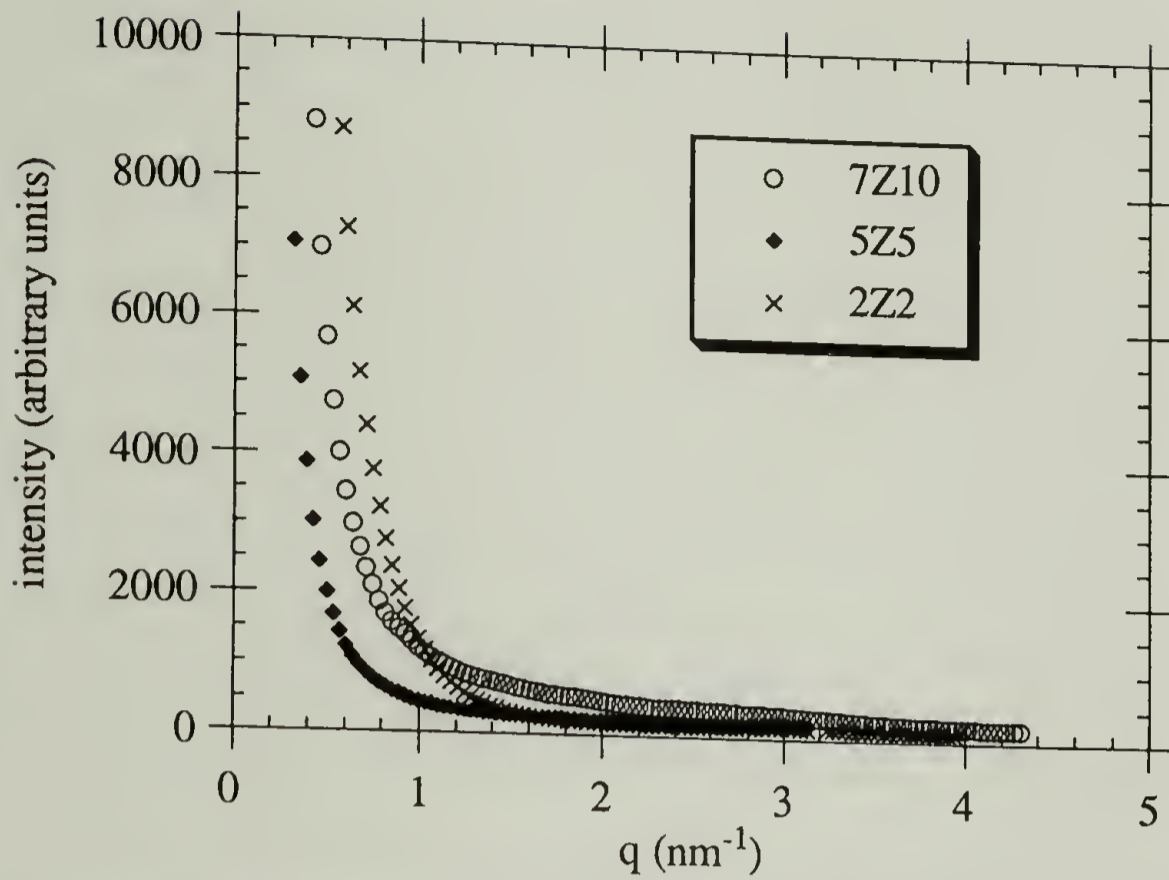


Figure 3.27: SAXS plots for zinc styrene/ethyl acrylate blends.

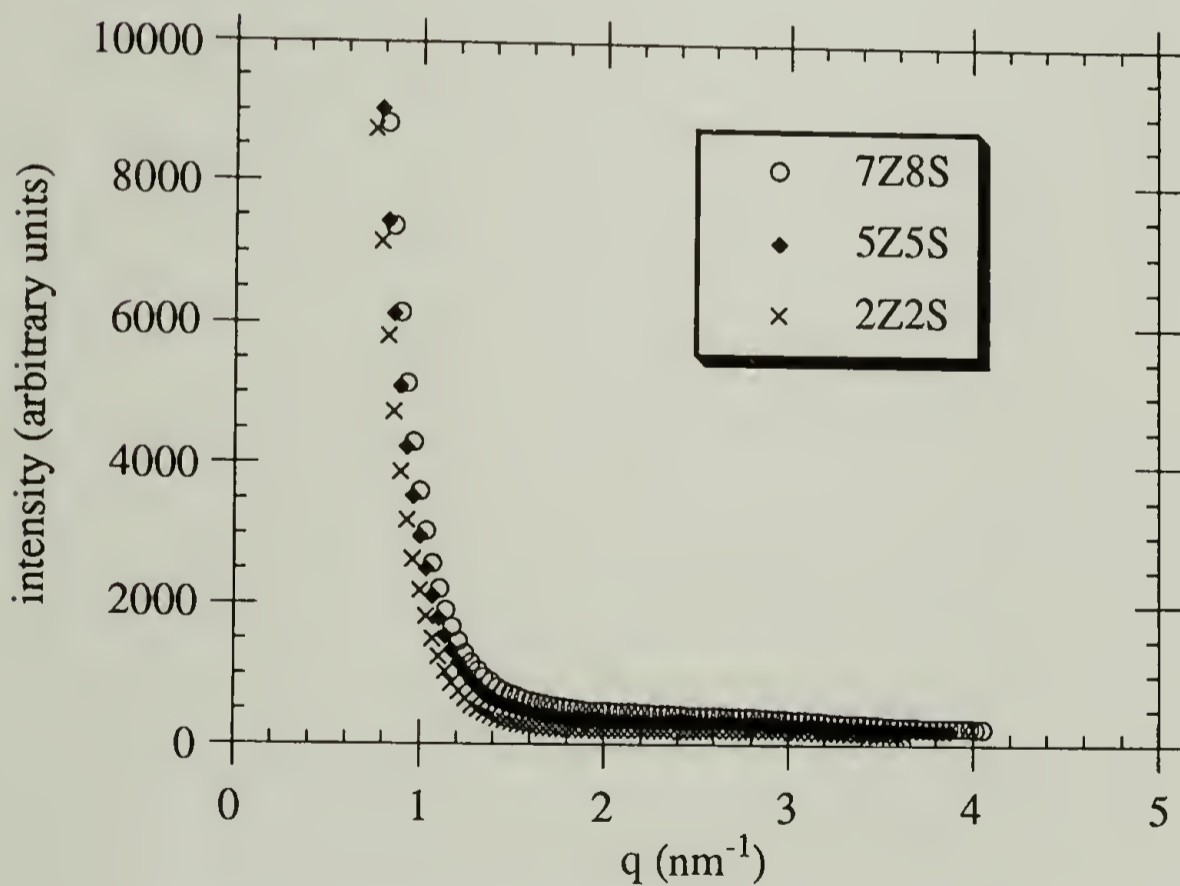


Figure 3.28: SAXS plots for zinc styrene/styrene blends.

probably due to the amounts of solvent added. When only small amounts are added the polar solvent acts to solvate the ions, resulting in a greater charge separation and a greater electrostatic driving force for aggregation. At saturation, however, the solvent increases the local dielectric constant, screening the charges and reducing the electrostatic attraction between ionic groups.

If the pyridine substituent in the blends is considered to be a diluent, it is clear that the blends fall into the category of high diluent levels, since the blends were prepared at a sulfonate/pyridine ratio of 1. It would appear that the absence of the ionic peak in the blends is due to the electrostatic screening effect of pyridine, resulting from the increased charge separation between interacting groups in the blends compared to the ionomers (see Section 3.2.2). Since the pyridine substituents are attached to polymer chains, there may also be an additional effect due to the increased steric requirements and higher level of cooperativity needed to allow four polymer chains to become part of a cluster in the case of the blends, compared to the requirements for only two polymer chains, as in the case of the ionomers.

Guinier plots based on the low angle upturn are shown in Figure 3.29 and the calculated radii for the clusters based on those plots are given in Table 3.6. It is obvious from Figure 3.29 that Guinier's Law is not followed in most of the materials. This result is due to the limited applicability of Guinier's Law to ionomers, and the large error in the data at low angles. Accurate data at low angles requires extremely accurate collimation, and precise measurements of the parasitic scattering and absorption coefficients. Even with desmearing, slit collimation is not likely to give the required accuracy at low angles. The only samples that appear to follow Guinier's Law reasonably well are the ZSPS/SVP blends. The value of the Guinier radii for these blends, approximately 30 Å, seems to correspond with what has been observed for the core plus shell radius. However, the absence of an ionic peak suggests that the short range order given by the core plus shell

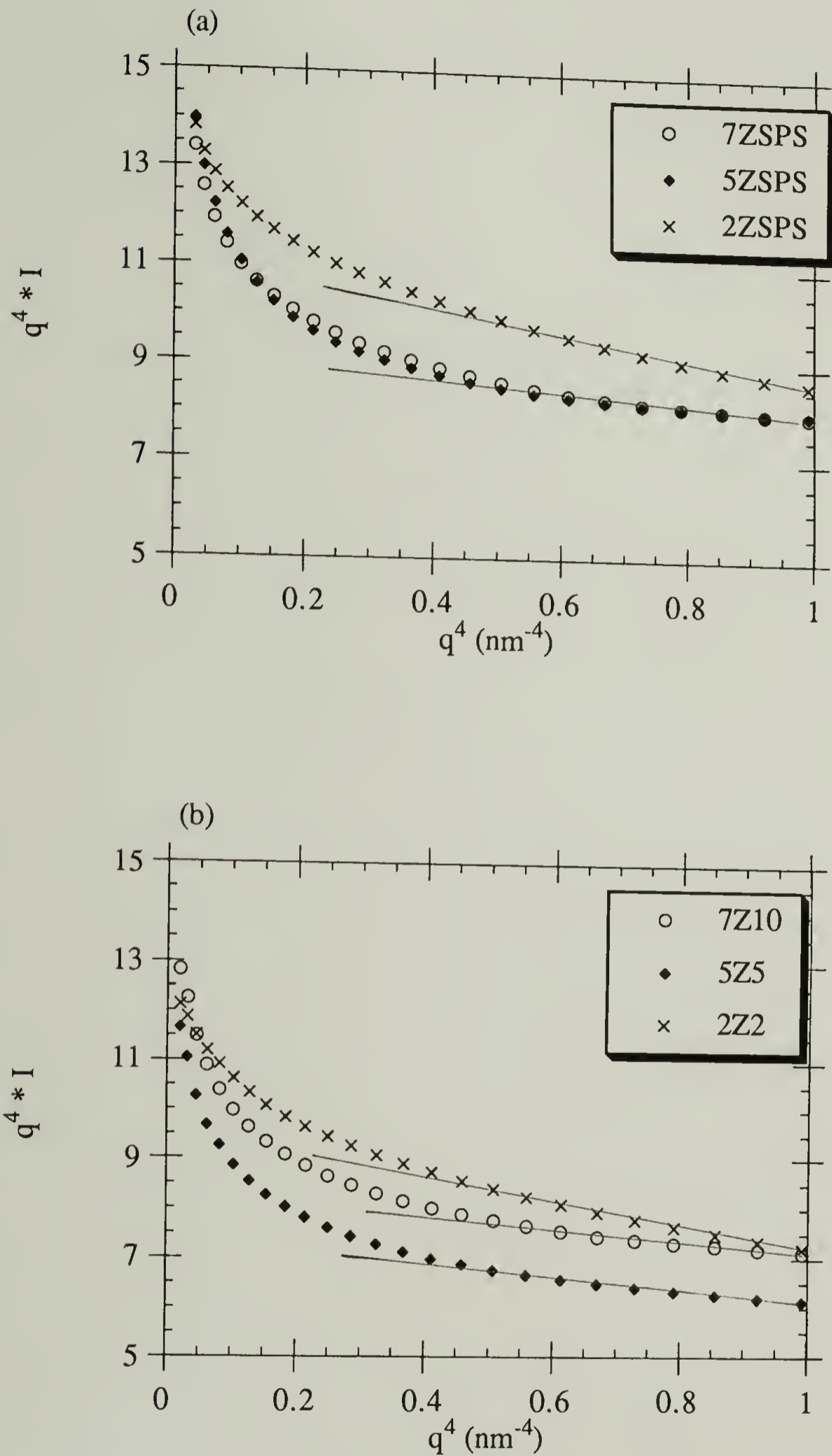


Figure 3.29: Guinier plots for (a) zinc ionomers, (b) zinc styrene/ethyl acrylate blends, and (c) zinc styrene/styrene blends.

continued on next page

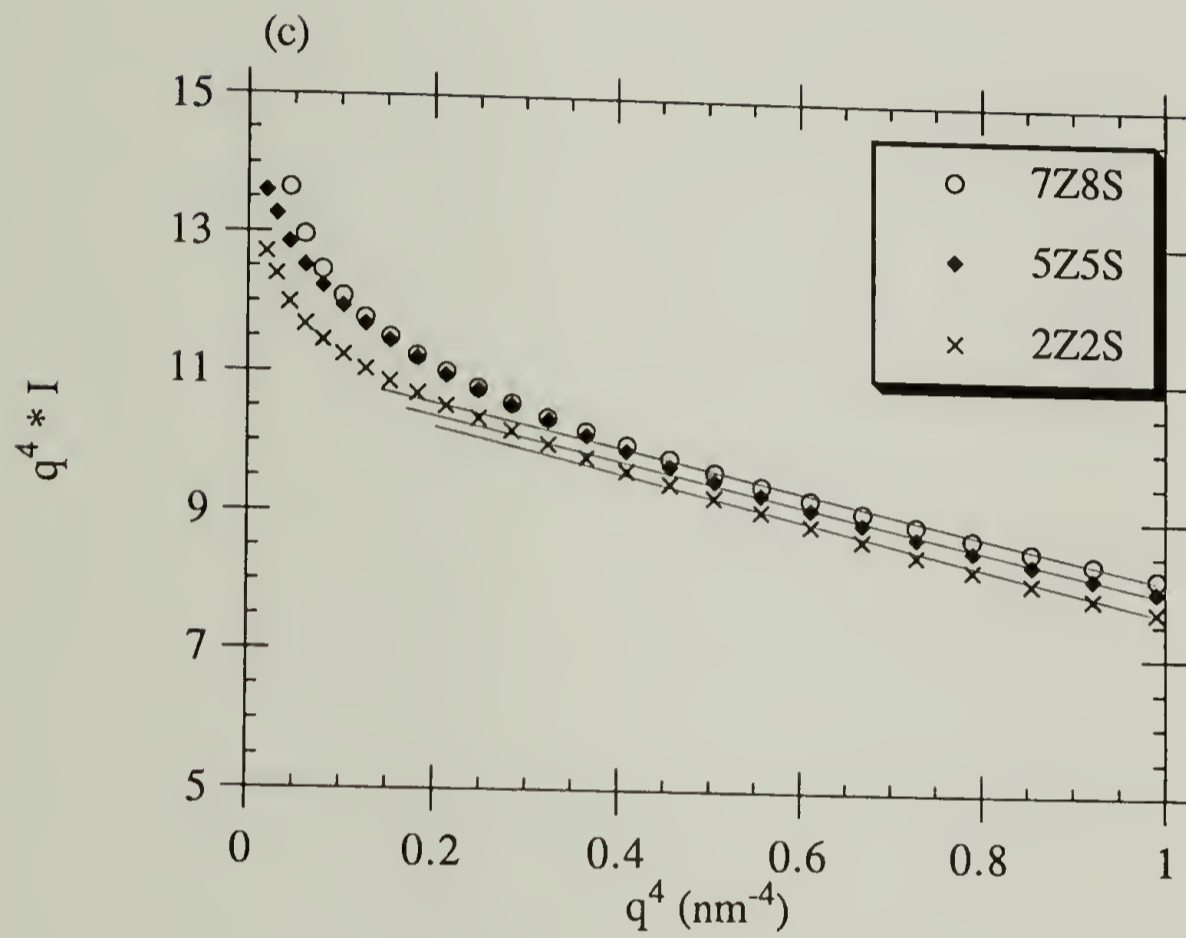


Figure 3.29 (continued)

Table 3.6 : Scattering parameters determined from Guinier and Porod analyses.

material	Guinier radius (Å)	Q (nm <sup>-3</sup> )	lim q <sup>4</sup> I (nm <sup>-4</sup> )	Os (nm <sup>-1</sup> )	L (Å)
2ZSPS	29.0 ± 2.0	25660	23950 ± 2000	0.147 ± 0.020	12.9 ± 0.6
5ZSPS	18.6	32610	58580	0.282	6.7
7ZSPS	20.9	33400	58460	0.275	6.9
2Z2	27.4	7620	7230	0.149	12.8
5Z5	20.8	6480	10100	0.245	7.8
7Z10	20.5	11380	17100	0.236	8.1
2Z2S	31.3	11080	8730	0.124	15.4
5Z5S	30.9	17380	11900	0.108	17.7
7Z8S	30.1	19490	16190	0.131	14.6



distances has been destroyed in the blends. Taggart<sup>28</sup> and MacKnight, et al.<sup>3</sup> have previously used a Guinier analysis to describe the upturn in ionomers, and in that case found radii of approximately 10 Å, corresponding to the core radii. In that case, however, the slit smeared data was used in the analysis. Given the limitations of applying Guinier's Law to ionomers and the requirement of extremely accurate low angle data, it must be concluded that no quantitative information can be obtained from a Guinier analysis of the data.

Better results can be obtained with a Porod analysis. The Porod plots are shown in Figure 3.30. Although the deviations from Porod's Law are fairly high, as seen by the positive slopes, the plots are linear, allowing the limiting values of  $Iq^4$  to be determined from equation 3.13a. In order to calculate the inhomogeneity length, an estimate of the cluster volume fraction must be made. MacKnight et al. have chosen 0.05, based on a radial distribution function analysis.<sup>3</sup> A fit of the depleted zone core-shell model to scattering data by Yarusso and Cooper results in a cluster volume fraction of 0.004-0.02.<sup>4</sup> Connolly has estimated the volume fraction from mechanical data based on the idea that the clusters act as filler particles, and found values between 0.05 and 0.15.<sup>16</sup> As a reasonable median value of these results, 0.05 was chosen for the purposes of these calculations.

The results of the analysis based on equations 3.13-16 are given in Table 3.6. The resulting values of the Porod inhomogeneity length ( $L$ ) are similar to the values determined by MacKnight, et al.<sup>3</sup> for ethylene ionomers, and correspond to the core size. The errors given in Table 3.6 are based solely on the errors in determining the slopes of the lines from equation 3.13. The actual errors are likely to be much higher due to the inherent limitations of applying Porod's Law to these systems.

The values for the ZSPS's and ZSPS/EAVP blends are quite similar. However, from the modulus data in Section 3.2.2 it is known that the number of ionic groups per cluster is much lower in the blends. Therefore, the density of the ionic groups in a cluster must be lower in the blends. This is consistent with the presence of the large pyridine substituent

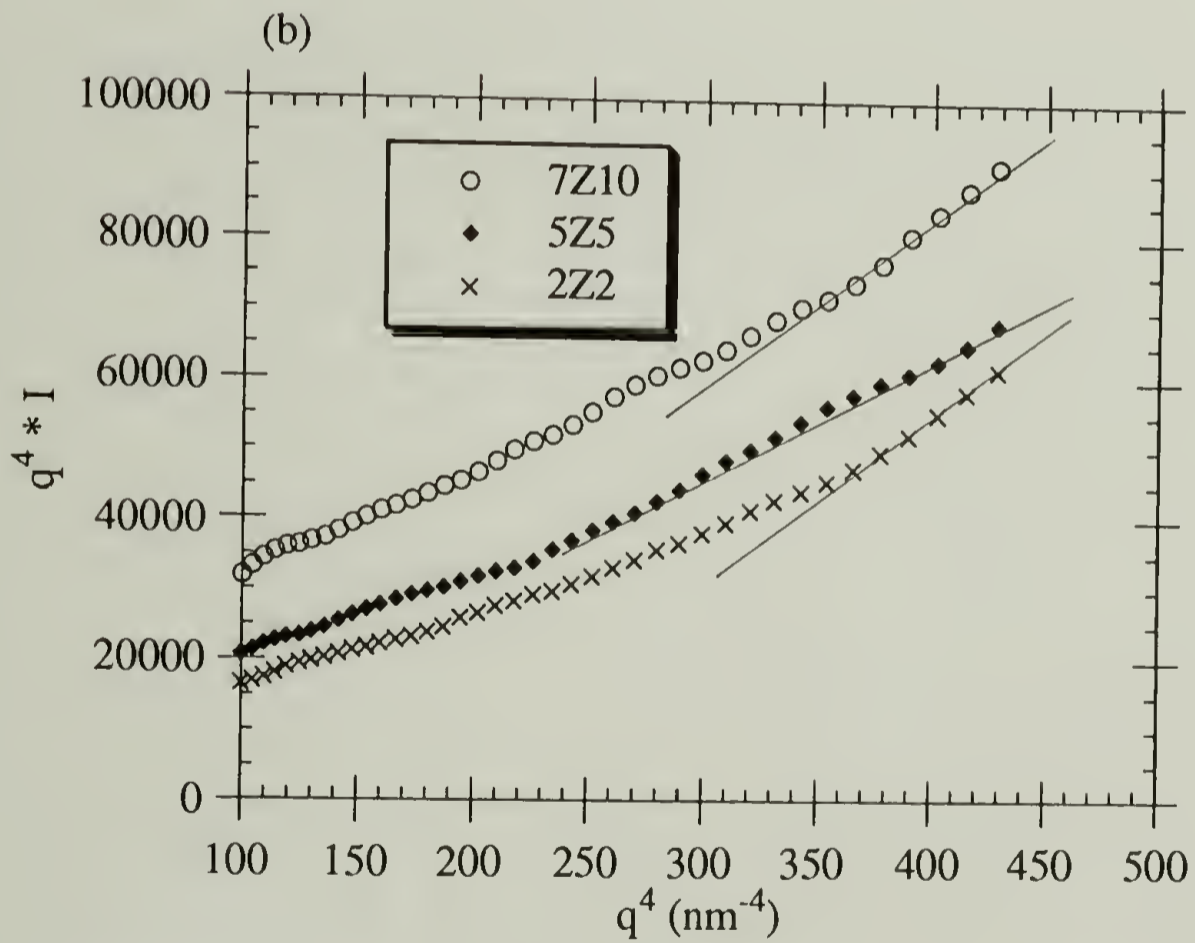
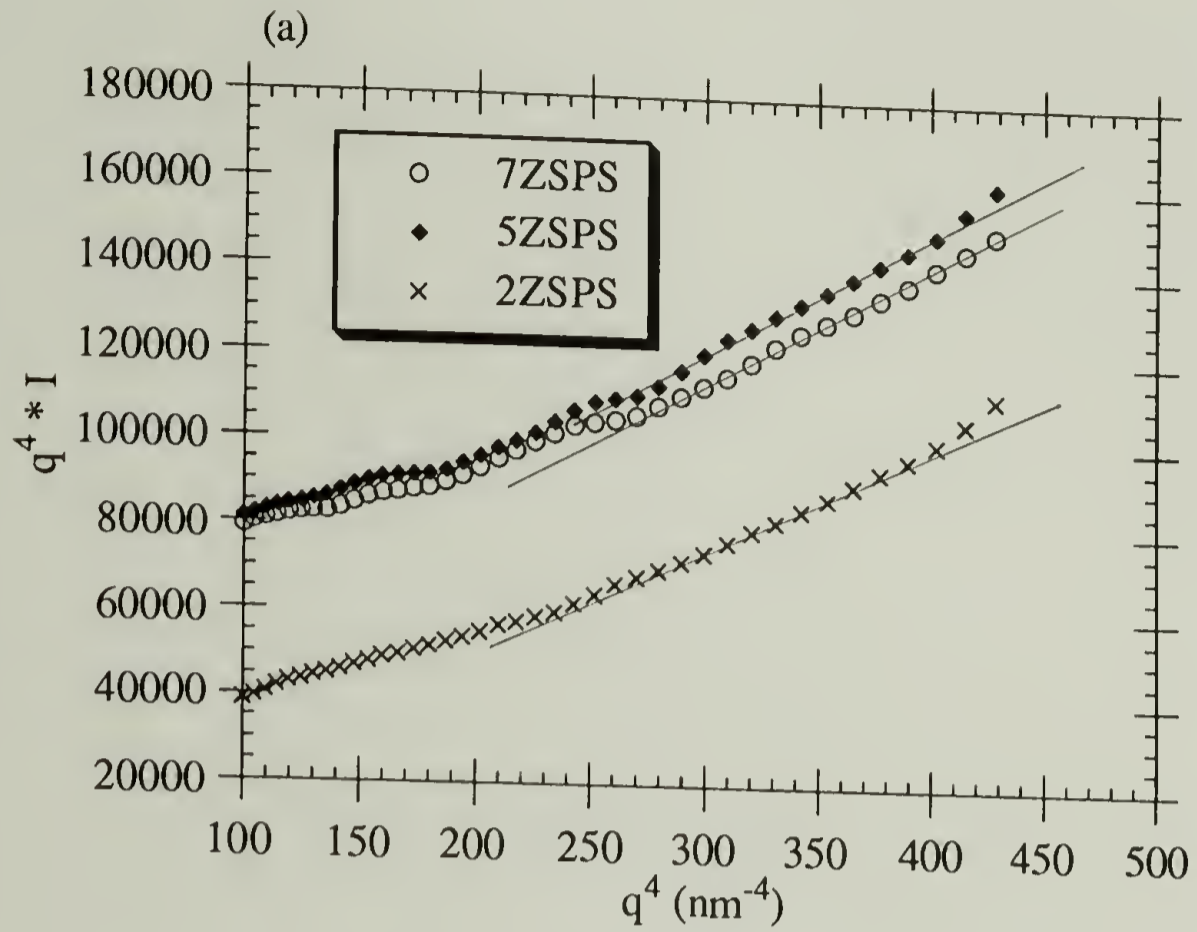


Figure 3.30: Porod plots for (a) zinc ionomers, (b) zinc styrene/ethyl acrylate blends, and (c) zinc styrene/styrene blends.

continued on next page

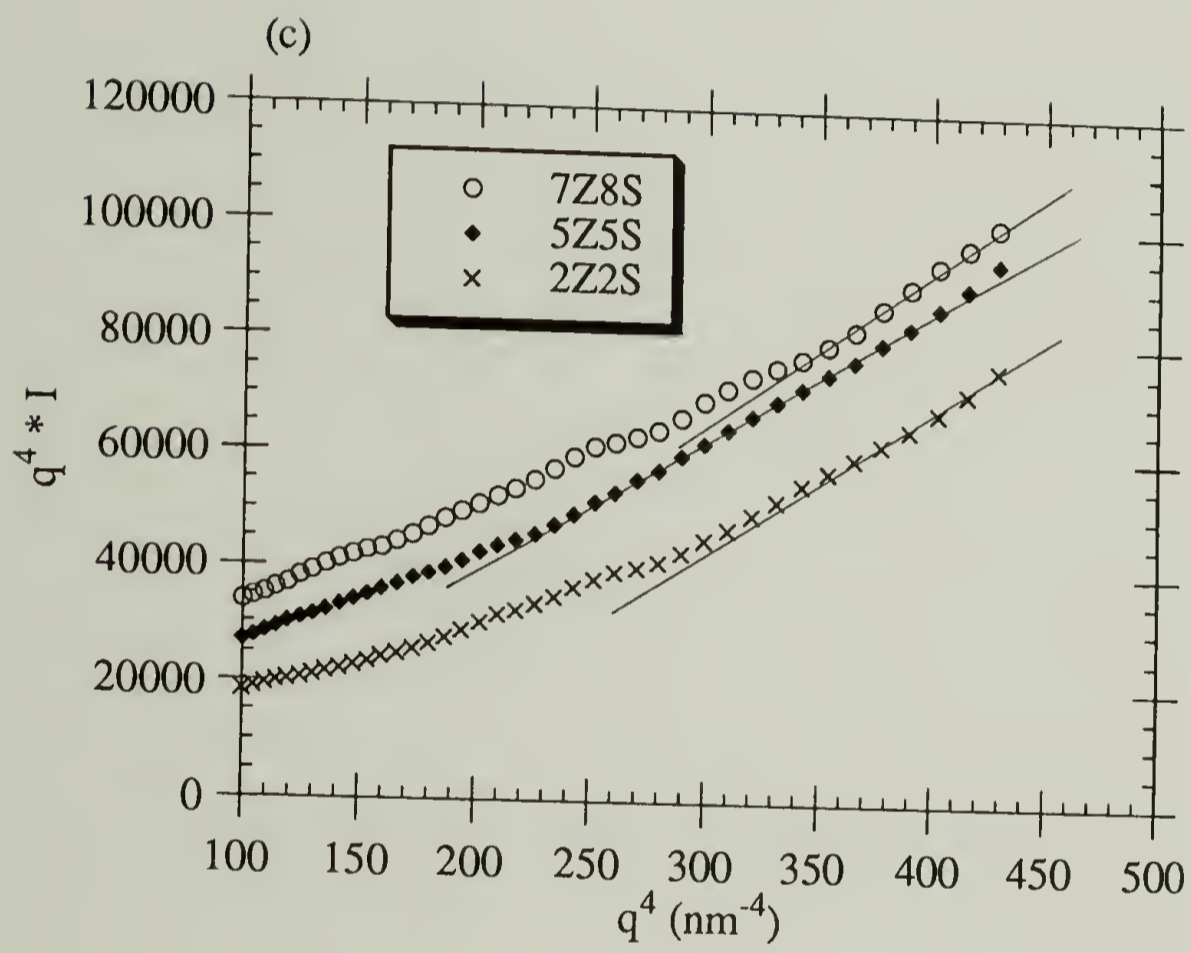


Figure 3.30 (continued)

and the additional polymer chain associated with each pyridine that must be incorporated into the cluster. The larger radius at the 2% substitution level may be because fewer ionic groups allow greater mobility, and thus the clusters are able to become more fully developed at the lower substitution level. The values of  $L$  for the ZSPS/SVP blends are higher than for either of the two materials. Although it is not clear why the values for this blend should be higher than for the ZSPS/EAVP blend, the results are still consistent with the decrease in ionic group density within the cluster due to pyridine substituents and the additional polymer chains associated with them.

### 3.3 Conclusions

Viscoelastic and small angle x-ray scattering measurements have shown the effect of blending on the aggregation behavior of ionomers. The cluster transition temperatures as measured by dynamic shear measurements are lowered for the blends compared to the ionomers. Comparison of the results for styrene/ethyl acrylate and styrene/styrene blends shows that both the pyridine substituent and the ethyl acrylate segments incorporated into the cluster act as internal plasticizers. Interestingly, even though the acid forms of sulfonated polystyrene do not show a cluster transition, the corresponding acid blends do show a cluster transition. The cluster transition in the acid blends is due to the acid/base interaction between sulfonic acid and pyridine which results in charge separation between the sulfonate anion and pyridinium cation. This charge separation provides the electrostatic interactions required for the formation of aggregates.

Activation energies for the cluster transitions occur in the order HSPS/SVP > ZSPS/SVP > ZSPS > ZSPS/EAVP. This order is rationalized on the basis of the degree of charge separation within the interactions, and provides evidence that the ionic cluster transition occurs due to dissociation and motion of the ionic groups.

The scattering data also support the view that the effect of blending is to plasticize the clusters. The suppression of the ionic peak is the same result that has been seen for ionomers plasticized with low molecular weight compounds. By considering that the cluster radius as determined by a Porod analysis is approximately the same in the blends and the ionomers, and that the functionality as determined by DMTA is lower in the blends than in the ionomers, it can be seen that the density of ionic groups in the cluster is much lower for the blends.

The interpretation of the data has been dependent on the depleted zone core-shell model for aggregation in ionomers. The reason for choosing this model is that the data do not support the other two major models.

The restricted mobility model of Eisenberg et al. states that the "cluster" is actually a region of restricted mobility of hydrocarbon chains.<sup>5</sup> These chains are restricted due to the crosslinking effect of multiplets, which are small aggregates consisting of ionic groups in contact with each other. The cluster transition in this model is the glass transition of the chains with restricted mobility. The action of a polar plasticizer is to "loosen" the multiplet, allowing greater mobility for the restricted hydrocarbon chains. If this were the case, one would expect the cluster transition temperatures and activation energies to occur in the same order because the same mechanism is involved for each of them. If one plasticizer were more effective than another, then the more effective plasticizer would result in a lower transition temperature and a lower activation energy. The results described in Section 3.2.2 show that this is not the case. For example, ZSPS has a higher transition temperature than the ZSPS/SVP blends, but the blends have the higher activation energy.

The second major model of aggregation in ionomers is the hard sphere liquid-like interference model of Yarusso and Cooper.<sup>4</sup> In this model the clusters are arranged with a liquid-like degree of order, and the ionic peak in SAXS measurements is due to a distance of closest approach of the clusters. However, the data presented in Section 3.2.3 show that the ionic peak is not present, even though the dynamic shear measurements show a

cluster transition. It is hard to imagine a situation in which the distance of closest approach is eliminated while still leaving the clusters intact, since it is the clusters that define that distance. Also, the model of Yarusso and Cooper explains the upturn in the SAXS curves as being due to long range inhomogeneities in the distribution of clusters. This explanation implies either that the Guinier scattering is due to very large size scales, or that the upturn eventually resolves into a peak. There is no evidence that the upturn is the high angle side of a peak, and the results presented both in this work and the work of MacKnight et al. show that in those systems which follow Guinier's Law the particle radius is no more than 30 Å.

The depleted zone core-shell model is also preferred over the others on physical grounds. It is unlikely that the restriction in mobility caused by ionic crosslinks in the Eisenberg model is sufficient to create an increase in  $T_g$  of 150° C, nor is it likely that the volume of the affected region is large enough to be considered a separate phase. Although regions of restricted mobility have been identified in networks,<sup>33</sup> the effects are nowhere near the magnitude that is proposed for ionomers.

The Yarusso and Cooper model implies a volume fraction of clusters of approximately 0.35. This value seems unreasonably high considering the small number of ionic groups on the polymer chains and the steric requirements involved in forming a cluster.

In summary, investigation of investigation of the viscoelastic behavior of the ionomer blends has shown for the first time that the ionic groups are aggregated, as they are in ionomers. Examination of the blends has also provided new insight into the nature of the aggregation in ionomers. Specifically, it is possible to conclude that the depleted zone core-shell model is best able to describe the morphology in both the blends and the ionomers.

### 3.4 References

1. MacKnight, W. J.; Earnest, T. R. *J. Poly. Sci. : Macromol. Rev.*, **16**, 41 (1981)
2. Fitzgerald, J. J.; Weiss, R. A. *J. Macromol. Sci.-Rev. Macromol. Chem. Phys.*, **C28**, 99 (1988)
3. MacKnight, W. J.; Taggart, W. P.; Stein, R. S. *J. Poly. Sci. : Symp.*, **45**, 113 (1974)
4. Yarusso, D. J.; Cooper, S. L. *Macromolecules*, **16**, 1871 (1983)
5. Eisenberg, A.; Hird, B.; Moore, R. B. *Macromolecules*, **23**, 4098 (1990)
6. Hird, B.; Eisenberg, A. *J. Poly. Sci. : Part B : Phys.*, **28**, 1665 (1990)
7. Weiss, R. A.; Lefelar, J. A. *Polymer*, **27**, 3 (1986)
8. Lundberg, R. D.; Makowski, H. S.; Westerman, L. *Poly. Prep.*, **19**, 310 (1978)
9. Fitzgerald, J. J.; Kim, D.; Weiss, R. A. *J. Poly. Sci. : Part C : Letters*, **24**, 263 (1986)
10. Weiss, R. A.; Fitzgerald, J. J.; Kim, D. *Macromolecules*, **24**, 1064 (1991)
11. Yano, S.; Nagao, N.; Hattori, M.; Hirasawa, E.; Tadano, K. *Macromolecules*, **25**, 368 (1992)
12. Simmons, A.; Eisenberg, A. *Poly. Prep.*, **27**, 341 (1986)
13. Alexander, L. E. *X-Ray Diffraction Methods in Polymer Science*, Robert E. Krieger Publishing Company, Malabar, Florida, 1985
14. Glatter, O. *J. Appl. Cryst.*, **7**, 147 (1974)
15. Eisenberg, A.; Navratil, M. *Macromolecules*, **7**, 90 (1974)
16. Connolly, J. M., Ph.D. Thesis, University of Massachusetts, 1989
17. Weiss, R. A.; Fitzgerald, J. J.; Kim, D. *Macromolecules*, **24**, 1071 (1991)
18. Eisenberg, A.; King, M. *Ion-Containing Polymers*, Academic Press, New York, 1977
19. Weiss, R. A.; Lefelar, J. A. *Polymer*, **7**, 3 (1986)
20. Sakurai, K.; Douglas, E. P.; MacKnight, W. J. *Macromolecules*, submitted
21. Eisenberg, A. *Macromolecules*, **3**, 147 (1970)
22. Sakurai, K.; Douglas, E. P.; MacKnight, W. J. *Macromolecules*, in press
23. Eisenberg, A.; King, M.; Navratil, M. *Macromolecules*, **6**, 734 (1973)

24. Aklonis, J. J.; MacKnight, W. J. *Introduction to Polymer Viscoelasticity*, John Wiley & Sons, New York, 1983
25. Pearson, D. S.; Graessley, W. W. *Macromolecules*, **11**, 528 (1978)
26. Ferry, J. D. *Viscoelastic Properties of Polymers*, John Wiley & Sons, New York, 1980
27. Plazek, D. J. *J. Phys. Chem.*, **69**, 3480 (1965)
28. Taggart, W. P., Ph.D. Thesis, University of Massachusetts, 1973
29. Peiffer, D. G.; Weiss, R. A.; Lundberg, R. D. *J. Poly. Sci. : Physics*, **20**, 1503 (1982)
30. Fitzgerald, J. J.; Kim, D.; Weiss, R. A. *J. Poly. Sci. : Letters*, **24**, 263 (1986)
31. Yarusso, D. J.; Cooper, S. L. *Polymer*, **26**, 371 (1985)
32. Fitzgerald, J. J.; Weiss, R. A. *Proc. Annu. Tech. Conf. Soc. Plast. Eng.*, 341 (1985)
33. Dickinson, L. C.; Morganelli, P.; Chu, C. W.; Petrovic, Z.; MacKnight, W. J.; Chien, J. C. W. *Macromolecules*, **21**, 338 (1988)



CHAPTER 4  
MECHANICAL PROPERTIES  
AND DEFORMATION BEHAVIOR

4.1 Introduction

One of the largest uses of polymers is in structural applications, and therefore it is important to understand their mechanical behavior. In tensile tests polymers can generally be divided into two classes: plastics and rubbers.<sup>1</sup> Plastics are characterized as having highly brittle behavior, with little or any plastic deformation. Their stress-strain curves are linear almost to the point of fracture. Rubbers are characterized by showing a yield point following the initial linear portion of the curve and a high level of elongation before failure, typically several hundred percent. Rubbers can be further characterized as crosslinked or not crosslinked. The major difference in the mechanical properties of the two is that the crosslinked systems show a dramatic increase in stress immediately before fracture while the uncrosslinked systems do not.

Polymer blends provide opportunities for enhancing the mechanical properties of polymers. Studies on miscible blends have shown that properties such as modulus and strength are higher than what would be predicted from linear additivity of the properties of the two components.<sup>2-5</sup> This has been explained on the basis of the reduction in volume upon mixing, which restricts the mobility of the chains in the blend.<sup>4,5</sup>

Immiscible polymers typically show properties that lie below linear additivity.<sup>6</sup> However, in some cases it can be advantageous to have an immiscible blend. Probably the best known example of this behavior is high impact polystyrene (HIPS).<sup>7,8</sup> HIPS is polystyrene containing approximately 20% rubber particles. The addition of the rubber particles results in increased ductility and greater impact strength. Some of the same

behavior can be seen when the minor phase is glassy, as in the case of polystyrene filled with glass beads.<sup>9</sup>

Some of the factors which are known to control the mechanical properties of immiscible blends are the size and volume fraction of the disperse phase and the amount of adhesion between the two phases at the interface.<sup>6-8</sup> Block copolymers have been successfully used to enhance the mechanical properties of immiscible blends.<sup>6,10,11</sup> When each block is miscible with one of the phases the copolymer spans the interface between the two, enhancing the interfacial adhesion.

Deformation mechanisms in polymers have been examined extensively.<sup>7-9,12-16</sup> There are two basic mechanisms for plastic deformation, crazing and shear banding. Crazes consist of highly drawn fibrils of polymer separated by voids. The amount of empty space in a craze can be as high as 50%. Shear bands are regions of oriented polymer. The major difference between the two mechanisms is that shear banding is a constant volume process, while crazing results in an increase in volume. Different polymers undergo different deformation mechanisms. For example, polystyrene undergoes crazing, while poly(phenylene oxide) deforms by shear banding.<sup>16</sup> The toughening in HIPS is caused by the presence of the rubber particles, which are able to act as both efficient nucleators and terminators of crazes. The extensive formation of crazes allows a high level of plastic deformation without fracture.

There have been few studies on the mechanical properties of ionomers or ionomer blends. An extensive study has been done by Bellinger on sulfonated polystyrene ionomers.<sup>17</sup> The ultimate strength of the ionomers was found to undergo a maximum as a function of sulfonation level. This was attributed to the ionic clusters acting as reinforcing particles at low sulfonation levels. At higher sulfonation levels the clusters become dominant in determining the properties, and the strength decreases. Extensive microscopic observations of deformation in blends of the ionomers with polystyrene showed that as the

amount of the ionomer in the blend increased there was a change in the deformation mechanism from crazing to shear banding.

There have been two studies of the mechanical properties of ionomer blends similar to the ones described in this work. Agarwal et al. examined the tensile properties of zinc neutralized sulfonated EPDM/poly(styrene-co-4-vinylpyridine) blends and found the maximum increase in tensile strength at a sulfonate to pyridine ratio of 1.<sup>18</sup> However, no attempt was made to measure the mechanical properties as a function of substitution level. Belfiore et al. saw a similar result for blends of a zinc-neutralized ethylene/methacrylic acid copolymer with poly(4-vinylpyridine).<sup>19</sup> The purpose of this chapter is to describe some preliminary investigations on the mechanical properties and deformation behavior of ionomer blends.

## 4.2 Results and Discussion

### 4.2.1 Experimental

**Blending.** The blends used are the same as the ones described in Chapter 2. For a description of the blending procedure and the nomenclature for the blends, see Section 2.2.1.

**Tensile Tests.** Tensile tests were performed in accordance with ASTM D882. Samples were compression molded into thin strips approximately 0.1 mm x 5 mm x 80 mm. The exact dimensions were measured for each sample. The molding temperatures were the minimum temperatures needed to cause flow, which were 175° C for the HSPS's and all SPS/EAVP blends, 200° C for the SPS/SVP blends, 250° C for the ZSPS's, and 30° C for the EAVP's. Samples were held at the molding temperature for 6 minutes, followed by quenching to room temperature.

Tensile tests were done at room temperature on an Instron tensile tester equipped with a 50 kg load cell, except for the tests for the EAVP's, for which a 20 g load cell was used. Samples were run with an initial gauge length of 50 mm at a constant crosshead speed of 5 mm/min. Three to five samples were run for each material and the results for the samples averaged. Moduli are given as the initial slope of the stress versus strain curve, stress to break and elongation at break as the values at the end of the test, and work to break as the integrated area under the curve.

**Fracture Surfaces.** Compression molded samples were placed in liquid nitrogen and freeze fractured under impact. The samples were coated with a thin layer of gold and examined using a Jeol 35CF scanning electron microscope operating at 20 kV.

#### 4.2.2 Mechanical Properties and Deformation Behavior

The stress-strain curves for the precursor materials are shown in Figures 4.1-4.3. The calculated values of modulus, strength at break, elongation at break, and work to break are given in Table 4.1. For the most part the values for the SPS's are similar to polystyrene. It has been reported by Bellinger that ionomers show an increase in strength with increasing sulfonation level up to 5% sulfonation level, followed by a decrease at higher sulfonation levels.<sup>17</sup> The same trends are seen for the ZSPS's here. Bellinger interpreted these results as being due to the clusters acting as reinforcing particles at low sulfonation levels. At higher sulfonation levels the clusters become more dominant in determining the properties, and the strength decreases. The HSPS's show the same increase in strength as the ZSPS's, but no subsequent decrease. Since there are no clusters in HSPS (see Chapter 3), the increase in strength is probably due to the hydrogen bonding interactions between sulfonic acid groups.

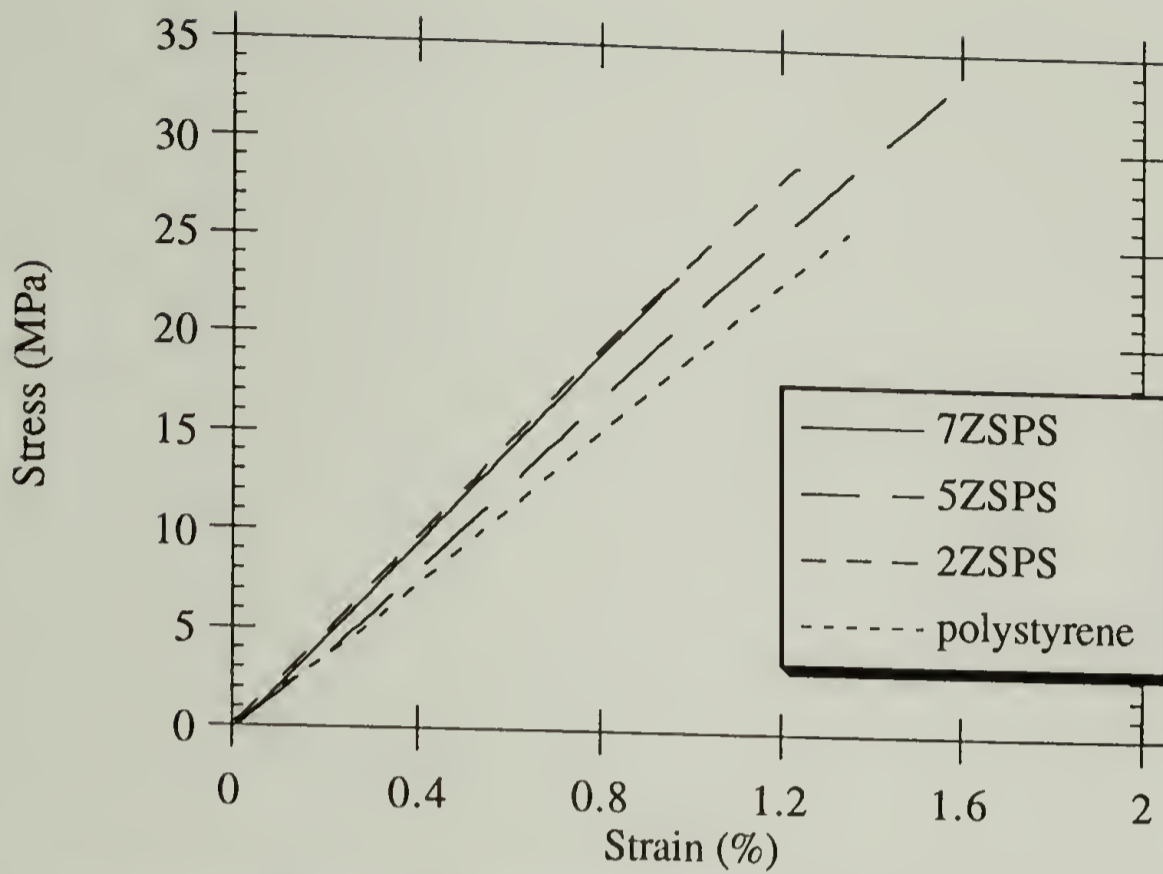


Figure 4.1: Stress-strain curves for zinc neutralized polystyrene ionomers.

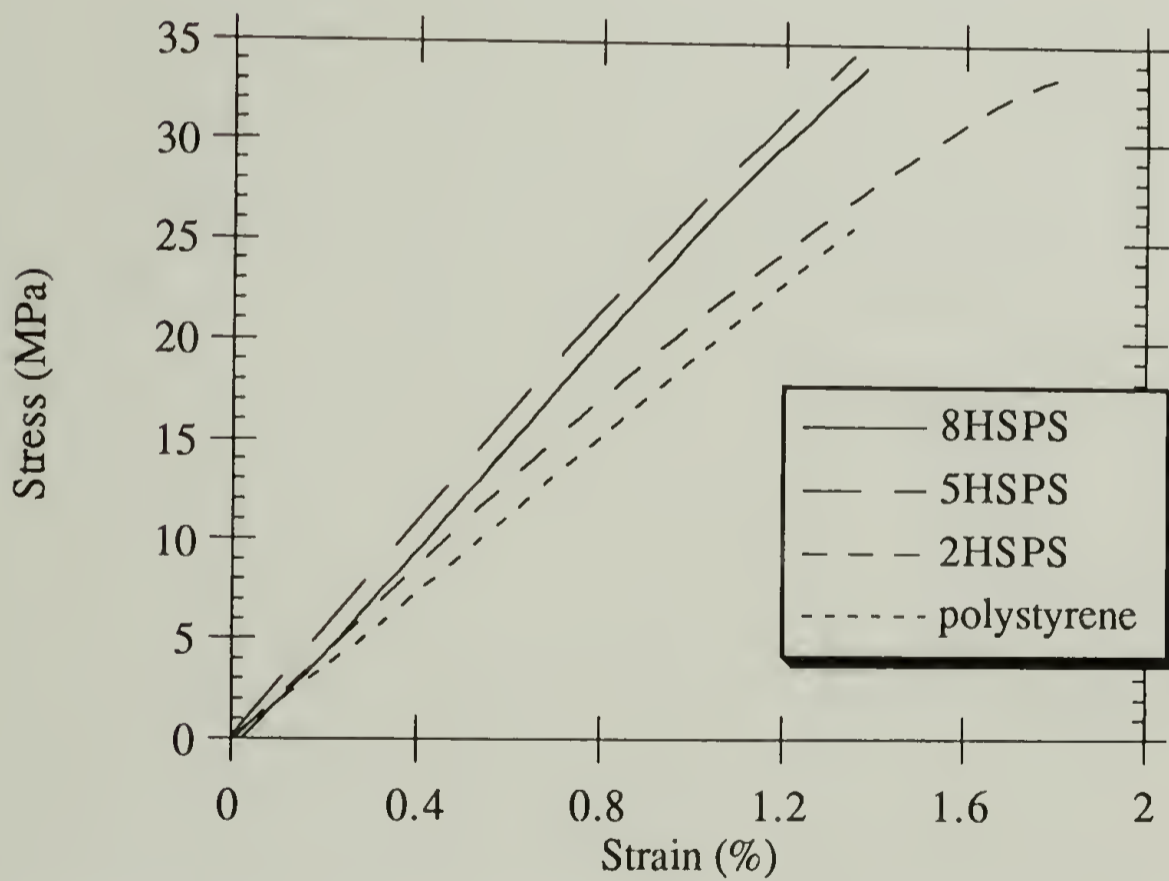


Figure 4.2: Stress-strain curves for acid forms of sulfonated polystyrene.

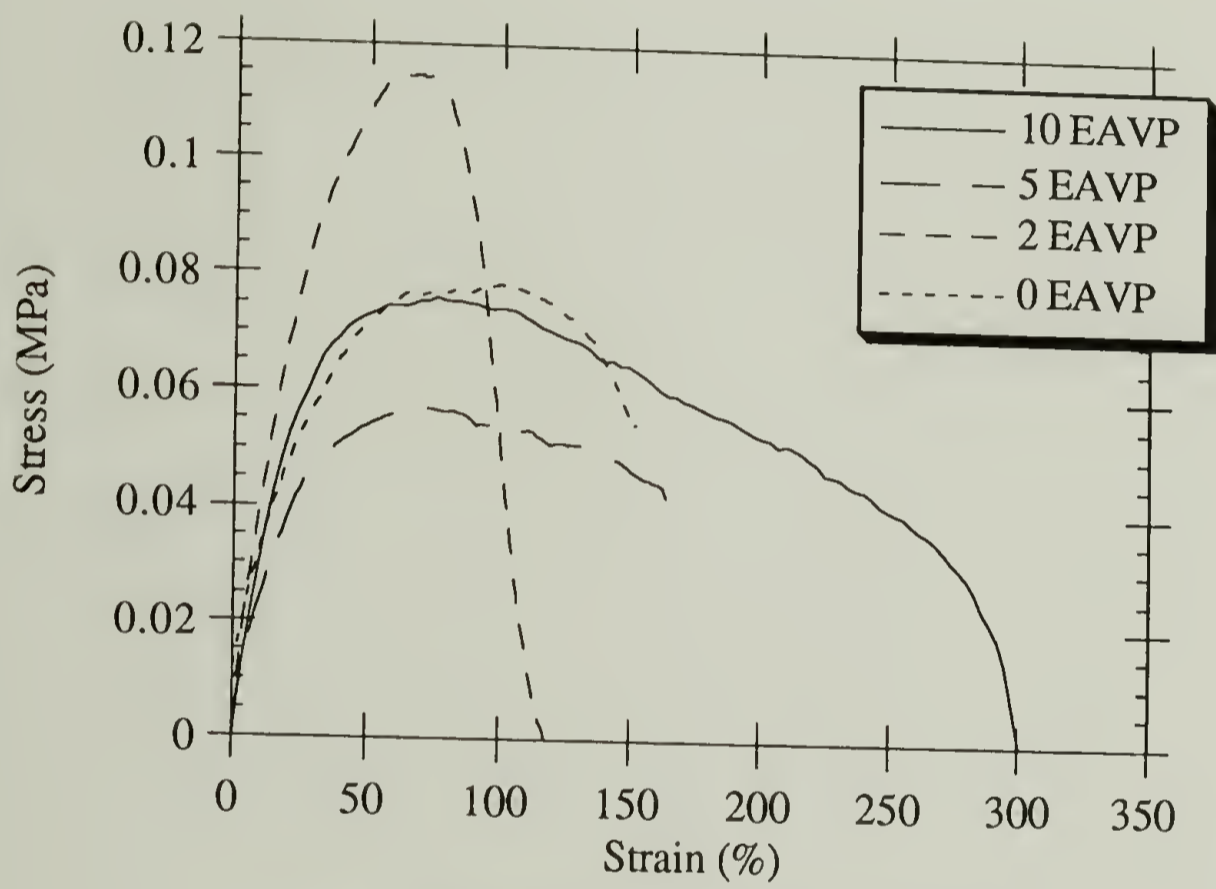


Figure 4.3: Stress-strain curves for EAVP's.

Table 4.1: Tensile test data for blend precursors.

material	modulus (MPa)	stress at break (MPa)	elongation at break (%)	yield strength (MPa)	elongation at yield (%)	energy to break (J/m <sup>3</sup> )
0SPS	1920 ± 130	24.7 ± 2.4	1.3 ± 0.1	-----	-----	0.16 ± 0.03
2HSPS	2170 ± 190	28.9 ± 4.7	1.5 ± 0.3	-----	-----	0.23 ± 0.10
5HSPS	2460 ± 430	34.8 ± 4.3	1.5 ± 0.4	-----	-----	0.25 ± 0.12
8HSPS	2400 ± 140	34.3 ± 2.7	1.5 ± 0.1	-----	-----	0.26 ± 0.04
2ZSPS	2600 ± 220	29.7 ± 1.0	1.2 ± 0.1	-----	-----	0.18 ± 0.01
5ZSPS	2260 ± 280	33.5 ± 0.8	1.5 ± 0.2	-----	-----	0.25 ± 0.03
7ZSPS	2550 ± 120	23.9 ± 2.1	1.0 ± 0.1	-----	-----	0.12 ± 0.03
0EAVP	0.25 ± 0.06	-----	-----	0.08 ± 0.00	94.0 ± 40.6	0.10 ± 0.05
2EAVP	0.41 ± 0.09	-----	-----	0.11 ± 0.02	83.7 ± 5.8	0.09 ± 0.05
5EAVP	0.21 ± 0.07	-----	-----	0.05 ± 0.01	73.0 ± 8.7	0.03 ± 0.01
10EAVP	0.48 ± 0.30	-----	-----	0.11 ± 0.07	77.7 ± 7.4	0.07 ± 0.04

The stress-strain curves for the EAVP's in Figure 4.3 reflect the rubbery nature of these materials. At high elongations the sample experiences a significant decrease in cross-sectional area as it draws, and so the engineering stress (the force divided by the original cross-sectional area), decreases. The true stress (the force divided by the actual cross-sectional area) is actually increasing throughout the test. Because the engineering stress decreased to almost zero at break, the ultimate strength and elongation values given for the EAVP's in Table 4.1 are at the peak of the stress-strain curve. The results show that the EAVP's have extremely poor properties.

Stress-strain curves for the blends are given in Figures 4.4-4.6. The calculated values for the properties are listed in Table 4.2. The results for blend 00 show that the properties are dominated by the rubbery phase. The gross phase separation and lack of any interfacial interactions causes the polystyrene phase to contribute almost nothing to the mechanical properties.

The results for the zinc blends show the effects of the change in phase behavior and the presence of interfacial interactions on the mechanical properties. Blend 2Z2, which is macrophase separated, has an ultimate strength and elongation greater than for the unfunctionalized blend. The high elongation shows that the rubbery phase still dominates the properties. However, the interactions have increased interfacial adhesion between the two phases, resulting in a higher strength. It is generally recognized that toughening mechanisms in rubber-modified plastics depends on efficient stress-transfer across the interface, which in turn depends on good interfacial adhesion.<sup>7,8</sup> In fact, the stress-strain curve for 2Z2 is similar to what is seen for HIPS, although the elongation is much higher for HIPS (around 40% elongation at break).<sup>7</sup> This difference may be because HIPS typically contains only 20% rubber particles, while these blends are approximately 50% rubber. Similar increases have been seen for the addition of diblock copolymers to immiscible polymer blends.<sup>6,10,11</sup> Like the ionic interactions here, block copolymers increase adhesion between the phases.



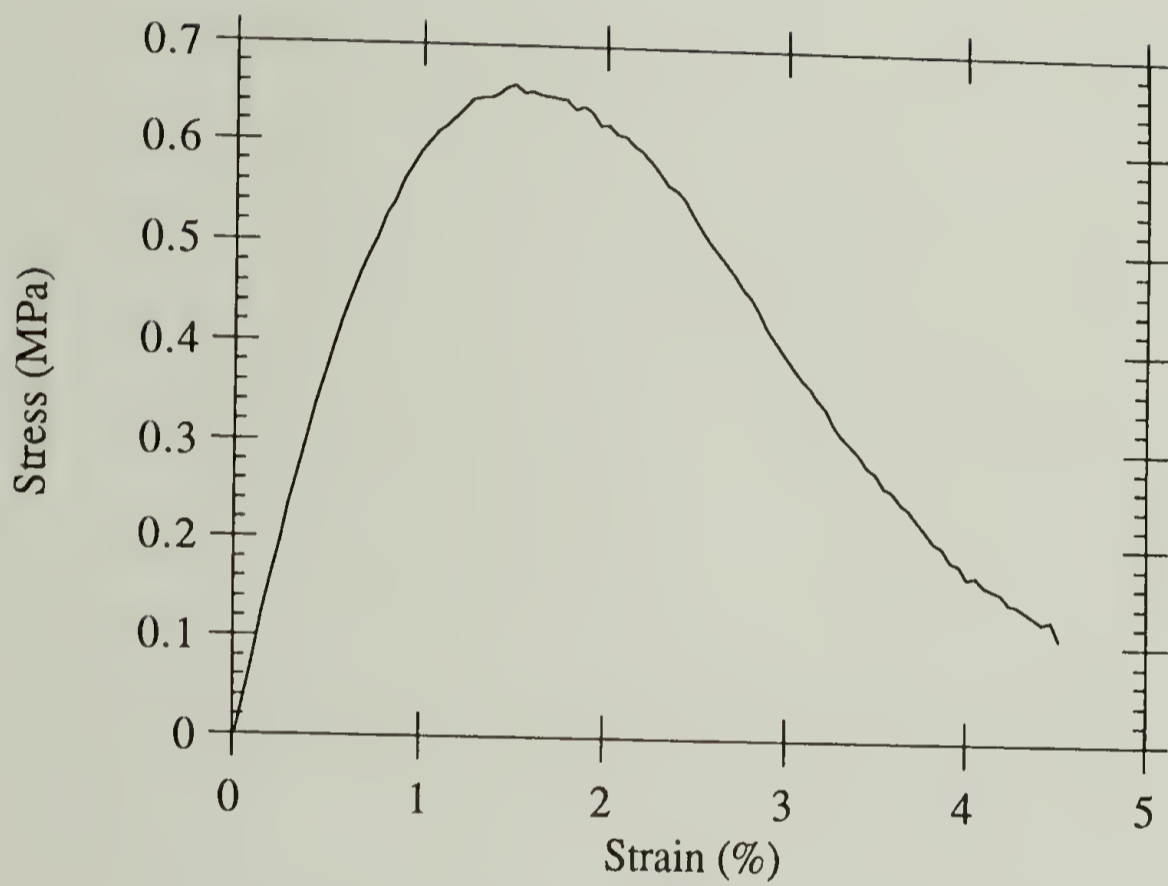


Figure 4.4 : Stress-strain curve for blend 00.

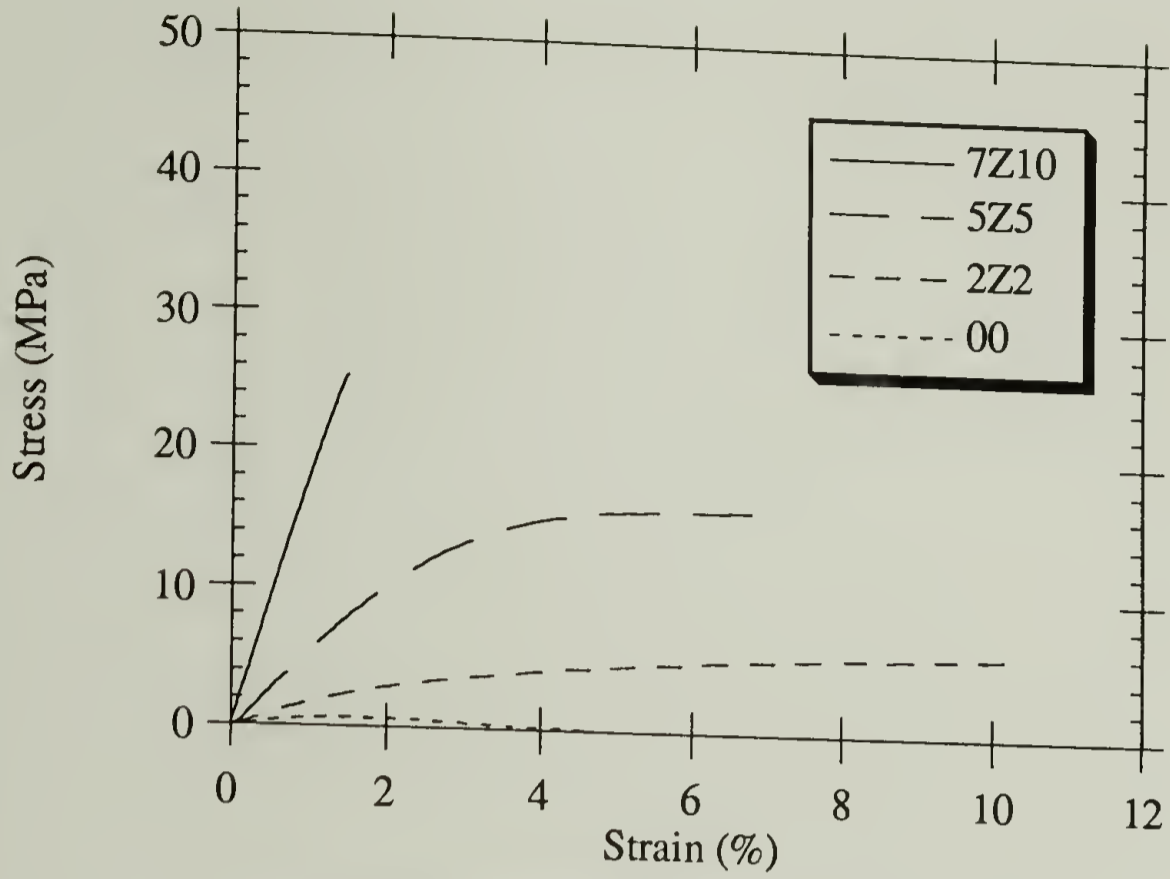


Figure 4.5: Stress-strain curves for zinc blends.

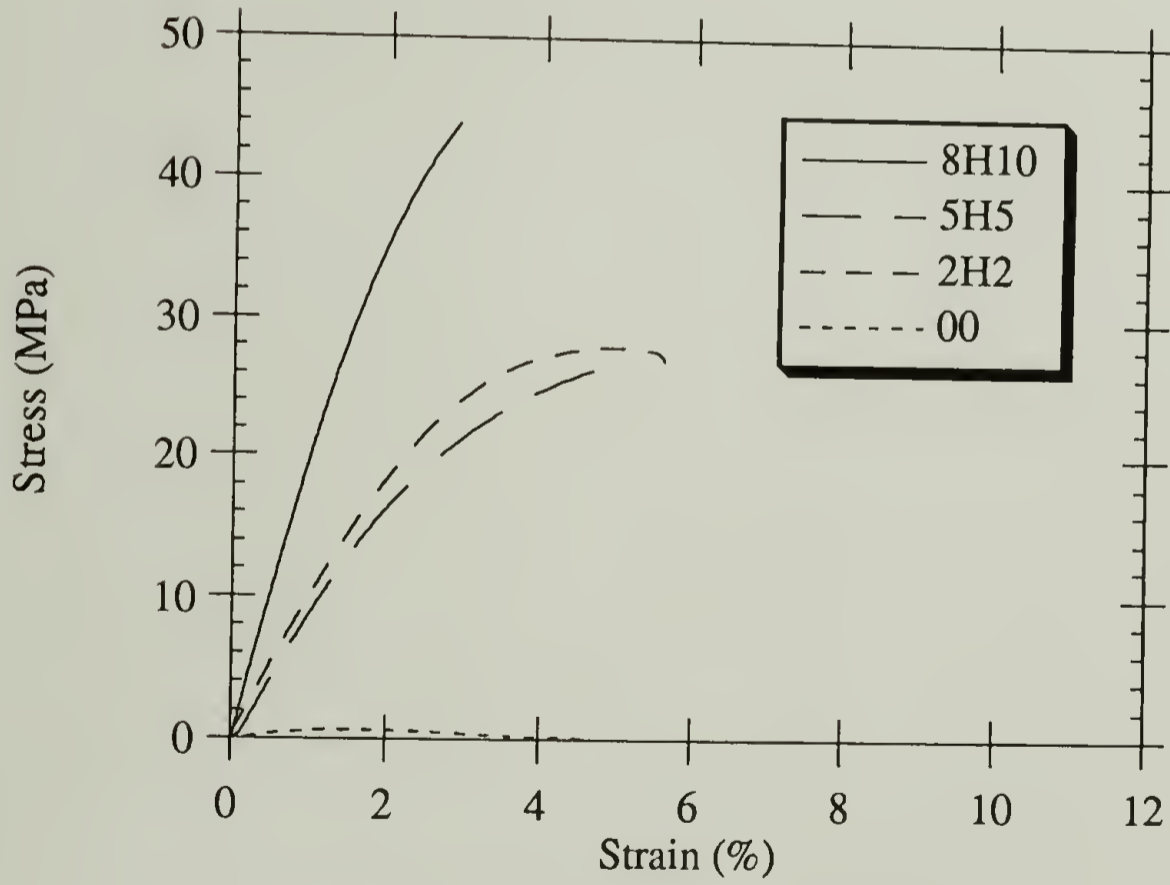


Figure 4.6: Stress-strain curves for acid blends.

Table 4.2: Tensile test data for ionomer blends.

material	modulus (MPa)	stress at break (MPa)	elongation at break (%)	yield stress (MPa)	elongation at yield (%)	energy to break ( $J/m^3$ )
00	$71.2 \pm 5.0$	$0.09 \pm 0.01$	$6.1 \pm 3.0$	$0.7 \pm 0.01$	$1.4 \pm 0.3$	$0.02 \pm 0.001$
2H2	$1040 \pm 180$	$24.6 \pm 2.2$	$5.0 \pm 0.7$	$26.6 \pm 2.0$	$4.5 \pm 1.0$	$0.75 \pm 0.38$
5H5	$1000 \pm 150$	$25.5 \pm 1.5$	$5.5 \pm 1.9$	$30.8 \pm 0.2$	$5.1 \pm 1.0$	$1.28 \pm 0.55$
8H10	$1900 \pm 280$	$44.7 \pm 3.7$	$3.3 \pm 0.5$	-----	-----	$0.87 \pm 0.26$
2Z2	$180 \pm 20$	$6.3 \pm 0.5$	$10.9 \pm 1.7$	-----	-----	$0.51 \pm 0.07$
5Z5	$580 \pm 30$	$14.2 \pm 0.2$	$8.8 \pm 2.7$	$15.5 \pm 0.7$	$6.2 \pm 0.6$	$1.08 \pm 0.43$
7Z10	$1650 \pm 160$	$26.5 \pm 1.7$	$1.5 \pm 0.3$	-----	-----	$0.19 \pm 0.08$

Blend 5Z5 shows a substantial increase in ultimate strength and a slight decrease in ultimate elongation compared to 2Z2. As the number of interacting groups increases the domain size becomes smaller and the number of interactions at the interface becomes greater, the ethyl acrylate phase to become less dominant in determining the mechanical properties. However, blend 5Z5 is still phase separated and the rubber phase still acts to substantially toughen the material. In fact, 5Z5 shows by far the highest toughness of any of the zinc blends.

The results of Chapter 2 showed that phase separation in blend 7Z10 occurs primarily on a length scale of less than 100 Å. At this level the domains are no longer expected to be mechanically active, and the mechanical properties for 7Z10 are essentially the same as for polystyrene.

The results for the acid blends are not as easy to interpret as for the zinc blends. Blend 5H5 shows mechanical properties that are similar to those of blend 5Z5. This is to be expected since their phase behavior is identical. However, the mechanical properties of 2H2 are more similar to 5Z5 than 2Z2. As was mentioned in Chapter 2, the DMTA low temperature transition is more prominent in 2Z2 than in 2H2 (see Figures 2.12 and 2.13). Since the transitions in DMTA are related to the mobility of the species, the acid/base interaction apparently has a greater effect in reducing chain mobility than the coordination interaction. This suggests that, although their effect on the phase behavior is the same, the acid/base interaction may be stronger than the coordination interaction. The difference between the mechanical properties of 2Z2 and 2H2 is that in 2Z2 the ethyl acrylate domains can still act as a separate phase, while in 2H2 the two phases are so strongly coupled that they do not act independently.

Mechanical properties for 8H10 are remarkable in that the ultimate strength is substantially higher than for either of the two components. Previous studies of miscible blends have found that mechanical properties generally are greater than would be predicted based on linear additivity of the properties of the two components.<sup>2-5</sup> This has been

interpreted as being due to the volume change upon mixing which restricts the free volume and decreases the mobility of the chains.<sup>4</sup> A quantitative theory for the volume change effect has found good agreement with experimental results.<sup>5</sup> Such an effect may explain the enhanced properties for 8H10. The substantial increase of  $T_g$  in the presence of specific interactions (see Chapter 2) demonstrates that the acid/base interaction is highly effective in reducing chain mobility. Although the previous studies do not show as much synergy as is seen for blend 8H10, the restrictions caused by the interactions may at least partially explain the increase in strength.

The increase in strength may also be due to the effect of the ionic clusters. Although HSPS does not contain ionic clusters, the acid blends do. The clusters have been proposed to act as reinforcing filler particles in ionomers,<sup>17,20</sup> and so the presence of clusters in 8H10 may act as a toughening agent. The high synergy results because the precursor sulfonated polystyrene does not contain these reinforcing particles, while the blend does.

The difference between 7Z10 and 8H10 remains to be explained. If the synergy in 8H10 is due to the restriction in chain mobility caused by volume change, then the difference between the acid and zinc blends would be due to a difference in the strength of the interactions. Visser and Cooper have proposed that deformation in ionomers occurs at least partially by rearrangement of the ionic groups.<sup>21</sup> In the case of the zinc blend, this would result in fewer restrictions on chain mobility as the ionic groups undergo rearrangement. The stronger interactions between ionic groups in the acid blends allow less rearrangement during deformation, and thus greater restrictions on the chain mobility.

If the synergy in 8H10 is due to the reinforcing effect of the clusters, then the apparent difference between 8H10 and 7Z10 is actually due to the difference between the precursors. For the zinc materials, 7ZSPS and 7Z10 both contain clusters, so the difference between the two is not great. However, for the acid materials 8HSPS does not contain clusters, while 8H10 does. Thus the presence of the clusters in the blend creates a substantial

increase in toughening over the precursor sulfonated polystyrene, and the appearance of substantial synergy.

Further information about deformation behavior can be obtained from examination of fracture surfaces. Figures 4.7-4.9 show SEM micrographs of the freeze-fractured surfaces of the blends. The trends seen in the micrographs follow the trends seen in the mechanical properties.

The micrograph for blend 00 in Figure 4.7 shows holes in the surface due to the loss of domains. This is clear evidence that there is no interfacial adhesion between the two phases, and is consistent with what has been described for the mechanical properties. However, the size of the holes is at least twice the size of the domains seen in the optical micrographs in Section 2.2.3. It is not clear why this is so, but it is important to note that the two techniques rely on different mechanisms. Optical microscopy depends on the refractive index difference between the phases, while SEM of a fracture surface depends on the mechanical properties.

Blend 2Z2 still shows evidence of phase separation, but now the particles have not completely been removed from the surface. In particular, there is a particle to the right of center in Figure 4.8a that has pulled away from the matrix but has still remained partially adhered. Thus, the interactions have resulted in increased adhesion at the interface. Again, the apparent domain sizes in the SEM micrograph do not match the results from optical microscopy.

The micrograph for 5Z5 in Figure 4.8b does not show any evidence of phase separated particles. As will be described below, the structure seen is evidence for the formation of crazes. Formation of crazes are well-known to be the primary mechanism of toughening in rubber-modified plastics, such as HIPS.<sup>7,8</sup> The formation of crazes in 5Z5 explains the high amount of toughening seen in the mechanical properties.

Blend 7Z10 shows a completely smooth surface in Figure 4.8c. This is consistent with the mechanical properties, which show brittle behavior.

50 microns

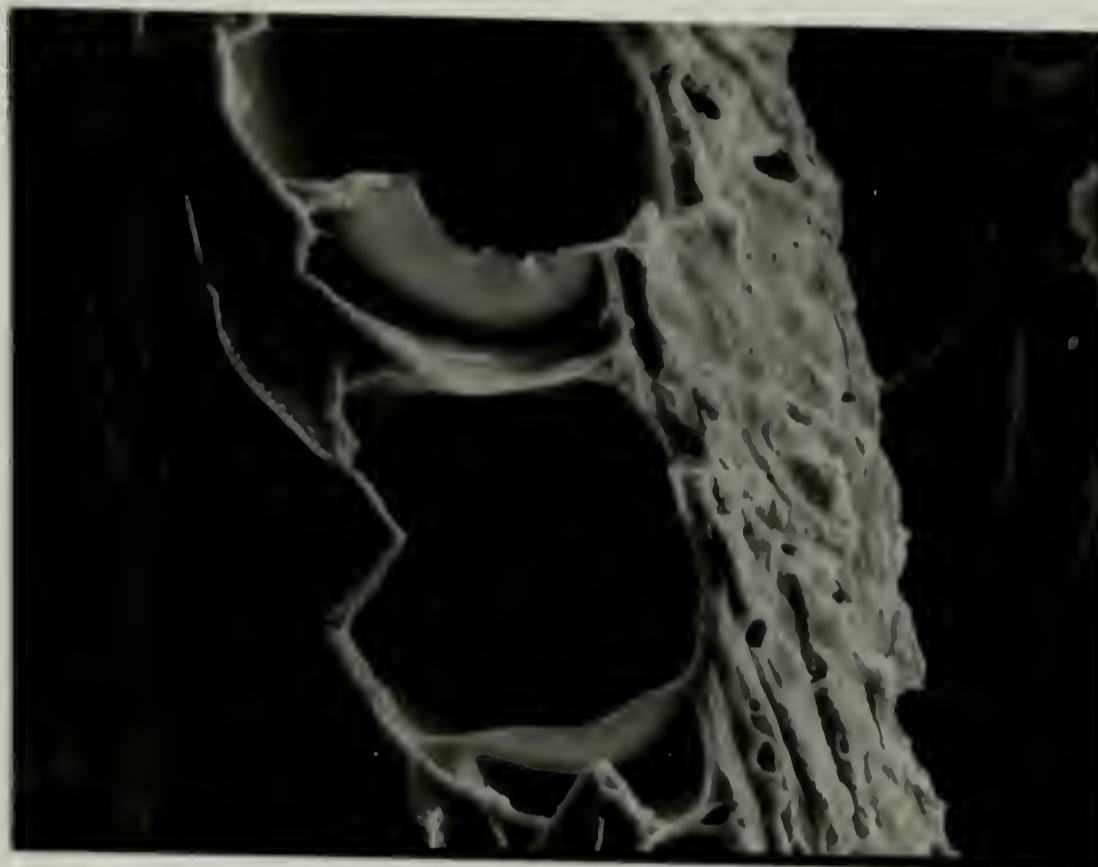
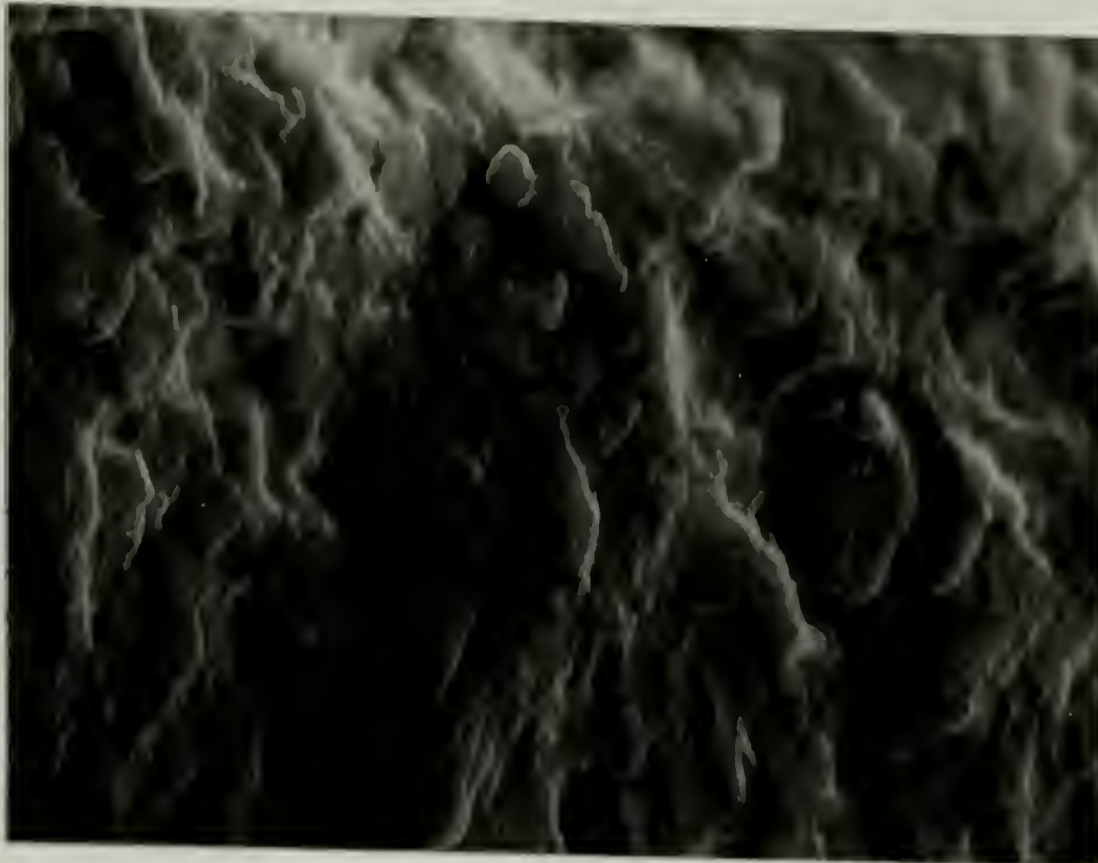


Figure 4.7: SEM of freeze-fractured surface of blend 00.

(a)

20 microns



(b)

20 microns

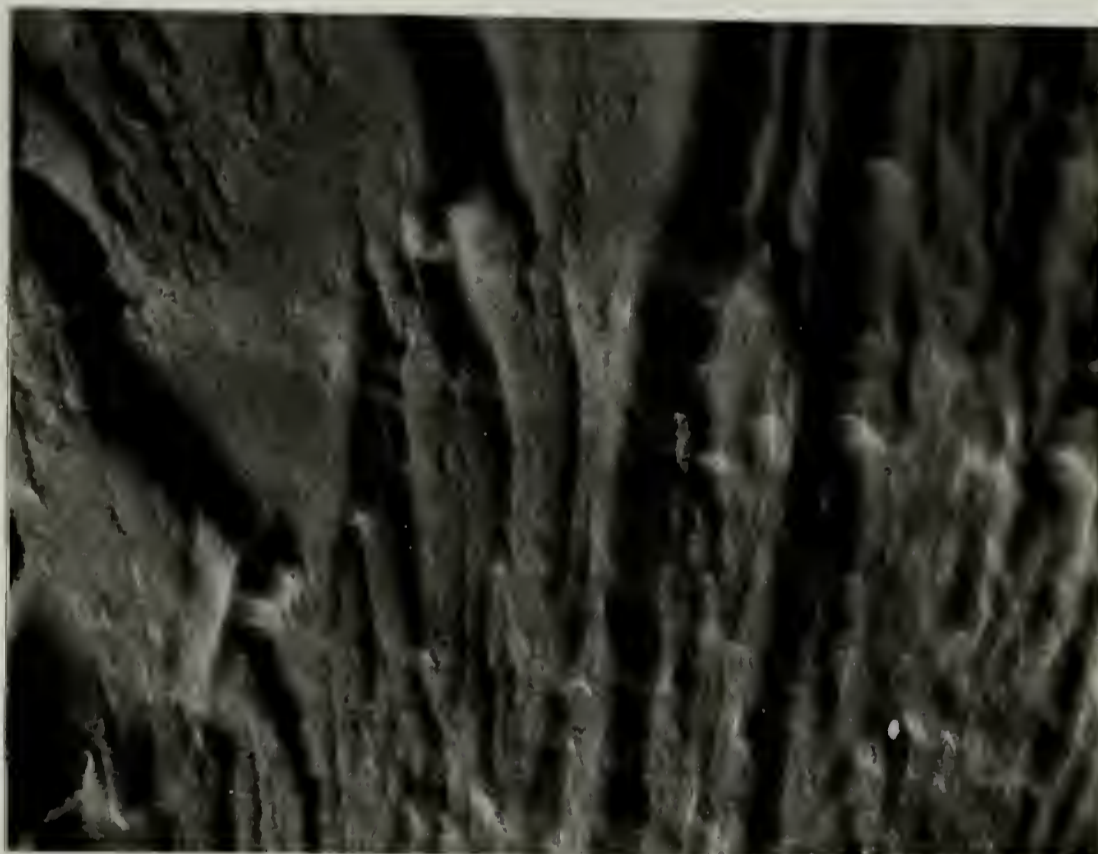


Figure 4.8: SEM of freeze-fractured surface of (a) blend 2Z2, (b) blend 5Z5 and (c) blend 7Z10

continued on next page



(c)

20 microns



Figure 4.8 (continued)

(a)

20 microns



(b)

20 microns



Figure 4.9: SEM of freeze-fractured surface of (a) blend 2H2, (b) blend 5H5 and (c) blend 8H10

continued on next page

(c)

20 microns



Figure 4.9 (continued)

The micrographs for the acid blends show very different behavior from the zinc blends, much as the mechanical properties do. There is no evidence of phase separation in the fracture surface of 2H2, as there was for 2Z2. Again, this is due to the greater strength of the acid/base interaction as compared to the coordination interaction.

The fracture surfaces of the acid blends all appear qualitatively similar. The surfaces are rough, although the scale of the features decreases as the substitution level increases. Extensive studies of deformation in polystyrene and polystyrene blends have shown similar features.<sup>7,8,12-14</sup> In many cases the rough region shows a regular structure of bands, and is known as the "hackle" region. This rough region occurs due to crack propagation through preexisting crazes. When the crack reaches the end of the craze the crack growth slows, and the stress concentration at the crack tip results in the formation of new crazes. These crazes are primarily in planes other than the plane of the existing crack. Further crack propagation occurs by the crack jumping to the plane of one of these secondary crazes and propagating through that craze. When the crack reaches the end of this craze it again slows, and the process is repeated.<sup>12,14</sup> The resulting fracture surface consists of rough features corresponding to the crack travelling through different planes.

Features such as those shown in Figure 4.9 are evidence for the extensive formation of crazes in the acid blends. Since crack propagation continues on the same plane to the end of a craze, the size of the features is related to the length of the crazes. The decrease in the size of the features with increasing substitution level results from the crazes becoming smaller and more numerous with increasing substitution level. Since crack growth slows at the end of a craze, more numerous and smaller crazes allows more plastic deformation to occur and results in an increase in toughness. In particular, the presence of crazes in blend 8H10 would suggest that the increase in strength is at least partially due to the reinforcing effect of the clusters.

### 4.3 Conclusions

The mechanical properties and fracture surfaces of the ionomer blends can be related to structural features which have been examined in other parts of this work. For the zinc blends, the main correlation is with the change in phase behavior with increasing substitution level. At 2% substitution level there is increased strength, although the fracture surface still shows the existence of two phases. However, better adhesion at the interface results in improved toughness. At 5% the phases are no longer distinct in the fracture surface. Instead, the fracture surface shows the rough character obtained when crazes are present. Since crazes are a well-known energy dissipation mechanism, it is possible to conclude that the formation of crazes is responsible for the increased toughness in blend 5Z5. Blend 7Z10 shows a smooth fracture surface and mechanical properties almost identical to polystyrene. At this level the phases are so small that they are no longer mechanically active, and fracture occurs in a brittle fashion.

The results for the acid blends do not correlate with the phase behavior in as straightforward a manner. Blend 5H5 exhibits behavior similar to 5Z5, but 2H2 is more similar to 5Z5 than to 2Z2. The difference between 2H2 and 2Z2 lies in the difference in the effectiveness of the interactions. The greater strength of the acid/base interactions results in a stronger coupling between the two phases. Thus, the ethyl acrylate phase cannot act independently and dominate the properties, as it does for 2Z2. The fracture surface for 2H2 shows evidence for enhanced toughening by the formation of crazes, but no evidence for separate particles. At the highest substitution level (blend 8H10) the fracture surface also shows evidence for the formation of crazes, and the strength is higher than for either of the two components. This synergy is likely due to a combination of the effects of the clusters acting as reinforcing particles and a loss in the mobility of the chains due to the interactions.

It should be noted that the results presented here are meant to be only a preliminary investigation of the mechanical properties and deformation behavior of the ionomer blends. The interpretation of the data is somewhat speculative, and clearly more intensive studies are needed to truly understand the effects of the interactions, ionic clusters, and changing phase size on the properties. Chapter 5 will present some recommendations for future work.

#### 4.4 References

1. Young, R. J. *Introduction to Polymers*, Chapman and Hall, London, 1983
2. Yee, A. F. *Poly. Eng. Sci.*, **17**, 213 (1977)
3. Joseph, E. A.; Lorenz, M. D.; Barlow, J. W.; Paul, D. R. *Polymer*, **23**, 112 (1982)
4. Kleiner, L. W.; Karasz, F. E.; MacKnight, W. J. *Poly. Eng. Sci.*, **19**, 519 (1979)
5. Yee, A. F.; Maxwell, M. A. *J. Macromol. Sci.-Phys.*, **B17**, 543 (1980)
6. Barlow, J. W.; Paul, D. R. *Poly. Eng. Sci.*, **24**, 525 (1984)
7. Bucknall, C. B. *Toughened Plastics*, Applied Science Publishers Ltd., London, 1977
8. Kinloch, A. J.; Young, R. J. *Fracture Behaviour of Polymers*, Elsevier Applied Science Publishers, London, 1983
9. Lavengood, R. E.; Nicolais, L.; Narkis, M. *J. Appl. Poly. Sci.*, **17**, 1173 (1973)
10. Traugott, T. D.; Barlow, J. W.; Paul, D. R. *J. Appl. Poly. Sci.*, **28**, 2947 (1983)
11. Fayt, R.; Jérôme, R.; Teyssié, P. *J. Poly. Sci. : Part B : Poly. Phys.*, **27**, 775 (1989)
12. Beahan, P.; Bevis, M.; Hull, D. *Proc. R. Soc. Lon., A*, **343**, 525 (1975)
13. Doyle, M. J.; Maranci, A.; Orowan, E.; Stork, S. T. *Proc. R. Soc. Lond. A*, **329**, 137 (1972)
14. Hull, D. *J. Mat. Sci.*, **5**, 357 (1970)
15. Bucknall, C. B.; Drinkwater, I. C. *J. Mat. Sci.*, **8**, 1800 (1973)
16. Bucknall, C. B.; Clayton, D.; Keast, W. E. *J. Mat. Sci.*, **7**, 1443 (1972)
17. Bellinger, M., Ph.D. Thesis, Rutgers University, 1992

18. Agarwal, P. K.; Duvdevani, I.; Peiffer, D. G.; Lundberg, R. D. *J. Poly. Sci. : Part B: Phys.*, **25**, 839 (1987)
19. Belfiore, L. A.; Pires, A. T. N.; Wang, Y.; Graham, H.; Ueda, E. *Macromolecules*, **25**, 1411 (1992)
20. Connolly, J. M., Ph.D. Thesis, University of Massachusetts, 1989
21. Visser, S. A.; Cooper, S. L. *Macromolecules*, **25**, 2230 (1992)

CHAPTER 5  
GENERAL CONCLUSIONS  
AND FUTURE WORK

5.1 Conclusions and Future Work

This work has, for the first time, extensively examined the properties and morphology of ionomer blends based on sulfonated polystyrene and copolymers that contain 4-vinylpyridine. The sulfonate groups interact with the pyridine substituents, resulting in substantial changes in their behavior compared to the individual blend components and the unfunctionalized blend.

The original motivation for this work grew out of an interest in understanding what effect specific interactions have on the phase behavior of otherwise immiscible blends. It has been shown from differential scanning calorimetry (DSC), dynamic mechanical thermal analysis (DMTA), and optical microscopy that the presence of the interactions results in a decrease in phase size as the number of interactions increases. This is consistent with a model for the phase behavior in which the ionic interactions act as crosslinks to restrict the size of the domains. Thus, all blends are phase separated on length scales smaller than the distance between interacting groups.

The model is supported by the data in several ways. It is clear from the thermal analysis that the domain size decreases with an increasing number of interactions. In particular, quantitative analysis of the phase composition and the effect of copolymer drift at the highest substitution level shows that the major phase is a mixed one, while the minor phase is due to longer ethyl acrylate segments created at the later stages of the copolymer synthesis. In terms of the model, most domains are smaller than the resolution limit of the DMTA, while the longer sequences result in a few domains that are large enough to be detected.



Optical microscopy also shows that the qualitative features of the model can describe the behavior of the blends. At 2% substitution level the domains are smaller and more homogeneous in size than the unfunctionalized blend due to the influence of the ionic crosslinks. Overall, the data show no difference between acid/base and coordination interactions, indicating that these interactions are strong enough and stable enough to be considered as crosslinks.

However, estimates of the domain sizes do not match the predictions of the model. One possible reason for this failure is the presence of aggregates of the ionic groups. Viscoelastic measurements of the blends show high temperature transitions due to ionic clusters, much as has been seen in ionomers. However, the transition temperatures are lowered due to internal plasticization by both pyridine and ethyl acrylate. The absence of an ionic peak in the x-ray scattering curves of the blends confirms that the clusters are disrupted. The calculated functionalities as determined from mechanical data decrease substantially upon blending, while the cluster core radii determined from a Porod analysis of the x-ray data do not change or increase upon blending, indicating that the concentration of ionic groups in the cluster has decreased upon blending. This change may be due to a combination of more restrictive steric requirements and the need for greater cooperativity in forming clusters in the blend.

One interesting result is that the acid blends show a cluster transition, while the acid form of sulfonated polystyrene does not. While this may appear surprising at first, it is easily explained as being due to the formation of a charge separated pair in the blend as a result of the proton transfer from sulfonic acid to pyridine.

The blends also provide an opportunity to gain further insight into the behavior of ionomers. For example, the activation energies for the high temperature cluster transition in viscoelastic measurements correlate with the strength of the electrostatic interactions between ionic groups, indicating that the cluster transition is associated with dissociation and motion of the ionic groups.

Consideration of the various models for ionomer morphology leads to the conclusion that the depleted zone core-shell model<sup>1</sup> is best able to explain the data. The restricted mobility model of Eisenberg, et al.<sup>2</sup> implies that the ionic cluster transition temperatures and the transition activation energies should occur in the same order with respect to interaction strength. The data, however, do not match this prediction. The hard sphere liquid-like interference model of Yarusso and Cooper<sup>3</sup> explains the peak in x-ray data as being caused by a preferred distance between clusters. However, data from this work show that the peak is eliminated upon blending, while viscoelastic measurements show that the clusters are still intact.

A preliminary investigation of the mechanical behavior of the ionomer blends can be related to the morphological results. For the zinc blends, the main correlation is with the change in phase behavior with increasing substitution level. At 2% substitution level there is increased strength, although the fracture surface still shows the existence of two phases. However, better adhesion at the interface results in improved toughness. At 5% substitution level the enhanced toughness is attributed to the extensive formation of crazes. At 7% substitution level the fracture surface is smooth and the mechanical properties are almost identical to polystyrene. At this level the phases are so small that they are no longer mechanically active.

The results for the acid blends show the effect of the greater strength of the acid/base interaction compared to the coordination interaction. The greater strength results in a stronger coupling between the two phases. For example, in blend 2H2 the ethyl acrylate phase cannot act independently and dominate the properties as it does for 2Z2. The fracture surface for 2H2 shows evidence for enhanced toughening by the formation of crazes, but no evidence for separate particles. At the highest substitution level (blend 8H10) the fracture surface also shows evidence for the formation of crazes, and the strength is higher than for either of the two components. This synergy is likely due to a combination of the

effects of the clusters acting as reinforcing particles and a loss in the mobility of the chains due to the interactions.

In summary, then, although the phase behavior is qualitatively determined by the crosslinking effect of the interactions, the view of the interactions as crosslinks is somewhat naive. The ionic groups are not independent, but are aggregated as in ionomers. Further, at higher temperatures the ionic groups can dissociate and allow flow to occur, and under loading there are toughening effects caused by aggregation of the groups and the different strengths of the interactions.

As in any investigation, there are many questions which remain unanswered. Unfortunately, the molecular weight distribution of the EAVP was not well controlled and the pyridine substituents in the copolymer were not distributed randomly. To overcome these problems, it may be possible to anionically polymerize butadiene followed by a postpolymerization reaction that introduces a pyridine or amide functionality. The resulting polymer is expected to have a narrow molecular weight distribution and a random distribution of functional groups. This scheme is similar to the approach used for synthesizing sulfonated polystyrene. The use of butadiene in place of ethyl acrylate may also provide some advantages for morphological investigations, described below.

The most obvious question remaining is that of the morphology and phase behavior at the highest substitution levels. There are three experiments which could possibly resolve this issue: transmission electron microscopy (TEM), small angle x-ray scattering (SAXS), and nuclear magnetic resonance spectroscopy (NMR). The SAXS data shown in Chapter 3 did not show any scattering that could be attributed to phase separated domains. (Note in particular the lack of scattered intensity for the acid blends shown in Figure 3.24.) Similarly, although TEM was attempted as part of this study a careful comparison with control samples was never able to reveal features that could be identified as a domain structure. Perhaps structural investigations utilizing blends of polystyrene and polybutadiene, for which TEM sample preparation techniques are well-known and which

are known to scatter x-rays, would show microphase separation at the higher substitution levels.

NMR relaxation time measurements have been used to examine phase separation at very small length scales.<sup>4-6</sup> Examination of the relaxation times for the backbone chains in these blends should show either the presence or absence of phase separation at length scales down to 10 Å. It would also be interesting to examine the relaxation times of the hydrocarbon chains in the ionomers. Differences between the relaxation times of the clusters and the matrix may provide further insight into the structure of the clusters. This is also another experiment in which comparison with the blends may provide further information on the nature of aggregation in ionomers.

Another important question that remains is whether or not these materials are at equilibrium. It is well-known that the relaxation times in ionomers are very long, which results in significant non-equilibrium effects.<sup>7</sup> The viscoelastic measurements described in Chapter 3 suggest that this is also true in the blends. It is not as clear whether the phase-separated structures in the blends are at equilibrium. The DSC annealing results in Chapter 2 indicate that there is no change in the phase separation with moderate amounts of annealing. This could be because the structure is at equilibrium, or because the presence of ionic interactions result in relaxation times that are so long that they are not accessible within the time frame of the experiments. In either case, it seems that the structure of the blends is governed by two very different relaxation times: one associated with the phase-separation between polystyrene and poly(ethyl acrylate) and one associated with the ionic aggregates. Further studies should be performed to establish more clearly the evolution of the morphology with time.

Because of the ionic nature of the interacting groups, dielectric measurements provide the opportunity for further examining relaxation behavior in the blend. A previous study on ionomers has found that interfacial polarization is a significant problem in the data analysis,<sup>7</sup> and a preliminary investigation of the dielectric properties of the blends in the

course of this work found the same problems. However, it may be possible to model the interfacial polarization from knowledge of the morphology adequately enough to account for the effect.

Clearly there is a great deal of work that needs to be done to understand the mechanical properties of these blends. For example, the use of notched fracture samples would allow a more accurate quantitative evaluation of the fracture toughness of the materials. More extensive investigations, such as transmission electron microscopy of deformed samples and measurements of volume change during deformation, would provide a better assessment of the roles that crazes and shear bands play in improving toughness.

Finally, in any scientific investigation it is important to maintain a perspective on the potential uses of the results. This work has been concerned with the development of a new class of materials with potentially useful properties. For example, the results from the mechanical properties tests point to potential uses as structural materials. Of course the specific blend investigated here is only a model system, but extension of these concepts to engineering thermoplastics may result in useful materials.

The controlled domain structure possible with these blends may result in new applications. For example, careful control of the morphology could result in membranes with interesting transport properties. Use of a conducting polymer as one of the components may result in useful electrical properties. The presence of ions opens up the possibility of using these blends as ionic conductors.

This work can only be considered a preliminary investigation of the structure and properties of ionomer blends. Further investigations will help to answer some of the questions that have been raised regarding their structure, morphology, and properties.

## 5.2 References

1. MacKnight, W. J.; Taggart, W. P.; Stein, R. S. *J. Poly. Sci. : Symp.*, **45**, 113 (1974)
2. Eisenberg, A.; Hird, B.; Moore, R. B. *Macromolecules*, **23**, 4098 (1990)
3. Yarusso, D. J.; Cooper, S. L. *Macromolecules*, **16**, 1871 (1983)
4. Jong, L.; Pearce, E. M.; Kwei, T. K.; Dickinson, L. C. *Macromolecules*, **23**, 5071 (1990)
5. Simmons, A.; Natansohn, A. *Macromolecules*, **24**, 3651 (1991)
6. Simmons, A.; Natansohn, A. *Macromolecules*, **25**, 1272 (1992)
7. Connolly, J. M., Ph.D. Thesis, University of Massachusetts, 1989

## BIBLIOGRAPHY

1. Flory, P. J. *J. Chem. Phys.*, **9**, 660 (1941)
2. Flory, P. J. *J. Chem. Phys.*, **10**, 51 (1942)
3. Huggins, M. L. *J. Chem. Phys.*, **9**, 440 (1941)
4. Scott, R. L. *J. Chem. Phys.*, **17**, 279 (1949)
5. Tompa, H. *Trans. Faraday Soc.*, **45**, 1142 (1949)
6. MacKnight, W. J.; Karasz, F. E. in *Comprehensive Polymer Science*, Vol. 7, S. L. Aggarwal, eds., Pergamon Press, New York, 1989, pp. 135
7. Flory, P. J.; Orwell, R. A.; Vrij, A. *J. Am. Chem. Soc.*, **86**, 3507 (1964)
8. Flory, P. J. *J. Am. Chem. Soc.*, **87**, 1833 (1965)
9. ten-Brinke, G.; Karasz, F. E.; MacKnight, W. J. *Macromolecules*, **16**, 1827 (1983)
10. Lu, X.; Weiss, R. A. *Poly. Mat. Sci. Eng.*, **64**, 75 (1991)
11. Painter, P. C.; Park, Y.; Coleman, M. M. *Macromolecules*, **21**, 66 (1988)
12. Painter, P. C.; Park, Y.; Coleman, M. M. *Macromolecules*, **22**, 580 (1989)
13. Coleman, M. M.; Lichkus, A. M.; Painter, P. C. *Macromolecules*, **22**, 586 (1989)
14. Brereton, M. G.; Vilgis, T. A. *Macromolecules*, **23**, 2044 (1990)
15. Kokhlov, A. R.; Nyrkova, I. A. *Macromolecules*, **25**, 1493 (1992)
16. Krause, S. *Pure and Appl. Chem.*, **58**, 1553 (1986)
17. Kwei, T. K.; Nishi, T.; Roberts, R. F. *Macromolecules*, **7**, 667 (1974)
18. Walsh, D. J.; Rostani, S. *Adv. Poly. Sci.*, **70**, 119 (1985)
19. Paul, D. R.; Newman, S., eds. *Polymer Blends*, Academic Press, New York, 1978
20. Bauer, R. F.; Dudley, E. A. *Rub. Chem. Tech.*, **50**, 35 (1977)
21. Yoshimura, N.; Fujimoto, K. *Rub. Chem. Tech.*, **42**, 1009 (1969)
22. Sperling, L. H.; Taylor, D. W.; Kirkpatrick, M. L.; George, H. F.; Bardman, D. R. *J. Appl. Poly. Sci.*, **14**, 73 (1970)
23. Xiao, H. X.; Frisch, K. C.; Frisch, H. L. *J. Poly. Sci. : Chem.*, **22**, 1035 (1984)

24. Pearce, E. M.; Kwei, T. K.; Min, B. Y. *J. Macromol. Sci.-Chem.*, **A21**, 1181 (1984)
25. Jong, L.; Pearce, E. M.; Kwei, T. K.; Dickinson, L. C. *Macromolecules*, **23**, 5071 (1990)
26. Ting, S. P.; Bulkin, B. J.; Pearce, E. M.; Kwei, T. K. *J. Poly. Sci. : Poly. Chem. Ed.*, **19**, 1451 (1981)
27. Ohno, N.; Kumanotani, J. *Polymer Journal*, **11**, 947 (1979)
28. Schneider, H. A.; Cantow, H.-J.; Percec, V. *Poly. Bull.*, **6**, 617 (1982)
29. Schneider, H. A.; Cantow, H.-J.; Maben, U.; Northfleet-Neto, H. *Poly. Bull.*, **7**, 263 (1982)
30. Simmons, A.; Natansohn, A. *Macromolecules*, **24**, 3651 (1991)
31. Simmons, A.; Natansohn, A. *Macromolecules*, **25**, 1272 (1992)
32. Smith, P.; Eisenberg, A. *J. Poly. Sci. : Letters*, **21**, 223 (1983)
33. Eisenberg, A.; Smith, P.; Zhou, Z.-L. *Poly. Eng. Sci.*, **22**, 1117 (1982)
34. Murali, R.; Eisenberg, A. *J. Poly. Sci. : Part B : Phys.*, **26**, 1385 (1988)
35. Zhou, Z.-L.; Eisenberg, A. *J. Poly. Sci. : Phys.*, **21**, 595 (1983)
36. Simmons, A.; Eisenberg, A. *Poly. Prep.*, **27**, 341 (1986)
37. Murali, R.; Eisenberg, A. *Poly. Prep.*, **27**, 343 (1986)
38. Natansohn, A.; Eisenberg, A. *Poly. Prep.*, **27**, 349 (1986)
39. Hara, M.; Eisenberg, A. *Macromolecules*, **20**, 2160 (1987)
40. Hara, M.; Eisenberg, A. *Macromolecules*, **17**, 1335 (1984)
41. Eisenberg, A.; Hara, M. *Poly. Eng. Sci.*, **24**, 1306 (1984)
42. Natansohn, A.; Eisenberg, A. *Macromolecules*, **20**, 323 (1987)
43. Rutkowska, M.; Eisenberg, A. *Macromolecules*, **17**, 821 (1984)
44. Rutkowska, M.; Eisenberg, A. *J. Appl. Poly. Sci.*, **30**, 3317 (1985)
45. Rutkowska, M.; Eisenberg, A. *J. Appl. Poly. Sci.*, **33**, 2833 (1987)
46. Rutkowska, M.; Eisenberg, A. *J. Appl. Poly. Sci.*, **29**, 755 (1984)
47. Natansohn, A.; Rutkowska, M.; Eisenberg, A. *Polymer*, **28**, 885 (1987)
48. Natansohn, A.; Rutkowska, M.; Eisenberg, A. *Poly. Eng. Sci.*, **27**, 1504 (1987)



49. Natansohn, A.; Murali, R.; Eisenberg, A. *Makromol. Chem., Macromol. Symp.*, **16**, 175 (1988)
50. Zhang, X.; Eisenberg, A. *Poly. Adv. Tech.*, **1**, 9 (1990)
51. Zhang, X.; Eisenberg, A. *J. Poly. Sci. : Part B : Phys.*, **28**, 1841 (1990)
52. Smith, P.; Hara, M.; Eisenberg, A. in *Current Topics in Polymer Science, Vol. II*, R. M. Ottenbrite, L. A. Utracki and S. Inoue, eds., Carl Hanser Verlag, New York, 1987, pp. 256
53. Peiffer, D. G.; Duvdevani, I.; Agarwal, P. K.; Lundberg, R. D. *J. Poly. Sci.: Letters*, **24**, 581 (1986)
54. Agarwal, P. K.; Duvdevani, I.; Peiffer, D. G.; Lundberg, R. D. *J. Poly. Sci. : Part B: Phys.*, **25**, 839 (1987)
55. Lundberg, R. D.; Phillips, R. R.; Peiffer, D. G. *J. Poly. Sci. : Part B : Phys.*, **27**, 245 (1989)
56. Belfiore, L. A.; Pires, A. T. N.; Wang, Y.; Graham, H.; Ueda, E. *Macromolecules*, **25**, 1411 (1992)
57. Register, R. A.; Sen, A.; Weiss, R. A.; Li, C.; Cooper, S. *J. Poly. Sci. : Part B : Phys.*, **27**, 1911 (1989)
58. Sakurai, K.; Douglas, E. P.; MacKnight, W. J. *Macromolecules*, in press
59. Sakurai, K.; Douglas, E. P.; MacKnight, W. J. *Macromolecules*, submitted
60. Aouadj, O.; Lassoued, A.; Djadoun, S. *Phys. Opt. Dyn. Phen. in Macr. Sys.*, p. 525 (1985)
61. Djadoun, S. *Poly. Bull.*, **9**, 313 (1983)
62. Djadoun, S. *Poly. Bull.*, **7**, 607 (1982)
63. Djadoun, S.; Goldberg, R. N.; Morawetz, H. *Macromolecules*, **10**, 1015 (1977)
64. Otocka, E. P.; Eirich, F. R. *J. Poly. Sci. : Part A-2*, **6**, 895 (1968)
65. Otocka, E. P.; Eirich, F. R. *J. Poly. Sci. : Part A-2*, **6**, 913 (1968)
66. Otocka, E. P.; Eirich, F. R. *J. Poly. Sci. : Part A-2*, **6**, 921 (1968)
67. Otocka, E. P.; Eirich, F. R. *J. Poly. Sci. : Part A-2*, **6**, 933 (1968)
68. MacKnight, W. J.; Earnest, T. R. *J. Poly. Sci. : Macromol. Rev.*, **16**, 41 (1981)
69. Fitzgerald, J. J.; Weiss, R. A. *J. Macromol. Sci.-Rev. Macromol. Chem. Phys.*, **C28**, 99 (1988)
70. Eisenberg, A. *Macromolecules*, **3**, 147 (1970)

71. Eisenberg, A.; King, M. *Ion-Containing Polymers*, Academic Press, New York, 1977
72. Eisenberg, A.; Navratil, M. *J. Poly. Sci. : Part B*, **10**, 537 (1972)
73. Eisenberg, A.; Navratil, M. *Macromolecules*, **6**, 604 (1973)
74. Eisenberg, A.; Navratil, M. *Macromolecules*, **7**, 90 (1974)
75. Navratil, M.; Eisenberg, A. *Macromolecules*, **7**, 84 (1974)
76. Connolly, J. M., Ph.D. Thesis, University of Massachusetts, 1989
77. Weiss, R. A.; Fitzgerald, J. J.; Kim, D. *Macromolecules*, **24**, 1071 (1991)
78. Lundberg, R. D.; Makowski, H. S.; Westerman, L. *Poly. Prep.*, **19**, 310 (1978)
79. Fitzgerald, J. J.; Kim, D.; Weiss, R. A. *J. Poly. Sci. : Part C : Letters*, **24**, 263 (1986)
80. Weiss, R. A.; Fitzgerald, J. J.; Kim, D. *Macromolecules*, **24**, 1064 (1991)
81. Yano, S.; Nagao, N.; Hattori, M.; Hirasawa, E.; Tadano, K. *Macromolecules*, **25**, 368 (1992)
82. Taggart, W. P., Ph.D. Thesis, University of Massachusetts, 1973
83. MacKnight, W. J.; Taggart, W. P.; Stein, R. S. *J. Poly. Sci. : Symp.*, **45**, 113 (1974)
84. Yarusso, D. J.; Cooper, S. L. *Macromolecules*, **16**, 1871 (1983)
85. Visser, S. A.; Cooper, S. L. *Macromolecules*, **25**, 2230 (1992)
86. Eisenberg, A.; Hird, B.; Moore, R. B. *Macromolecules*, **23**, 4098 (1990)
87. Fitzgerald, J. J.; Weiss, R. A. *Proc. Annu. Tech. Conf. Soc. Plast. Eng.*, 341 (1985)
88. Weiss, R. A.; Lefelar, J. A. *Polymer*, **27**, 3 (1986)
89. Fitzgerald, J. J.; Kim, D.; Weiss, R. A. *J. Poly. Sci. : Letters*, **24**, 263 (1986)
90. Yarusso, D. J.; Cooper, S. L. *Polymer*, **26**, 371 (1985)
91. Niwa, M.; Matsumoto, T.; Kagami, M.; Kajiyama, K. *Sci. Eng. Rev. Doshisha Univ.*, **25**, 192 (1984)
92. Tamikado, T. *J. Poly. Sci.*, **43**, 489 (1960)
93. Hoffman, R. in *Applied Polymer Light Microscopy*, D. A. Hemsley, eds., Elsevier Applied Science, London, 1989, pp. 151
94. Beckman, E. J.; Karasz, F. E.; Porter, R. S.; MacKnight, W. J.; Hunsel, J. V.; Koningsveld, R. *Macromolecules*, **21**, 1193 (1988)

95. Couchman, P. R. *Macromolecules*, **11**, 1156 (1978)
96. Lin, A. A.; Kwei, T. K.; Reiser, A. *Macromolecules*, **22**, 4112 (1989)
97. Mayo, F. R.; Lewis, F. M. *J. Am. Chem. Soc.*, **66**, 1594 (1944)
98. Odian, G. *Principles of Polymerization*, John Wiley & Sons, New York, 1981
99. Meyer, V. E.; Lowry, G. G. *J. Poly. Sci.*, **A3**, 2843 (1965)
100. Bares, J. *Macromolecules*, **8**, 244 (1975)
101. Russell, T. P.; Jérôme, R.; Charlier, P.; Foucart, M. *Macromolecules*, **21**, 1709 (1988)
102. Lu, X.; Weiss, R. A. *Poly. Mat. Sci. Eng.*, **64**, 163 (1991)
103. Lu, X.; Weiss, R. A. *Macromolecules*, **24**, 4381 (1991)
104. Hird, B.; Eisenberg, A. *J. Poly. Sci. : Part B : Phys.*, **28**, 1665 (1990)
105. Yano, S.; Nagao, N.; Hattori, M.; Hirasawa, E.; Tadano, K. *Macromolecules*, **25**, 368 (1992)
106. Alexander, L. E. *X-Ray Diffraction Methods in Polymer Science*, Robert E. Krieger Publishing Company, Malabar, Florida, 1985
107. Glatter, O. *J. Appl. Cryst.*, **7**, 147 (1974)
108. Weiss, R. A.; Lefelar, J. A. *Polymer*, **7**, 3 (1986)
109. Eisenberg, A.; King, M.; Navratil, M. *Macromolecules*, **6**, 734 (1973)
110. Aklonis, J. J.; MacKnight, W. J. *Introduction to Polymer Viscoelasticity*, John Wiley & Sons, New York, 1983
111. Pearson, D. S.; Graessley, W. W. *Macromolecules*, **11**, 528 (1978)
112. Ferry, J. D. *Viscoelastic Properties of Polymers*, John Wiley & Sons, New York, 1980
113. Plazek, D. J. *J. Phys. Chem.*, **69**, 3480 (1965)
114. Peiffer, D. G.; Weiss, R. A.; Lundberg, R. D. *J. Poly. Sci. : Physics*, **20**, 1503 (1982)
115. Dickinson, L. C.; Morganelli, P.; Chu, C. W.; Petrovic, Z.; MacKnight, W. J.; Chien, J. C. W. *Macromolecules*, **21**, 338 (1988)
116. Young, R. J. *Introduction to Polymers*, Chapman and Hall, London, 1983
117. Yee, A. F. *Poly. Eng. Sci.*, **17**, 213 (1977)
118. Joseph, E. A.; Lorenz, M. D.; Barlow, J. W.; Paul, D. R. *Polymer*, **23**, 112 (1982)

119. Kleiner, L. W.; Karasz, F. E.; MacKnight, W. J. *Poly. Eng. Sci.*, **19**, 519 (1979)
120. Yee, A. F.; Maxwell, M. A. *J. Macromol. Sci.-Phys.*, **B17**, 543 (1980)
121. Barlow, J. W.; Paul, D. R. *Poly. Eng. Sci.*, **24**, 525 (1984)
122. Bucknall, C. B. *Toughened Plastics*, Applied Science Publishers Ltd., London, 1977
123. Kinloch, A. J.; Young, R. J. *Fracture Behaviour of Polymers*, Elsevier Applied Science Publishers, London, 1983
124. Lavengood, R. E.; Nicolais, L.; Narkis, M. *J. Appl. Poly. Sci.*, **17**, 1173 (1973)
125. Traugott, T. D.; Barlow, J. W.; Paul, D. R. *J. Appl. Poly. Sci.*, **28**, 2947 (1983)
126. Fayt, R.; Jérôme, R.; Teyssié, P. *J. Poly. Sci. : Part B : Poly. Phys.*, **27**, 775 (1989)
127. Beahan, P.; Bevis, M.; Hull, D. *Proc. R. Soc. Lon., A*, **343**, 525 (1975)
128. Doyle, M. J.; Maranci, A.; Orowan, E.; Stork, S. T. *Proc. R. Soc. Lond. A*, **329**, 137 (1972)
129. Hull, D. *J. Mat. Sci.*, **5**, 357 (1970)
130. Bucknall, C. B.; Drinkwater, I. C. *J. Mat. Sci.*, **8**, 1800 (1973)
131. Bucknall, C. B.; Clayton, D.; Keast, W. E. *J. Mat. Sci.*, **7**, 1443 (1972)
132. Bellinger, M., Ph.D. Thesis, Rutgers University, 1992

